Appendix C
Hydrodynamic, Wave, and Sediment Transport Modeling

Mississippi Barrier Island Restoration

Prepared for US Army Corps of Engineers

june 2013

PREFACE

This document consists of two parts:

Part I – Morphological study for the restoration of the Ship Island

Part II – Optimization of closure methods

Part I

CH2MHILL

Deltares
Enabling Delta Life

Royal HaskoningDHV
Enhancing Society Together

Mississippi Barrier Island Restoration

Prepared for: USACE

Final

June 2013

CH2MHILL Royal HaskoningDHV Deltares

Mississippi Barrier Island Restoration

1204473-000

Title
Mississippi Barrier Island Restoration

Project 1204473-000
Reference 1204473-000-HYE-0031
Pages 180

Keywords
Barrier islands, Coastal morphology

Summary
The main goal of the restoration of the barrier islands in the Mississippi Coastal Improvements Program (MsCIP) is to restore the sediment budget, including littoral zone geologic processes around Ship, Horn, and Petit Bois islands as close to their natural state as possible. The United States Army Corps of Engineers (USACE), Mobile District, has commissioned CH2MHILL, Royal HaskoningDHV and Deltares to carry out a modeling study that addresses parts of the additional studies identified in the MsCIP Comprehensive Plan and Integrated Programmatic Environmental Impact Statement.

The objective of the study is to address the following key questions:
1 How will closing of Camille Cut and nearshore sand placement at the southeast end of Ship Island impact sediment transports?
2 Will sand extracted from offshore borrow sites negatively impact erosion and deposition on the barrier islands?
3 How will closing of Camille Cut and nearshore sand placement at the southeast end of Ship Island impact operation and maintenance at Ship Island Pass?

These key questions were addressed by investigating the impact of the restoration design on hydrodynamics, sediment transport and morphology, using numerical models.

In summary, the three key questions are addressed as follows:
1 The post-restoration configuration primarily has a local effect on the transport pattern along and around Ship Island under hurricane conditions. During year-averaged conditions the effect is minimal. Transports along the tips of Ship Island and through the passes are expected to increase slightly (0-10% under year-averaged conditions).
2 Due to its small size and limited excavation depth the borrow area south of Ship Island will not negatively impact the overall morphological development of the restored Ship Island.
3 The restoration is expected to result in a limited increase of the sedimentation of Ship Island Pass, primarily during hurricane events. For year-averaged conditions the effect is predicted to be minimal. It was found that for the restored Ship Island during severe hurricanes sedimentation in the channel increased with 10% to 30%, while for milder hurricanes the increase is expected to be in the order of 0% to 10%.

This report constitutes the final report.

Version	Date	Author	Initials	Review	Initials	Approval	Initials
01 (draft)	May 2012	Team		Prof. L.C. van Rijn		W.M.K. Tilmans	
02	Nov 2012	Team		Prof. L.C. van Rijn		W.M.K. Tilmans	
03 (final)	June 2013	Team		Prof. L.C. van Rijn		W.M.K. Tilmans	

State
final

Contents

List of Figures

1 Introduction

1.1 Study objective

The main goal of the restoration of the barrier islands in the Mississippi Coastal Improvements Program (MsCIP) is to restore the sediment budget, including littoral zone geologic processes around Ship, Horn, and Petit Bois islands as close to their natural state as possible. The restoration effort seeks to return sediment into the system within the barrier islands to pre-Hurricane Camille conditions as much as possible given the realities of navigation channel dredging, climate change (sea level rise, increased frequency of storms, etc.) and other anthropogenic activities. The scale of the restoration is based on adding approximately the same volume of sand to the system that has been removed over the past decades (upwards of approximately 22 Mcy, see USACE, 2009a,b) due to (maintenance) dredging. More recent MsCIP studies by Byrnes et al. (2011), which considered both the volume of sediment removed from maintenance dredging and associated placement of dredged sediment within the system indicate that approximately 13 Mcy has been removed from the littoral system of the barrier islands. Restoring the Mississippi barrier islands to a condition similar to the natural system that functioned before human intervention (generally defined as the pre-Camille conditions) offers the best opportunity to ensure the long-term viability of these islands.

A sketch of the Comprehensive Coastal Improvement Program is shown in Figure 1.1. An overview of all barrier islands, passes, navigation channels and ports in the study area is given in Figure 1.2.

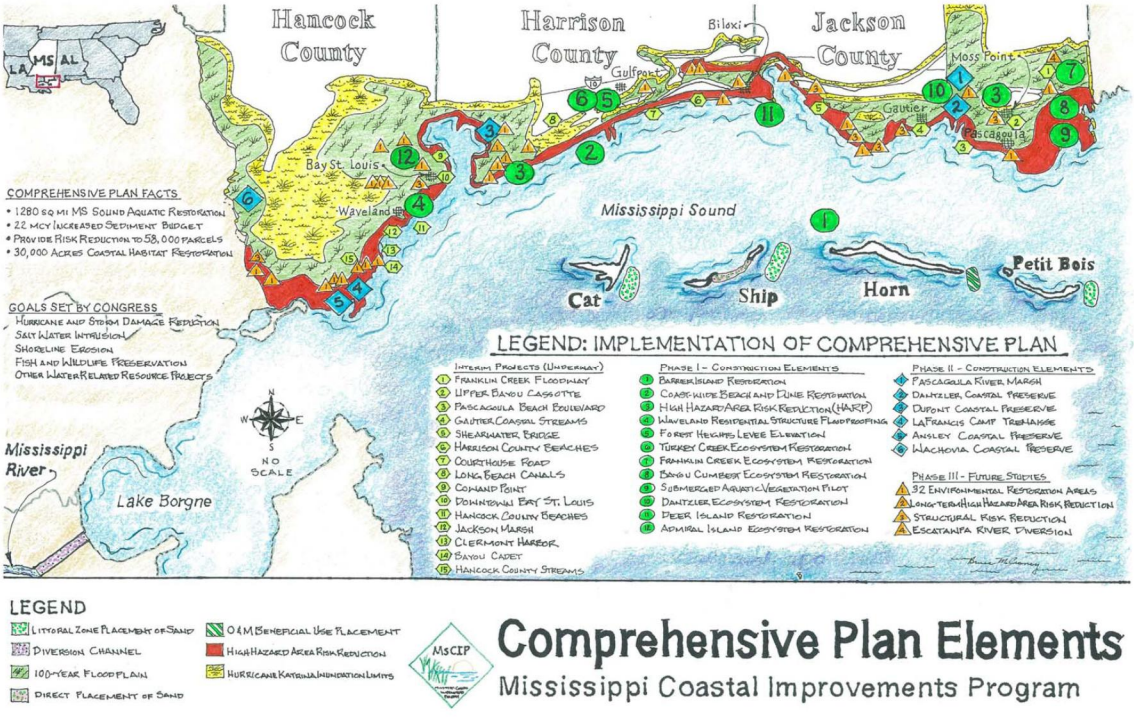

Figure 1.1 MsCIP Comprehensive Plan Elements (source: http://www.mscip.usace.army.mil/)

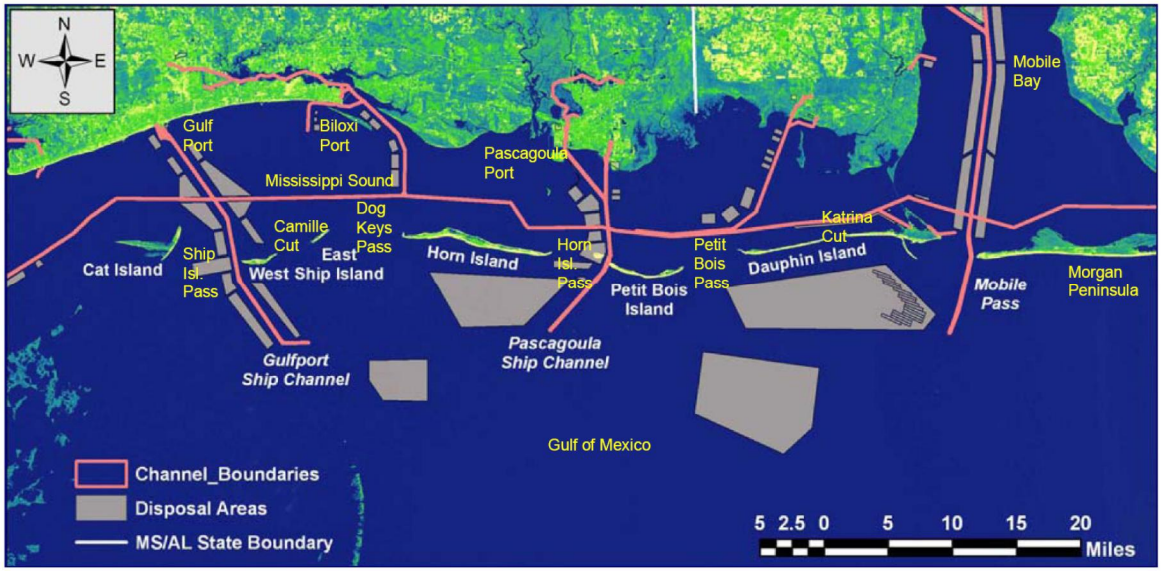

Figure 1.2 Overview of islands, passes, channels and ports (based on figure in Byrnes et al (2011))

The US Army Corps of Engineers (USACE), Mobile District, has commissioned CH2MHILL, Royal HaskoningDHV and Deltares to carry out a modeling study that addresses parts of the additional studies identified in the MsCIP Comprehensive Plan and Integrated Programmatic Environmental Impact Statement.

The objective of the study is to address the following key questions:

1 How will closing of Camille Cut and nearshore sand placement at the southeast end of Ship Island impact sediment transports?

4 Will sand extracted from offshore borrow sites negatively impact erosion and deposition on the barrier islands?

5 How will closing of Camille Cut and nearshore sand placement at the southeast end of Ship Island impact operation and maintenance at Ship Island Pass?

These key questions will be addressed by investigating the impact of restoration designs on hydrodynamics, sediment transport and morphology. The overall approach will be to incorporate the designs in numerical models and perform a comparison relative to the base scenario for a range of representative conditions. The considered baseline and restoration cases are (see Section 2.4 for a more detailed description):

1a Baseline 1a, using post-Katrina topography and bathymetry, including the recent (early 2012) widening of the Gulf Port navigation channel and the planned sediment placement at the northern side of Ship Island.

1b Baseline 1b, as in baseline 1a, with presence of the borrow source in Ship Island Pass, as a reference for Design 2b.

2a Closing of Camille Cut and nearshore sand placement at the southeastern shore of Ship Island, for the situation with and without presence of Ship Island offshore borrow area.

2b Closing of Camille Cut and nearshore sand placement at the southeastern shore of Ship Island, for the situation with presence of the borrow source in Ship Island Pass.

A summary of the cases described above is presented in Table 1.1.

Case	Camille Cut closure	SE sand placement Ship Isl.	Ship Isl. offshore borrow area	Ship Isl. Pass borrow area	Widened Gulf Port channel	north sand placement Ship Isl.
1a	no	no	no	no	yes	yes
1b	no	no	no	yes	yes	yes
2a	yes	yes	no + yes	no	yes	yes
2b	yes	yes	no	yes	yes	yes

Table 1.1 Summary of baselines and restoration designs to be studied

Phase 1 of the study (i.e. the original scope) comprised the following eight tasks:

Task 1 Desk-Top Study, Data Collection and Review
Task 2 Construction and calibration of a Delft3D Comprehensive Numerical Model of the Mississippi Coastal Cell (MCC-model)
Task 3 Evaluation of Barrier Island Restoration Design
Task 4 Reporting of Tasks 1 to 3
Task 5 Scoping, Project Management, Internal Reviews, and Workshops
Task 6 On-Site Collaboration and Support
Task 7 Modeling Training
Task 8 Provision of Modeling Software (Optional Task)

During the course of the first phase of the study additional topics were identified that were important for the evaluation of the Ship Island restoration and the sediment balance of the Mississippi Coastal Cell (MCC). Furthermore, it became apparent that a number of detailed processes of potential relevance for Ship Island Pass could not be fully addressed in the defined Phase 1 work. Therefore, a Phase 2 was defined in which both the hurricane aspects and the more detailed processes at West Ship Island and Ship Island Pass were addressed in two additional tasks:

Task 9 Comprehensive Evaluation of Effect of Hurricanes and Tropical Storms
Task 10 Detailed Evaluation of Sediment Balance of Ship Island Pass

In the present report all tasks are described.

1.2 Project team

The CH2MHILL-Royal HaskoningDHV-Deltares management team included David Stejskal (CH2MHILL), Marius Sokolewicz, Winfried Pietersen and Linda Mathies (Royal HaskoningDHV) and Hans de Vroeg and Dirk-Jan Walstra (Deltares). Most of the work was carried out at Deltares' Delft office. The remaining team members focused on the modeling and consisted of Cilia Swinkels, Jaap van Thiel de Vries, Arjen Luijendijk, Wiebe de Boer, Roderik Hoekstra (all Deltares), Frank Dekker, Tijmen Smolders and Johan Henrotte (all Royal HaskoningDHV). The Quality Control was carried out by Prof. Dr. Leo van Rijn (Deltares).

1.3 Outline of the report

In this report all modeling activities and results are described and the key questions are addressed. A description of the modeling strategy is given in Chapter 2. This chapter also includes a description of the cases which have been modeled in this study. A summary of the

most relevant data on the environmental conditions is presented in Chapter 3. The setup and results of the tidal modeling are described in Chapter 4, the setup and results of the wave modeling in Chapter 5. The sediment transport modeling for year-averaged conditions, hurricanes and cold fronts is described in Chapter 6. On the basis of all results the sediment budget for the MCC area is described in Chapter 7. This chapter includes a comparison of the results with the sediment balance presented in Byrnes et al. (2011), with dredging volumes from the passes and with model results from other studies. The considerations in this chapter focus on the large scale MCC-model. In Chapter 8 the restored Ship Island is evaluated by considering the morphological development of the restored Ship Island for both the medium term (4 years) and for hurricane impact. Finally, Chapter 9 synthesizes the results into a morphological evaluation of the restored Ship Island and addresses the key questions introduced in this chapter.

1.4 Disclaimer

This study has been performed in support of the Supplemental Environmental Impact Study for the Mississippi Coastal Improvement Program. The study resulted in an assessment of morphological aspects of the restoration of Ship Island, the results of which are presented in this report. These results are for use for the Supplemental Environmental Impact Study for the Mississippi Coastal Improvement Program.

It is noted that model simulations have their limitations, and the accuracy of model predictions is subject to these limitations - partly due to the inherent unpredictable (chaotic) behavior of weather systems. Models show trends in morphological processes, and their results should always be interpreted by experienced morphological experts. Even then, due to the nature of the considered processes, predictions are only an approximation of reality.

For the purpose of this assessment, a modeling tool has been set-up. This modeling tool can be used for the evaluation of alternative approaches for restoration of the barrier island which were not the subject of this study. However, it is noted that the use of the tool requires expert knowledge, and that the modeling results should always be interpreted by experienced morphological experts to conclude on the morphological impacts.

.

2 Study approach and modeling strategy

2.1 Introduction

In this chapter the overall study approach to address the key questions (Chapter 1) is presented. The study approach, discussed in the next section, is aimed at evaluating the restored Ship Island and the potential impact on its direct surroundings. Although the primary interest is on a relatively small scale, larger spatial scales need to be included. This relates to the nature of the phenomena that need to be included (e.g. hurricanes and tide) that require evaluation on larger scales. Furthermore, a thorough understanding of the sediment dynamics and morphology on Ship Island scale also requires knowledge of sediment pathways and morphological characteristics of the coastal cell to which it belongs. The study approach gives a general description of the main study components, how these are interconnected and how the restored Ship Island is evaluated. As the study is primarily based on the application of models, the models and the associated modeling strategy are explained in Section 2.3. Finally the components of the restoration effort (Table 1.1) are further detailed in Section 2.4.

2.2 Study Approach

Evaluation of the restoration efforts at Ship Island starts with a sound understanding of the observed morphological developments and the associated sediment budget of the morphological system to which Ship Island belongs. In the present study, previous work (Byrnes et al., 2011; Rosati et al., 2009) in which the morphological cell is bounded in the East by the Fort Morgan Peninsula and in the West by Cat island is followed (here referred to as the Mississippi Coastal Cell or MCC).

As a first step the sediment budget is derived from model predictions on the MCC-scale which include all relevant processes and forcing conditions (averaged conditions, tropical storms and hurricanes). The predicted sediment budget is compared with budgets derived from the bathymetric surveys (Byrnes et al., 2011) and the historic dredging figures. For the averaged conditions a set of representative wave conditions was selected. However, such an approach is not feasible for the hurricanes due to their highly dynamic and intermittent character. Instead, all relevant hurricanes that occurred during the period over which the existing sediment budget was determined (1917-2010) are considered. The model-based sediment budget allows for further spatial detailing of the sediment pathways and can also be used to estimate the contributions of the various forcing components.

Next, the detailed sediment transport mechanisms and morphology in the Ship Island area are evaluated. Processes that govern the transports around West Ship Island are investigated. After having established the dominant forcing mechanisms a number of detailed multi-annual morphodynamic simulations based on averaged forcing conditions are run to evaluate the restored Ship Island. The considered cases (see Table 1.1) are chosen such that insight is obtained into the combined and separate impact of the sand placements and the borrow areas that comprise the restoration of Ship Island.

To evaluate the long term stability of the restored Ship Island, it is subjected to a range of characteristic hurricanes. The predicted post-hurricane bathymetries are subsequently used to evaluate the recovery potential covering a 4 year period again based on averaged conditions excluding hurricanes.

This study relies heavily on the application of process-based hydrodynamic and morphological models to address the key questions. The models are used to identify and quantify the impact of the various elements (i.e. nourishments and borrow areas) that make up the restoration of Ship Island.

Hydrodynamic and morphological models of the area have been set up, based on Deltares' Delft3D modeling suite, a generic process based morphodynamic model (Lesser et al., 2004) and the XBeach model, a hurricane impact model (Roelvink et al., 2009).

Although the MCC is the largest considered scale in the evaluation, larger domains are required to accurately incorporate wave, tidal, wind and hurricane forcing conditions. A cascade of models has been set up which, at the largest scale, starts with the Gulf of Mexico and subsequently scales down to the Gulf coast (Mississippi river to the north-east coast of Florida), the Mississippi coastal cell (MCC) and finally Ship Island.

The evaluation of the restoration effort is primarily based on its influence on the sediment pathways and morphological development relative to the existing (pre-restoration) situation. Therefore, the models will both be applied on the existing situation and the restored Ship Island. Key aspects such as the potential increased back filling of Ship Island Pass and the morphological evolution of the restored Ship Island under averaged and hurricane conditions are addressed by aggregating model results to indicators. These indicators describe/quantify a particular aspect such as sedimentation rates, volumes losses or the littoral drift at specific locations. The effect of the restoration is established based on the modified indicators.

In the following section the adopted modeling strategy and the individual models are described in more detail.

2.3 Overview of models and modeling strategy

2.3.1 Introduction

First a general overview is provided of the Delft3D and XBeach models and domains used in the present study. In the final sub-section the study approach is coupled to a modeling strategy in which the interaction between the various models and the key questions is provided.

2.3.2 Gulf of Mexico model (GoM-model) and Panhandle model (PAN-model)

Two existing models (hydrodynamics and waves) have been considered to provide tidal and hurricane boundary conditions for the models on the MCC and Ship Island scale (see Figure 2.1). The largest model covers the entire Gulf of Mexico (GoM). As the resolution of GoM-model is too course for a direct coupling to models on MCC-scale, an intermediate scale model is used. This so-called PAN-model has a higher resolution (about 2x2 km in the area of the Mississippi Sound) and covers the northeastern corner of the Gulf.

Besides the tidal forcing on the open boundaries, the size of the GoM-model domain also requires the inclusion of the internal tide generating forces. The PAN-model is nested in the GoM-model and thus obtains its boundary conditions from the overall model. Both models were calibrated for tidal water levels at relevant tidal stations along the shoreline of the Gulf of Mexico. Both models are also used to provide boundary conditions for hurricane conditions. For these events both models were forced with space and time varying wind and pressure fields.

2.3.3 Mississippi Coastal Cell model (MCC-model)

The MCC-model is a depth-averaged (2DH) hydrodynamic and sediment transport model for the MCC-area which has specifically been constructed for the present study. It has an alongshore dimension of approximately 150 km (93 mi), see Figure 2.1 for an indication of the extent of the computational grid. The model includes forcing conditions for tides, river discharges, waves and wind. The MCC-model predicts waves, tide, wind and (breaking) wave driving currents and the associated initial sediment transports (i.e. no bed updating) based on the post-Katrina bathymetry and topography provided by USACE. For details on the bathymetry data reference is made to Section 3.3.

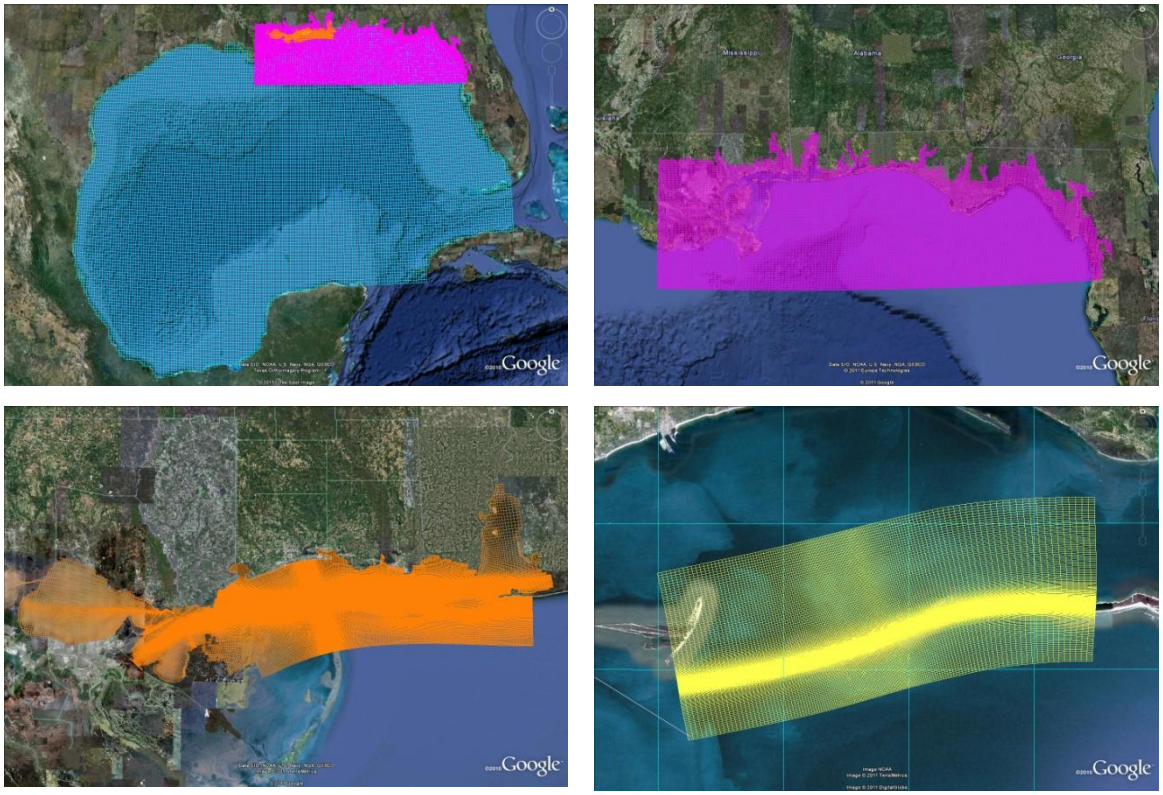

Figure 2.1 Overview of model grids used in the hurricane model train, sequentially presented from large scale to small scale (top left: Gulf of Mexico grid; top right: Panhandle grid; bottom left: Mississippi Coastal Cell grid; bottom right: Ship Island grid)

The MCC-model is used to derive the overall sediment budget for the MCC-area which is primarily based on initial transport predictions for average and hurricane conditions. Morphodynamic simulations are performed for Ship Island and its surroundings using a smaller model (see next section) for which the MCC-model provides the boundary conditions.

The hydrodynamic calibration and validation of the MCC-model were performed using measured water levels, currents and waves and model predictions of these parameters provided by USACE. These data are described in Chapter 3. The construction, calibration and validation of the hydrodynamic MCC-model are described in Chapter 4. In Chapter 5 the wave model is discussed.

2.3.4 Ship Island model (Delft3D SPI-model)

For the area around Ship Island, a detailed 2D morphological model was set up, and is nested in the MCC-model. The alongshore extent of the detailed model is about 30 km (19 mi) to include the inlets enclosing East and West Ship Island (see Figure 2.1). The grid resolution in the vicinity of the island is about 10x10 m to incorporate the surf zone dynamics and the associated sediment transports. The model includes all relevant hydrodynamic processes and has identical settings as the MCC-model to ensure consistency. The SPI-model is used to predict waves, tide, wind and (breaking) wave driving currents; the associated sediment transports; and the morphological development over 4 years. The SPI model is used to investigate the morphodynamic development of the restored Ship Island relative to the present situation (i.e. post-Katrina without restoration). Different configurations, as described in Section 2.4, were studied to assess the effects of the nourishments and borrow areas on the morphological development of Ship Island. The morphological development for averaged conditions was evaluated after 2 and 4 years.

As the SPI-model is a cut-out from the MCC-model and uses the same model settings, no further calibration and validation of this model is performed.

2.3.5 Ship Island model (XBeach SPI-model)

An XBeach model is used to determine the morphological development of Ship Island due to hurricane impact. The model covers the same domain as the Delft3D SPI-model (Figure 2.1) but has a higher resolution in the cross-shore to account for the detailed hydrodynamic and transport processes on the island. The resolution in cross-shore direction gradually decreases from 5 m on and around Ship Island to 30 m at the distal model boundaries. The longshore resolution is 20 m at Ship Island and decreases to 75 m at the lateral model boundaries.

XBeach is a different model to Delft3D and it contains more detailed descriptions of the hydrodynamic processes relevant for the nearshore processes during hurricane conditions. In contrast, the transport formulations are parameterized and less advanced than in Delft3D. Therefore a limited validation of the XBeach model using hurricane Katrina is presented (i.e. the model is applied with default settings without a calibration) prior to its application to evaluate the restored Ship Island.

2.3.6 Modeling Strategy

The coupling and interaction between the four models and the relevant processes are highlighted in Figure 2.2. The two largest models (GoM-model and PAN-model) provide the boundary conditions (tidal and/or hurricane induced) for the smaller models. The MCC-model is used to evaluate the contributions of the average wave climate and the hurricanes to the overall sediment budget. Furthermore, the MCC-model is used to drive both the Delft3D- and XBeach-based SPI-models. These are used to predict the morphological development for the averaged and hurricane conditions, respectively.

.

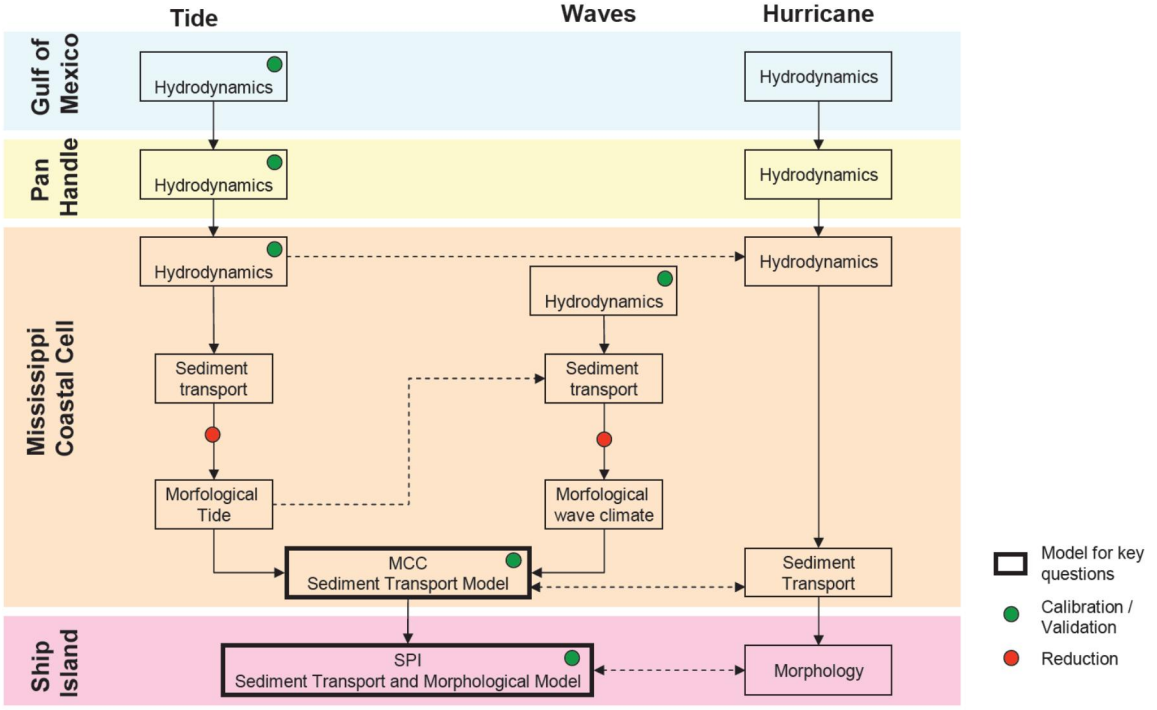

Figure 2.2 Illustration of Modeling Strategy

2.4 Definition of Cases

2.4.1 Introduction

The impact of the restoration design is primarily addressed by evaluating the predicted sediment transports and morphodynamic development relative to a baseline case. To separate the impact of the different elements of the restoration (e.g. sand placements and borrow areas), a number of cases have been defined in which several combinations of the restoration elements are considered. For all sand placements we assume identical sediment characteristics as naturally occurring at Ship Island (D_{50} = 0.30 mm, D_{10} = 0.225 mm, D_{90} = 0.750 mm). The following elements of the Ship Island restoration were provided by USACE:

- Camille Cut closure: Sand placement between East and West Ship Island up to a height of 2.14 m (7 ft) above NAVD.
- North sand placement on West Ship Island: Sediment placement of about 600,000 cy (about 500,000 m^3) along the northern shore of West Ship Island, see Figure 2.4 (area between 'sand placement limits'). The fill was placed at an elevation of 1.7 m (5.5 ft) above NAVD. The sand for this nourishment has been borrowed from the Ship Island Pass borrow area.
- South-east sand placement on East Ship Island: Sand placement at the south-eastern shore of East Ship Island.
- Ship Island Pass borrow source: Borrow area is located west of West Ship Island (Figure 2.4). It is approximately 250 m (820 ft) wide and 700 m (2300 ft) long with an average depth of about -10 m NAVD.
- Ship Island borrow area: The borrow area is located between 1.6 and 2.4 km (1 and 1.5 mi) south of Ship Island in ambient water depths of approximately 10 m (33 ft). The borrow area is approximately 180 m (590 ft) wide (north-south direction) and

1800 m (5900_ft) long (east-west direction) with an average cut depth of approximately 2.5 m (8 ft).

The total volume of the sand placements is about 17 Mm^3 (22 Mcy) Approximately 0.8 Mm^3 (1 Mcy) is anticipated to come from the offshore Ship Island Borrow. Other sources of material are being considered by the USACE for the remaining part.

2.4.2 Cases

In the this section, the considered cases are described.
The post-Katrina bathymetry and topography (see Section 3.3) are the basis of the models applied in the present study. The widened Gulf Port Channel and the North sand placement at West Ship Island are included in all cases. Two base line scenarios are used in which the Ship Island Borrow source is included and excluded. The restoration cases include the Camille Cut closure, but the borrow areas are separately considered. The baseline and restoration cases are:

1a Baseline 1a, using Post Katrina topography and bathymetry, including widening of the Gulf Port navigation channel and sediment placement at the northern side of Ship Island (see Figure 2.4).

1b Baseline 1b, as in baseline 1a, with presence of the borrow source in Ship Island Pass [1](see Figure 2.4), as a reference for Case 2b

2a Closing of Camille Cut and nearshore sand placement at the southeastern shore of Ship Island, for the situation with (Case 2a-1) and without presence of Ship Island borrow area (Case 2a-2)

2b Closing of Camille Cut and nearshore sand placement at the southeastern shore of Ship Island, for the situation with presence of the borrow source in Ship Island Pass.

Case	Camille Cut closure	SE sand placement	Offshore borrow area	Ship Isl. Pass borrow area
1a	no	no	no	no
1b	no	no	no	yes
2a	yes	yes	no + yes	no
2b	yes	yes	no	yes

Table 2.1 Summary of baselines and restoration designs to be studied

Case 1a: Baseline <u>without</u> Ship Island Pass borrow area

The baseline situation is the reference against which design 2a will be compared to assess the relative effect of the planned closure of Camille Cut, the borrow areas and sand placement along the southeastern shore of Ship Island (see Figure 2.3).

1. *Material taken from Ship Island Pass is currently being and historically on a few occasions been placed along the north shore of West Ship Island in the vicinity of Fort Mass.*

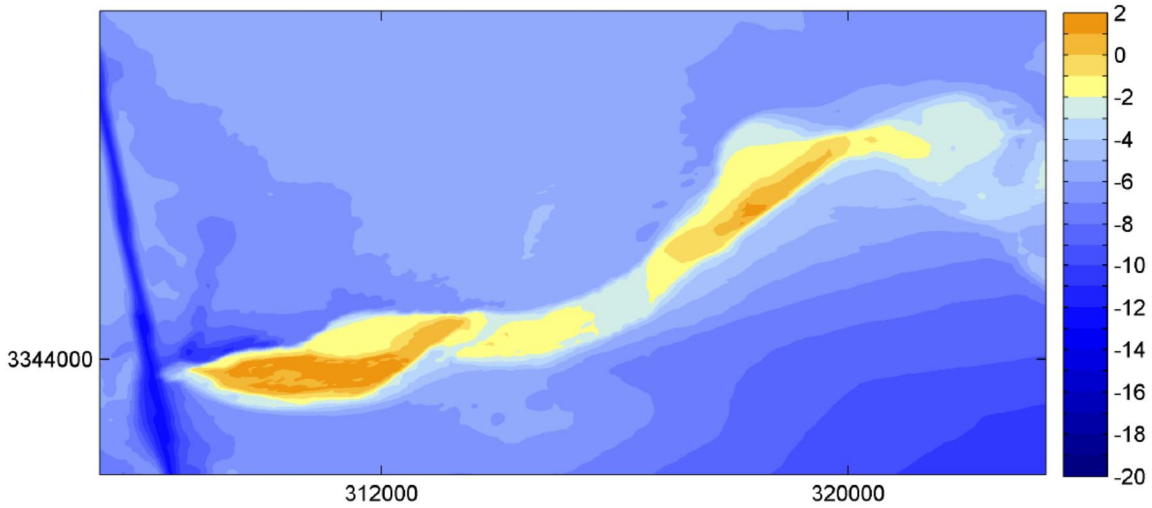

Figure 2.3 Baseline situation (model bathymetry), levels in m with respect to MSL

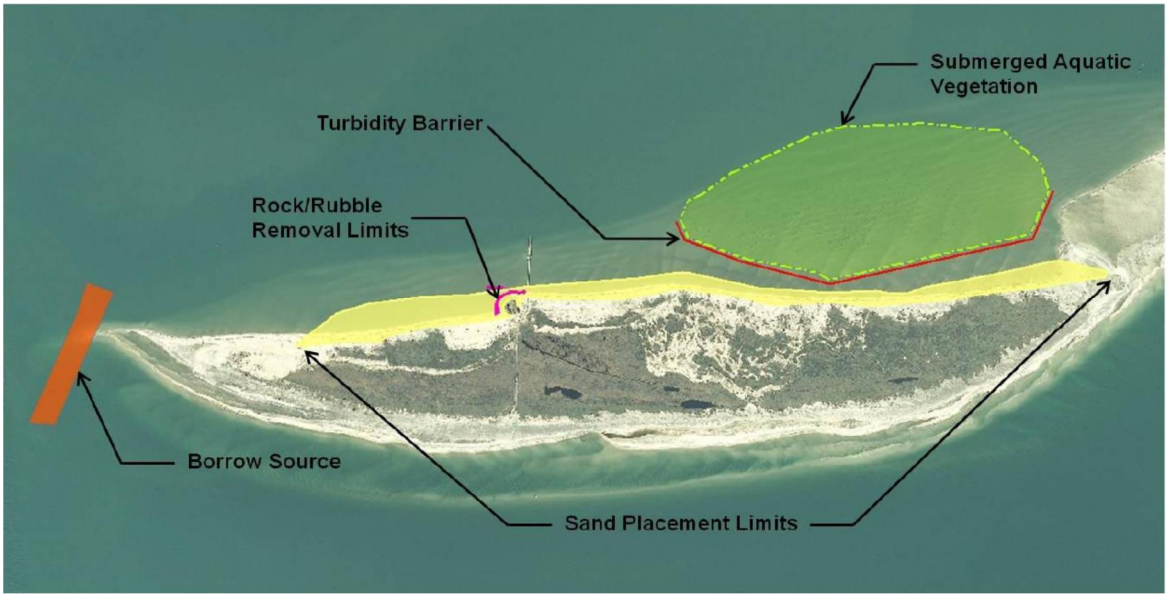

Figure 2.4 West Ship Island, Sketches of northern sand placement and Ship Island Pass 'Borrow Source' (source: USACE -ASBPA presentation)

Case 1b: Baseline <u>with</u> Ship Island Pass borrow area

Due to its relatively small size the Ship Island Pass borrow source is expected to backfill quickly. Therefore, it was decided to consider an additional baseline case. The additional baseline case is, besides the borrow source in Ship Island Pass, identical to Case 1a. Figure 2.5 shows a detail of the model bathymetry with the borrow source located just west of Ship Island.

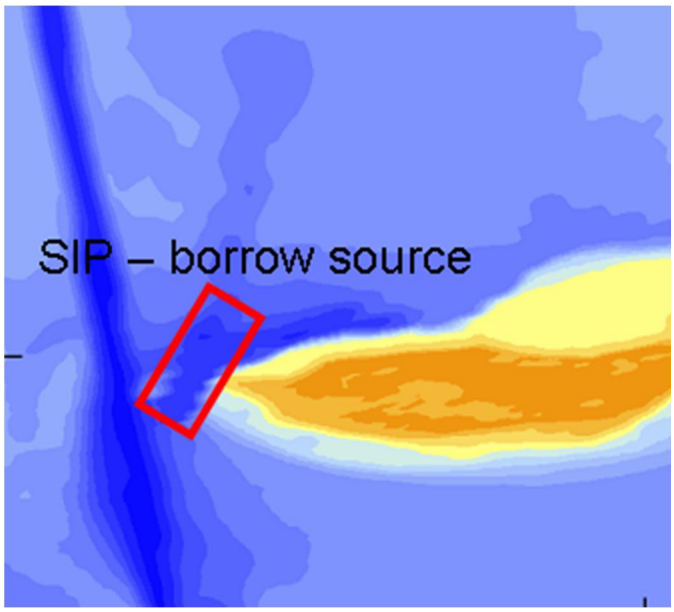

Figure 2.5 Ship Island Pass (SIP) borrow source in the model bathymetry

Case 2a: Closure of Camille Cut, South-east sand placement Ship Island, without the Ship Island Pass borrow area

In Case 2a Camille Cut is closed and the South-east sand placement is implemented (both according to the closure design provided by USACE, see Figure 2.6). The design template for Camille Cut consists of an approximate 700 foot wide equilibrated island crest width of elevation +7 feet (NAVD88). The fill slope from the island crest to the mean high water line is approximately 1-foot vertical and 50-foot horizontal (1V:50H) along the Gulf of Mexico side. On the Mississippi Sound side the slope for the island crest to the mean high water line is approximately 1V:15H.

For Case 2a, the effect of the offshore Ship Island borrow area on the erosion and deposition on Ship Island will be investigated by running the model with and without the offshore borrow area (defined as Cases 2a-1 and 2a-2, respectively). The location of the Ship Island borrow area is indicated in Figure 2.6.

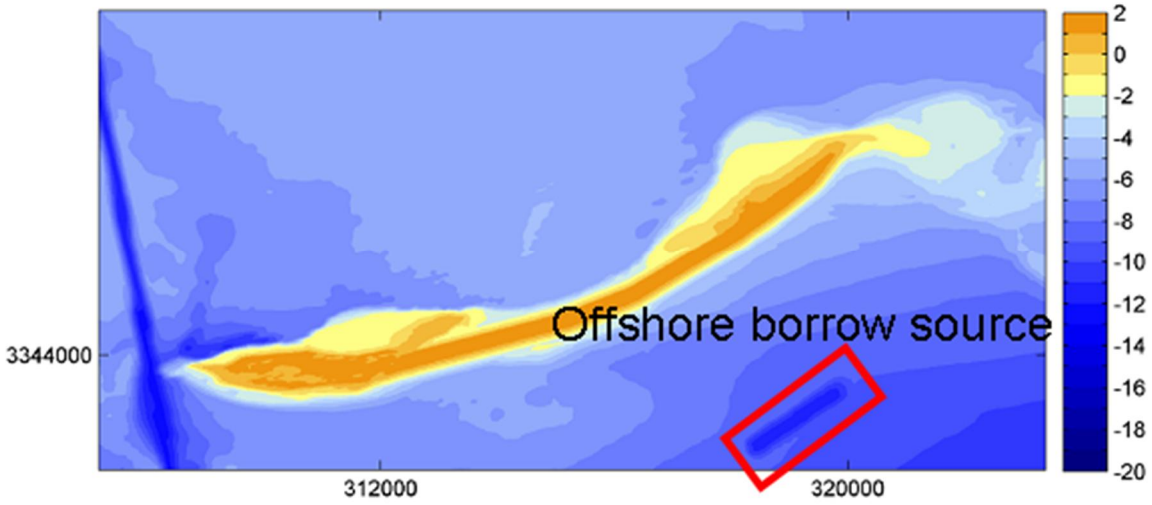

Figure 2.6 Camille Cut Closure, sand placement at southeastern shore and Ship Island borrow area (model bathymetry with offshore borrow area in place)

Case 2b: Closure of Camille Cut, South-east sand placement Ship Island and with the Ship Island Pass borrow area.

The difference between Case 2b and Case 2a is that in Case 2b the Ship Island borrow area is included in the bathymetry (see Figure 2.5). For the assessment of the impact of the planned activities the results of this run will be compared with the baseline run Case 1b.

3 Environmental conditions

3.1 Introduction

In this chapter the data that formed the basis for the model input or model verification/calibration are described. For a description of how these data were used as model input, reference is made to Chapters 4 to 8, in which the setup of the models is described.

3.2 General description of project area

The littoral system relevant for the barrier island dynamics consists (from East to West) of Fort Morgan Peninsula (located just east of Mobile Pass), Dauphin Island, Petit Bois Island, Horn Island, Ship Island, and Cat Island. The barrier islands are low and vegetated. They form the offshore boundary of the Mississippi Sound.

The net sand transport along the Gulf coast of the barrier islands is westward directed. The islands are composed of beach sand provided by the updrift beaches east of Mobile Pass and from the ebb-tidal shoals at the entrance.

Ship Island was temporarily breached into two islands in 1947, had naturally recovered by 1950, but then was permanently breached by Hurricane Camille in 1969. In 2005, East and West Ship Island nearly had reconnected, but hurricane Katrina separated both islands again. Presently, the islands appear to be evolving independently, with West Ship Island having higher dunes than East Ship Island (see Byrnes et al. (2011)).

Dauphin Island breached in 1917 in response to a 1915 hurricane, and reformed in 1957. In 2005 the island breached again as a result of hurricane Katrina.

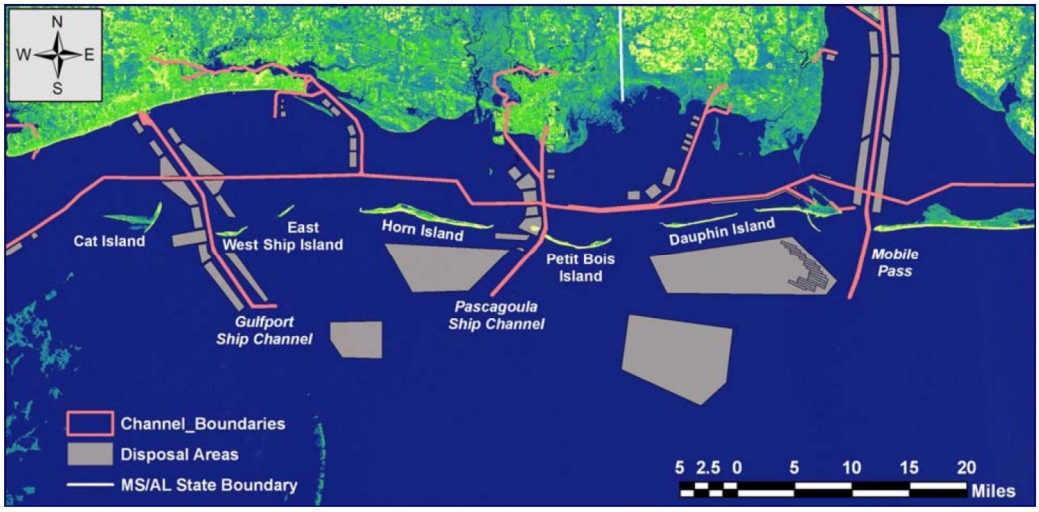

Figure 3.1 Islands and channels in the study area (source: Byrnes et al. (2011))

Tidal passes with ebb-tidal shoals interrupt the littoral system, see Figure 3.2. Several navigation channels run through the passes, including: Mobile Pass Channel, Pascagoula Ship Channel and Gulfport Ship Channel. The Gulf Infracoastal Waterway (GIWW) runs more or less parallel to the islands in the Mississippi Sound. The channels serve the ports of Mobile, Pascagoula, Biloxi and Gulfport.

Dredging of the navigation channels was initiated in 1897, and in the course of time the channel dimensions have been increased. Since September 1993 the depth of Pascagoula Bar channel (through Horn Island Pass) is kept at 44 ft (13.4 m) below NAVD. The channel width is 450 ft (137 m) [2]. Since September 1991 Gulfport Bar channel is kept at a depth of 38 ft (11.6 m) below NAVD and a width of 300 ft (90 m). In 2011 this channel has been widened to about 300-400 ft. Natural water depths in the passes are 10 to 20 ft (3 to 6 m) below NAVD, except for Ship Island Pass where a relatively deep natural channel always has been present (see Figure 3.19, lower box).

Regular maintenance dredging is carried out in the navigation channels. Maintenance dredging graphs for the channel sections in the passes, presented by Byrnes et al. (2011), indicate average dredging volumes over the last decade of about 360,000 cy/yr for Horn Island Pass and about 210,000 cy/yr for Ship Island Pass.

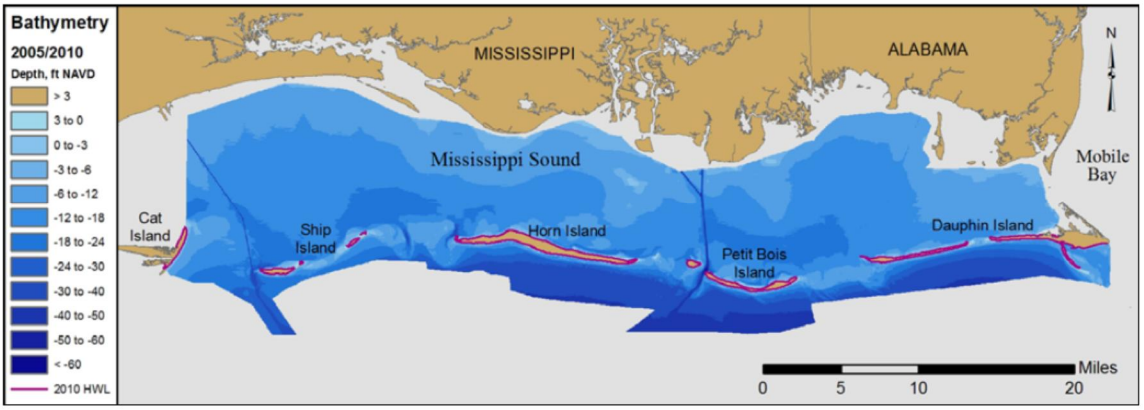

Figure 3.2 Bathymetry 2005/2010 (source: Byrnes et al. (2011))

2. *Authorized to 550 ft but currently constructed only to 450 ft*

3.3 Bathymetry

An overview of the data available for the schematization model bathymetry is presented in Table 3.1.

Name (source)	Coordinate System	Vertical projection	Date	Coverage	Resolution
USGS 2008 – 2009 (USACE)	NAD 83 UTM zone 16N	NAVD 88 (orthometric height (GEOID03))	June 2008 & June 2009	West Ship Island to Dauphin Island, from shoreline to 2km offshore	50m (gridded)
ADCIRC Model bathymetry (USACE)	WGS84 (latitude/longitude)	NAVD 88 (orthometric height (GEOID03))	Patch of many sources	Mississippi Bay	Min. 100m – Max 1500m (gridded)
Byrnes *et al* Sediment budget bathymetry (USACE)	WGS84 (latitude/longitude)	NAVD 88 (orthometric height (GEOID03))	Patch of many sources	West Mississippi Bay	25m (gridded)
USGS Lidar (USACE)	NAD 83 UTM zone 16N	NAVD 88 (orthometric height (GEOID03))	September 2005 (processed in 2007)	Merged parts of Mississippi barrier islands	5m (gridded)
Katrina Cut (USACE)	Alabama State Plane NAD83 West	MLLW in feet (based on NAVD88 epoch 01)	April 2010	'Katrina Cut'	100m longshore; 1m cross-shore
GEBCO (database, GEBCO website)	WGS84 (latitude/longitude)	NAVD 88 (orthometric height (GEOID03))	Patch of many sources	Global	30-arc second (gridded)
Digital Elevation Map (database, NOAA website)	WGS84 (latitude/longitude)	MHW (meters)	Patch of many sources	Global	1/3 arc second (gridded)

Table 3.1 Overview of the metadata of the bathymetrical datasets

3.4 Water levels and currents

Time series of measured water levels were downloaded from the NOAA website (tidesandcurrents.noaa.gov) for a total of 7 tidal stations in the Mississippi Sound region. Time series of computed water levels with the ADCIRC model were provided by USACE at a total of 18 stations. Also, sets of harmonic constituents for a total of 10 stations in the region were collected, which are applied for both the calibration of the PAN and the MCC-model. Sources of the harmonic constituent sets were the NOAA website, the XTide database and the IHO database. The reference time of the collected sets were all adjusted to GMT. The locations of the different water level stations are shown in Figure 3.3.

The calibration of the tidal model in this study was mainly performed on the basis of the harmonic constituents sets so that the wind and air pressure effects and potential measuring

errors are excluded from the observed water level times series. The NOAA and ADCIRC time series and Acoustic Doppler Current Profiler (ADCP) current measurements were used for model validation.

In addition, ADCP current measurements were available for selected transects as provided by USACE (ERDC, 2010). The current profiles were measured using a vessel-mounted ADCP at a total of six transects between the barrier islands Ship Island Pass, Camille Cut, Dog Keys Passes, Petit Bois Pass, Katrina Cut and Pass Aux Herons, as indicated in Figure 3.4.

For a consistent comparison with the predicted (depth-averaged) velocities, the measured ADCP velocity measurements need to be averaged over the water column. A review using in-house analysis software revealed a large degree of noise in the data (both in magnitude and direction), in particular in shallow water depths. This is illustrated in Figure 3.5 where two consecutive current profiles (6 seconds apart) are presented. As a complete analysis was beyond the scope and a quick scan of depth-averaged values seemed to cancel out a considerable part of the noise, time-series of depth-averaged currents were derived by averaging the measured unfiltered current profiles over all bins for each measured time-step.

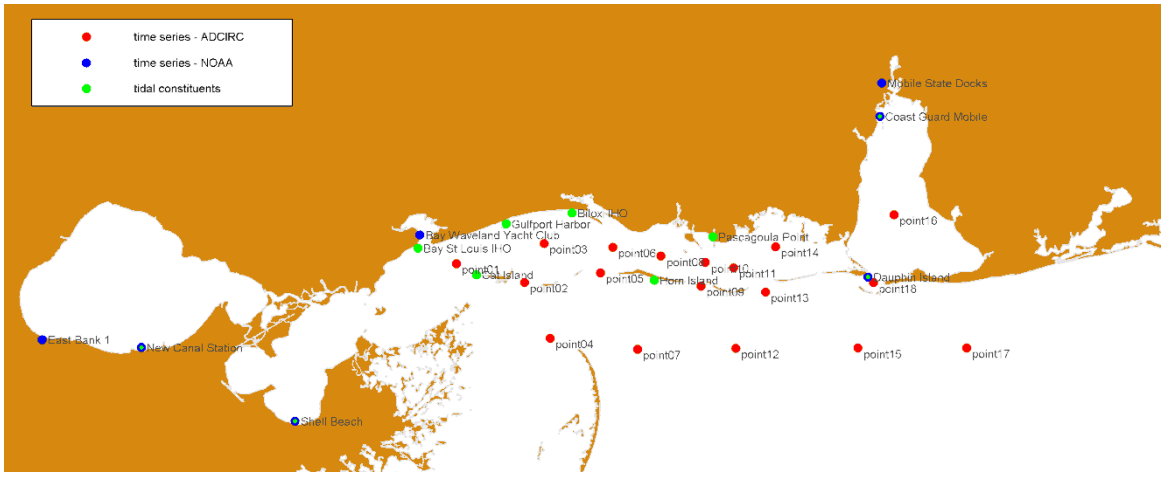

Figure 3.3 Location of water level stations.

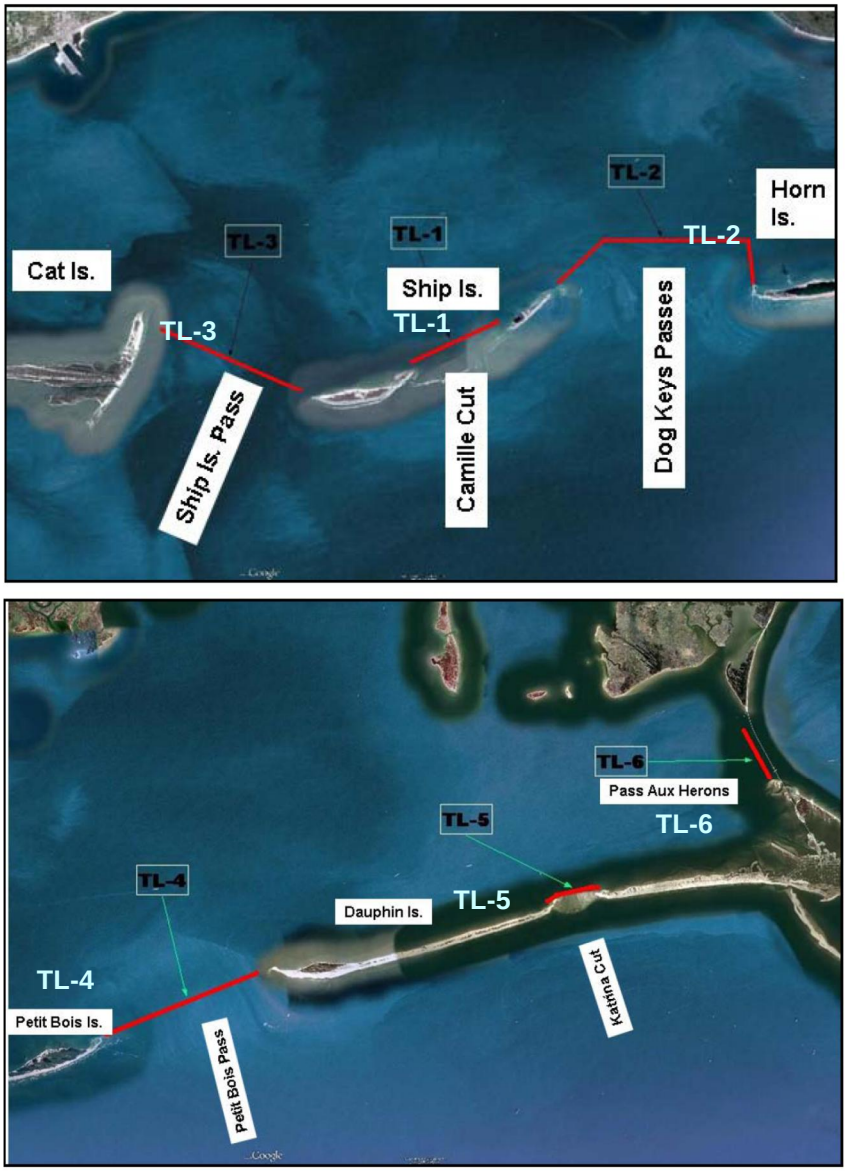

Figure 3.4 Location of ADCP transects (ERDC, 2010).

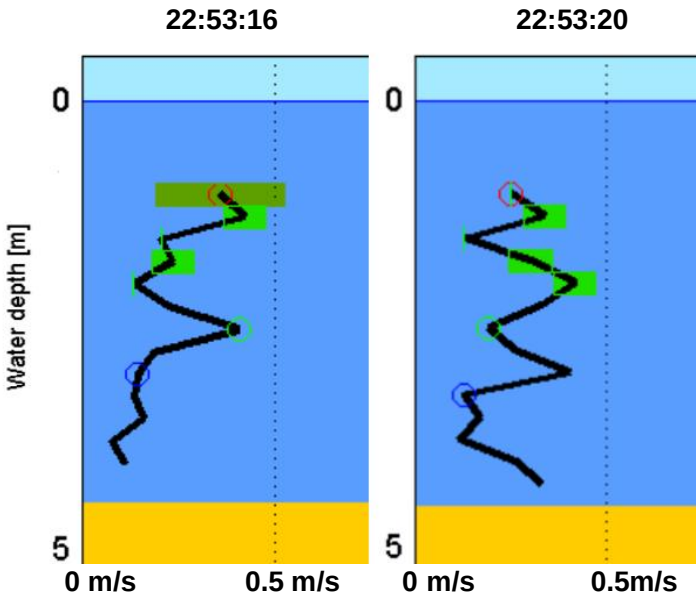

Figure 3.5 Vertical profiles of ADCP measurements at transect TL5.

3.5 Wind and waves

3.5.1 Introduction

The following data sources are available and were investigated for the wave modeling study:

- NDBC measured wave and wind data, available online at http://www.ndbc.noaa.gov/
- WIS hindcasted wave and wind data, available online at http://frf.usace.army.mil/wis2010/hindcasts.shtml?dmn=gom
- ERA-Interim reanalysis wave and wind data (http://www.ecmwf.int/research/era/do/get/era-interim), available online at http://data-portal.ecmwf.int/data/d/interim_daily/ (1.5 degrees resolution, research only). In a later stage of the project these data have been purchased from ECMWF at a higher resolution (0.75 degrees), reference is made to Chapter 5.
- NCEP/NCAR reanalysis wind data, available online at http://www.cpc.ncep.noaa.gov/products/wesley/reanalysis.html

The different data sources are discussed below.

3.5.2 NDBC data

The National Data Buoy Center (NDBC) data provides measured wind and wave data, available from the NOAA website. Many measurement stations in the vicinity of the project area are available. However, as indicated in Deltares (2011b) the number of years for which data are available is limited. Furthermore, the data contain a lot of gaps (missing data, no measurements). To derive a reliable mean wave and wind climate, at least 5 years of continuous wave and wind data should be available simultaneously at different data points. As the NDBC data does not fulfill these criteria, the data cannot be used as sole data source for the mean wave climate study.

Note that the NDBC data are considered of high-quality and are used for calibration and validation of the offshore data and modeling results. For these actions, NDBC Station 42040 and 42007 are used, see Figure 3.6.

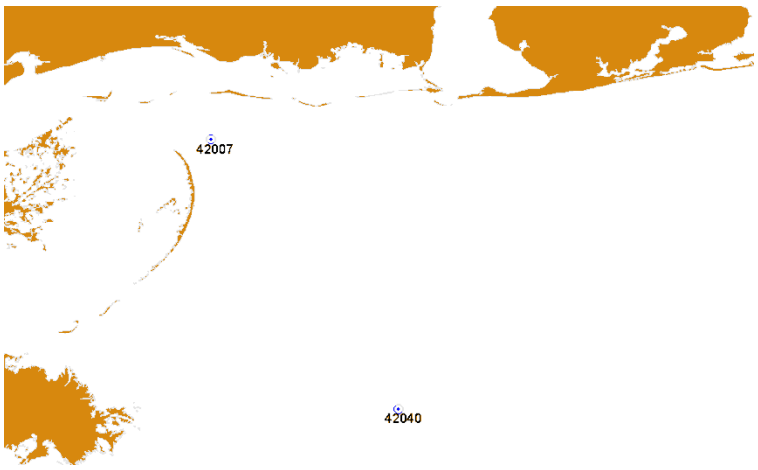

Figure 3.6 NDBC Wave buoys used for data and model validation and calibration

3.5.3 WIS data

The Wave Information Studies (WIS) data contains hindcasted wave and wind information, uninterrupted, with an hourly resolution for the period 1980 to 1999. Comparison of the data with measurements (NDBC-data) showed an underestimation of the higher peak periods. This is illustrated in Figure 3.7 in which the frequency tables for two stations at approximately the same location are presented. In the NDBC dataset (station 42007) approximately 35% of the wave conditions contain a higher peak period than 5.5 seconds. In the WIS data set (station 73143) this is only 10% of the data. The underestimation of wave peak periods will have an impact on the computed sediment transports by waves. Therefore, the WIS data was not used to determine the offshore wave and wind scenarios (the wave model wind forcing and boundary wave conditions).

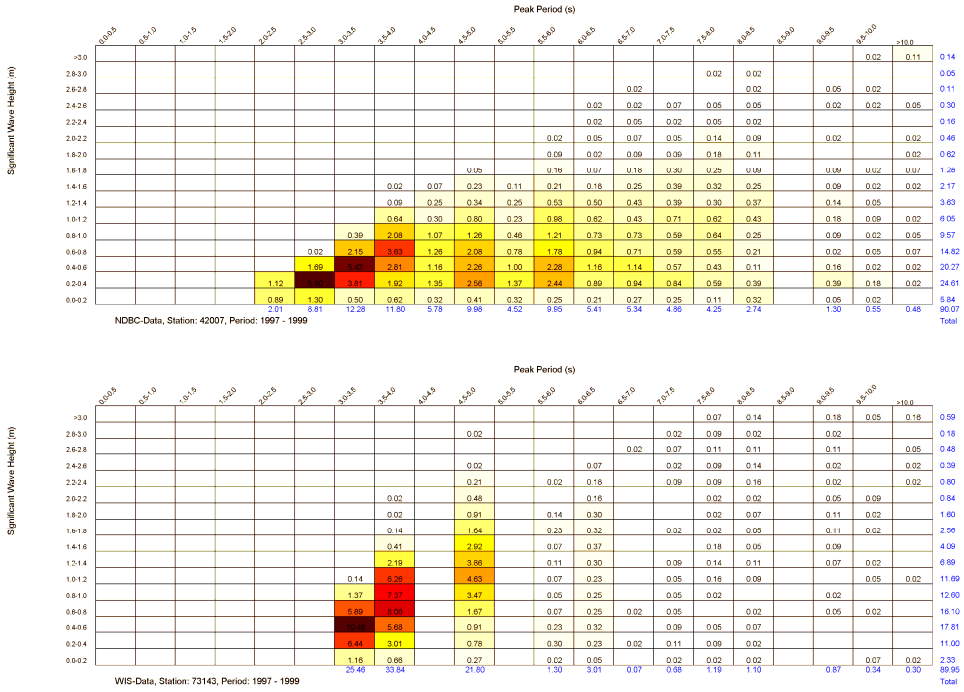

Figure 3.7 Frequency tables of wave height versus peak period for NDBC measurement station 42007 (upper) and WIS station 73143 (lower).

3.5.4 ERA Interim data

The European Center for Medium-Range Weather Forecasts (ECMWF) has carried out several reanalysis of wind and wave information, which are called the European Reanalysis (ERA). The most recent of those, the ERA-interim reanalysis, provides data with a spatial resolution of about 1ºx1º and covers the period 1989 – 2010. The wave model used in the reanalysis is the third generation WAM model, which is coupled with an atmospheric model. The quality of the ERA-interim data is considered to be good and is higher than that of the ECMWF operational model for data up to 2005. The ERA-interim wave and wind data were acquired for this project for the period 1989 to 2010, with a spatial resolution of 1ºx1º around the project area (between 270 – 275 degrees East and 28 – 30 degrees North) and a temporal resolution of 6 hrs. The ERA-Interim significant wave height and wind speed roses are presented in Figure 3.8 and Figure 3.9.

For the ERA-Interim data the same comparison with NDBC wave peak periods, as done for the WIS data, was made in order to verify the applicability of the data. This comparison is shown in Figure 3.10. Note that the comparison is based on a more offshore data location than in Figure 3.6 (NDBC station 42040). From Figure 3.10 it can be observed that the higher wave peak periods are present in the ERA-Interim dataset and that the peak periods for the different datasets are distributed in a comparable way.

Following the comparison between ERA-Interim and NDBC wave peak periods, a detailed comparison was made for significant wave height, wind speed and wave direction as well. For this purpose the time resolution of both datasets must be brought as close to each other as possible. For the observed wave conditions (wave height, peak period and mean wave direction), a three hour average is determined (+/- 1.5 hr around the ERA-Interim time point). For wind conditions (wind speed and direction) no averaging is applied. The comparisons between the ERA-Interim and NDBC data are shown in Figure 3.11.

The red dotted line is the symmetric slope line (which estimate is printed on top of the figure) and gives an indication for the deviation of the ERA-Interim data from the NDBC measurements. It can be observed that the significant wave heights of ERA-Interim are approximately 10% lower than those of the NDBC data. On the other hand, the correlation between both datasets is rather high, above 90%. The underestimation of the peak significant wave heights by the ERA data is commonly known and the data will be corrected for this underestimation. The correction is described in Section 5.3. For wave peak periods, wind speed and wind directions, although with some scatter, the ERA-Interim data are found to match the NDBC measurements well. Detailed error statistics for the different parameters are presented in Table 3.2.

For the wave directions, a consistent deviation between the ERA-Interim and the NDBC data can be observed, reflected by the bias of approximately 12º-deg. This may (partly) be caused by the definition of the wave direction in both datasets. The wave direction in the NDBC data is defined as the direction *from which the wave at the dominant peak period is coming*. The ERA-Interim wave directions are mean wave directions based on the 2D wave spectrum. The wave directions of the ERA-Interim data are not corrected for the observed deviation from the measured NDBC wave directions.

Overall, the ERA-Interim data is considered a suitable data source for the wave modeling study.

	Hs (m)	Tp (s)	Dir (°N)	U10 (m/s)	Udir (°N)	Hs corrected (m)
mean ERA-Interim	0.96	5.6	118	5.7	110	1.04
mean NDBC	1.04	5.7	131	5.7	107	1.04
Bias	0.08	0.11	12.50	0.00	-3.61	0.00
RMSE	0.28	1.05	38.64	1.32	28.73	0.24
Scatter Index	27.80	18.58	6.47	23.03	6.05	22.64
Symetric slope	1.12	1.03	1.00	1.00	1.00	1.02
Correlation coefficient	0.92	0.70	0.69	0.90	0.82	0.94

Table 3.2 Error statistics for the ERA-Interim data

3.5.5 NCEP/NCAR reanalysis wind data

The last data source that has been reviewed is the NCEP/NCAR reanalysis data. These data are a result from the NCEP / NCAR reanalysis project carried out by the National Center for Environmental Predication and the National Center for Atmospheric Research. The data is available at location (271.8750, 29.5234) for the period between 1980 and 2010 with a 6-hr time resolution. The NDBC wind measurements and the NCEP/NCAR wind data are compared in Figure 3.12. It can be seen that the *NCEP/NCAR* reanalysis wind data deviates from the measured wind data. The deviation is larger than that of the ERA-Interim wind data and the correlation with the measurements much lower (correlation coefficient is 0.69 instead of 0.90 for the ERA-Interim data). Therefore, the NCEP data are not used further in this study.

3.5.6 Conclusion

From the available datasets described above, the ERA-Interim dataset was found to be the most suitable dataset for the wave climate study.

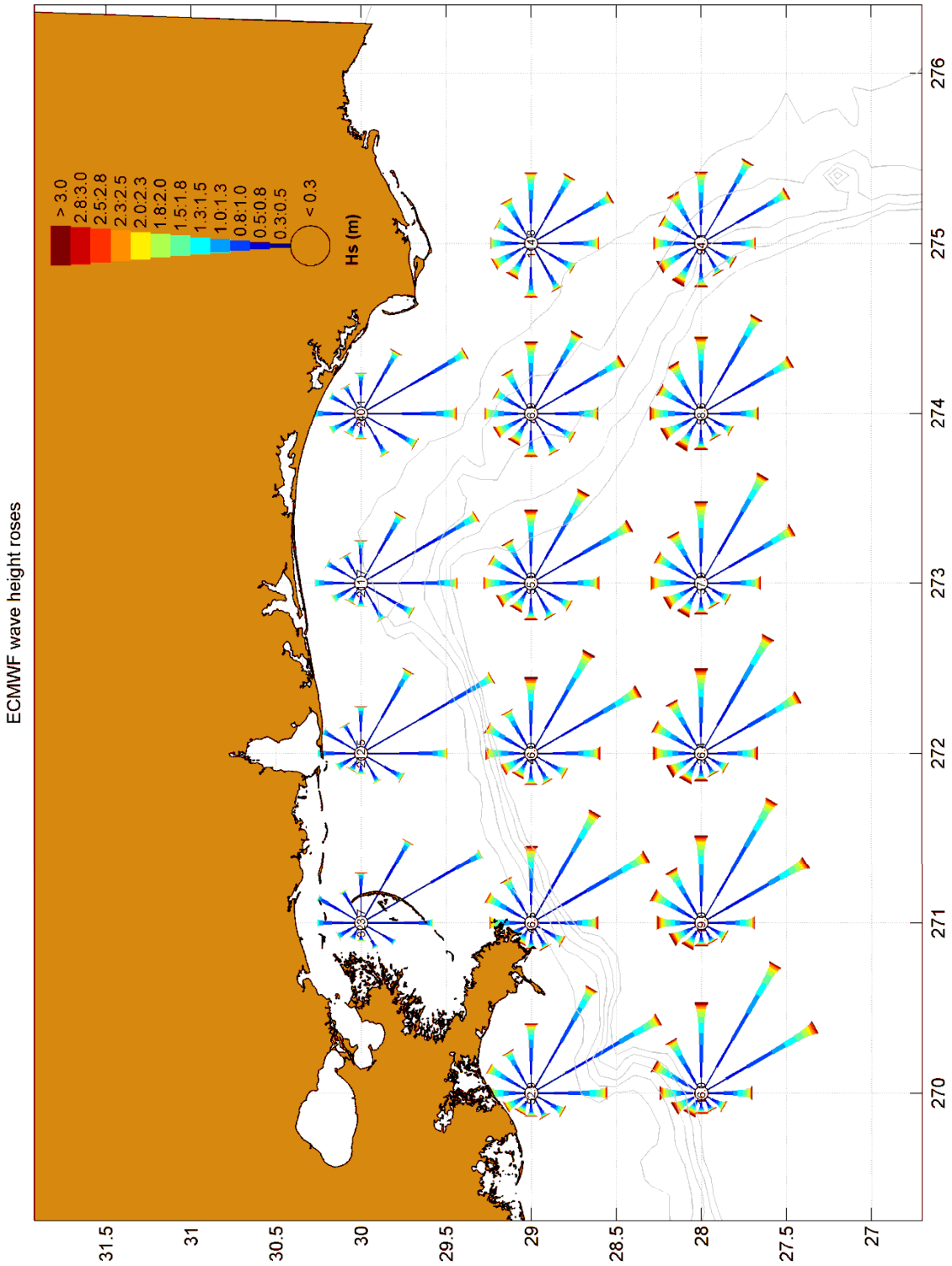

Figure 3.8 ECMWF year-average wave height roses (period 1989-2010).

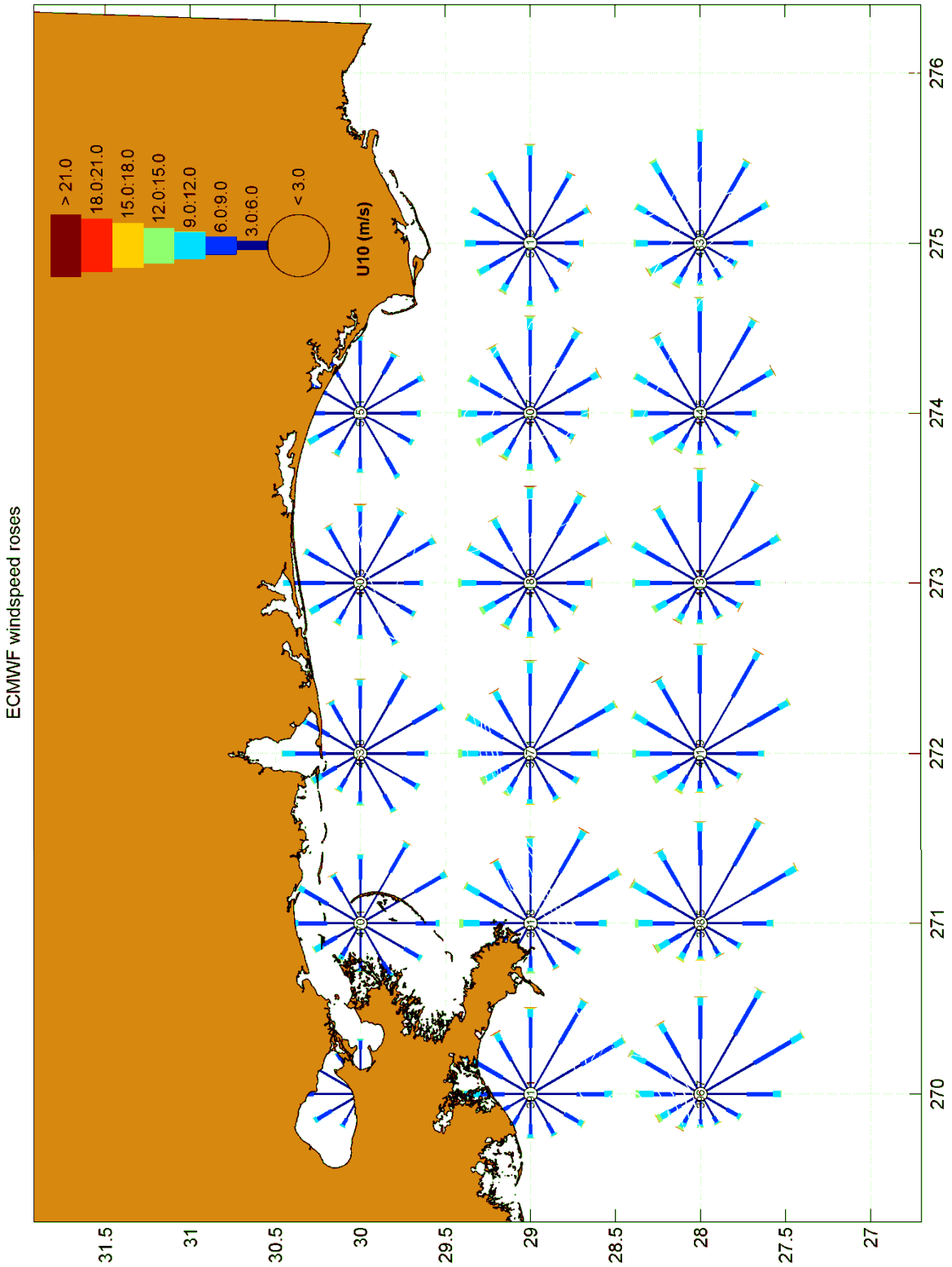

Figure 3.9 ECMWF year-average wind speed roses (period 1989-2010).

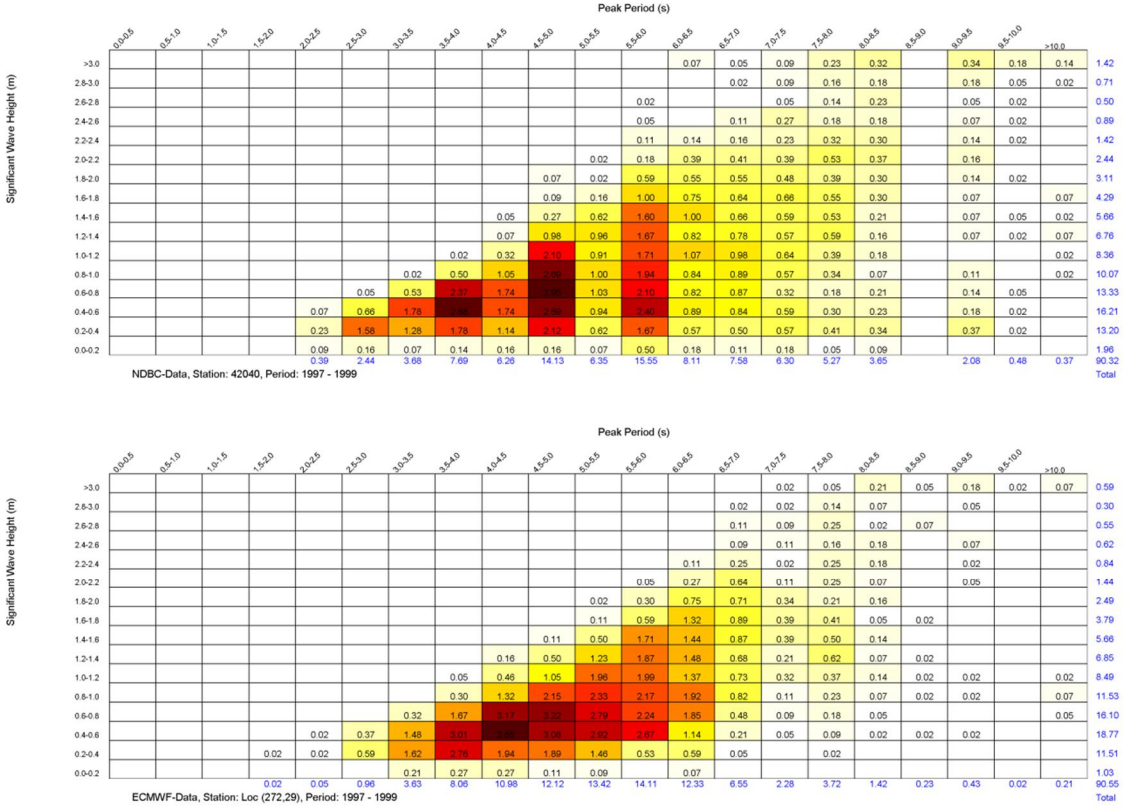

Figure 3.10 Frequency tables of wave height versus peak period for NDBC measurement station 42040 (upper) and ECMWF (lower).

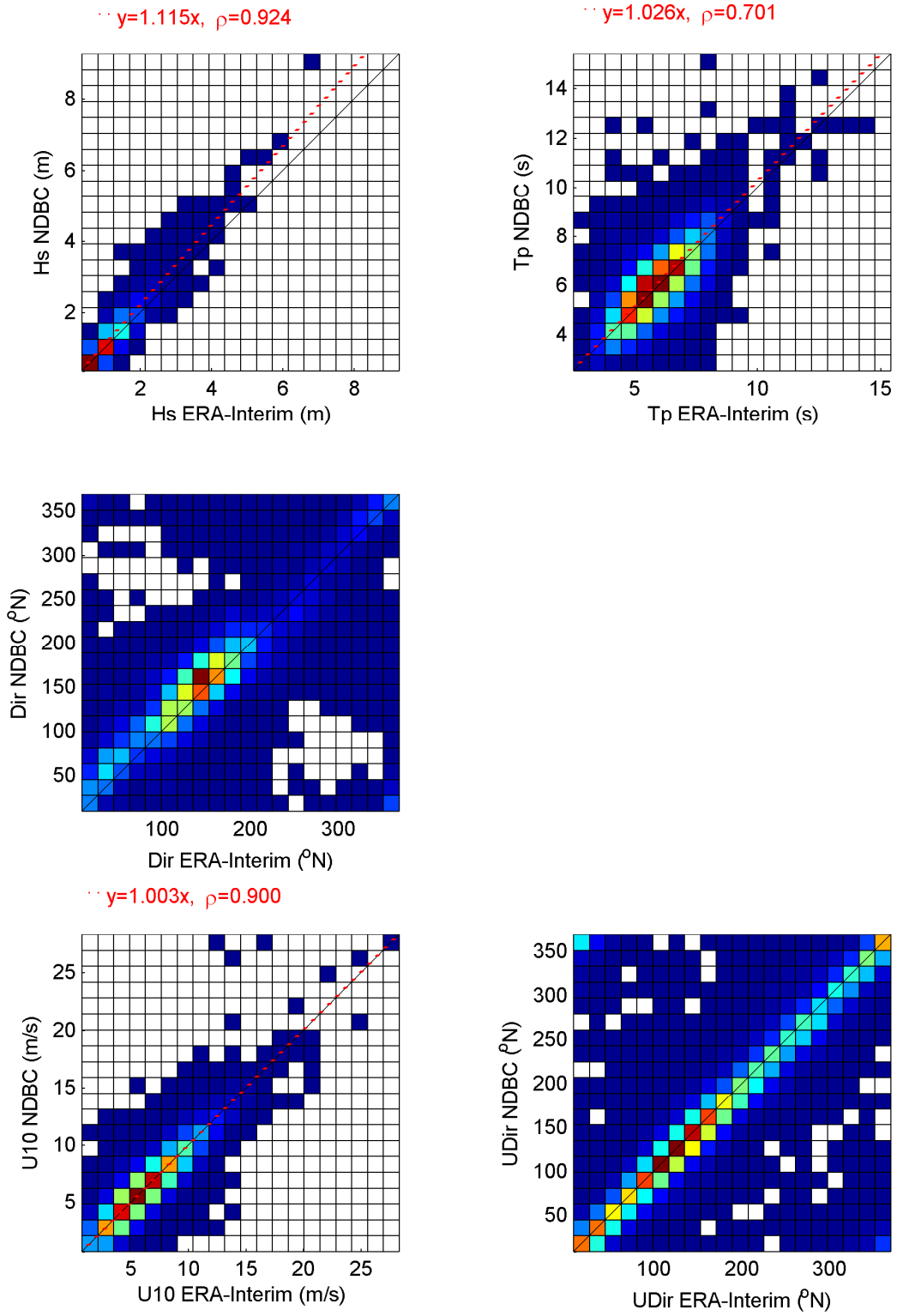

Figure 3.11 Scatter plots of ERA-Interim data at location (272,29) and NDBC data at station 42040.

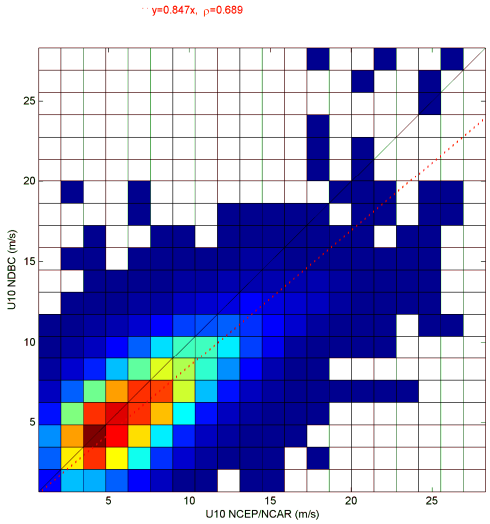

Figure 3.12 Comparison between NCEP/NCAR at location 272, 29 and NDBC wind speeds at station 42040.

3.6 Sediment characteristics

A comprehensive overview of the seabed characteristics in the area is found in USACE (2010). In this report, an investigation and background of the proposed sand borrow areas is presented. The report describes the geologic setting and physiography of the Mississippi barrier islands and presents a compatibility assessment of available sediments for the barrier islands restoration. For this investigation, an overview of grain sizes, gradation of the sand along with the shape of the grains that comprise the islands is given, including a color analysis of the sediment. Generally, the sediment of the barrier islands can be classified as medium, poorly graded sand with a sub-angular to rounded shape.

For two transects along West Ship Island and Horn Island, the distribution of sediment on the islands was analyzed. Figure 3.13 shows the results for the Ship Island transect, showing variation of sediment grain sizes across the islands. The coarsest material (450 µm) is found at the sound side of the island and the finest material (215 µm) in the surf zone. Furthermore, the variation over depth at Ship Island was investigated at three locations, which showed a range in the order of 60µm in the upper 5 feet (1.5 m).

To gain insight into the sediment characteristics of the potential borrow areas, VibraCore samples were collected at several locations around the barrier islands. In the potential borrow area south of Camille Cut and East Ship Island 54 borings were completed to fully define the sand deposits (see Figure 3.14). The average D_{50} grain size was found to be 200 µm and the predominant color was light grey in this borrow site. Other areas where extensive borings were collected and analyzed are offshore of Cat Island, in the Mississippi Sound and in all passes (Ship Island, Dog Keys, Horn Island and Petit Bois).

During the course of the project, the most recent USGS sediment data (June 2011) became available. This extensive data set collected along the nearshore of the barrier islands within the National Park Service Boundaries confirmed the presence of rather coarse material along the barrier island (see Figure 3.15).

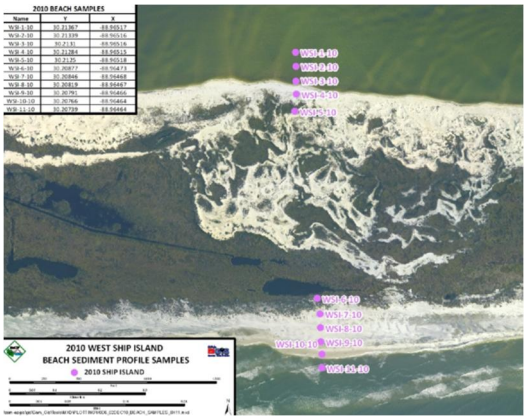

Location	% Pass Mesh #20	% Pass Mesh #40	% Pass Mesh #60	% Pass Mesh #100	% Pass Mesh #200	D50 µm
WSI-1-10	99.8	77.6	17.6	3.9	1	335
WSI-2-10	99.6	70.6	13.1	3.4	1.4	354
WSI-3-10	94.4	45	7.2	0.7	0.6	450
WSI-4-10	99.8	69	7.3	5.5	0.3	364
WSI-5-10	99.9	97.3	53	10.7	0.9	243
WSI-6-10	100	99	47	2.4	0.2	257
WSI-7-10	100	95	39.4	5.6	2.7	276
WSI-8-10	99.8	84.8	32.3	5.4	1.7	298
WSI-9-10	100	95.8	27.8	7.6	1.3	299
WSI-10-10	99.8	70.2	8.9	5.8	0.5	360
WSI-11-10	99.6	95.5	68.7	5.3	1.1	215

Figure 3.13 Location of sampling locations for West Ship Island beach transect and sieve passing and D50 values. From USACE, 2010.

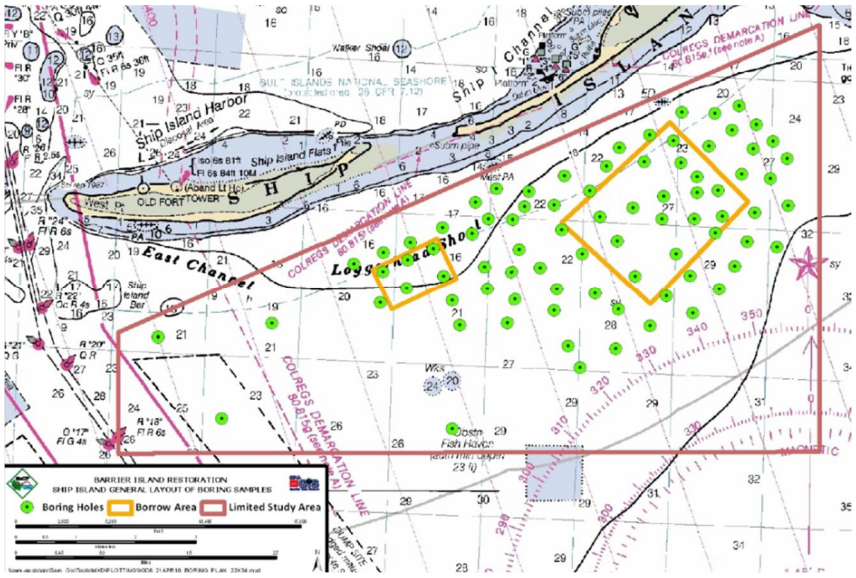

Figure 3.14 General layout of the borings completed for the investigation for borrow material from Ship Island borrow area. From USACE, 2010.

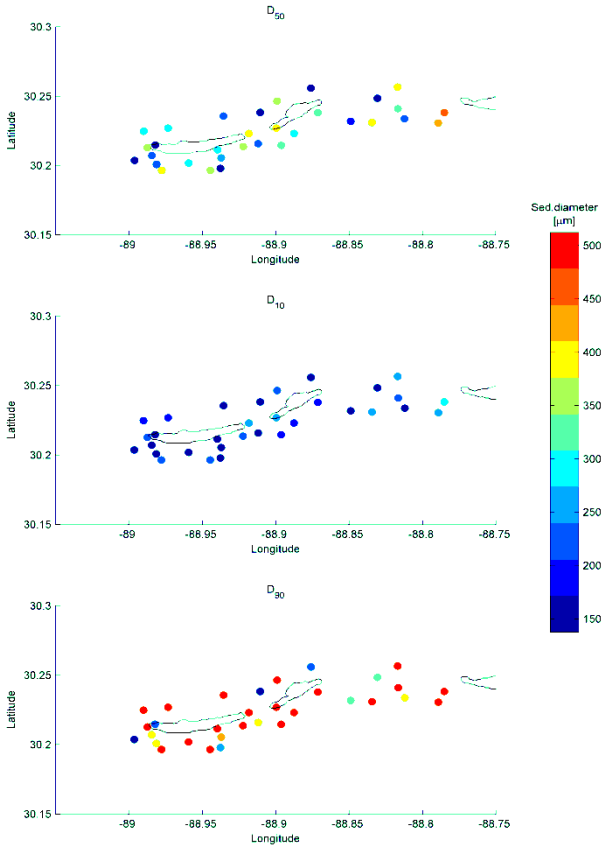

Figure 3.15 D50, D10 and D90 values around Ship Island. From USGS, 2011.

3.7 River discharges

From USGS Stream Flow Annual Reports, yearly average river discharges over the period 1971 – 2010 are available for most rivers in the Mississippi sound area. These are presented in Table 3.3.

No annual reports were provided for the Jordan River and the West-Pascagoula River. Average discharges were therefore estimated from the ADCIRC model input provided by the USACE. This data covers the period March 11th 1998 to September 30th 1998. The data excludes the winter period, so no yearly average values could be derived directly from the data.

Based on a comparison of the USGS data of the available rivers to the model input, it was concluded that the average taken over the first 35 days of the ADCIRC time series can be considered as representative for yearly average values. Estimations of the year-average river discharges for the Jordan River and West-Pascagoula River are also presented in Table 3.3.

River	Discharge (m^3/s)
Pearl River	282
Jordan River	23*
Wolf River	17
Biloxi River	6
West Pascagoula River	368*
East Pascagoula River	246
Escatawpa River	32
Alabama River	888
Tombigbee River	677

Table 3.3 Year-average river discharges based on USGS stream flow reports or estimated from Adcirc model input (*)

3.8 Hurricanes

In order to derive a sediment budget that is consistent with the budget study of Byrnes et al. (2011) the same period from 1917 to 2010 is also considered for the hurricanes. According to the NOAA hurricane database (http://www.csc.noaa.gov/hurricanes/#) 1423 hurricanes and tropical storms have occurred in this period. The North Atlantic hurricane database (HURDAT) contains data for all tropical cyclones in the Atlantic Ocean, Gulf of Mexico and Caribbean Sea, since 1851. This dataset was used to derive hurricane wind fields, which were imposed to Delft3D to simulate the hydrodynamic response.

The category 4 and 5 hurricanes that have occurred in the Gulf of Mexico and the hurricanes and tropical storms with wind speeds exceeding 39 mph which made landfall within 500 km of Ship Island are considered. This reduces the number of hurricanes to 208 (see Figure 3.16). The selected hurricanes are listed in Appendix A.

Selected hurricanes are evaluated in Delft3D, in which a hurricane module is available that generates space and time varying wind and pressure fields that are imposed as forcing conditions on the hydrodynamic and wave modules (Deltares, 2011c). The adopted method is a somewhat improved version of the Holland (1980) approach. Main advantage of this method is that it only requires the specification of a limited number of input parameters which are mostly available for all the historic hurricanes in HURDAT (see Chapter 6 for more details).

The following five parameters are required for each hurricane:

- the location of the cyclone centre,
- the radius of maximum wind,
- the maximum wind speed,
- the central pressure and
- the current motion vector of the vortex.

The radius of maximum wind speed is not available in HURDAT and for the older hurricanes the central pressure is usually absent. In the present study the radius of maximum wind speed was determined based on Hsu and Yan (1999), which describe the radius of maximum windspeed (and the standard deviation herein) for 59 hurricanes as a function of hurricane category (which is directly related to maximum wind speed). For the older hurricanes the central pressure was also determined from the maximum wind speed as described in Deltares, 2011c; Eq. 6.1.

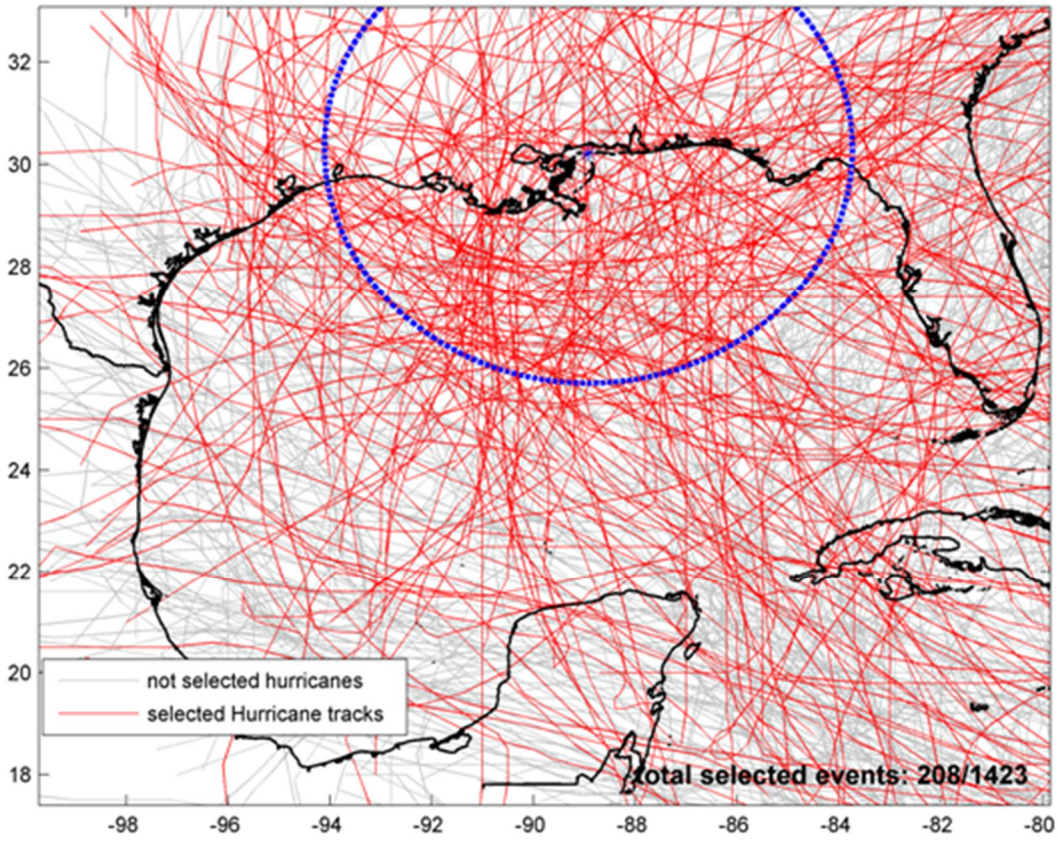

Figure 3.16 Tracks of hurricanes from 1917 to 2010.

3.9 Coastal system

3.9.1 Morphodynamic development of the barrier islands

Byrnes et al. (2011) studied the Mississippi coastal system based on observed island changes between 1917 and 2010. Byrnes' main findings with respect to the morphological development of the Mississippi barrier islands are summarized in Figure 3.17.

Dauphin Island tends to extend in a westward direction. Petit Bois, Horn and Ship Island tend to erode at their eastern ends and to accrete at their western ends, thus they migrate westward. Erosion rates at the eastern ends tend to be larger than the accretion rates at the western ends. Cat Island tends to erode at its southern end. For all islands the Gulf shorelines have eroded between 1848 and 2010, while at most locations the Sound shorelines also have eroded (but to a lesser extent than the Gulf shorelines).

For all islands, the above MSL surface areas tend to decrease. In Rosati et al. (2009) it is reported that in the period 1848 till 1986 Horn Island has had a significantly lower change in area (15%) as compared to Petit Bois (34%), Ship (38%) and Cat (29%) Islands.

In Byrnes et al. (2011) typical rates of change – as found by other authors and based on their own analysis – are discussed. Values found by Byrnes et al. (2011) and by Waller & Malbrough (1976) are summarized in Table 3.4. The values of Byrnes et al. are

representative for the period 1917 to 2010, the values of Waller et al. for the period 1848 to 1973.

According to Morton (2007) the three predominant processes causing land loss of the islands are: (1) unequal lateral transfer of sand related to greater updrift erosion compared to downdrift deposition, (2) barrier narrowing resulting from simultaneous erosion of the Gulf and Soundside shores, and (3) barrier segmentation related to storm breaching. According to Morton the main causes of the island land loss are frequent intense storms (particularly if these cause breaching of the islands), relative sea level rise and a deficit in the sediment budget (caused by a reduction in sand supply due to dredging of the navigation channels through the passes and tidal deltas). The latter factor causes the acceleration of the rate of land loss observed in the last decades.

Island	Westward growth rate (ft/yr) Byrnes/Waller	Eastern tip erosion rate (ft/yr) Byrnes/Waller	Erosion rate Gulf shoreline (ft/yr) Waller
Dauphin	+150 / -	-	-
Petit Bois	+84 / +118	-258 / -322	-5.9 (west) to -11.5 (east)
Horn	+94 / +125	-130 / -119	-2
Ship	+28 / +38	-44 / -44	-9.8
Cat	-	-	-7.9

Table 3.4 Barrier island changes (source: Byrnes et al. (2011))

Morton (2007) reports that repeated beach profile surveys between 1989 and 1993 by Chaney and Stone (1996) demonstrate that the Mississippi Sound shore eroded throughout the year, but rates of erosion were highest in the winter months when relatively high waves were generated in the Sound during the passage of cold fronts.

In Byrnes et al. (2011) the coastline retreat due to relative sea level rise is estimated at about 0.76 ft/yr (about 0.25 m/yr), which is in the order of only 4-5% of observed island shoreline retreats.

Inlet shoals and channels play an important role in the littoral sand transport between the islands. Channel orientation is primarily north-south, and overall deposition on ebb shoals is skewed to the west. Except for Mobile Pass and its ebb shoal, all other channels and ebb shoals do not extend very far offshore. The ebb shoal at Dog Keys Pass is the most extensive shoal system, followed by the shoal at Horn Island Pass. Ship Island Pass has a relatively deep natural inlet (see Figure 3.18), but here ebb shoal deposits are not well developed.

Figure 3.18 shows observed cross-sections through the passes for several points in time. The channels migrate to the west, forced by the westward migration of the islands. In the last decades the distinct channel in Petit Bois Pass has more or less disappeared. Changes in Horn Island Pass in the last decades are governed largely by the small dredged material disposal island in this entrance. Dog Keys Pass is the largest entrance in the island chain and it contains two well-developed channels. Originally, Dog Keys Pass was the primary channel, but in the last decades Little Dog Keys Pass has become the dominant channel in terms of depth. In Ship Island Pass the channel has shifted westward (similar as for the other passes), but channel characteristics have been very consistent. The bottom just west of the channel has remained remarkably stable.

Dredging of the channels at Horn Island Pass and Ship Island Pass started in the late 1890's. Since then, the maintenance of these channels has controlled the degree to which further island growth in a westward direction could occur. Sand dredged from the Pascagoula navigation channel (running through Horn Island Pass) has been placed primarily at the small island west of the channel (see 2nd box in Figure 3.17) and in the ebb shoal littoral zone. Sandy material dredged form Ship Island Pass has typically been placed in the littoral zone site and the fine grain sediment was taken to the ODMDS (Ocean Dredged Material Disposal Site).

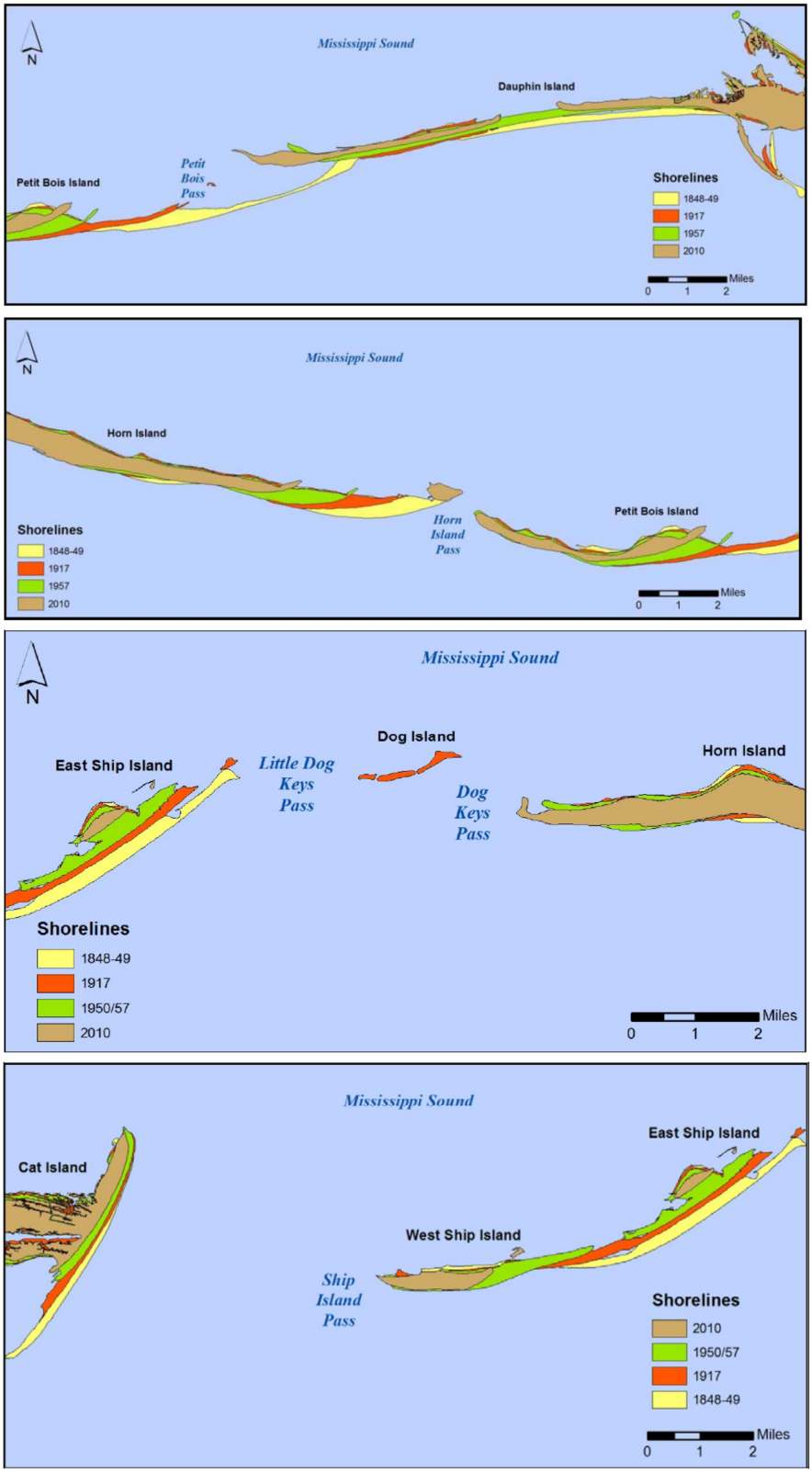

Figure 3.17 Illustration of barrier island migration (source: Byrnes et al. (2011))

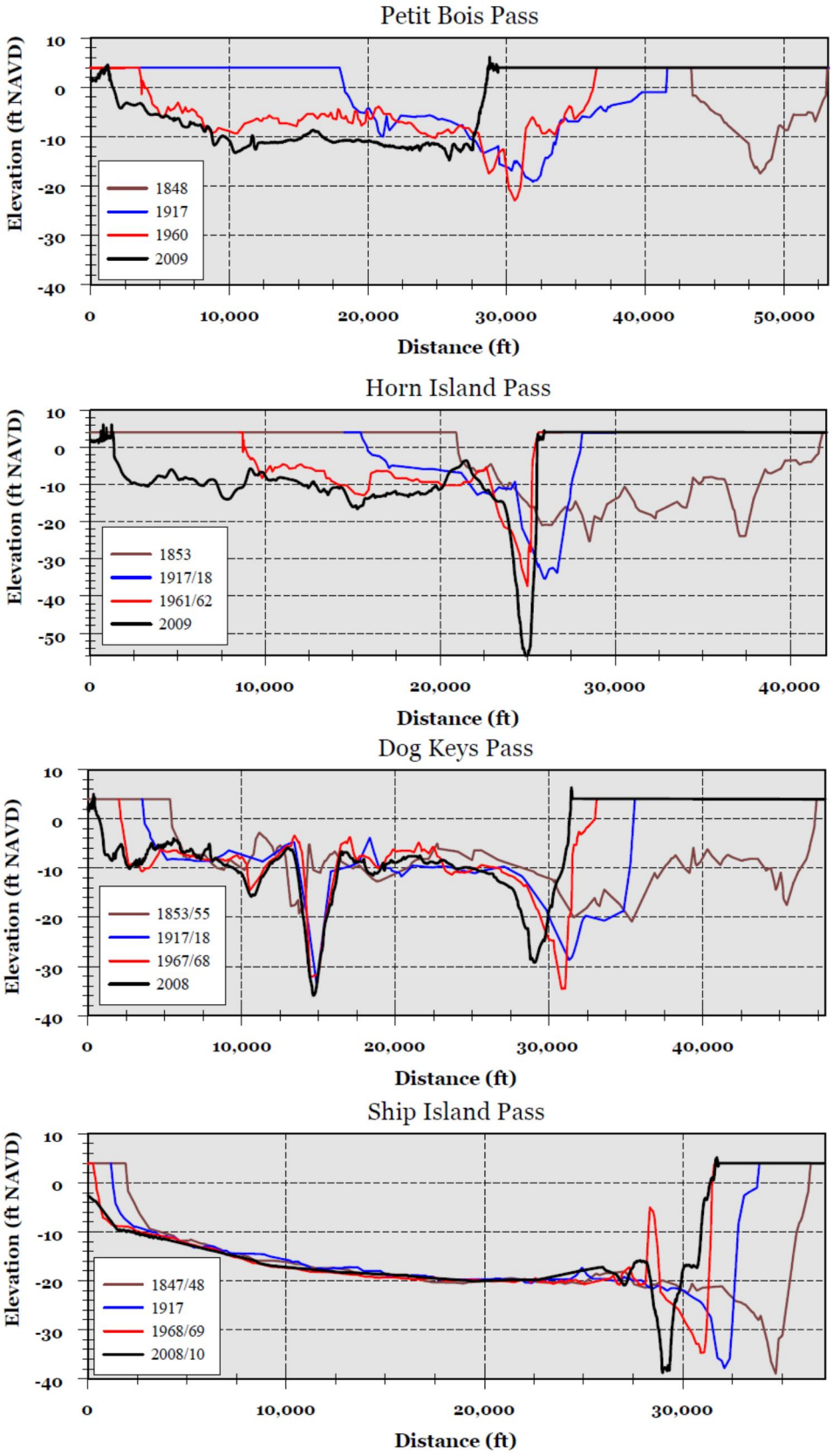

Figure 3.18 Observed development of the passes (after Byrnes et al., 2011).

3.9.2 Sediment balance of the barrier islands

In the available study reports historical erosion and accretion patterns have been derived, averaged over long periods of time (several decades), and sediment balances have been presented for the zone above -30 ft based on interpretation and computational results. The most recent balance as presented in Byrnes et al. (2011) is shown in Figure 3.19.

The balance is determined by:

Q_{in} = Sediment transport into area
Q_{out} = Sediment transport out of area
P = Sand placement in the area
R_m = Maintenance dredging, dredged material placed outside area
R_n = Capital dredging, dredged material placed outside area

On the basis of computations carried out in previous USACE studies and based on sedimentation rates in the navigation channels near the barrier islands, in Byrnes et al. (2011) the net longshore transport along the Gulf shoreline of the islands is estimated at 400,000 to 500,000 cy/yr (about 300,000 to 400,000 m^3/yr), see Figure 3.19.

The large scale sediment balance shown in Figure 3.19 is based on small scale balances for the boxes 1 to 5, which are presented in Figure 3.20. Along the barrier islands the westward directed longshore sediment transport is the dominant factor for the balance. In the passes and breaches cross-shore transport plays an important role. In Chapter 7 the balances will be discussed in more detail and compared with the model results.

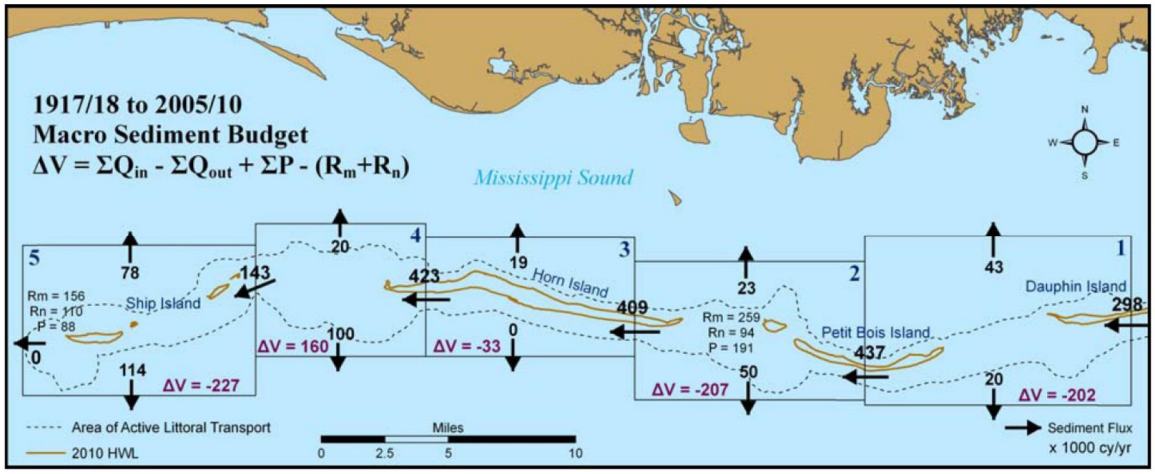

Figure 3.19 Large-scale sediment balance for period 1917/20 to 2005/10 (in 10^3 cy/yr) (source: Byrnes et al., 2011).

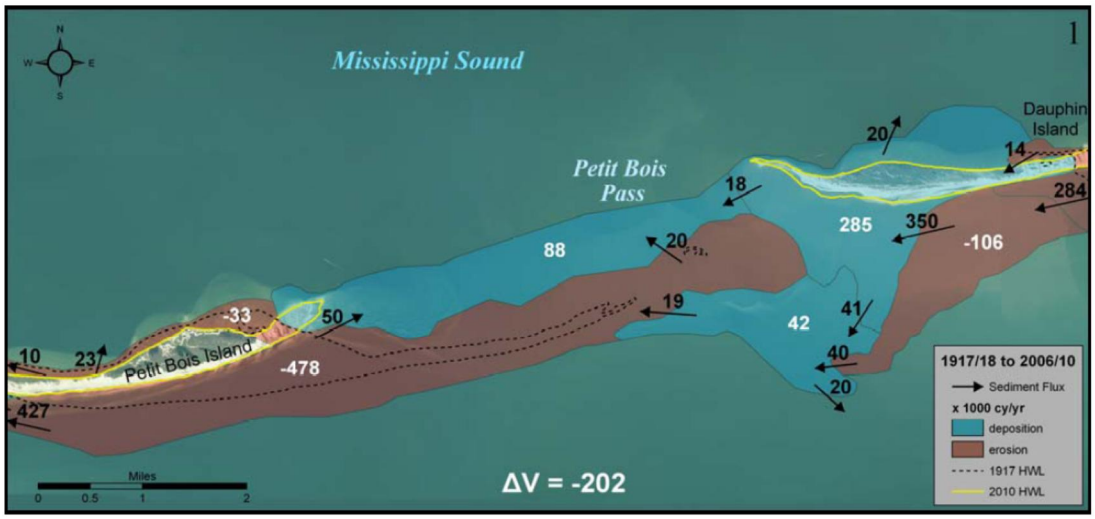
1
Mississippi Sound
Dauphin Island
Petit Bois Pass
Petit Bois Island
20
14
18
284
285
350
-106
88
20
19
42
41
40
20
-33
50
10
23
-478
427
1917/18 to 2006/10
Sediment Flux
x 1000 cy/yr
deposition
erosion
1917 HWL
2010 HWL
Miles
0 0.5 1 2
ΔV = -202

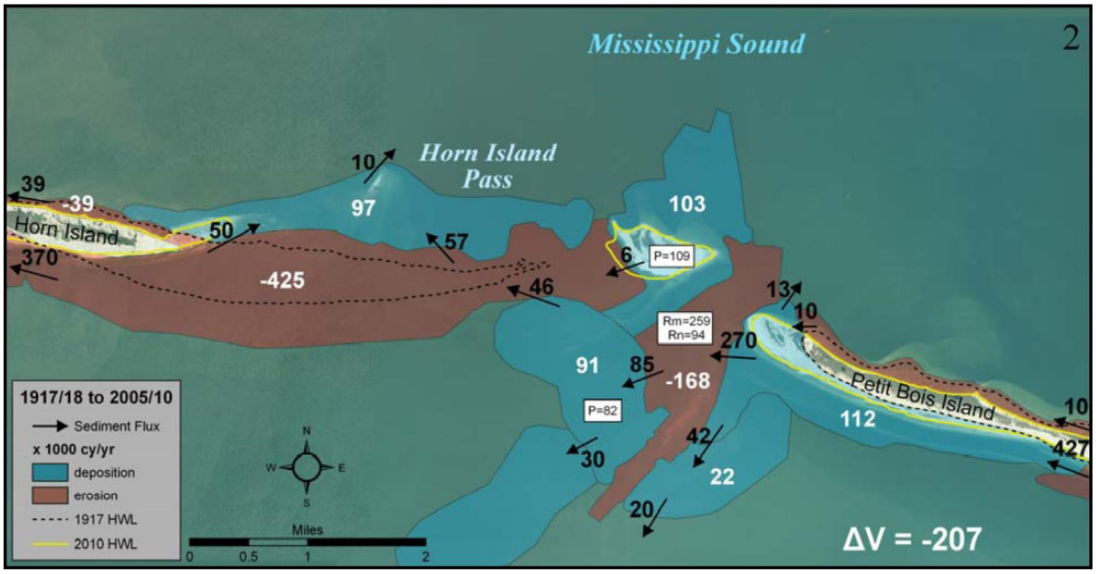
2
Mississippi Sound
Horn Island Pass
Horn Island
Petit Bois Island
10
39
-39
97
103
50
57
370
-425
46
6
P=109
13
10
Rm=259
Rn=94
270
91
85
-168
P=82
112
10
427
42
30
22
20
1917/18 to 2005/10
Sediment Flux
x 1000 cy/yr
deposition
erosion
1917 HWL
2010 HWL
Miles
0 0.5 1 2
ΔV = -207

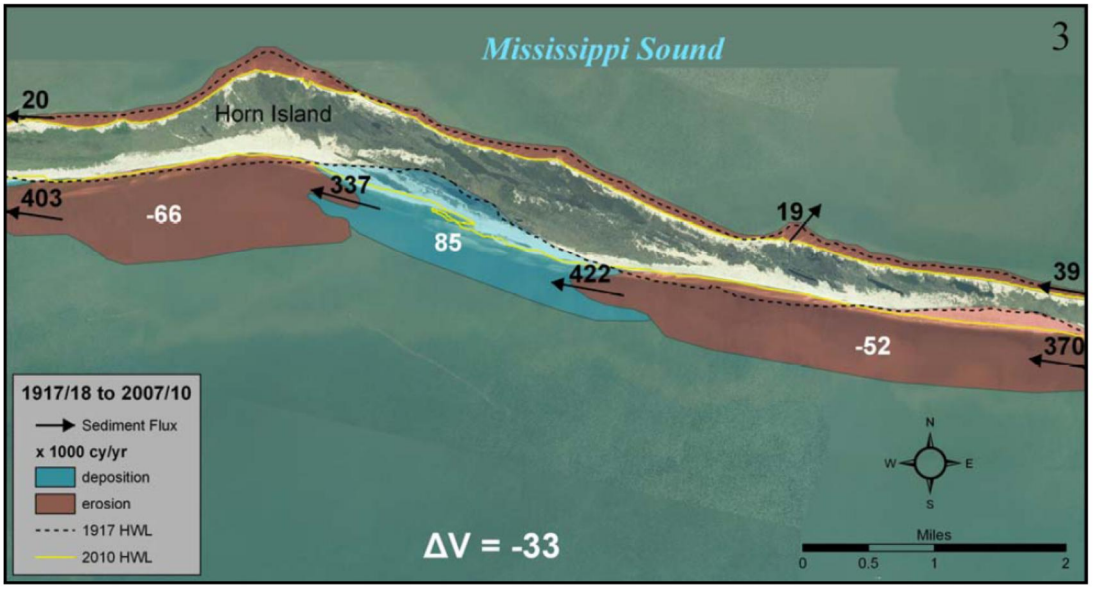
3
Mississippi Sound
Horn Island
20
403
-66
337
85
19
422
39
-52
370
1917/18 to 2007/10
Sediment Flux
x 1000 cy/yr
deposition
erosion
1917 HWL
2010 HWL
Miles
0 0.5 1 2
ΔV = -33

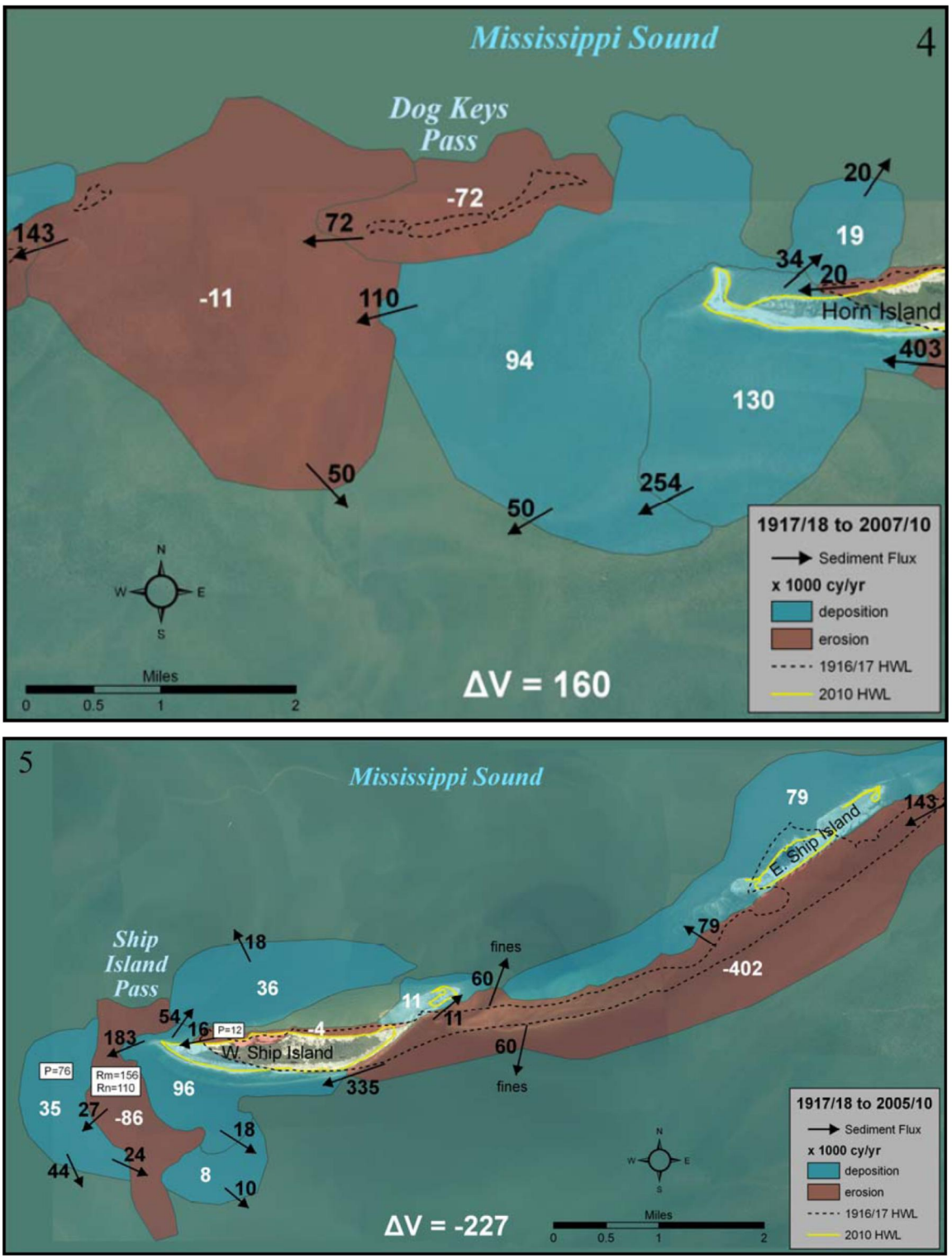

Figure 3.20 Detailed sediment balance for the boxes shown in Figure 3.19 for the period 1917/20 to 2005/10 (in 10^3 cy/yr) (source: Byrnes et al., 2011).

4 Hydrodynamic modeling

4.1 Introduction

This chapter describes the setup of the Mississippi Coastal Cell (MCC) model. The MCC-model is a two-dimensional depth-averaged (2DH) model covering the Mississippi coastal cell and barrier islands. In the following chapters the hydrodynamic MCC-model is extended to include additional forcing mechanisms (e.g. wind and waves) and the sediment transport and morphology will be activated. In this Chapter, the setup and verification/calibration of the hydrodynamic part of the MCC-model (tides, wind and river input excluding hurricanes) will be described.

4.2 Model setup

4.2.1 Model area, bathymetry and grid

The MCC-model consists of a curvi-linear computational grid covering the Mississippi coast and parts of the adjacent Alabama and Louisiana coasts. The model ranges from Gulf Shores, Alabama in the east to Lake Borgne and Lake Pontchartrain in Louisiana in the west. It covers the Mississippi and Alabama barrier islands, including Ship Island. The grid is projected in WGS84, UTM16 coordinates. The grid has a resolution of about 10 x 10 m in the vicinity of East and West Ship Island, with a gradually decreasing resolution towards the model boundaries. The gridlines are aligned such that they are orientated perpendicular to the shoreline of the barrier islands. Figure 4.1 shows the bathymetry of the MCC-model for the baseline case. The computational grid is presented in Figure 4.2.

The bathymetry for the baseline case (used for calibration of the model, not yet including Katrina Cut Closure) was created by interpolation of different bathymetric data sets to the computational grid. The order in which the data sets were considered is as follows:

1. Latest bathymetric data used in Byrnes et al. (2011)
2. Lidar data of topography surveyed in 2007 (file: USGS_2007_lidar 5mGrid)
3. USGS single-beam and swath bathymetric data surveyed in 2008 and 2009 (file: 2008_2009GUISbathy_v3.xyz)
4. ADCIRC model bathymetry (which was corrected for unrealistic steps in the bottom by DEM data)
5. Gulfport Channel data based on AutoCAD drawings (file: X001C909.dwg)
6. Katrina Cut survey data (kc042010.xyz, kc042110.xyz, kc042210.xyz)
7. Areas not covered by the above data sets were filled in with Digital Elevation Map (DEM) data downloaded from the NOAA website (files: mobile_al_navd88.grd, new_orleans_navd_88.grd, biloxi_ms.asc and northern_gulf_coast_navd_88.grd)

The final constructed model bathymetry is converted from the NAVD vertical reference level to MSL according to a spatial varying conversion field. This field was generated with the VDATUM software from NOAA. Some uncertainty regarding the accuracy of the datum conversion exists, as two different spatial data sets had to be used in VDATUM, which do not exactly match at their interface. A difference of approximately 0.1m is observed between the two data sets. The sensitivity of the results for this difference is discussed in Section 4.3.1.

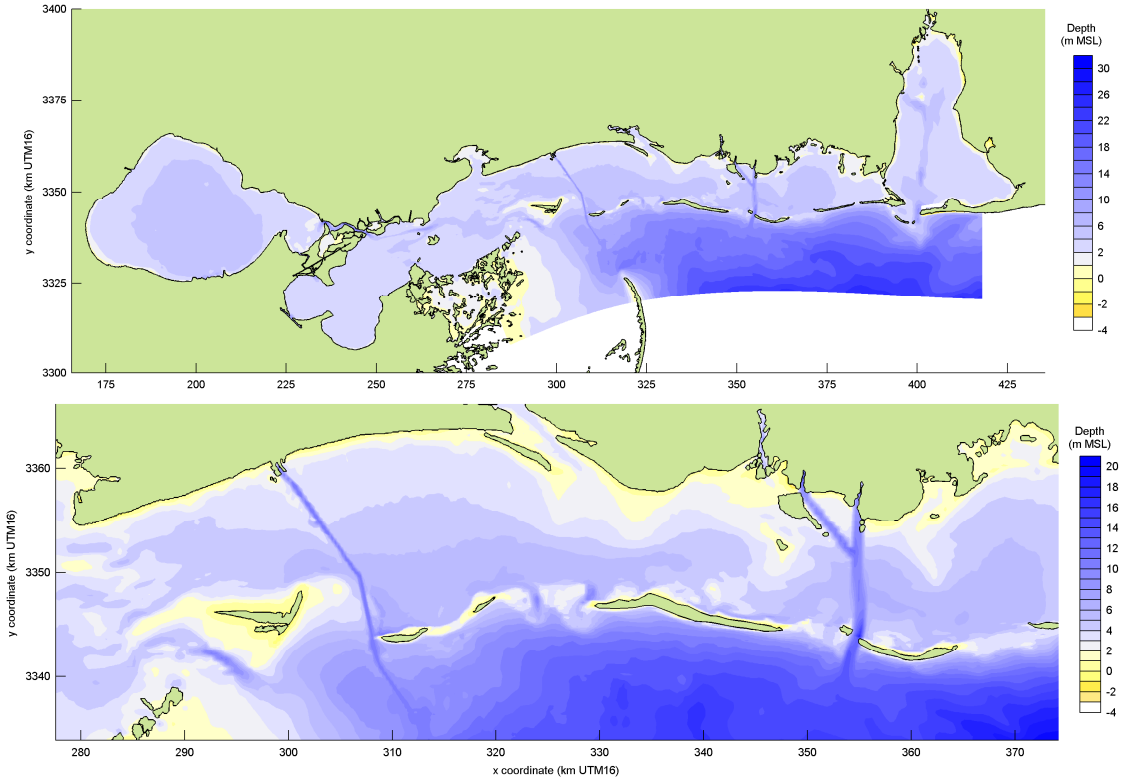

Figure 4.1 Model area and model bathymetry of the MCC hydrodynamic model (upper) and details around the barrier islands (lower). Note that due to the lower grid resolution towards the east, Pascagoula Ship Channel and Mobile Ship Channel are schematized wider than in reality.

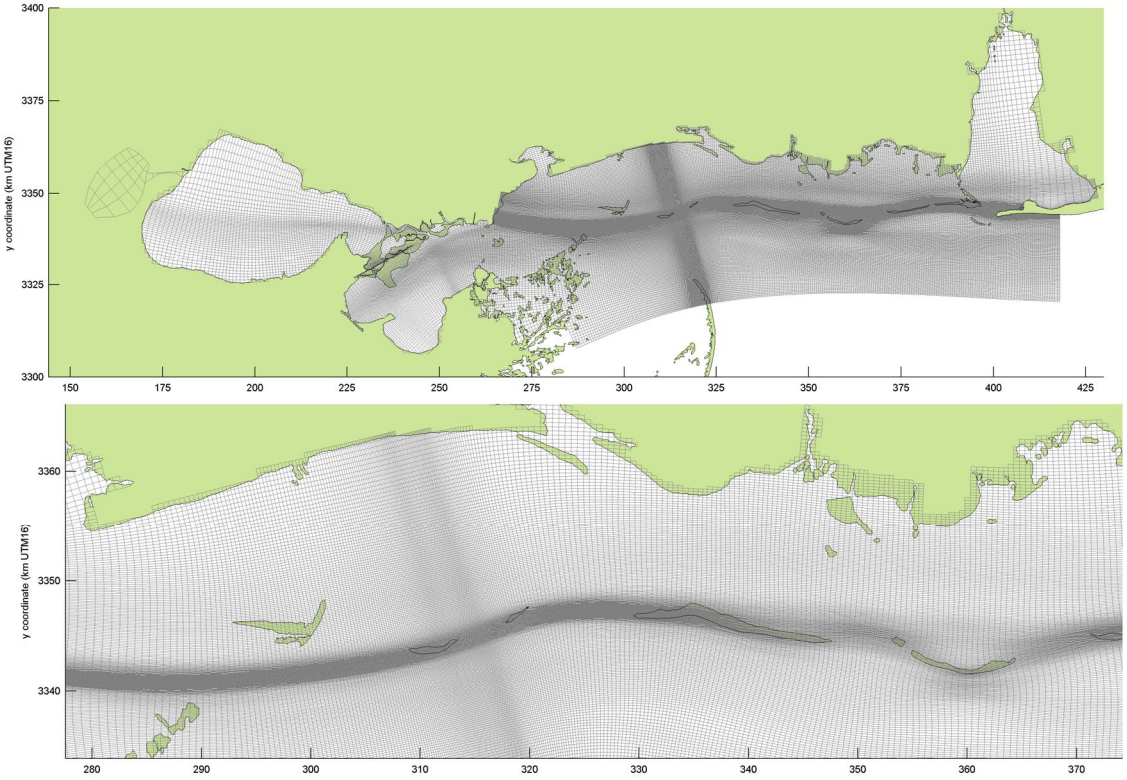

Figure 4.2 Computational grid of the MCC hydrodynamic model (presented grid 2 times coarser than actual grid)

4.2.2 Tidal boundary conditions

Tidal boundary conditions for the MCC-model are obtained by a two-stages nesting in existing models; the Gulf of Mexico (GoM) model and a smaller higher-resolution model of the north-eastern area of the Gulf (PAN), see Figure 4.3. The PAN model ultimately provides the tidal boundary conditions for the MCC-model.

The GoM model covers the entire Gulf of Mexico. The bathymetry of the GoM model is based on Gebco-08 data. Two open boundaries are defined at the south-east side of the model. At these open boundaries water level boundary conditions are imposed based on astronomical components from Topex Poseidon.

A higher resolution model covering the north-eastern corner of the Gulf (PAN) was nested in the GoM model, as shown in Figure 2.1. The resolution of the PAN model is in the order of 2x2 km in the area of the Mississippi sound. The south and west boundary of this model are open. The bathymetry of the PAN model is also based on Gebco-08 data. The model takes into account internal tide generating forces. The PAN model was nested within the GoM, so water level boundary conditions for the PAN model were derived from the GoM model with the nesting procedure.

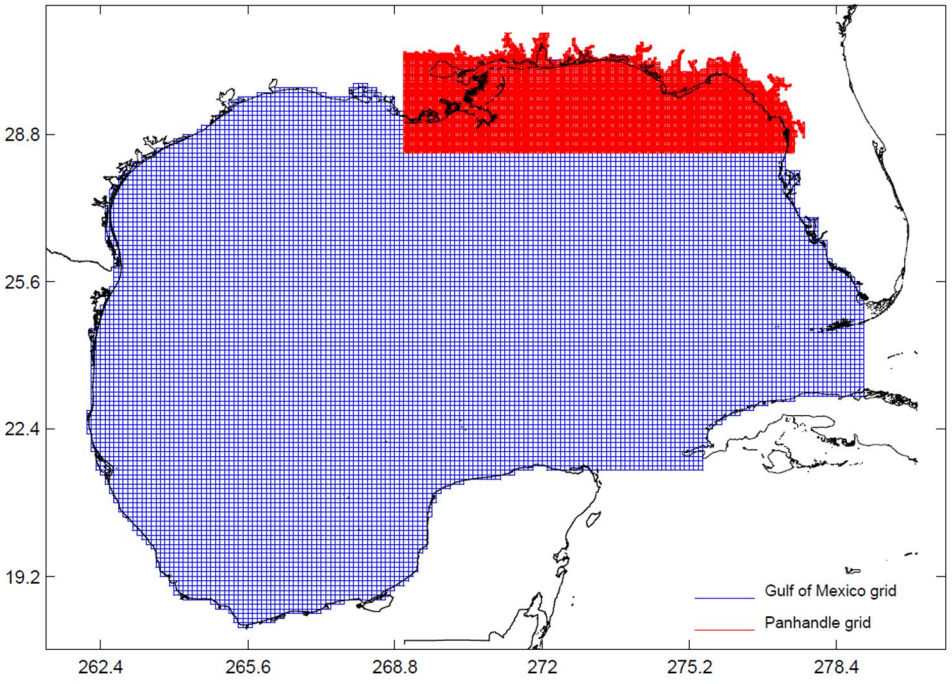

Figure 4.3 Computational model grids of the GoM (blue) and PAN model (red).

Several runs have been performed with the GoM and PAN. On the basis of an analysis of the results, the boundary conditions for the MCC were selected. In the MCC-model, water level forcing at the open sea boundaries was applied. The tidal constituents were derived by interpolating sets of tidal constituents from surrounding PAN model grid points to the defined boundary sections of the MCC-model. The model applies six (6) sections at the southern boundary at open sea and three (3) sections between the Chandeleur Islands and the mainland. The lateral boundary (east) is of Neumann type, which determines the alongshore water level gradient at the boundary. The Neumann boundary allows the model to compute the water level and velocity distribution in cross-shore direction so that it matches the water levels at sea and other forcing mechanisms (wind and waves).

4.2.3 River discharges

The river input in the MCC is included in the model as constant discharges based on yearly average values, as discussed in Section 3.7. Yearly average discharges are incorporated in the model as presented in Table 3.3.

4.2.4 Model settings

Bed roughness

Based on model experience in shallow tidal environments, a Manning coefficient of 0.02 $s/m^{1/3}$ was initially used in the MCC-model to account for the effect of bottom friction. However, the Manning roughness coefficient was varied as part of the model calibration.

Computational timestep and timezone

Based on the Courant criterion for surface wave propagation <10, the timestep for the hydrodynamic computation is set to 10 s. The model is run in GMT times.

Horizontal eddy viscosity

A uniform horizontal eddy viscosity of 0.1 m^2/s was applied. This is a common value for this kind of application with the grid resolution used. However, the eddy viscosity was varied as part of the model calibration.

Delft3D has a functionality to adjust the eddy viscosity for variation in velocities and grid resolution, called HLES (Horizontal Large Eddy Simulation). The sensitivity of the model results to the viscosity (uniform values of 1, 0.1 and HLES) was tested and it was found that the differences were only minor. Locally, eddies in the lee of the barrier islands show some variation in intensity, however, their location is fixed and differences in flow magnitudes are a few percent compared to the results with uniform viscosity values. For reasons of computational efficiency and simplicity, a uniform value for the eddy viscosity was used. From comparison of results and analysis of computed eddy viscosity values by HLES, it was found that a uniform value of 0.1 m^2/s is a representative value.

4.2.5 Wind boundary conditions (sensitivity)

During the set-up and calibration of the MCC-model, various sets of measured water levels, currents and wind were analyzed and compared with model results. This analysis is presented in Annex D.

The analysis indicated the significance of wind-induced water levels (surges) and currents in the study area. It was found that the magnitude of wind-induced currents in the study area can be in the same order as the magnitude of tidal currents, and can hence probably not be neglected. This is mainly related to cold front events, which will be described in Section 6.4.

4.3 Model calibration and validation

In this section, the calibration and performance of the hydrodynamic MCC-model is presented and discussed. The MCC-model was calibrated on the basis of tidal information by comparing the model results with water level data and tidal constituents from NOAA, available in both the frequency domain as in the time domain, and current measurements in the time domain. Calibration of a tidal model is more objectively performed in the frequency domain (by comparing astronomical constituents) because in this way the effect of meteorological forcing on the water levels is excluded from the analysis.

A numerical model is a schematization of the real world and the higher the quality of the input data (bathymetry, boundary conditions), the more accurate the modeling results. Typically, the following accuracy criteria of tidal models for the prediction of water levels after calibration are to be achieved:

- Amplitude of main water level constituents (O1, K1, N2, M2, S2, ..) should be within 10% from the observed amplitudes
- Phases of main water level constituents (O1, K1, N2, M2, S2, ..) should be within 20 minutes from the observed phases

As currents tend to be more variable (e.g. as a result of direct or indirect wind effects and local bathymetry features), mean deviations of around 20% of the observed current magnitudes can generally be achieved. However, during some events the model may deviate by a larger amount. The available current data and model results could not be compared in a quantitative sense, since the MCC currents represent depth-averaged velocities, whereas the current data downloaded from NOAA represent surface currents. A discussed in Section 3.4 the ADCP data (which include depth information) show considerable scatter in both magnitudes and directions. Therefore, only a qualitative assessment can be made between computed and observed currents.

The objective of the calibration study is to be well within the above given accuracy margins for water levels and to assess the ability of the model to compute the currents correctly.

4.3.1 Description of calibrated model settings

In the calibration process, the MCC-model was first calibrated for tide only, after which wind and pressure effects were included in the model to compare modeled and observed water levels and currents. In the calibration, the sensitivity of model results to several key parameters has been tested. Below, the most important of these settings and the effect on the model results are briefly discussed:

- Tidal corrections at the open boundaries
- Bottom roughness
- Bathymetry
- River discharges
- Wind and pressure

Results of the calibrated model will be presented in Section 4.3.2.

Tidal corrections at the open boundaries

Different corrections to the boundary conditions, derived from the PAN model, have been applied by defining amplitude ratios and phase differences for the three main constituents: O1, Q1 and K1. The correction values were chosen on the basis of Fourier analysis of the computed water levels, which were then compared to known tidal constituents at several main tidal stations. In the model, the major components (O1, Q1 and K1) initially appeared to exhibit a phase lag of about 10º to 15º with respect to the observations; the amplitudes were generally represented well. Further optimization of the corrections to the boundary conditions included the constituents P1, M2 and S2. The correction settings that gave the best agreement with observations are presented in Table 4.2.

Tidal constituent	Amplitude correction factor (-)		Phase correction (º)	
	Gulf of Mexico	Chandeleur Sound	Gulf of Mexico	Chandeleur Sound
O1	1.0	1.1	10	-10
Q1	1.0	1.0	15	15
K1	1.0	1.1	15	0
P1	1.1	1.1	10	0
M2	0.7	1.0	-5	-5
S2	1.0	1.0	0 (east) to 20 (west)	20

Table 4.2 Optimum boundary corrections of tidal constituents at the open boundaries of MCC

Bottom roughness

A series of sensitivity runs was carried out with different settings for the bed roughness parameters, based on typical values for muddy to sandy tidal environments. The effect of the bottom roughness has been verified by applying the following friction formulations and values:

- Chézy = 65 $m^{1/2}/s$
- Manning = 0.026 $s/m^{1/3}$ and 0.020 $s/m^{1/3}$
- Van Rijn roughness predictor, which computes the local bed roughness based on the sediment diameter (uniform value of 300 µm) and instantaneous flow velocities.

The simulation with a Manning value of 0.020 $s/m^{1/3}$ showed the best performance with respect to the tidal range in the Mississippi Sound as a whole and was therefore selected.

Model bathymetry

After inclusion of the tidal corrections, a number of sensitivity run were carried out with local adaptations of the model bathymetry to further improve the tidal propagation through the area. The following sensitivities were verified:

- As a phase lag of the main tidal constituents was observed in Lake Pontchartrain, the entrance channel to Lake Pontchartrain was widened and deepened to advance the tidal phasing in the lake. The improvement to the phasing of the main tidal constituents at New Canal Station was a few degrees, hence this adaptation was accepted.
- As there were uncertainties about the conversion from the NAVD vertical reference level to MSL (see Section 4.2.1), the effect of an overall raise of the seabed by 0.1m was tested. This appeared not to have a significant effect on the tidal propagation, however it slightly reduced the tidal range in the shallow embayments. Therefore this adaptation was not accepted.

After the above model modifications, the tidal propagation in the MCC-model was found to be satisfactory. The model was then used to simulate the March 2010 period, for which ADCP measurement data were available. In this process, further adjustments were made to the model:

River discharges

The effect of inclusion of the river discharges was verified. Taking into account the river discharges led to a minor improvement in computed flow magnitudes.

Wind and pressure

The effect of inclusion of wind and pressure was verified based on incorporation of spatial uniform wind and pressure values in the model. Including meteorological forcing led to a

major enhancement of the computed water levels and currents with respect to the observations. Further improvement was achieved by also including wind and pressure in the PAN model, so that the overall surge in the region is incorporated in the MCC boundary conditions.

4.3.2 Results

Model performance in the frequency domain

The capability of the calibrated model to correctly representing the propagation of the tide in the Mississippi Sound was assessed in the frequency domain by comparing observed and computed amplitudes and phases of a set of main tidal constituents. The comparison was made for water levels at a total of 10 stations. The harmonic analyses, performed with Delft3D-TRIANA (Deltares, 2009), was based on one month simulations and carried out for the eight (8) largest constituents.

The results of TRIANA are presented in the form of tables which include for each of the main constituents the mean amplitude and phase differences and ratios, the root mean square of the differences and ratios (or error) between computed and observed amplitudes and phases and the vector differences. Figure 4.4 and Table 4.3 present the computed and observed amplitude (Hc and Ho) and the computed and observed phase (Gc and Go) of the three main constituents for 10 tidal stations. On the basis of this, it can be observed that:

- the model shows that it accurately represents the propagation of the water levels (vertical tide).
- the main constituents (O1, K1, P1) are well represented by the model. The computed amplitudes are generally within 10% and the computed phases are within 20 minutes (i.e. about 5°/hr for the diurnal constituents) from the observed values.
- the water levels at the stations Shell Beach and New Canal Station do not perform within the set accuracy criteria for amplitudes and phases and at station Coast Guard Mobile not for the accuracy criteria for amplitudes only. The three stations are located in embayments with a shallow bathymetry (~3-4 m); consequently, correct representation of the bottom topography and bed roughness is very important for accurate modeling of the tidal propagation in these areas. Moreover, accurate schematization of the entrances to Lake Pontchartrain and Mobile Bay is crucial in order to achieve correct tidal propagation towards the bays. The accuracy achieved at the three shallow stations is considered good enough for the present study, also taking into account that the stations are located away from the area of interest.

Station	Component	Hc	Ho	Hc/Ho	Gc	Go	Gc-Go
Biloxi IHO	**O1**	**0.16**	**0.16**	**1.03**	**30.7**	**37.9**	**-7.2**
	K1	**0.17**	**0.17**	**0.97**	**47.4**	**47.9**	**-0.6**
	P1	**0.06**	**0.05**	**1.18**	**46.5**	**41.9**	**4.6**
Dauphin Island	**O1**	**0.14**	**0.14**	**1.01**	**26.6**	**41.9**	**-15.3**
	K1	**0.14**	**0.14**	**0.99**	**42.1**	**50.6**	**-8.5**
	P1	**0.05**	**0.04**	**1.08**	**41.2**	**49.9**	**-8.7**
Gulfport Harbor	**O1**	**0.16**	**0.16**	**1.02**	**35.7**	**32.0**	**3.7**
	K1	**0.17**	**0.17**	**0.96**	**52.9**	**41.0**	**11.9**
	P1	**0.06**	**0.04**	**1.28**	**52.0**	**43.6**	**8.4**
Horn Island	**O1**	**0.15**	**0.16**	**0.94**	**23.2**	**26.8**	**-3.6**
	K1	**0.16**	**0.16**	**0.97**	**39.0**	**38.3**	**0.7**
	P1	**0.05**	**0.05**	**0.98**	**38.1**	**37.4**	**0.7**
Pascagoula Point	**O1**	**0.15**	**0.16**	**0.98**	**24.1**	**28.3**	**-4.2**
	K1	**0.16**	**0.14**	**1.08**	**40.1**	**33.8**	**6.3**
	P1	**0.05**	**0.05**	**1.08**	**39.2**	**33.4**	**5.8**
New Canal Station	**O1**	**0.03**	**0.04**	**0.88**	**194.9**	**177.5**	**17.4**
	K1	**0.03**	**0.03**	**0.81**	**222.6**	**181.5**	**41.1**
	P1	**0.01**	**0.01**	**0.83**	**221.7**	**181.2**	**40.5**
Shell Beach	**O1**	**0.11**	**0.13**	**0.84**	**96.7**	**82.9**	**13.8**
	K1	**0.11**	**0.14**	**0.80**	**120.6**	**98.2**	**22.4**
	P1	**0.04**	**0.04**	**0.88**	**119.7**	**95.5**	**24.2**
Bay St. Louis	**O1**	**0.13**	**0.14**	**0.95**	**57.8**	**66.0**	**-8.1**
	K1	**0.14**	**0.15**	**0.89**	**77.4**	**71.3**	**6.0**
	P1	**0.05**	**NaN**	**NaN**	**76.5**	**NaN**	**NaN**
Cat Island	**O1**	**0.14**	**0.15**	**0.96**	**46.6**	**44.2**	**2.5**
	K1	**0.14**	**0.16**	**0.89**	**64.6**	**54.1**	**10.5**
	P1	**0.05**	**0.05**	**0.98**	**63.7**	**50.2**	**13.6**
Coast Guard Mobile	**O1**	**0.16**	**0.14**	**1.14**	**59.4**	**56.1**	**3.3**
	K1	**0.16**	**0.15**	**1.11**	**79.4**	**70.3**	**9.1**
	P1	**0.05**	**0.05**	**1.13**	**78.5**	**69.2**	**9.3**

Table 4.3 Computed and observed amplitudes (Hc, Ho) and phases (Gc, Go)

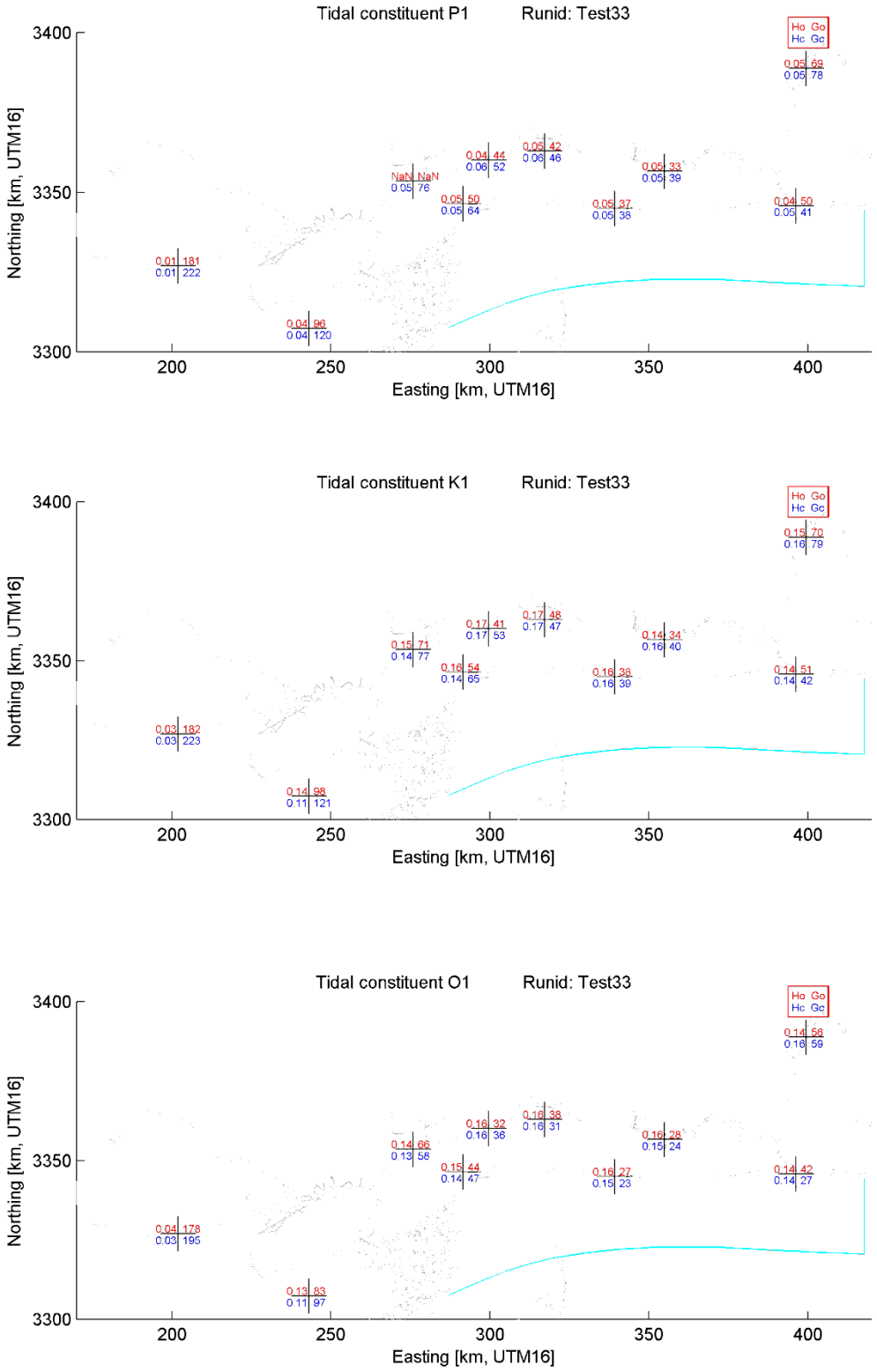

Figure 4.4 Computed and observed amplitudes and phases.

Model performance in the time domain

The accuracy of the MCC-model is not only based on a comparison on the frequency domain (comparison of amplitudes and phases of tidal constituents), but also in the time domain by comparing time series of observed and computed water levels and currents. The comparison in the time domain is presented below for respectively water levels and currents for March 2010.

Water levels and currents - NOAA observations

Time series of computed water levels (run33, tide only, no wind and pressure included) for three representative stations are plotted against predicted water levels in Figure 4.5. Predicted water levels are derived from tidal predictions on the basis of the available constituents sets. The plotted time series cover a typical spring-neap cycle in March 2010. From these figures the following can be observed:

- Generally the model results are an accurate representation of the predicted tidal water levels;
- At the station Shell Beach differences to a maximum of about 10 cm can be observed during spring tides.

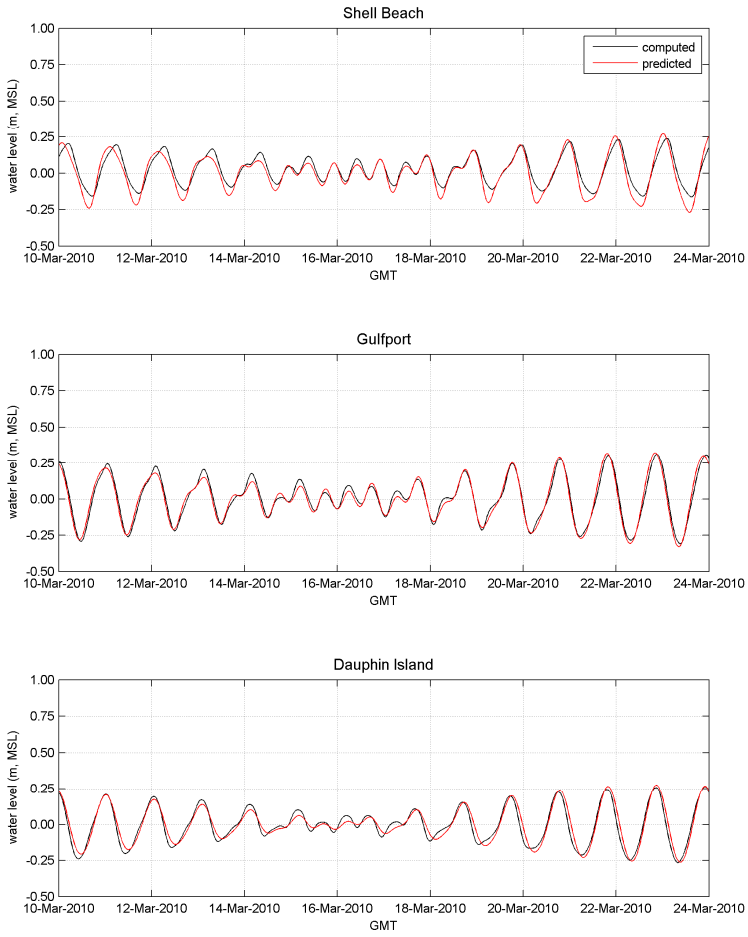

Figure 4.5 Comparison of computed and predicted (based on tidal constituents) water levels.

Time series of computed water levels (run33, tide including wind and pressure) for three representative stations are plotted against observed and predicted water levels in Figure 4.6

Predicted water levels are derived from tidal predictions on the basis of the available constituents sets. The plotted time series cover a typical spring-neap cycle in March 2010.

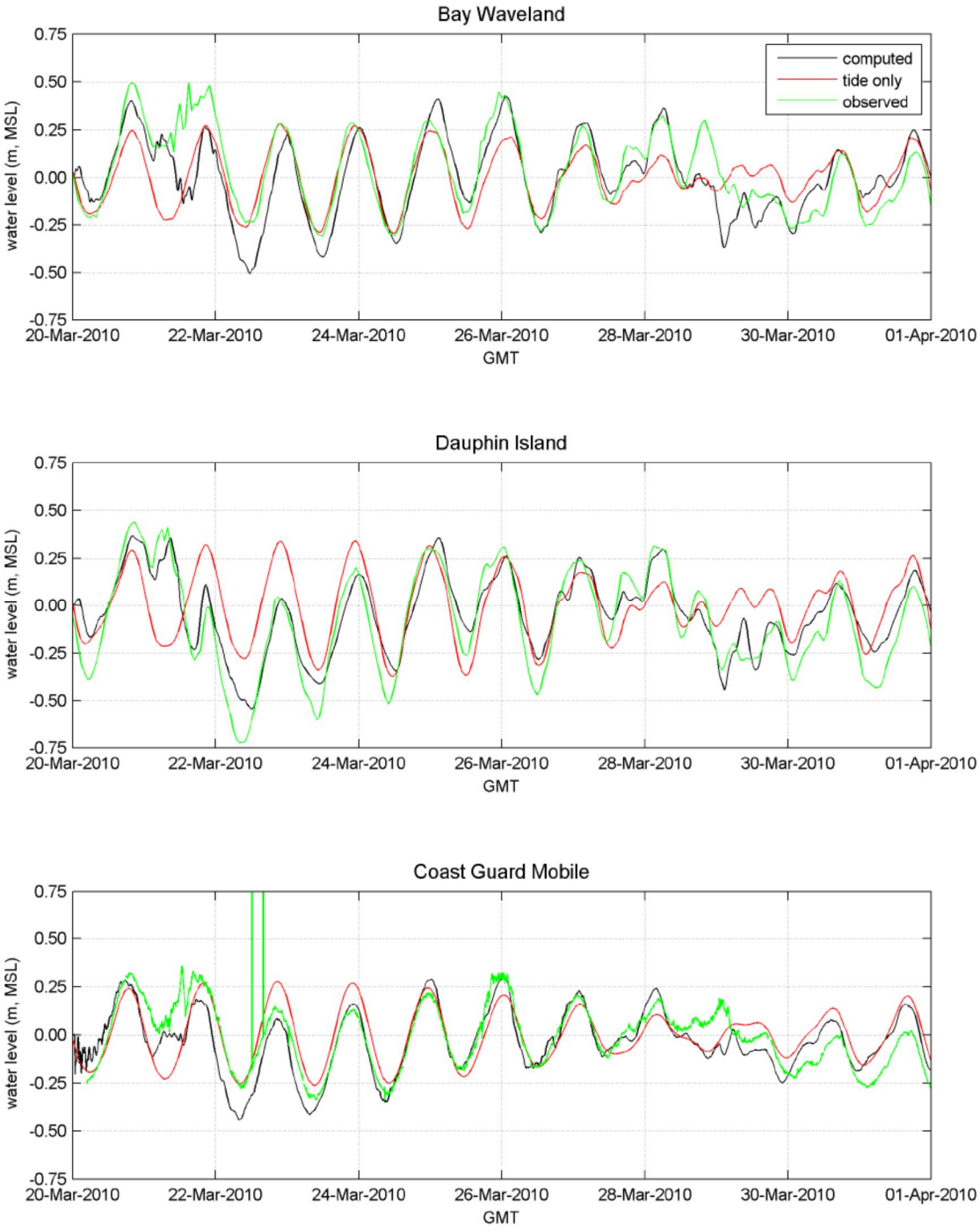

Figure 4.6 Comparison of computed, predicted (tidal constituents) and observed water levels.

From these figures the following can be observed:

- Generally the model results are an accurate representation of the observed water levels; however, deviations with the observations in the order of 25 cm can be observed. In the simulation, spatially uniform wind and pressure has been considered. It is expected that applying a spatial varying wind and pressure field will enhance the model performance. For a discussion on the effect of wind reference is made to Appendix D.

Model results of the ADCIRC model were provided by USACE for 18 selected locations. Time series of computed water levels and currents (run33, tide including wind and pressure) for two of the stations are plotted against the ADCIRC model results in Figure 4.7 and 4.8. From the comparison with the ADCIRC results the following can be concluded:

- The two models generally show good agreement in computed water levels and currents, however;
- At certain moments significant differences in water levels can be observed between the two models. Typically the ADCIRC model computes larger variation in water levels due to meteorological effects than the MCC-model. A plausible explanation could be the difference in forcing of the two models; whereas the MCC incorporates uniform wind and pressure forcing, the ADCIRC model is driven by spatial varying wind fields but neglects the effects of pressure.
- Comparison of the modeled water levels with nearby observations shows that the MCC results generally agree well with the observation.
- The flow directions typically agree well between the MCC and ADCIRC results.
- The MCC flow magnitudes are typically somewhat lower than the ADCIRC results (~10%). This can possibly be explained by the lower water level variations computed in the MCC, leading to smaller head differences in the area.
- Especially point 5 and point 9 (not presented) show large differences in flow magnitudes, with much lower peak velocities computed by the MCC (~40% lower). These two points are located in tidal inlets (Dog Key Pass and Horn Island Pass respectively); small deviations in the exact location and depths between the two models may explain the differences here[3].

It is concluded that the MCC-model shows good agreement in computed water levels and currents with observations.

3. *Sensitivity runs have been performed to improve the performance of the water levels in the Sound as a whole. No further simulations have been carried out to improve the modeled velocities locally, as it was expected that the differences in model schematization between MCC and ADCIRC would be dominant in the inlets.*

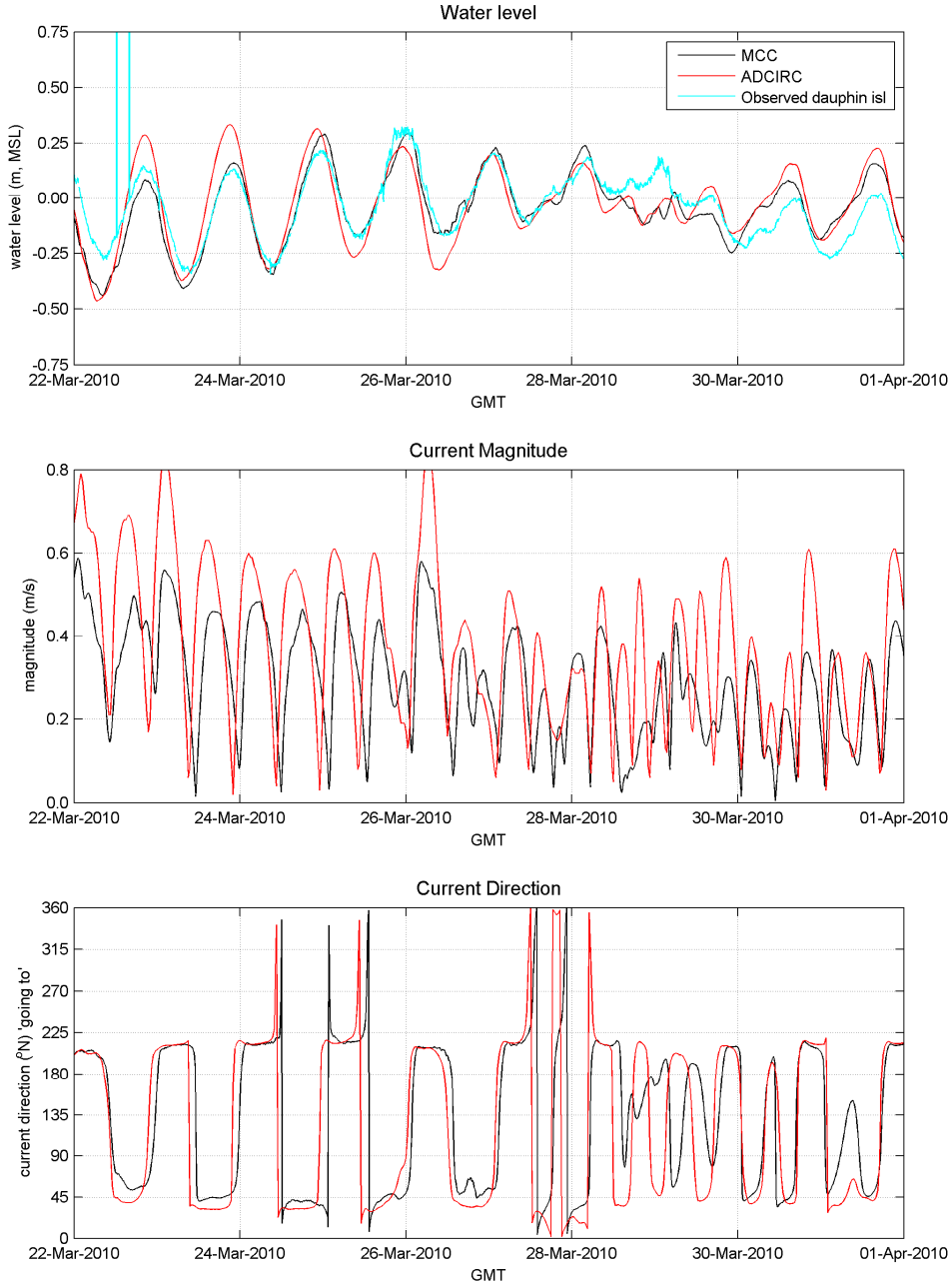

Figure 4.7 Comparison water levels and currents Dauphin Island.

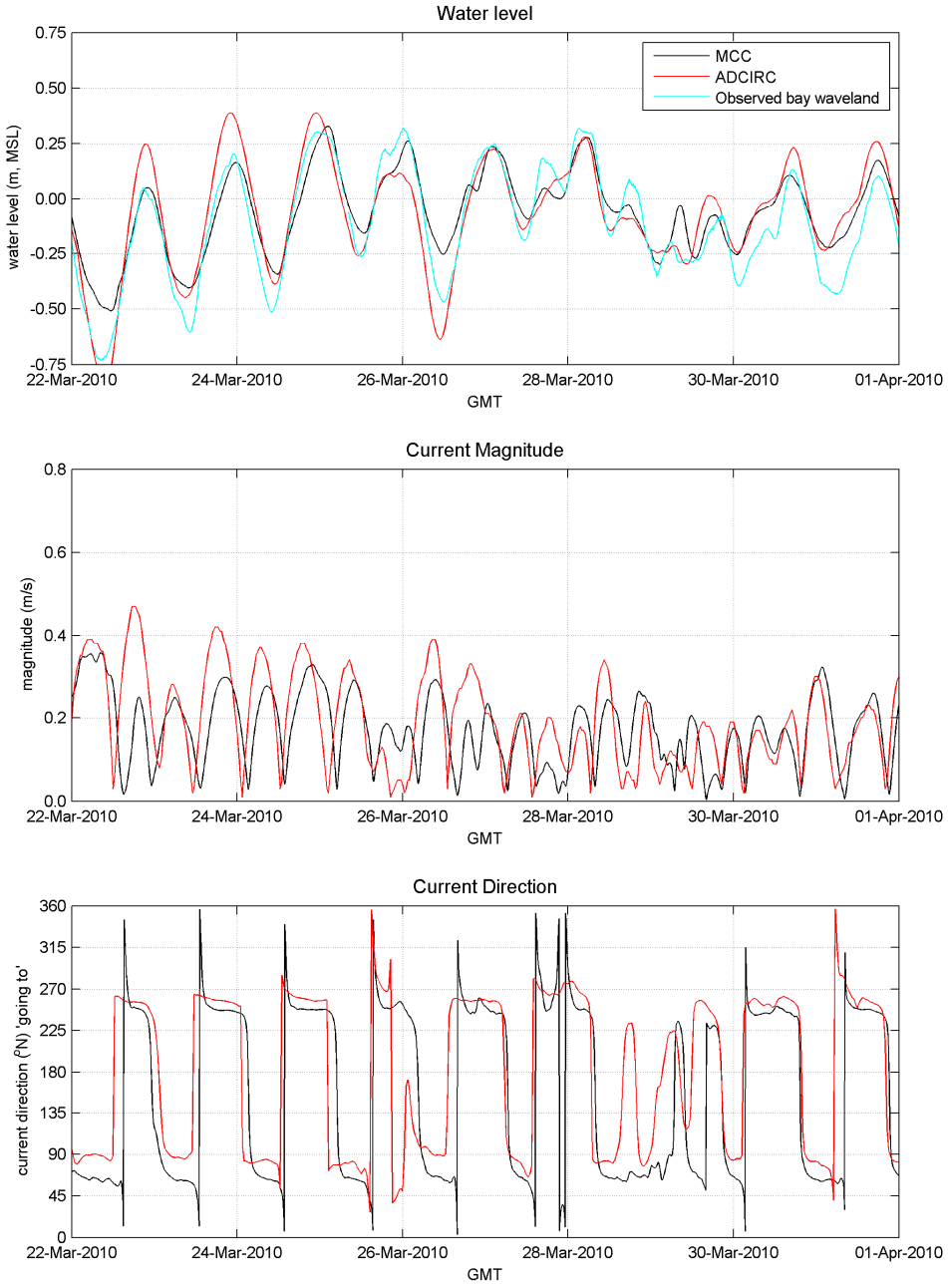

Figure 4.8 Comparison water levels and currents Bay Waveland.

Currents - ADCP measurements

The results of the flow modeling are compared with the ADCP transect measurements by ERDC (2010) as provided by USACE. Current profiles were measured at a total of six transects between the barrier islands, as indicated in Figure 3.4.

Comparison between measured and computed current vectors are presented for two arbitrarily selected time stamps at transects TL1, TL2 and TL3 in Figures 4.9 to 4.14 respectively. Given the noise of the measurement and the fact that the exact bathymetry at the time of the ADCP measurements is by definition not included in the model depth schematization, the comparison should be qualitatively interpreted.

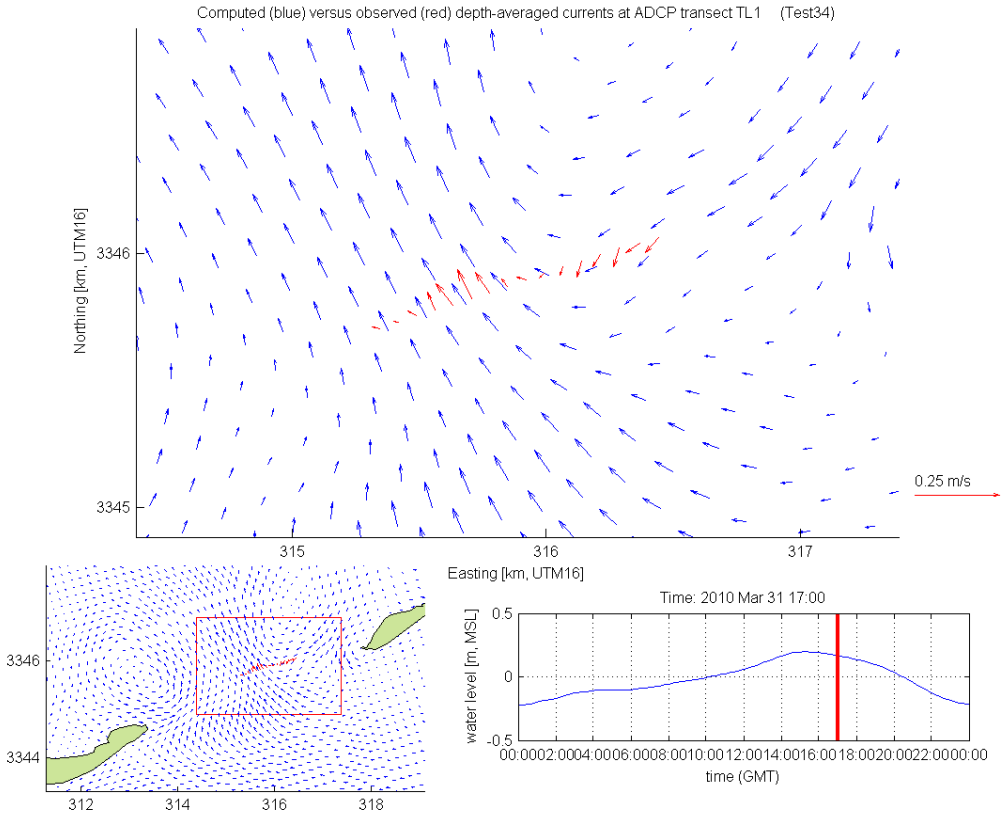

Figure 4.9 Comparison between computed and measured depth-averaged current vectors at transect TL1.

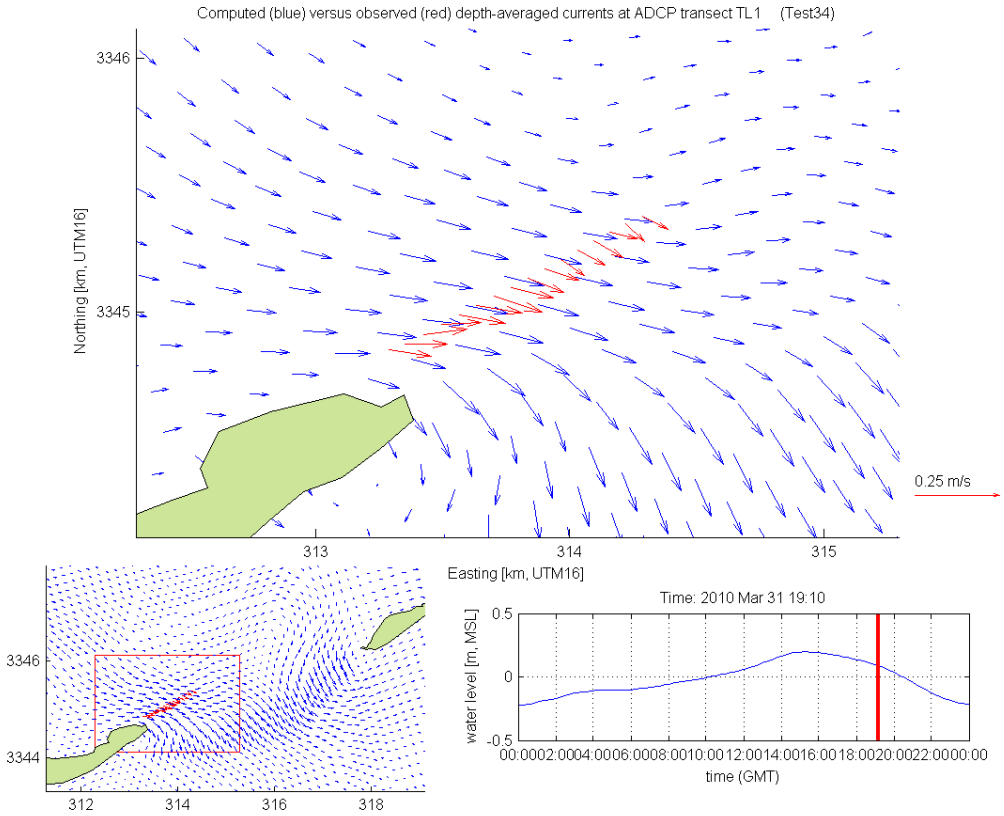

Figure 4.10 Comparison between computed and measured depth-averaged current vectors at transect TL1.

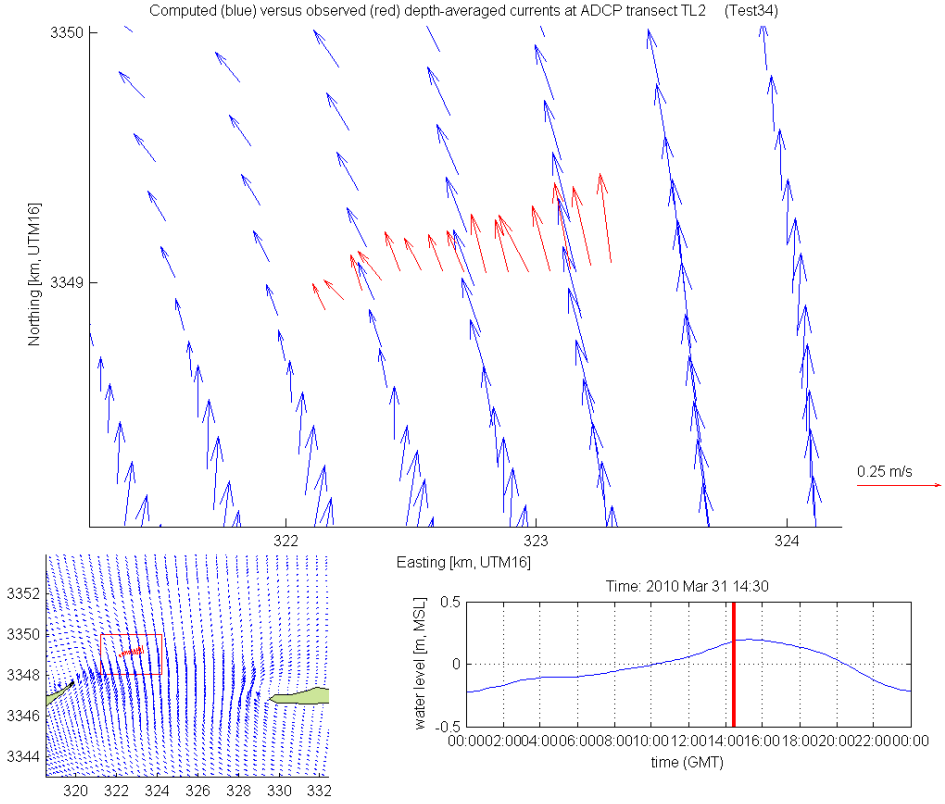

Figure 4.11 Comparison between computed and measured depth-averaged current vectors at transect TL2.

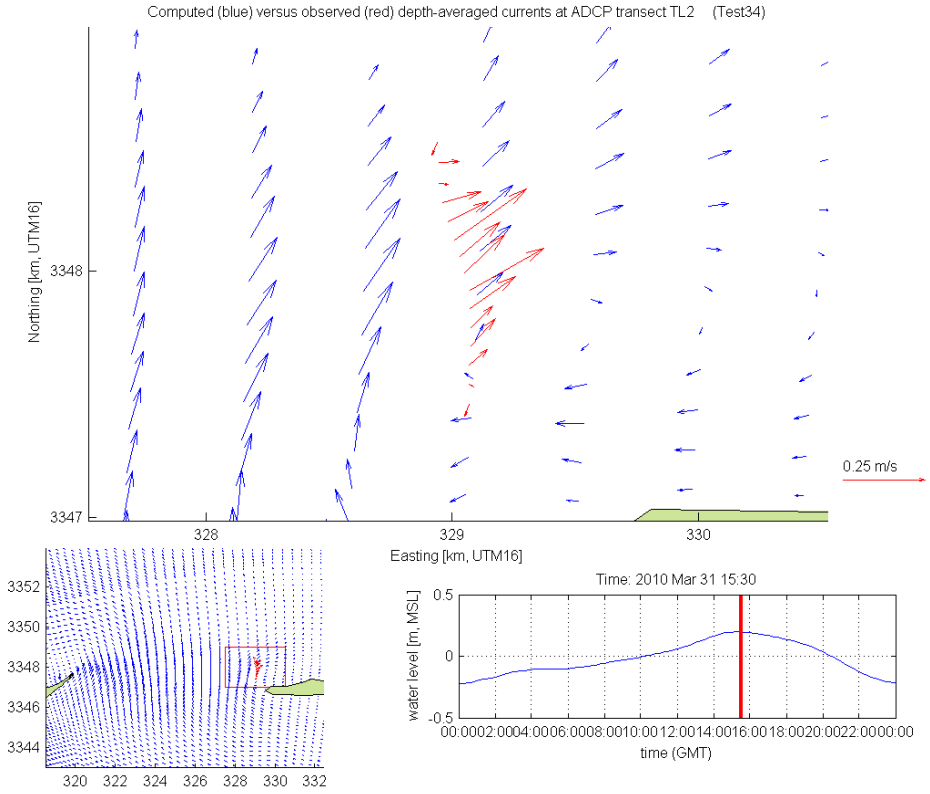

Figure 4.12 Comparison between computed and measured depth-averaged current vectors at transect TL2.

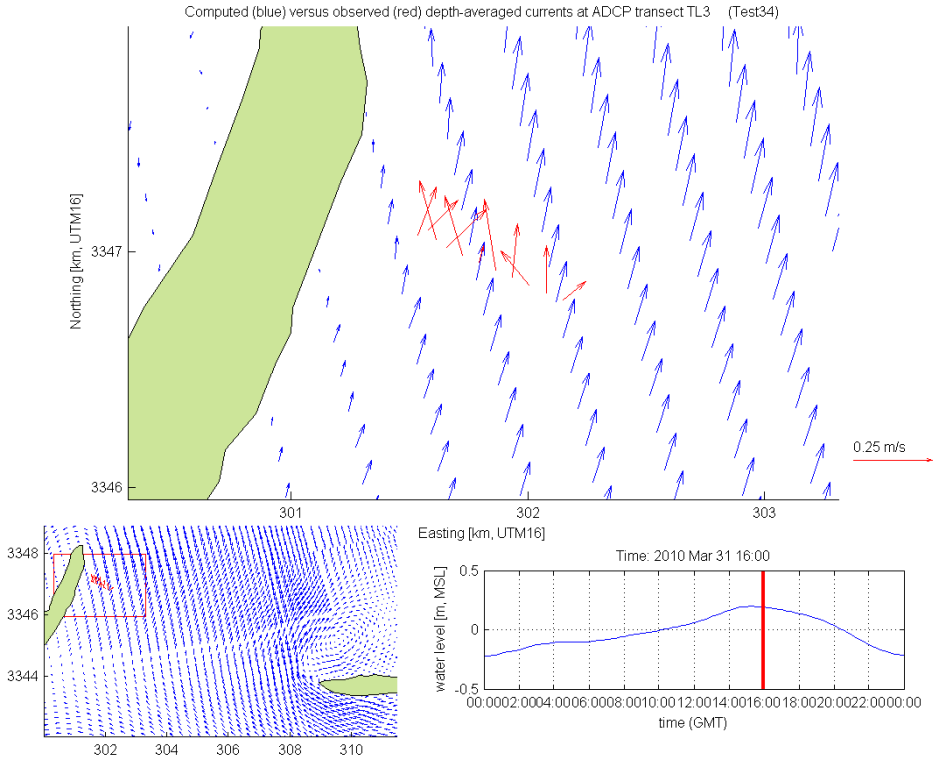

Figure 4.13 Comparison between computed and measured depth-averaged current vectors at transect TL3.

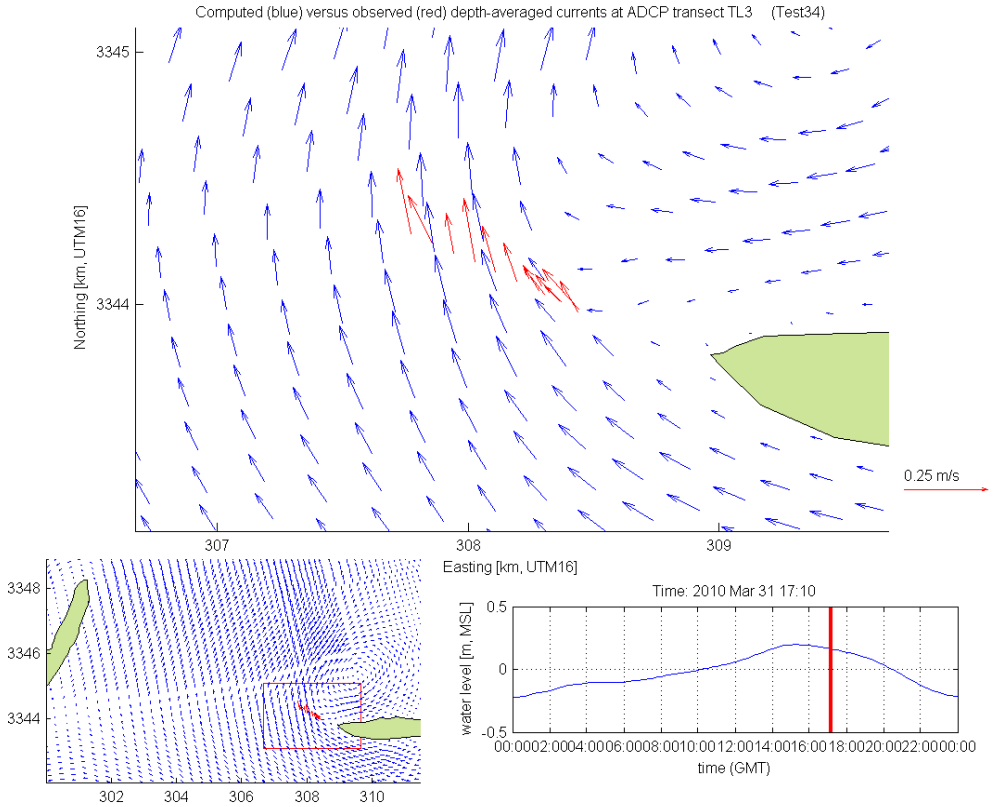

Figure 4.14 Comparison between computed and measured depth-averaged current vectors at transect TL3.

From the comparison with the ADCP data the following can be concluded:

- Qualitatively the model results show good agreement in flow patterns with the ADCP data; especially the match in flow directions is reasonable and the model captures complex eddy structures that seem to be present in ADCP data too (e.g. Figure 4.9 and 4.12)
- The agreement in flow magnitudes is poor, but as the noise level in the ADCP data is high this is not a reason to reject the model results or to further tune the model.

4.4 Conclusion

The calibration of the MCC was successful and the model performance is considered acceptable for the purpose of the study. The calibrated hydrodynamic MCC will therefore serve as the basis for the modeling. Inclusion of waves in the MCC is described in Chapter 5.

5 Wave modeling

5.1 Introduction

One of the forcings of the littoral sediment transport is the mean wave climate. In this Chapter, the mean wave climate - excluding hurricanes and tropical storms - along the Mississippi barrier islands is determined by means of wave transformation modeling. Below, the wave modeling strategy and results are presented.

In Section 5.2 the methodology for the wave modeling is discussed. The data set selection and validation are described in Section 5.3. The setup of the wave model is presented in Section 5.4. The model performance, calibration and results are described in Section 5.5, and in Section 5.6 the results are discussed.

5.2 Approach

In order to determine the mean wave climate along the Mississippi barrier islands, the known wave climate from an offshore location will be transformed to nearshore the islands. The transformation will be carried out by means of a hybrid approach to downscale offshore wave climates to coastal areas. This approach consists of the following three steps:

1 Schematization/classification - Characterization of the offshore climate using a number of scenarios.
2 Transformation - Reduced wave model computations (wave propagation modeling) using the defined scenarios.
3 Time series reconstruction - Determination of the relationships between offshore and nearshore parameters from the data for each scenario. Construction of the nearshore time series by transforming the offshore time series using the relationships found.

In order to retrieve a reliable wave climate, at least five years of data should be available. Several data sources were available for the determination of offshore wave and wind conditions. All available datasets were reviewed in order to select the most suitable dataset for the present wave modeling study. The selected dataset was validated, compared with available measurements and if required corrected. These steps and results are described in Section 5.3. The validated and corrected dataset is the basis for Step 1 above; the classification of the data into representative offshore wave and wind conditions.

From the wave propagation modeling, Step 2 above, nearshore wave heights, periods and directions are determined on the basis of offshore conditions. In this project the wave propagation modeling was carried out with the numerical modeling package Delft3D-WAVE, which is based on the SWAN wave model. SWAN is developed by the University of Delft and Deltares and includes all relevant wave processes such as refraction, shoaling and wave breaking. The SWAN wave model is regularly applied in wave propagation modeling all over the world. More information can be found on www.swan.tudelft.nl.

In the wave modeling, a nested modeling approach is followed, consisting of multiple computational grids in order to get detailed high resolution wave information in the project area. Within the modeling package Delft3D-Wave automated nesting facilities are available for the transfer of wave information between the different computational grids. In Section 5.4 the wave model setup is described.

On the basis of the wave propagation modeling results of the representative conditions, offshore wave time series can be transformed to local / nearshore time series, Step 3 above, using the Deltares in-house data analysis software ORCA (Van Os and Caires, 2011). Transformed time series were compared with available measurements nearshore on both climate and time series level. Based on this, the accuracy of the wave modeling results was determined and the wave model setup adjusted in order to improve the accuracy. In Section 5.5 the modeling results and the validation of the results are presented. Possible factors that influence the modeling results are discussed in Section 5.6.

Conclusions on the determination of the mean wave climate for the purpose of sediment transport modeling are drawn in Section 5.7

5.3 Data Analysis

5.3.1 Data source selection

The following available data sources were investigated for the wave modeling study:

- NDBC measured wave and wind data, available online at http://www.ndbc.noaa.gov/
- WIS hindcasted wave and wind data, available online at http://frf.usace.army.mil/wis2010/hindcasts.shtml?dmn=gom
- ERA-Interim reanalysis wave and wind data (http://www.ecmwf.int/research/era/do/get/era-interim), available online at http://data-portal.ecmwf.int/data/d/interim_daily/ (1.5 degrees resolution, research only). It has been purchased from ECMWF at a higher resolution (0.75 degrees)
- NCEP/NCAR reanalysis wind data, available online at http://www.cpc.ncep.noaa.gov/products/wesley/reanalysis.html

The different data sources were discussed in Section 3.5 From the initial data analysis, the ERA-Interim dataset was found to be the most suitable dataset as input for the wave climate study. The data validation and correction of the ERA-Interim against NDBC buoy data is presented below.

5.3.2 Data Validation and Correction

The NDBC and ERA-Interim data were quality checked in order to get reliable and consistent datasets, which can be used for data calibration/correction, model setup and validation of the modeling results. The quality control of the data was carried out before the comparison of the different datasets as presented in the previous section. The quality controls applied where the following:

1. Outliers in the significant wave height and wind speed time series were identified and removed. Outliers were identified as follows:
   - for deviations from the mean over a fixed period, $x_i - \overline{x} > crt_1 \cdot std(x)$, where $\overline{x} = \frac{1}{N}\sum_{i=1}^{N} x_i$, $std(x) = \sqrt{\frac{1}{N}\sum_{i=1}^{N}(x_i - \overline{x})^2}$, N is the number of records (in the period over which $\overline{x}$ and $std(x)$ are determined) and crt_1 the number of standard deviations a value can be allowed to deviate from the mean, for both the wind and wave data crt_1 was made equal to 6;
   - for deviations in magnitude from one time step to the next, $x_{i+1} - x_i > crt_2 \cdot std(x)$, where crt_2 is the number of standard deviations a value can be allowed to deviate from the previous. The criteria value crt_2 was set equal to 2 for wave data and 3 for wind speed data.

2. NaN values were synchronized, since if the observation of one variable is faulty the observations of the other variables at the same time are probably also faulty.

Following the data quality check, the ERA-Interim data are corrected on the basis of the measured NDBC data. Basis for the correction are the measured NDBC data at station 42040 and the ERA-Interim data at station location (lat,lon) = (272,29). Although the locations are approximately 30 km apart, they are both located in deep water where the wave conditions are not influenced by the depth or coast. This should result in similar conditions at both stations.

Based on a linear regression analysis, it was found that for different directional sectors and different wave height classes, different correction factors should be applied. The correction of the significant wave height ERA-Interim data was carried out as summarized in Table 5.1. As indicated in this table, a correction factor is only applied on the wave heights for offshore waves that propagate towards the Mississippi coast. The original and corrected wave heights are presented in Figure 5.1.

Directional sector	**Hs 0.0 – 0.5 m**	**Hs 0.5 – 1.0 m**	**Hs 1.0 – 1.5 m**	**Hs 1.5 – 2.0 m**	**Hs 1.5 – 2.0 m**	**Hs > 2.5 m**
315 – 75	1	1	1	1	1	1
75 – 165	1.05	1.15	1.15	1.15	1.15	1.15
165 – 225	1	1.1	1.2	1.2	1.2	1.2
225 - 315	1	1	1	1	1	1

Table 5.1 Correction factors for ECMWF wave heights based on a comparison with NDBC wave data.

The deviation in wave direction is less straightforward and difficult to correct. As indicated in the previous section, part of the deviation in wave directions depends on the definition of wave directions that is applied. The wave directions from NDBC are defined as *the directions for which the wave at the dominant periods are coming*. The wave directions from ECMWF data are defined as *the weighted average direction of the two dimensional wave spectrum*. The observed difference in wave directions is at least partly caused by the difference in these definitions. Therefore, it was decided not to apply a correction on wave directions.

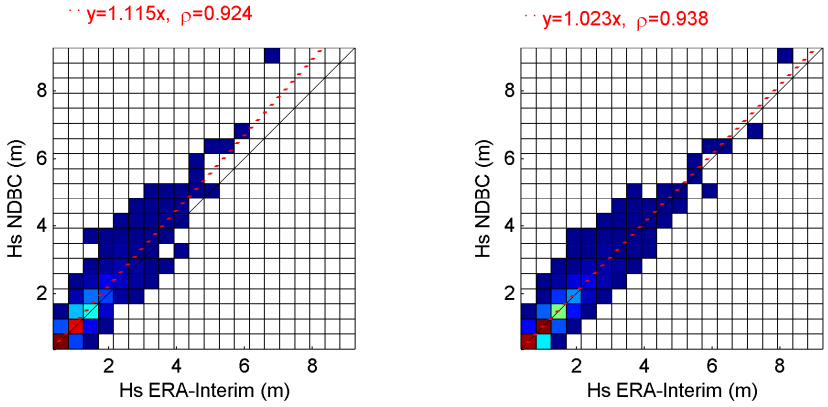

Figure 5.1 Scatter plots of ERA-Interim data at location (272,29) and NDBC data at station 42040; left original ERA-Interim data, right: corrected ERA-Interim data.

5.4 Model setup

5.4.1 Model area, bathymetry and grid

A nested wave modeling approach was adopted to transform the offshore wave conditions to nearshore. The computational domains are presented in Figure 5.2. Three computational grids were applied:

- Overall: to transform wave data from offshore to nearshore (resolution 1.5 x 1.5 km, in red)
- MCC: to provide wave conditions at the MCC domain (resolution approximately 250 x 100 m around Ship Island, in blue)
- Detailed: to provide detailed wave information around the barrier islands in the breaker zone (approximately 10 x 50 m around Ship Island, in black)

The boundaries of the overall domain correspond with the wave information locations of the ERA-Interim dataset, which are also indicated in Figure 5.2. The wind information available at all ERA data points is applied in the wave model for the specification of a spatial varying wind field[4].

The bathymetry for each computational domain is presented in Figure 5.3

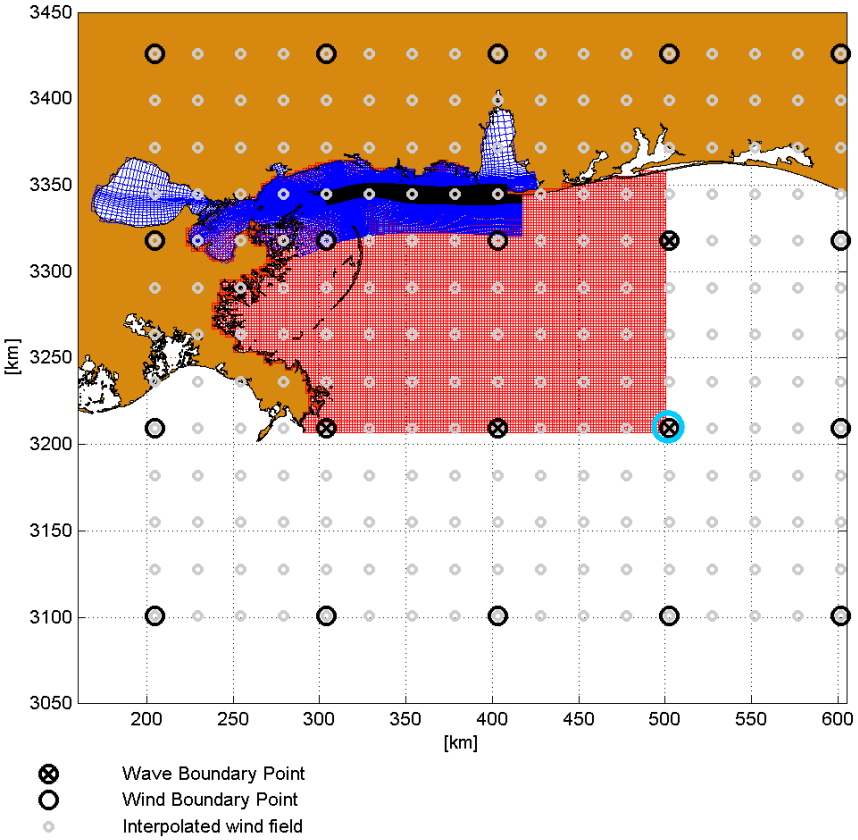

Figure 5.2 Computational domains for the wave model and wind and wave boundary points.

4. *The wave modeling was carried out with a spatially varying wind field, while for the flow modeling a uniform wind field was applied. For the wave modeling corresponding spatial wind information was available, while for the flow modeling period such information was not available. The wave model domain is considerably larger than the flow model domain. Therefore spatial variation in wind strength and –direction is more relevant in the wave model than in the smaller flow domain (MCC), warranting the application of a uniform wind field in the flow model.*

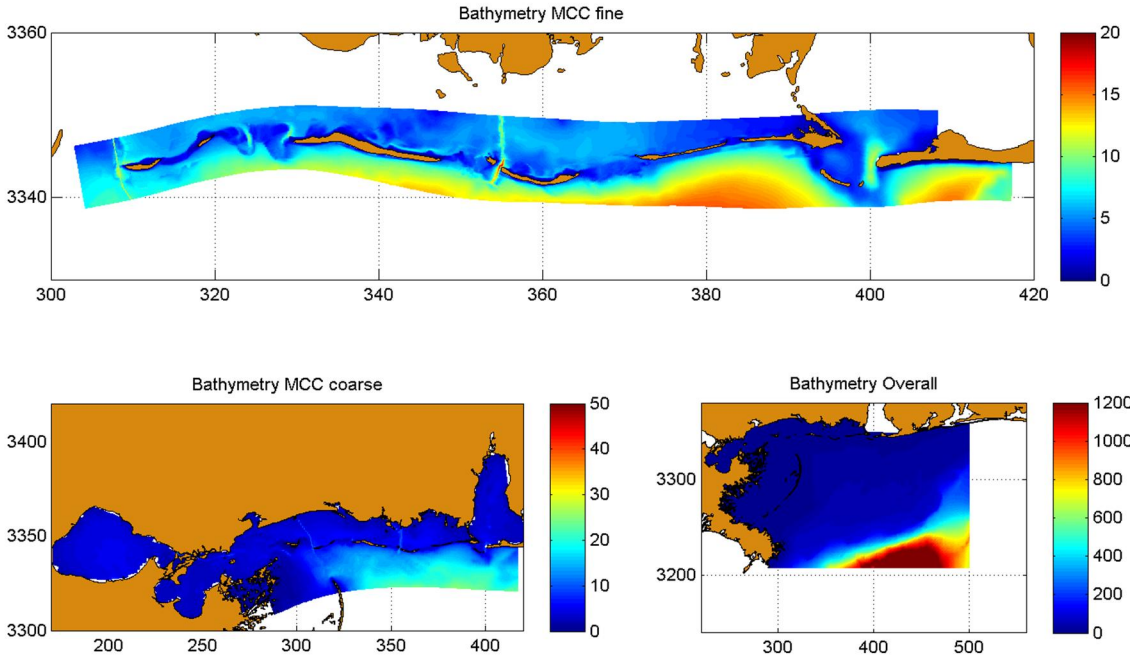

Figure 5.3 Bathymetry of the different computational domains used in the wave modeling.

5.4.2 Wave and wind boundary conditions

The ERA-Interim data described in Section 3.5 and 5.3 is used as the basis for the schematization of the normal wave boundary conditions. The boundary locations for the wave model are indicated in Figure 5.2. Wave and wind data of ERA-Interim were classified in order to get a set of representative wave and wind boundary conditions. The reference station for the classification was station (273,29) at the lower right corner of the computational domain. The classification was carried out for this station in the following way:

- All relevant tropical storms and hurricane conditions (e.g. all named storms in the area of interest) are removed from the dataset. The effect of hurricanes is studied separately, see Chapter 6. The events that were removed from the dataset are indicated in Table 5.2.
- A classification on the basis of Hs-Dir was carried out. A variable class definition was applied in order to get a higher resolution of classes for offshore wave directions that propagate towards the shore (i.e. southeasterly directions). The classes are indicated in Figure 5.4.

For each class, the average wind and wave condition at the reference station is computed based on all entries in the class. In this way, 165 conditions are identified based on bin sizes of 10ºdeg to 30ºdeg for the wave direction and 0.5 m for the wave height. A full wave and wind climate is subsequently formulated by binning all simultaneous occurring entries at the other ERA-Interim stations as well. In this way, the spatial coherence in wave and wind along the model boundaries is taken into account (i.e. prescription of spatially varying wave conditions on the model boundaries). See Table 5.3 for an overview of the binned wave climate.

	start			stop		
Name	**year**	**month**	**day**	**year**	**month**	**day**
Elena	1985	8	28	1985	9	4
Juan	1985	10	26	1985	11	1
Beryl	1988	8	8	1988	8	10
Florence	1988	9	7	1988	9	11
Andrew	1992	8	16	1992	8	28
Alberto	1994	6	30	1994	7	7
Beryl	1994	8	14	1994	8	19
Erin	1995	7	31	1995	8	6
Opal	1995	9	27	1995	10	6
Josephine	1996	10	4	1996	10	16
Danny	1997	7	16	1997	7	27
Earl	1998	8	31	1998	9	8
George	1998	9	15	1998	10	1
Helene	2000	9	15	2000	9	25
Allison	2001	6	5	2001	6	15
Barry	2001	8	2	2001	8	8
Bertha	2002	8	4	2002	8	9
Hanna	2002	9	12	2002	9	15
Isodore	2002	9	14	2002	9	27
Ivan	2004	9	2	2004	9	24
Arlene	2005	6	8	2005	6	14
Cindy	2005	7	3	2005	7	11
Dennis	2005	7	4	2005	7	18
Katrina	2005	8	23	2005	8	31
Fay	2008	8	15	2008	8	28
Gustav	2008	8	25	2008	9	5
Claudette	2009	8	16	2009	8	17
Ida	2009	11	4	2009	11	10
Bonnie	2010	7	22	2010	7	24

Table 5.2 Overview of hurricanes and tropical storms that have been removed from the ERA interim dataset (1989 – 2010) before classification.

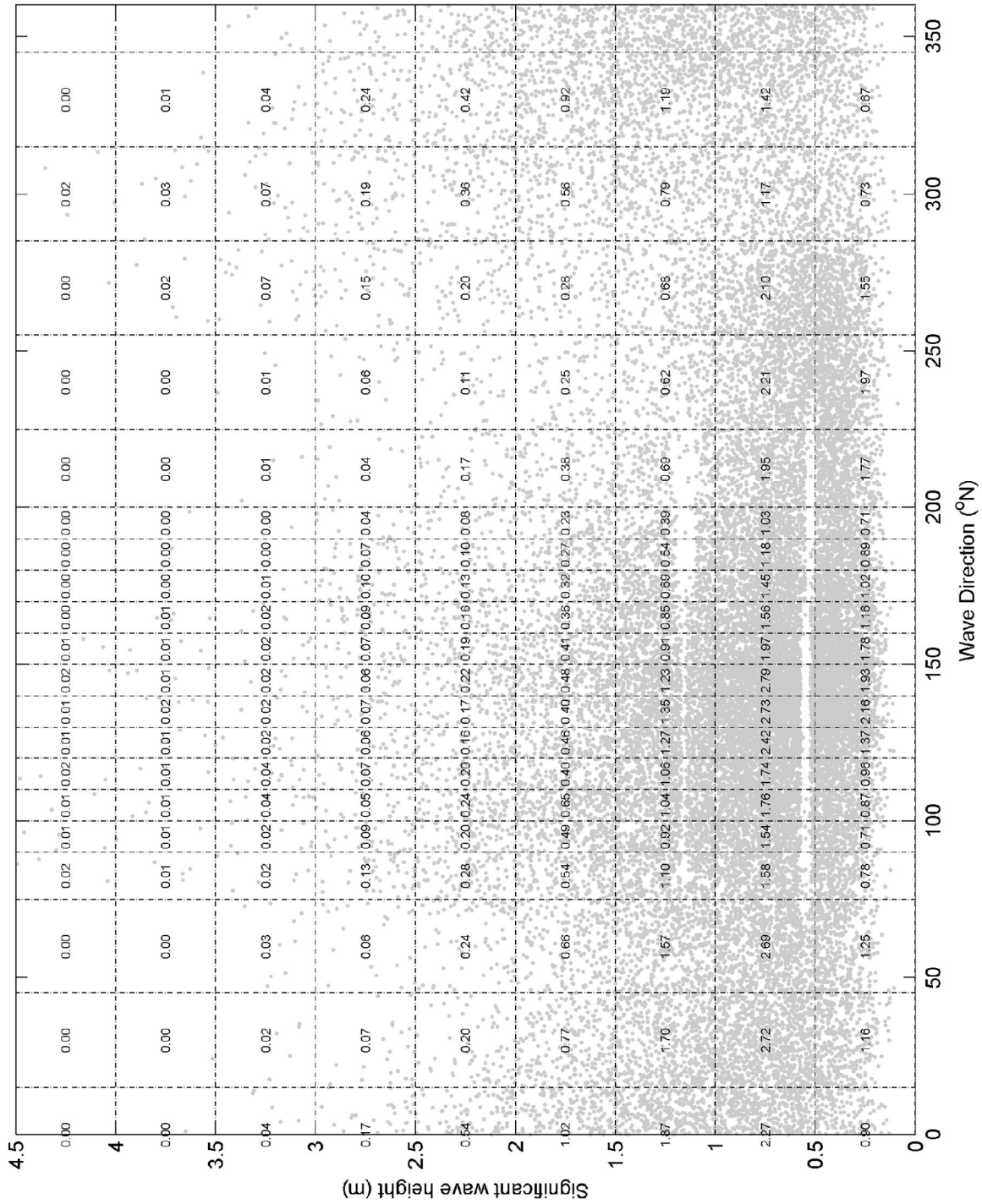

Figure 5.4 Hs-Dir classification of ERA-Interim wave data at the reference location (273,29), dots indicate the conditions; the numbers indicate the percentage of occurrence (total 100%).

Scenario	Class	Number of events	Duration (%)
1	345.0<Dir>15.0,0.0<Hs>0.5	281	0.8994
2	15.0<Dir>45.0,0.0<Hs>0.5	363	1.1618
3	45.0<Dir>75.0,0.0<Hs>0.5	392	1.2546
4	75.0<Dir>90.0,0.0<Hs>0.5	245	0.7842
5	90.0<Dir>100.0,0.0<Hs>0.5	221	0.7073
6	100.0<Dir>110.0,0.0<Hs>0.5	273	0.8738
7	110.0<Dir>120.0,0.0<Hs>0.5	301	0.9634
8	120.0<Dir>130.0,0.0<Hs>0.5	429	1.3731
9	130.0<Dir>140.0,0.0<Hs>0.5	674	2.1572
10	140.0<Dir>150.0,0.0<Hs>0.5	604	1.9332
11	150.0<Dir>160.0,0.0<Hs>0.5	555	1.7763
12	160.0<Dir>170.0,0.0<Hs>0.5	362	1.1586
13	170.0<Dir>180.0,0.0<Hs>0.5	320	1.0242
14	180.0<Dir>190.0,0.0<Hs>0.5	277	0.8866
15	190.0<Dir>200.0,0.0<Hs>0.5	221	0.7073
16	200.0<Dir>225.0,0.0<Hs>0.5	553	1.7699
17	225.0<Dir>255.0,0.0<Hs>0.5	617	1.9748
18	255.0<Dir>285.0,0.0<Hs>0.5	483	1.5459
19	285.0<Dir>315.0,0.0<Hs>0.5	228	0.7297
20	315.0<Dir>345.0,0.0<Hs>0.5	210	0.6721
21	345.0<Dir>15.0,0.5<Hs>1.0	708	2.266
22	15.0<Dir>45.0,0.5<Hs>1.0	849	2.7173
23	45.0<Dir>75.0,0.5<Hs>1.0	840	2.6917
24	75.0<Dir>90.0,0.5<Hs>1.0	494	1.5811
25	90.0<Dir>100.0,0.5<Hs>1.0	480	1.5395
26	100.0<Dir>110.0,0.5<Hs>1.0	550	1.7603
27	110.0<Dir>120.0,0.5<Hs>1.0	544	1.7411
28	120.0<Dir>130.0,0.5<Hs>1.0	755	2.4197
29	130.0<Dir>140.0,0.5<Hs>1.0	852	2.7301
30	140.0<Dir>150.0,0.5<Hs>1.0	870	2.7877
31	150.0<Dir>160.0,0.5<Hs>1.0	616	1.9716
32	160.0<Dir>170.0,0.5<Hs>1.0	487	1.5587
33	170.0<Dir>180.0,0.5<Hs>1.0	452	1.4499
34	180.0<Dir>190.0,0.5<Hs>1.0	369	1.181
35	190.0<Dir>200.0,0.5<Hs>1.0	323	1.0338
36	200.0<Dir>225.0,0.5<Hs>1.0	609	1.9492
37	225.0<Dir>255.0,0.5<Hs>1.0	692	2.2148
38	255.0<Dir>285.0,0.5<Hs>1.0	656	2.0996
39	285.0<Dir>315.0,0.5<Hs>1.0	366	1.1714
40	315.0<Dir>345.0,0.5<Hs>1.0	445	1.4243
41	345.0<Dir>15.0,1.0<Hs>1.5	585	1.8724
42	15.0<Dir>45.0,1.0<Hs>1.5	530	1.6963
43	45.0<Dir>75.0,1.0<Hs>1.5	492	1.5747
44	75.0<Dir>90.0,1.0<Hs>1.5	344	1.101
45	90.0<Dir>100.0,1.0<Hs>1.5	287	0.9186
46	100.0<Dir>110.0,1.0<Hs>1.5	324	1.037
47	110.0<Dir>120.0,1.0<Hs>1.5	330	1.0562
48	120.0<Dir>130.0,1.0<Hs>1.5	398	1.2738
49	130.0<Dir>140.0,1.0<Hs>1.5	421	1.3507
50	140.0<Dir>150.0,1.0<Hs>1.5	382	1.2258
51	150.0<Dir>160.0,1.0<Hs>1.5	283	0.909
52	160.0<Dir>170.0,1.0<Hs>1.5	265	0.8546
53	170.0<Dir>180.0,1.0<Hs>1.5	215	0.6881
54	180.0<Dir>190.0,1.0<Hs>1.5	167	0.5377
55	190.0<Dir>200.0,1.0<Hs>1.5	122	0.3905
56	200.0<Dir>225.0,1.0<Hs>1.5	214	0.6881
57	225.0<Dir>255.0,1.0<Hs>1.5	195	0.6241
58	255.0<Dir>285.0,1.0<Hs>1.5	212	0.6785
59	285.0<Dir>315.0,1.0<Hs>1.5	248	0.7938
60	315.0<Dir>345.0,1.0<Hs>1.5	372	1.1906
61	345.0<Dir>15.0,1.5<Hs>2.0	320	1.0242
62	15.0<Dir>45.0,1.5<Hs>2.0	241	0.7713
63	45.0<Dir>75.0,1.5<Hs>2.0	205	0.6561
64	75.0<Dir>90.0,1.5<Hs>2.0	169	0.5409
65	90.0<Dir>100.0,1.5<Hs>2.0	154	0.4929
66	100.0<Dir>110.0,1.5<Hs>2.0	204	0.6529
67	110.0<Dir>120.0,1.5<Hs>2.0	123	0.3969
68	120.0<Dir>130.0,1.5<Hs>2.0	143	0.4577
69	130.0<Dir>140.0,1.5<Hs>2.0	126	0.4033
70	140.0<Dir>150.0,1.5<Hs>2.0	146	0.4769
71	150.0<Dir>160.0,1.5<Hs>2.0	128	0.4129
72	160.0<Dir>170.0,1.5<Hs>2.0	113	0.3617
73	170.0<Dir>180.0,1.5<Hs>2.0	100	0.3201
74	180.0<Dir>190.0,1.5<Hs>2.0	82	0.2657
75	190.0<Dir>200.0,1.5<Hs>2.0	71	0.2272
76	200.0<Dir>225.0,1.5<Hs>2.0	119	0.3809
77	225.0<Dir>255.0,1.5<Hs>2.0	78	0.2496
78	255.0<Dir>285.0,1.5<Hs>2.0	89	0.2849
79	285.0<Dir>315.0,1.5<Hs>2.0	175	0.5601
80	315.0<Dir>345.0,1.5<Hs>2.0	288	0.9218
81	345.0<Dir>15.0,2.0<Hs>2.5	170	0.5441
82	15.0<Dir>45.0,2.0<Hs>2.5	62	0.1984
83	45.0<Dir>75.0,2.0<Hs>2.5	76	0.2432
84	75.0<Dir>90.0,2.0<Hs>2.5	86	0.2753
85	90.0<Dir>100.0,2.0<Hs>2.5	60	0.1952
86	100.0<Dir>110.0,2.0<Hs>2.5	73	0.2368
87	110.0<Dir>120.0,2.0<Hs>2.5	63	0.2016
88	120.0<Dir>130.0,2.0<Hs>2.5	49	0.1568
89	130.0<Dir>140.0,2.0<Hs>2.5	51	0.1664
90	140.0<Dir>150.0,2.0<Hs>2.5	67	0.2176
91	150.0<Dir>160.0,2.0<Hs>2.5	58	0.1856
92	160.0<Dir>170.0,2.0<Hs>2.5	48	0.1568
93	170.0<Dir>180.0,2.0<Hs>2.5	42	0.1344
94	180.0<Dir>190.0,2.0<Hs>2.5	32	0.1024
95	190.0<Dir>200.0,2.0<Hs>2.5	24	0.0768
96	200.0<Dir>225.0,2.0<Hs>2.5	52	0.1696
97	225.0<Dir>255.0,2.0<Hs>2.5	32	0.1056
98	255.0<Dir>285.0,2.0<Hs>2.5	64	0.2048
99	285.0<Dir>315.0,2.0<Hs>2.5	113	0.3617
100	315.0<Dir>345.0,2.0<Hs>2.5	130	0.4161
101	345.0<Dir>15.0,2.5<Hs>3.0	53	0.1696
102	15.0<Dir>45.0,2.5<Hs>3.0	21	0.0672
103	45.0<Dir>75.0,2.5<Hs>3.0	20	0.064
104	75.0<Dir>90.0,2.5<Hs>3.0	40	0.128
105	90.0<Dir>100.0,2.5<Hs>3.0	29	0.0928
106	100.0<Dir>110.0,2.5<Hs>3.0	16	0.0512
107	110.0<Dir>120.0,2.5<Hs>3.0	23	0.0736
108	120.0<Dir>130.0,2.5<Hs>3.0	19	0.064
109	130.0<Dir>140.0,2.5<Hs>3.0	23	0.0736
110	140.0<Dir>150.0,2.5<Hs>3.0	18	0.0576
111	150.0<Dir>160.0,2.5<Hs>3.0	21	0.0704
112	160.0<Dir>170.0,2.5<Hs>3.0	27	0.0864
113	170.0<Dir>180.0,2.5<Hs>3.0	29	0.096
114	180.0<Dir>190.0,2.5<Hs>3.0	22	0.0736
115	190.0<Dir>200.0,2.5<Hs>3.0	11	0.0384
116	200.0<Dir>225.0,2.5<Hs>3.0	11	0.0352
117	225.0<Dir>255.0,2.5<Hs>3.0	18	0.0608
118	255.0<Dir>285.0,2.5<Hs>3.0	47	0.1504
119	285.0<Dir>315.0,2.5<Hs>3.0	60	0.192
120	315.0<Dir>345.0,2.5<Hs>3.0	75	0.24
121	345.0<Dir>15.0,3.0<Hs>3.5	12	0.0384
122	15.0<Dir>45.0,3.0<Hs>3.5	5	0.016
123	45.0<Dir>75.0,3.0<Hs>3.5	9	0.0288
124	75.0<Dir>90.0,3.0<Hs>3.5	7	0.0224
125	90.0<Dir>100.0,3.0<Hs>3.5	7	0.0224
126	100.0<Dir>110.0,3.0<Hs>3.5	11	0.0352
127	110.0<Dir>120.0,3.0<Hs>3.5	14	0.0448
128	120.0<Dir>130.0,3.0<Hs>3.5	6	0.0192
129	130.0<Dir>140.0,3.0<Hs>3.5	4	0.016
130	140.0<Dir>150.0,3.0<Hs>3.5	5	0.016
131	150.0<Dir>160.0,3.0<Hs>3.5	7	0.0224
132	160.0<Dir>170.0,3.0<Hs>3.5	6	0.0192
133	170.0<Dir>180.0,3.0<Hs>3.5	3	0.0096
134	190.0<Dir>200.0,3.0<Hs>3.5	1	0.0032
135	200.0<Dir>225.0,3.0<Hs>3.5	4	0.0128
136	225.0<Dir>255.0,3.0<Hs>3.5	3	0.0096
137	255.0<Dir>285.0,3.0<Hs>3.5	21	0.0672
138	285.0<Dir>315.0,3.0<Hs>3.5	23	0.0736
139	315.0<Dir>345.0,3.0<Hs>3.5	13	0.0416
140	345.0<Dir>15.0,3.5<Hs>4.0	1	0.0032
141	15.0<Dir>45.0,3.5<Hs>4.0	1	0.0032
142	75.0<Dir>90.0,3.5<Hs>4.0	4	0.0128
143	90.0<Dir>100.0,3.5<Hs>4.0	2	0.0064
144	100.0<Dir>110.0,3.5<Hs>4.0	3	0.0096
145	110.0<Dir>120.0,3.5<Hs>4.0	3	0.0096
146	120.0<Dir>130.0,3.5<Hs>4.0	4	0.0128
147	130.0<Dir>140.0,3.5<Hs>4.0	5	0.016
148	140.0<Dir>150.0,3.5<Hs>4.0	4	0.0128
149	150.0<Dir>160.0,3.5<Hs>4.0	3	0.0096
150	160.0<Dir>170.0,3.5<Hs>4.0	4	0.0128
151	180.0<Dir>190.0,3.5<Hs>4.0	1	0.0032
152	190.0<Dir>200.0,3.5<Hs>4.0	1	0.0032
153	255.0<Dir>285.0,3.5<Hs>4.0	5	0.016
154	285.0<Dir>315.0,3.5<Hs>4.0	10	0.032
155	315.0<Dir>345.0,3.5<Hs>4.0	2	0.0064
156	75.0<Dir>90.0,4.0<Hs>Inf	5	0.016
157	90.0<Dir>100.0,4.0<Hs>Inf	4	0.0128
158	100.0<Dir>110.0,4.0<Hs>Inf	2	0.0064
159	110.0<Dir>120.0,4.0<Hs>Inf	5	0.016
160	120.0<Dir>130.0,4.0<Hs>Inf	4	0.0128
161	130.0<Dir>140.0,4.0<Hs>Inf	2	0.0064
162	140.0<Dir>150.0,4.0<Hs>Inf	5	0.016
163	150.0<Dir>160.0,4.0<Hs>Inf	3	0.0096
164	255.0<Dir>285.0,4.0<Hs>Inf	1	0.0032
165	285.0<Dir>315.0,4.0<Hs>Inf	5	0.016

Table 5.3 Binned wave climate.

5.4.3 Initial Model settings

Initially, the following parameter settings were applied in the wave model:

Wave spectrum

- At the wave model boundary a JONSWAP spectrum with a peak enhancement factor of 3.3 is assumed.
- At the wave model boundary, a directional spreading of approximately 25ºdeg (power function, with power = 4) is assumed.

Physical parameters

(see http://swanmodel.sourceforge.net/online_doc/swanuse/node28.html)

- Third-generation mode for wind growth, quadruplet interactions and whitecapping, with wind growth and whitecapping according to the Westhuizen option.
- Constant depth induced breaking ($\alpha = 1$, $\gamma = 0.73$)
- Constant JONSWAP bottom friction (friction coefficient = 0.067 m^2s^{-3})[5]
- No non-linear triad interactions
- No diffraction

Numerical parameters

- Extension of the frequency space: from 0.03 to 2.5 Hz divided over 43 bins. The directional space was kept default with 36 bins of 10 degrees
- Accuracy:
    - Relative change Hs-Tm01: 0.01
    - Relative change Hs with respect to mean: 0.01
    - Relative change Tm01 with respect to mean: 0.01
    - Percentage of wet points: 99%
    - Maximum number of iterations: 50
    - Alpha: 0.001

5.5 Model results, performance and calibration

5.5.1 Initial modeling results

The initial modeling results are illustrated in Figure 5.5 for one of the 165 conditions that were modeled with the wave model SWAN. Comparable plots are made (not presented) for each condition in order to verify the wave modeling results. The processes of refraction, wave energy dissipation due to bottom friction and breaking, wave blocking by the islands and wave penetration into Mississippi Sound can be observed in the figure. Furthermore, it can be seen that the nesting of the different computational domains was correctly implemented. On the basis of this analysis it was concluded that the processes and boundary conditions were included in a correct way in the SWAN wave model.

5. *The bottom friction is computed based on the empirical model of JONSWAP (Hasselmann et al., 1973). The coefficient of the JONSWAP formulation is set at 0.067 m2/s3, which is a typical value for wind sea.*

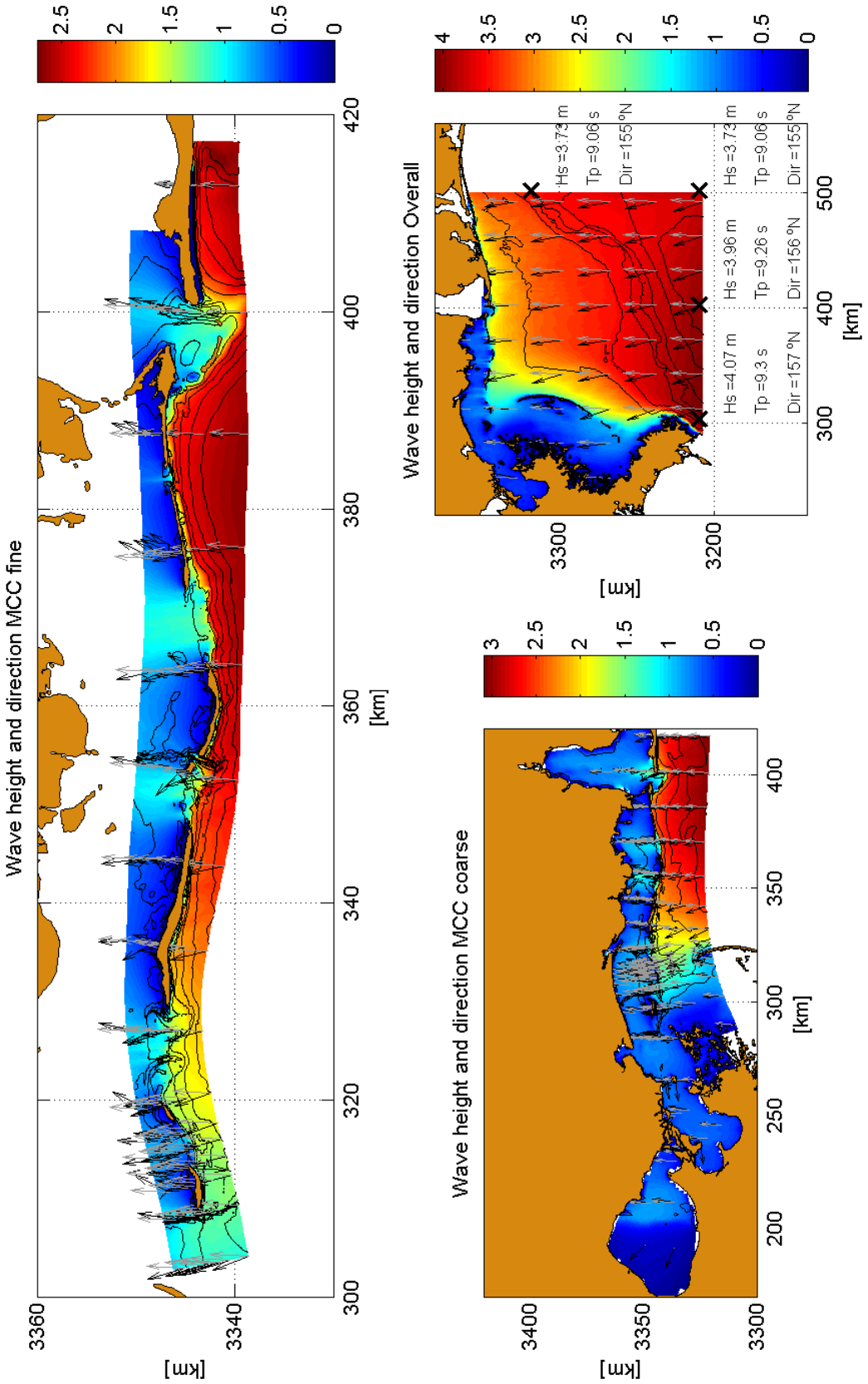

Figure 5.5 Example of computed wave heights and directions for the different computational domains. Grey arrows: wind vectors, black arrows: wave vectors.

5.5.2 Model performance

To assess the quality of the wave transformation with the initial model settings, transformed time series, based on the computations, are compared to measurements at the NDBC buoys 42040 (offshore) and 42007 (nearshore) for the period 2001-2008. The climates are compared qualitatively by means of wave roses in Figure 5.6. It can be observed that the modeled wave directions come more from the southeast while the measured wave directions come more from the east. This is true for both station 42040 (offshore) and station 42007 (nearshore). Furthermore, the wave height roses indicate that the higher wave heights in the measured wave climates are missing in the modeled wave climates.

Scatter plots for H_s, T_p and Dir provide a more quantitative insight in the agreement between the model results and measurements (see Figure 5.7). Here we focus especially on the waves coming from offshore directions (85ºN-185ºN), since these conditions are most important for the sediment transports near Ship Island. The results for wave heights are in line with what was observed from the wave height roses; there is a severe underestimation of Hs, which is largest at the nearshore station. The peak periods and wave directions are modeled relatively well.

The linear fit through the data provides an indication of the deviation between the measurements and the modeling results. It can be observed that the initial modeled significant wave heights deviate from the measurements by approximately 29% at station 42007 and 21% at station 42040. Further improvement in model results is therefore required.

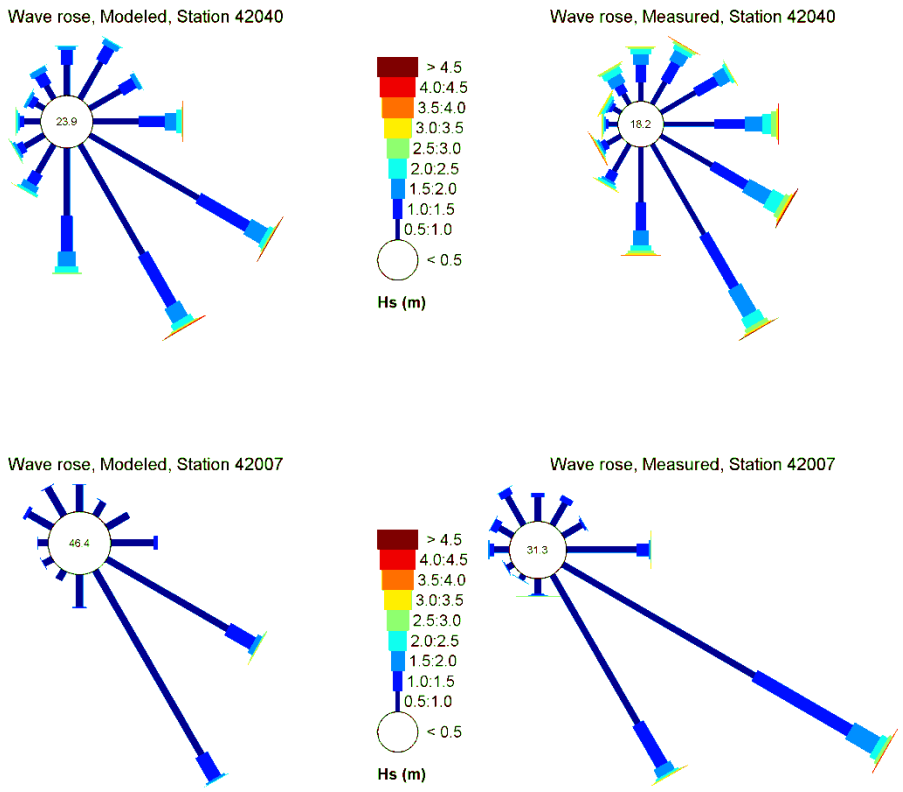

Figure 5.6 Comparison of modeled and observed (NDBC) wave height roses at station 42020 (offshore location, see Figure 3.6) and station 42007 (nearshore location, see Figure 3.6).

5.5.3 Model calibration

In Table 5.4, statistical results are presented for several model settings that were tested in the model calibration phase.

In Section 5.3.1, it was found that the ERA-Interim wind speeds match the observed wind speeds at offshore locations very well. From further analysis, however, it is now found that the nearshore wind speeds in the ERA-Interim data set are much lower than measured nearshore wind speeds. As a first step to improve the model results with respect to the measurements, a uniform (offshore) wind instead of a space-varying wind is therefore applied. This modification results in a better model performance (see Table 5.4), especially at the nearshore buoy location (42007). Additionally, a different formulation for the third-generation mode for wind input, quadruplets and white capping (as advised by Rogers et al. (2003) instead of the default SWAN Westhuizen option) and a decreased bottom friction coefficient (0.038 m^2s^{-3} instead of 0.067 m^2s^{-3}, leading to lower wave energy dissipation) lead to further improvement of the model results. The final modeled significant wave heights show an underestimation of approximately 8% (symmetric slope of 0.92) and a correlation coefficient of 0.84 with respect to the nearshore measurements (Scenario 4 in Table 5.4).

In the model calibration phase, the effects of a different classification approach were also investigated. Instead of a classification based on wave height and wave direction (Hs-Dir), a classification based on wind speed and wind direction (U10-Udir) was tested. This modification leads to better agreement between the modeled and measured Hs (scenario 5 to 7 in Table 5.4), suggesting that the schematization of the wind climate is important for the accuracy in the modeled nearshore wave heights. A symmetric slope of 1.01 and a correlation coefficient of 0.84 is found for Scenario 7. Note that the nearshore correlation coefficient and the RMSE do not improve compared to the Hs-Dir classification. Furthermore it can be observed that the agreement in wave directions with the U10-Udir classification does not improve compared to the Hs-Dir classification and that the bias in directions actually becomes larger.

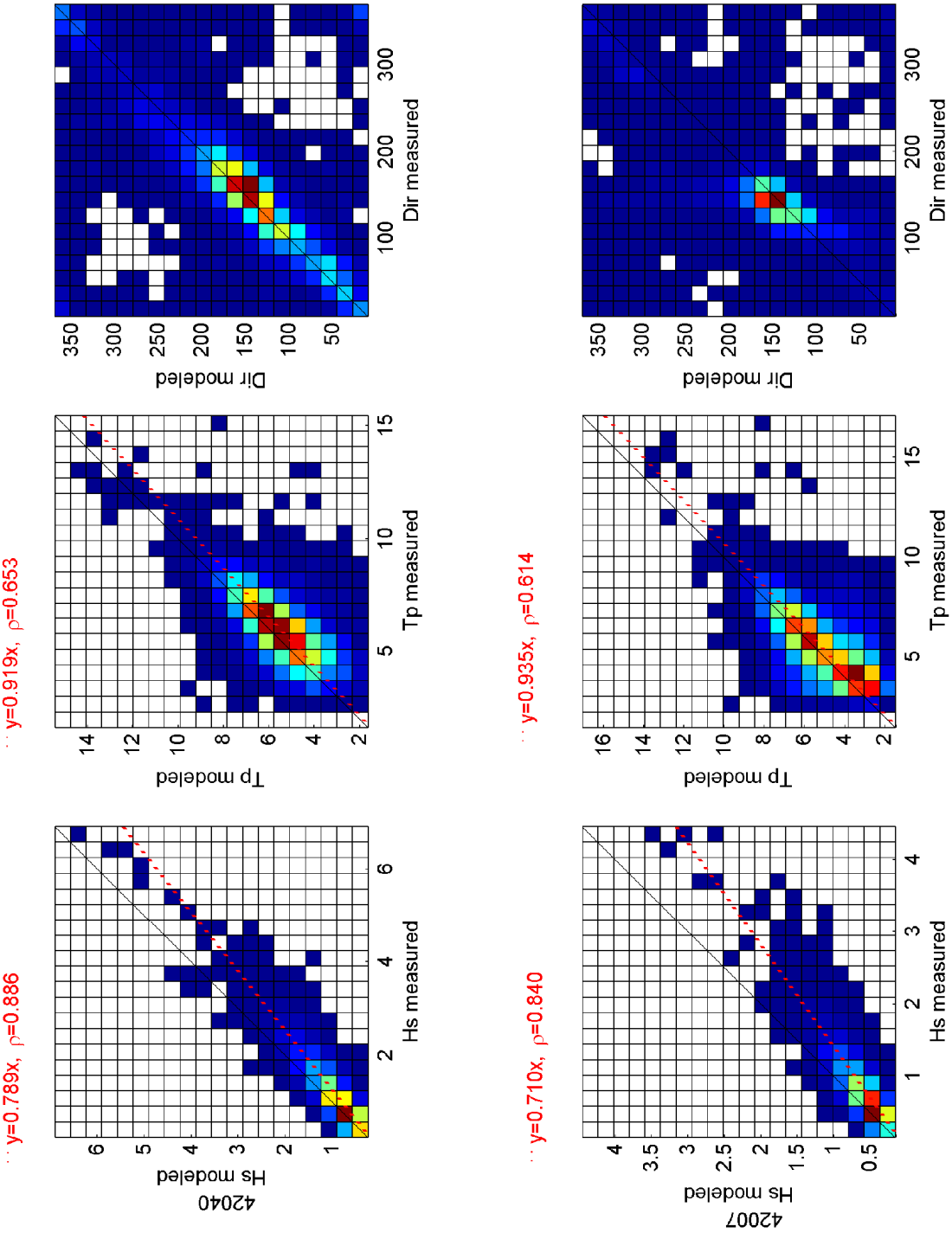

Figure 5.7 Scatter plots of modeled versus measured wave data. Upper panels: NDBC station 42040, lower panels: NDBC station 42007 (see Figure 3.6 for locations of wave stations).

Error Statistics for different modeling scenarios

Scenario 1	Hs-Dir Classification
Scenario 2	As Scenario 1, with Uniform wind
Scenario 3	As Scenario 2, with Rogers
Scenario 4	As Scenario 3, with reduced bed roughness
Scenario 5	U10-Udir Classification
Scenario 6	As Scenario 5, with Rogers
Scenario 7	As Scenario 6, with reduced bed roughness

	Period 2001-2008 42040 Hs-Dir				**U10-Udir**			**42007 Hs-Dir**				**U10-Udir**		
Scenario	1	2	3	4	5	6	7	1	2	3	4	5	6	7
Hs														
Mean measured	1.03	1.03	1.03	1.03	1.03	1.03	1.03	0.68	0.68	0.68	0.68	0.67	0.67	0.67
Mean model	0.83	0.85	0.89	0.89	0.89	0.94	0.94	0.49	0.57	0.61	0.63	0.62	0.66	0.68
Bias	-0.2	-0.17	-0.14	-0.14	-0.13	-0.09	-0.09	-0.18	-0.11	-0.06	-0.04	-0.06	-0.01	0
RMSE	0.38	0.32	0.29	0.29	0.28	0.26	0.26	0.3	0.25	0.23	0.23	0.23	0.23	0.23
Scatter Index	31.26	26.63	25.29	25.21	24.48	23.64	23.6	34.94	32.98	33.45	33.03	33.43	33.62	34.06
Symmetric Slope	0.79	0.82	0.85	0.85	0.87	0.91	0.91	0.71	0.83	0.88	0.92	0.92	0.97	1.01
Correlation Coefficient	0.89	0.92	0.93	0.93	0.93	0.93	0.93	0.84	0.84	0.84	0.84	0.84	0.84	0.84
Tp														
Mean measured	5.66	5.66	5.66	5.66	5.66	5.66	5.66	5.06	5.06	5.06	5.06	5.05	5.05	5.05
Mean model	5.16	5.19	5.23	5.23	5.44	5.43	5.43	4.66	4.65	4.6	4.73	4.67	4.79	4.88
Bias	-0.5	-0.47	-0.43	-0.43	-0.22	-0.23	-0.23	-0.4	-0.41	-0.46	-0.33	-0.38	-0.26	-0.18
RMSE	1.3	1.25	1.21	1.21	1.11	1.11	1.11	1.51	1.47	1.49	1.44	1.4	1.33	1.31
Scatter Index	21.19	20.43	20	19.97	19.14	19.11	19.11	28.79	27.92	28.12	27.71	26.59	25.87	25.69
Symmetric Slope	0.92	0.92	0.93	0.93	0.96	0.96	0.96	0.94	0.93	0.92	0.94	0.92	0.94	0.96
Correlation Coefficient	0.65	0.67	0.68	0.68	0.71	0.7	0.7	0.61	0.6	0.61	0.62	0.6	0.64	0.65
Dir														
Mean measured	130.06	130.1	130.1	130.1	130.16	130.16	130.16	126.39	126.41	126.41	126.41	126.45	126.45	126.45
Mean model	126.45	123.56	122.81	122.81	119.27	117.92	117.88	133.19	125.82	126.14	126.18	120.82	121.35	121.41
Bias	-3.6	-6.55	-7.29	-7.29	-10.89	-12.24	-12.28	6.8	-0.59	-0.27	-0.23	-5.63	-5.1	-5.04
RMSE	39.66	38.07	38.01	38.03	38.78	38.85	38.87	47.51	45.03	45.26	45.17	45.81	45.62	45.6
Scatter Index	6.44	6.62	6.51	6.53	6.69	6.86	6.87	6.72	6.31	6.22	6.28	6.55	6.38	6.34
Symmetric Slope	-	-	-	-	-	-	-	-	-	-	-	-	-	-
Correlation Coefficient	0.67	0.69	0.69	0.69	0.68	0.68	0.68	0.5	0.54	0.53	0.54	0.52	0.53	0.53

Table 5.4 Overview of deviation between modeled and measured wave parameters for different modeling scenarios at NDBC station 42040 (offshore location, see Figure 3.6).

5.5.4 Selected wave model settings

Based on the findings in Section 5.5.3 the settings advised by Rogers et al. (2003) were applied and the bottom friction coefficient was decreased to 0.038 (scenario 4 above).

Section 5.5.3 also indicates that the U10-Udir classification leads to more accurate significant wave heights compared to the Hs-Dir classification. The deviation in wave heights for the U10-Udir classification at station 42007 (nearshore) is 1%, while the deviation for the Hs-Dir classification is 8%. The nearshore correlation coefficient and the RMSE for the significant wave heights are not improved with the U10-Udir classification. The resulting wave peak period for both classification methods give comparable error statistics when comparing the results with buoy measurements. The modeled wave directions with the Hs-Dir classification show a slightly better match with the measured wave directions for both the offshore (42040) and nearshore (42007) locations compared to the U10-Udir classification.

It is not fully understood why the U10-Udir classification gives better results with respect to the measured significant wave heights. Looking to the layout of the area of interest it is expected that the offshore waves are dominant in the wave climate. Therefore, a Hs-Dir classification at the offshore boundary would result in better results compared to a U10-Udir classification. It is also not fully clear why the Hs-Dir classification results in an underestimation of the significant wave heights, which is already observed at the offshore wave measurement location (station 42040). Possibly, this may be related to a swell component; issues that may influence the deviation in wave modeling results and measurements are further discussed in Chapter 6.

For the sediment modeling study the results of the Hs-Dir classification were applied for reasons described below.

Although the deviation between the wave modeling results for the Hs-Dir classification and the measurements are larger compared to the U10-Udir classification, the deviation is still small and acceptable from a modeling point of view. Furthermore the Hs-Dir classification resulted in a lower RMSE and higher correlation for wave directions. Considering only the wave periods and directions, the model performance of both classification methods are comparable.

It is expected that the deviation between the wave modeling results and the measurements for the Hs-Dir classification are related to the spectral shape, which is only partly reproduced by the spectral wave forcing at the boundary of the model.

When applying the wave modeling results in the sediment modeling study the deviation between the wave measurements and modeling results are taken into account by studying the sensitivity of the computed transports to increased wave heights.

5.6 Discussion

5.6.1 General

From the results it became clear that the modeled wave heights are significantly lower than the measured wave heights. Although improvements were achieved during the wave model calibration/validation process, the underestimation of the wave heights was not fully resolved. Furthermore, a deviation in wave direction still existed. Several issues may play a role in the deviation between the measured and modeled wave heights. These issues are discussed in the following sections.

5.6.2 Influence of period on error statistics

In the previous chapter a comparison was made between the modeling results and the measurements on the basis of error statistics. It was observed that the statistics are sensitive to the period for which statistics are drawn. The statistics for three different periods and both classification methods at nearshore station 42007 are indicated in Table 5.5. A variation of 2% to 3% in the symmetric slope can be observed. The model performance of the Hs-Dir classification for the period 2007-2008 is comparable to the model performance of the U10-Udir classification. This supports the selection of the Hs-Dir classification instead of the U10-Udir classification.

Location	**42007**				**42007**		
Classification method	**Hs-Dir**				**U10-Udir**		
Period	2001 - 2008	2001 - 2002	2007 - 2008		2001 - 2008	2001 - 2002	2007 - 2008
Hs							
Mean measured	0.68	0.64	0.75		0.67	0.64	0.74
Mean model	0.63	0.59	0.72		0.68	0.64	0.77
Bias	-0.04	-0.05	-0.03		0	-0.01	0.03
RMSE	0.23	0.22	0.22		0.23	0.22	0.23
Scatter Index	33.03	33.04	29.33		34.06	34.79	30.8
Symmetric Slope	0.92	0.92	0.94		1.01	1.01	1.04
Correlation Coefficient	0.84	0.84	0.86		0.84	0.85	0.85
Tp							
Mean measured	5.06	4.93	5.32		5.05	4.93	5.31
Mean model	4.73	4.49	4.96		4.88	4.66	5.12
Bias	-0.33	-0.43	-0.35		-0.18	-0.27	-0.19
RMSE	1.44	1.37	1.43		1.31	1.22	1.31
Scatter Index	27.71	26.33	26.02		25.69	24.19	24.41
Symmetric Slope	0.94	0.92	0.94		0.96	0.94	0.96
Correlation Coefficient	0.62	0.65	0.65		0.65	0.68	0.67
Dir							
Mean measured	126.41	121.65	127.48		126.45	121.74	127.56
Mean model	126.18	123.92	121.04		121.41	119.14	117.85
Bias	-0.23	2.26	-6.44		-5.04	-2.61	-9.72
RMSE	45.17	43.04	41.96		45.6	43.24	42.23
Scatter Index	6.28	6.45	6.26		6.34	6.47	6.13
Symmetric Slope	-	-	-		-	-	-
Correlation Coefficient	0.54	0.58	0.56		0.53	0.58	0.55

Table 5.5 Influence of period on the error statistics at NDBC station 42007 (nearshore location, see Figure 3.6).

5.6.3 Comparison with measurements at Ship Island

Wave measurements at Ship Island were carried out between March – July 2010. The stations at which the data were collected are indicated in Figure 5.8. The error statistics for the month April 2010 at these two stations for both classification methods are provided in Table 5.6. The modeling results are based on the transformation of the offshore wave time series of ERA-Interim station (272,29) to the nearshore Gulf and Sound gage. It can be observed that the model performance at the Gulf side is better compared to the model performance at the Sound side. Overall the error statistics show a larger deviation between the modeling results and the measurements compared to the deviation at NDBC measurement station 42040 and 42007.

The time series comparison for the month April 2010 is presented in Figure 5.9 and Figure 5.10 for the Gulf and Sound Gage, respectively. In the measurements a daily pattern is visible in wave heights, wave peak periods and wave directions at both stations. This daily pattern cannot be observed in the modeling results. The pattern may be induced by the tidal water levels and currents. As this is not included in the wave modeling, the pattern is not reproduced by the modeling results. This is one of the causes of weak error statistics for these stations.

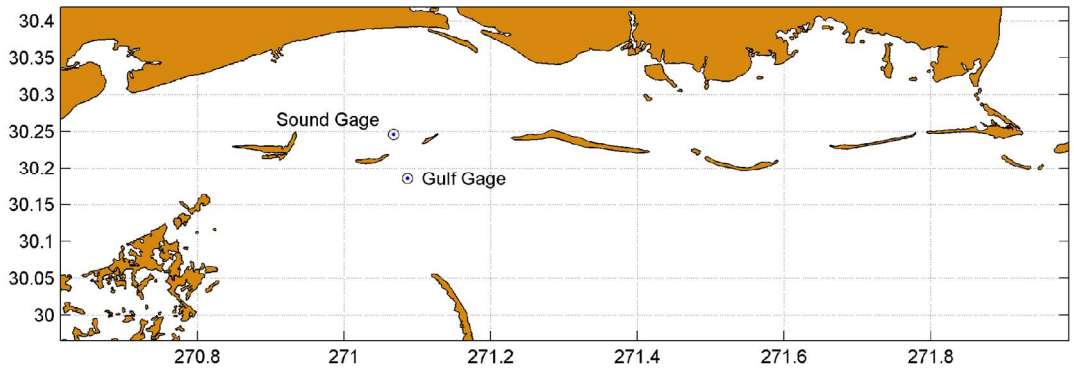

Figure 5.8 Wave measurement stations around Ship Island.

The general patterns in measured wave heights, wave peak periods and wave directions are well reproduced at both stations by the modeling results. The wave heights at the sound side are depth limited and the water levels will determine to a large extent the wave heights. For the sediment transport computations the tidal variation in water levels and currents is included.

The RMSE for the Gulf gage is 0.25 m and for the Sound gage 0.22 m for the period April 2010 (classification method Hs-Dir). These values are similar to the values reported in ERDC (2011), see Table 5.7. These values are rather high compared to the average wave heights for both stations in the same period (0.57 m for the Gulf gage and 0.31 m for the Sound gage).

	Period April 2010			
	Gulf Gage		**Sound Gage**	
	Hs-Dir	**U10-Udir**	**Hs-Dir**	**U10-Udir**
Scenario	4	7	4	7
Hs				
Mean measured	0.57	0.57	0.31	0.31
Mean model	0.54	0.59	0.43	0.45
Bias	-0.03	0.02	0.11	0.14
RMSE	0.25	0.26	0.22	0.26
Scatter Index	44.11	44.48	59.86	68.34
Symmetric Slope	0.9	1.02	1.28	1.4
Correlation Coefficient	0.74	0.76	0.54	0.54
Tp				
Mean measured	4.79	4.79	3.39	3.39
Mean model	4.32	4.4	3.29	3.69
Bias	-0.47	-0.39	-0.1	0.3
RMSE	1.97	1.76	1.66	1.85
Scatter Index	39.88	35.8	48.95	54.03
Symmetric Slope	0.9	0.91	0.93	1.06
Correlation Coefficient	0.38	0.49	0.18	0.16
Dir				
Mean measured	145.69	145.69	133.85	133.85
Mean model	123.45	119.21	133.46	130.12
Bias	-22.23	-26.48	-0.38	-3.73
RMSE	56.75	61.49	60.76	61.95
Scatter Index	4.42	6.45	4.82	9.38
Symmetric Slope	-	-	-	-
Correlation Coefficient	0.29	0.25	0.28	0.25

Table 5.6 Error statistics for Gulf Gage and Sound Gage station for the month April 2010.

Parameter	Gulf Gage	Sound Gage
RMSE	**0.27 m**	**0.23 m**
Bias	**0.16 m**	**0.16 m**
Scatter Index	**45%**	**76%**

Table 5.7 Performance of ST-WAVE model for wave height in the ERDC (2011) wave modeling study

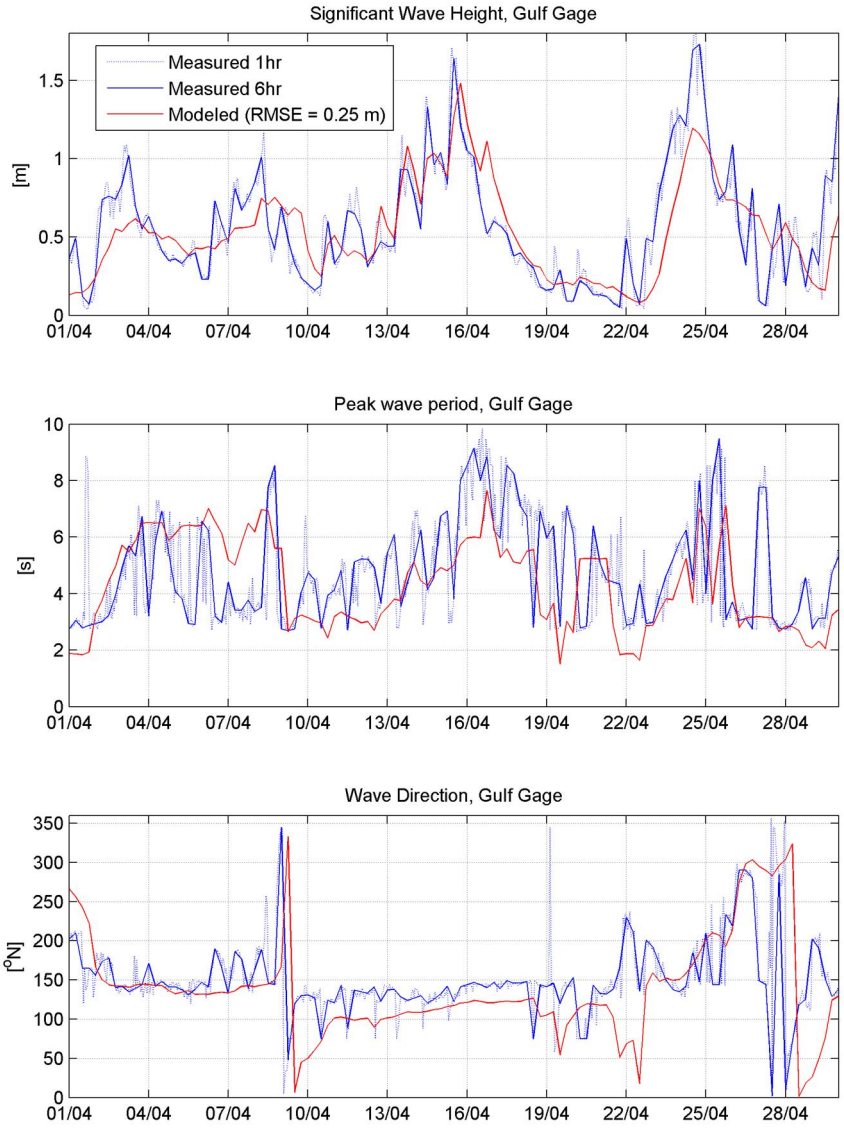

Figure 5.9 Comparison of measured and modeled wave data at the Gulf gage.

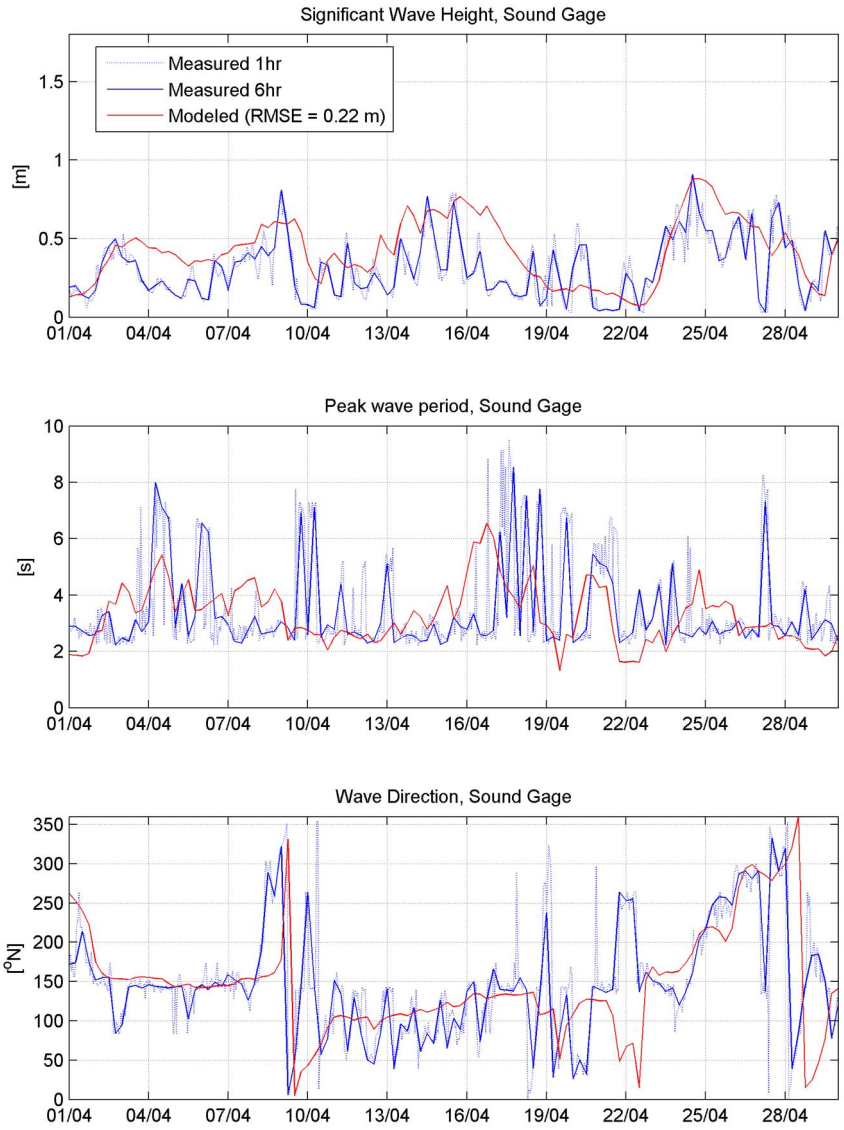

Figure 5.10 Comparison of measured and modeled wave data at the Sound gage.

5.6.4 Loss of energy in the wave model

During data validation (Section 5.3.2), the ERA-Interim significant wave heights at station (272,29) were corrected on the basis of measured wave heights at station 42040. The correction yielded a 5%-20% increase in significant wave height, depending on the directional sector (only eastern to southern directions) and wave height classes. This approach assumes that the wave heights at station 42040 and at station (272,29) are comparable. For southern wave directions this is a reasonable assumption, as waves are already fully grown over the Gulf of Mexico.

From the comparison of the measured data with transformed data at station 42040, a deviation (underestimation) of 14% was observed for the directional sector 85 to 185°N. The same comparison is made for the wave heights at the boundary of the model (the ERA-Interim data at station 272,29) and the transformed wave heights for station 42040 (see Figure 5.11). A deviation of approximately 7% is observed between the significant wave heights at the boundary of the model and the wave heights at station 42040, for the

directional sector 85 to 185°N. This indicates an energy loss between the boundary of the model and station 42040.

The reason for the reduction in wave heights is not clear. The area is deep, so bottom friction does not play a role. Other possibilities are too low wind speeds. The wind speeds at station (272,29) however match very well with the observed wind speeds at station 42040 (see as was shown in Figure 3.10). Therefore, this is expected not to be the cause of the reduction in wave heights from the boundary of the model towards station 42040.

The reduction in wave heights with approximately 6% for the southern wave directions (85 – 210°N) between the boundary of the model and station 42040 partly explains the deviation between the measured wave heights and the modeled wave heights. A possible solution could be to increase the wave heights at the boundary of the model again with 6%. This is not included in the wave model as the cause for the energy loss is not well understood. In the sediment transport modeling the sensitivity of the sediment transport to higher waves will be investigated.

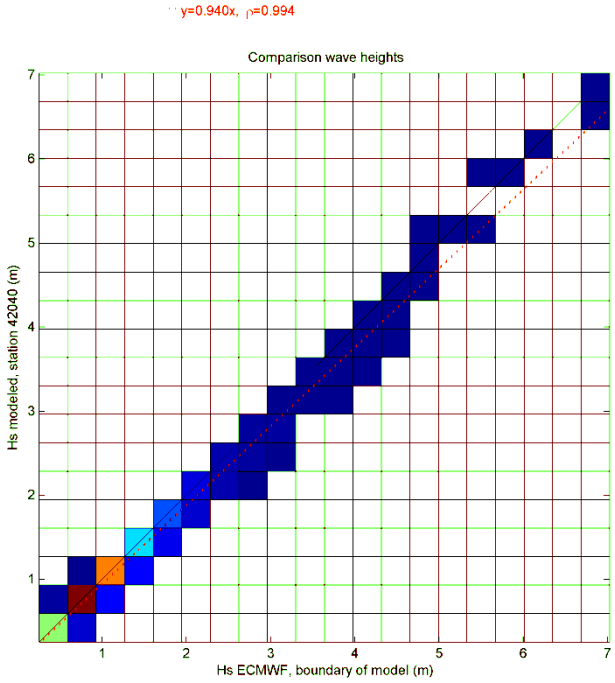

Figure 5.11 Comparison between wave heights at the model boundary and modeled wave heights at station 42040 (offshore station).

5.6.5 Deviation in wave direction

In the wave height roses (see Figure 5.6) a deviation in wave directions was observed. The deviation in wave direction is also observed in the time series, especially when waves are coming from southeastern directions. This is illustrated Figure 5.12 at station 42040 for a short period of time in June/July 2010. The deviation is approximately 15° – 30°deg.

A possible cause for the deviation in wave direction may be the definition of the wave direction. The measured wave directions from NDBC are defined as the *directions from which the waves at the dominant period are coming*. The ERA-Interim and the modeled wave directions are mean wave directions, based on the 2D-wave spectrum.

A comparable deviation between the ERA-Interim data and the NDBC data was found in Section 5.3. The wave modeling did not improve the match in wave directions at station 42040.

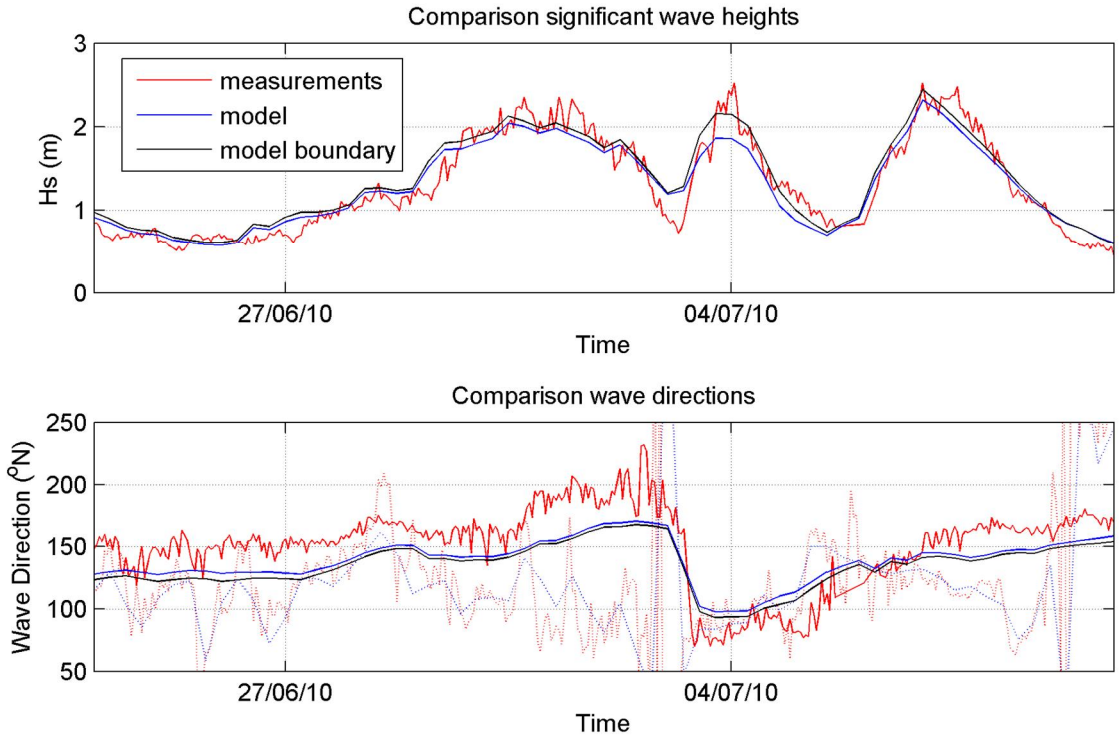

Figure 5.12 Illustration of deviation between wave directions at station 42040 (offshore station) for southeastern waves.

5.6.6 Other possible causes of deviation

Low time resolution of data

The ERA-Interim data, which is applied in the classification of the data, has a 6 hr time-resolution. It is suggested in discussion with USACE that the relatively low resolution of the data may lead to an underestimation of the higher wave heights. As weather patterns may develop and resolve quickly in the Gulf of Mexico, the high peaks might not be well covered in the ERA-Interim data.

In the time series plots included in this chapter (e.g. Figure 5.9 and 5.10) the difference between the hourly and 6 hourly resolution data can be observed. Although variation is visible within the 6 hourly time-frame, the period of storms (e.g. higher waves) is usually larger than 1 day and is well reproduced with the 6 hourly resolution data. Furthermore, although the ERA-interim has only 6 hourly resolution data, the ERA-interim wave and atmospheric models transfer information each 20 minutes. Therefore it is expected that the time resolution of the ERA-Interim data is not a limitation.

Parameter specification of the wave model boundaries

The wave model, which is applied in this study, is driven by parametric description of the wave spectrum at the boundary (Hs, Tp, Dir). In case the spectral shape is complex (e.g. bi-modality in frequency and/or directional space) the parameter specification of the wave conditions is not adequate to represent the wave spectrum in a proper manner.

From a first analysis of measured wave spectra, they did not show complex spectral shapes, like multiple peaks in frequency space or directional space. This suggest that the spectral shape can be adequately represented by parametric description. However, no detailed comparison of measured and modeled wave spectra is carried out.

5.7 Conclusion

The modeled significant wave heights show an underestimation of approximately 8% compared to available measurements.

It was decided not to increase the modeled wave heights, but to keep in mind possible slight wave height underestimation during the interpretation of the results.

6 Sediment transport modeling

6.1 Introduction

In this chapter the sediment transport modeling is presented for the year-averaged conditions (Section 6.2), for the hurricanes (Section 6.3) and for the cold fronts (Section 6.4).

For these three contributions a different modeling approach was applied, which is first discussed in each section, followed by a presentation and discussion of the results. Each section is concluded with an analysis of the relative importance of individual conditions for the transport.

In this chapter the modeling approach and results are presented. A comparison of the results with available data and other studies is presented in Chapter 7.

6.2 Modeling of transport due to year-averaged conditions

6.2.1 Approach

6.2.1.1 Introduction

For a description of the overall modeling strategy and the interaction between the various models, refer to Chapter 2. In this section the sediment transport modeling is described in more detail. A distinction has been made between the transport along the Gulf-oriented shorelines and the transport along the Sound-oriented shoreline.

The different steps for the transport modeling for the year-averaged conditions are illustrated in Figure 6.1. To compute the annual sediment transport generated under year-averaged conditions, the wave climate was schematized into a reduced set of 139 onshore-directed wave conditions (see Chapter 5). The wave climate was based on the period 1989-2010. Sediment transport computations were made for the yearly averaged wave conditions, from which the named events were excluded. In this report these wave conditions are referred to as *year-averaged conditions*.

The modeling was based on the calibrated hydrodynamic model (described in Chapter 4), in which the sediment transport calculation is activated. The hydrodynamic model was coupled to the wave model (described Chapter 5). A two-way coupling between both models was established which allows for the wave forcing and other relevant wave parameters to be used in the flow and transport calculations whereas the water levels and current velocities are transferred to the wave model.

For each of the year-averaged wave conditions, the sediment transport was computed for the MCC-model domain. These simulations were forced with each wave condition (wave height, wave period and incident wave angle combination) combined with a representative ‘morphological tide’ (to be discussed later in Section 6.2.2). In this way for each wave condition a tide-averaged sediment transport field was obtained. This transport field was subsequently scaled with the waves percentage of occurrence. The annual year-averaged transport was obtained by summation of all 139 weighted transport fields. The simulations presented in this chapter have been conducted without updating the bathymetry.

Gross sediment transports have been assessed by integrating negative sediment transports (to the West) and positive sediment transports (to the East) separately. The net sediment transport for each individual wave condition has been considered, variation in the direction of the alongshore sediment transport over a tide has not been taken into account.

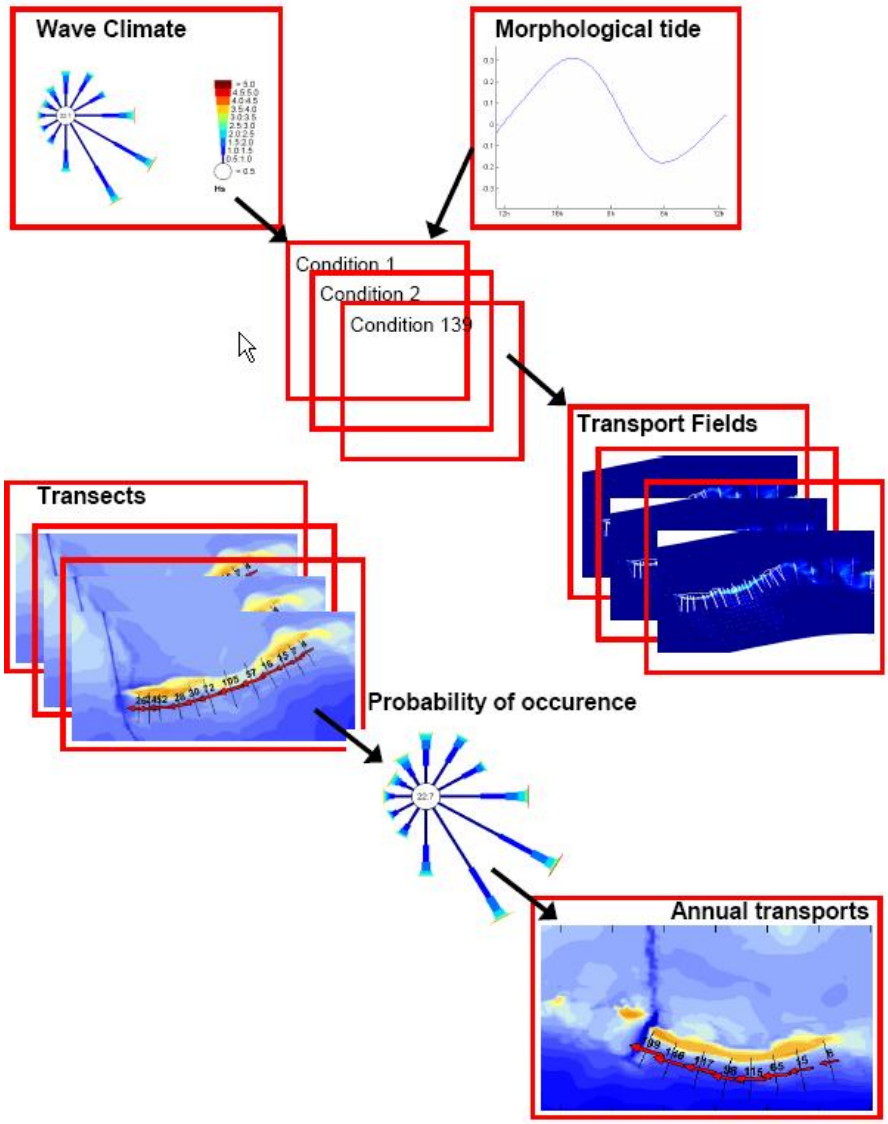

Figure 6.1 Approach for assessment of year average transport fields.

6.2.1.2 *Morphological tide*

Sediment transports along the Mississippi barrier islands and through the passes are induced by wind and wave-driven currents, tidal currents and their interaction. It has been assumed that the long-term residual sediment transports can be described by averaging over a complete neap-spring cycle. Combining a spring-neap cycle with the 139 wave conditions would result in unacceptable long run-times. To save computational the spring-neap tidal cycle is approximated by a single representative a so-called *morphological tide*.

Van Rijn (1993) showed that in most cases a spring-neap tidal cycle can be represented by a single tide with an amplitude about 10% larger than the average tide. This straightforward schematization technique was applied in the present study, as indicative simulations revealed

that the tidal motion has a relatively small effect on the computed longshore transports. This resulted in a morphological tide with a range of 0.5 m.

6.2.1.3 Coupling of the hydrodynamic and wave model

A two-way coupling between the flow and wave models was established which allowed for the wave forcing (based on spatial gradients in the radiation stresses) and other relevant wave parameters to be used in the flow and transport calculations whereas the water levels and current velocities were transferred to the wave model. As the water levels and velocities vary over the tide it was essential that the data exchanged between the models was updated regularly. In the model simulations a coupling interval of 60 minutes ensured accurate predictions of waves, current velocities and sediment transports.

6.2.1.4 Model settings

The most applicable additional model parameter settings relevant for the sediment transport simulations are presented below. Refer to Chapters 4 and 5 for a detailed description of the wave and flow model parameter settings reference.

Sediment characteristics

The sediment around the barrier islands is characterized as fine to medium sand. Based on sediment sample data (see Section 3.6) a mean sediment diameter D_{50} of 300 µm was applied for the sediment transport calculations. Although the D_{50} may spatially vary around the barrier islands, a uniform D_{50} has been applied in the sediment transport modeling. The sediment fall velocity has been computed based on the D_{50} following the Van Rijn (1993) formulations. The sediment diameters D_{10} and D_{90} were set at $0.75*D_{50}$ and $1.5*D_{50}$ respectively. Dss (Diameter suspended sediment) was set at $1*D_{50}$, since no specific data on the suspended material was available.

Transport formula and parameters

The transport formulation of Van Rijn (1993), which is the default option in Delft3D, has been used to compute the sediment transport rates along the barrier islands. Wave-related suspended and bed load transport factors have been set to 0.2; this is a common value for depth-averaged transport model applications with Delft3D. This deviates from the default value of 1, which is valid for 2DV or 3D applications (i.e. simulations with a vertical grid). The remaining transport parameters were set to default values.

Other parameters

Other important model settings were:

- The influence of turbulence has been taken into account by the definition of a uniform horizontal background eddy viscosity of 0.5 m^2/s.
- The bottom stress due to wave forces was computed according to Van Rijn (2004).
- The time step for the hydrodynamic and sediment transport computations was 12 s.

6.2.2 Year-averaged transports on MCC-scale

The computed annual littoral net longshore transport integrated over all normal wave conditions is shown in Figure 6.2 for the coast between West Ship Island and Dauphin Island. Figure 6.3 shows the computed large-scale sand budget under year-averaged conditions.

The upper panel in Figure 6.2 shows the bathymetry around the barrier islands, the lower shows the computed net transport. The transports are cross-shore integrated between MSL -8 m and the coastline. Along all barrier islands the computed sediment transport is directed towards the west, which is consistent with other sediment budget analyses carried out for the

MCC area (for example Cipriani and Stone, 2001; Byrnes et al., 2011, see Chapter 7). Due to the relatively irregular bathymetry the initial transport pattern is rather scattered. However, despite this scatter a large-scale transport pattern can be distinguished in the longshore transports.

Along Dauphin Island the computed net transport shows a slowly increasing trend from about 10,000 cy/yr in the east to about 40,000 cy/yr in the west. At Katrina Cut the transport has been blanked, since at this location cross-shore processes dominate the littoral drift. These cross-shore processes are not the subject of discussion and therefore this area has been blanked.

Also along the main part of Petit Bois the sediment transport increases from east to west which is primarily originating from the convex shoreline shape. The varying shoreline angle results in an increase of the incident wave angle towards the western part of the island. At the eastern end of the island the transport is about 10,000 cy/yr whereas close to the western end the transport reaches a maximum of about 75,000 cy/yr. At this location the shoreline orientation deviates about 40ºdeg from the computed year-average direction of the nearshore wave energy[6]. In general maximum longshore transports are observed at this incident wave angle. For smaller and larger angles of wave incidence the transport is smaller which can induce shoreline instabilities (see e.g. Ashton and Murray, 2004). The accreting transport gradient at the western tip of Petit Bois (the most western 1-2 km) implies that this part of the shoreline is moving seaward. Figure 3.20 (Box 2), in which the HWL of 1917 and 2010 derived from maps are compared, confirms this tendency. The shoreline at the western end of the island has moved seaward in the considered period. Figure 3.20 shows that along the eastern part of the island the shoreline has retreated. This can be explained by the erosive gradient computed with the MCC model. Thus, given the large scale shape of the Petit Bois shoreline and the shoreline orientations relative to the waves, the computed large scale transport pattern along the island can be explained, and observed shoreline behaviour seems to confirm the computed pattern.

The pattern along Horn Island shows considerable scatter, which is most likely the result of relatively large alongshore non-uniformities in the nearshore bathymetry. Still, a large-scale pattern can be observed with a transport of about 20,000 cy/yr at the eastern end, which increases to a maximum of about 100,000 cy/yr at the location where the shoreline orientation deviates about 40ºdeg from the estimated year-average direction of the nearshore wave energy (see footnote 6). The western part of Horn Island has an orientation considerably more normal to the incoming waves. Therefore, along this section the transports are considerably smaller (about 20,000 cy/yr). Due to the convex shape of the western part, the transport increases from east to west along this section. In the area where the transport drops from 100,000 to 25,000 cy/yr accretion should be expected, which can indeed be observed in Figure 3.20 (Box 3). Along the eastern part the computed overall erosive gradient agrees with the observed shoreline retreat in Figure 3.20.

For Ship Island the computed large scale longshore transport pattern is largely affected by the presence of Camille Cut. At Camille Cut the transport has been blanked, since at this

6. *With our modeling tool Unibest-CL+ the equilibrium orientation of the shorelines of Dauphin Island, Petit Bois and Horn Island was computed at about 160º N (shore-normal), based on the nearshore wave climate. For Ship Island it was computed at about 140ºN. The equilibrium orientation is an indication of the weighed direction of the year-average wave energy. The wave-induced longshore transport is very sensitive for the orientation of the shoreline relative to this wave energy.*

location cross-shore processes with a considerable longshore component dominate the littoral drift. These cross-shore processes are not subject of discussion in this chapter and therefore this area has been blanked. Along East Ship Island an increasing transport from east to west from about 5,000 to 50,000 cy/yr is computed which can be explained by the slight convex shape of the shoreline. Along West Ship Island a maximum transport of about 50,000 cy/yr is found at the location where the shoreline orientation deviates about 40ºdeg from the estimated year-average direction of the nearshore wave energy (reference is made to footnote 1 and the discussion of the transport pattern of Petit Bois earlier in this section). The accreting transport gradient at the western end of West Ship Island implies that this part of the shoreline is moving seaward. Figure 3.20 (Box 5), in which the HWL of 1917 and 2010 derived from maps are compared, confirms this tendency.

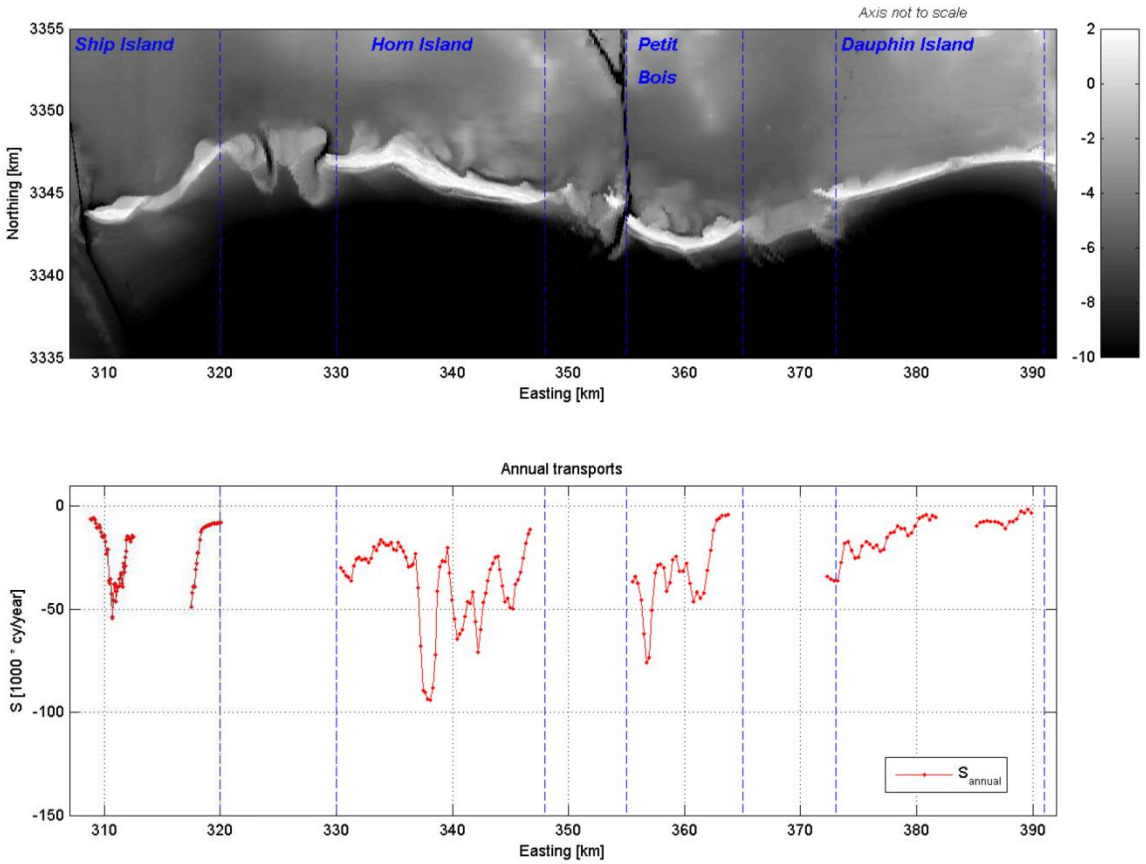

Figure 6.2 Upper Panel: MCC area with locations of transects. Lower Panel: Annual net littoral transport along Gulf side barrier islands for average wave conditions (- = westward directed).

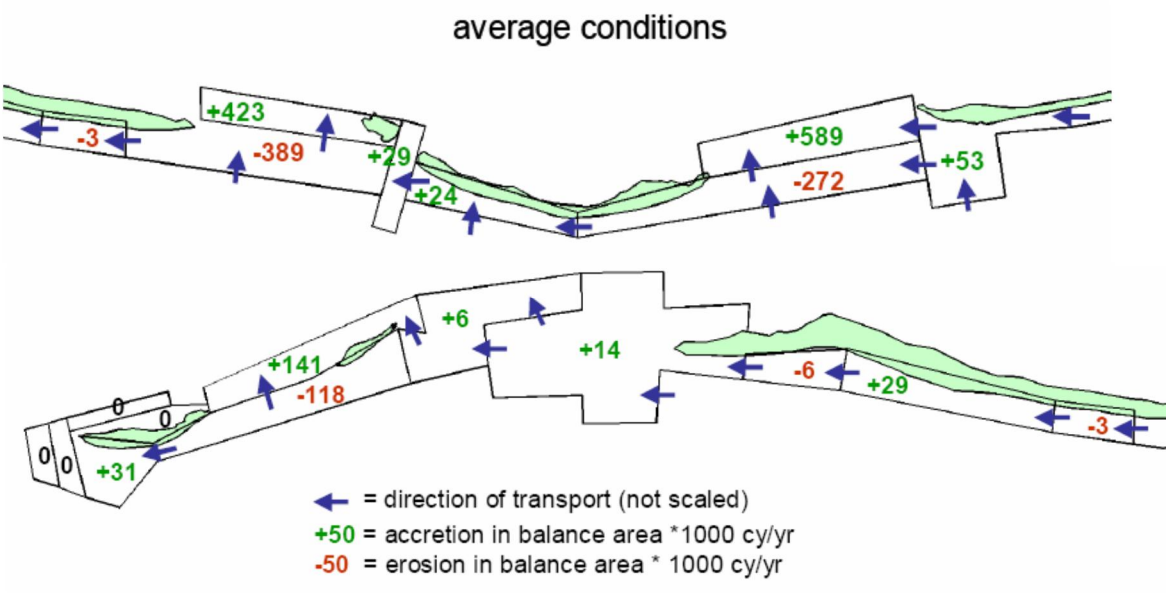

Figure 6.3 Computed sediment balance due to year-average conditions.

For all islands except East Ship Island the computed net transport at the western end is larger than the transport at the eastern end. This would indicate an overall[7] erosion of the Gulf-orientated shorelines, which is confirmed by observations in Byrnes et al. (2011).

For all islands the net transport at their eastern end is somewhat smaller than the net transport at the western end of the updrift (eastward) located island. This may be an indication that a significant part of the sediment is not crossing the passes to feed the next island in the littoral chain. This may result in some shoaling of the passes, but the sediment could also be transported out of the littoral zone (into the Sound or offshore).

It is concluded that the predicted longshore transport distributions can be largely explained by the individual island geometries and the results seem consistent with previous work. This does not automatically imply that the transport patterns can fully explain the observed morphological development of the barrier islands over the past decades. A typical example is the abrupt change in the shoreline orientation of Horn Island. The response of the model is as to be expected, i.e. a large local gradient in the longshore transport. This gradient will tend to smooth out the discontinuity. Still, in nature this discontinuity has remained present for at least the last century, though some tendency of smoothing can be observed (see Figure 3.20, Box 3).

The net littoral transport and the gross littoral transports in western and eastern direction are compared in Figure 6.4. The gross littoral transport to the west is close to the net littoral transport as the gross littoral transport to the east is almost negligible. This is to be expected on the basis of the nearshore wave roses (see Figure 6.6) which indicate that the occurrence of waves generating transport towards the east is very low due to the proximity of the Mississippi river delta. The specific contribution of each wave condition will be discussed in more detail in Section 6.2.3.

7. *Averaged over the entire barrier shoreline length. At some spots local accretion occurs, mainly near the western tips of the barriers.*

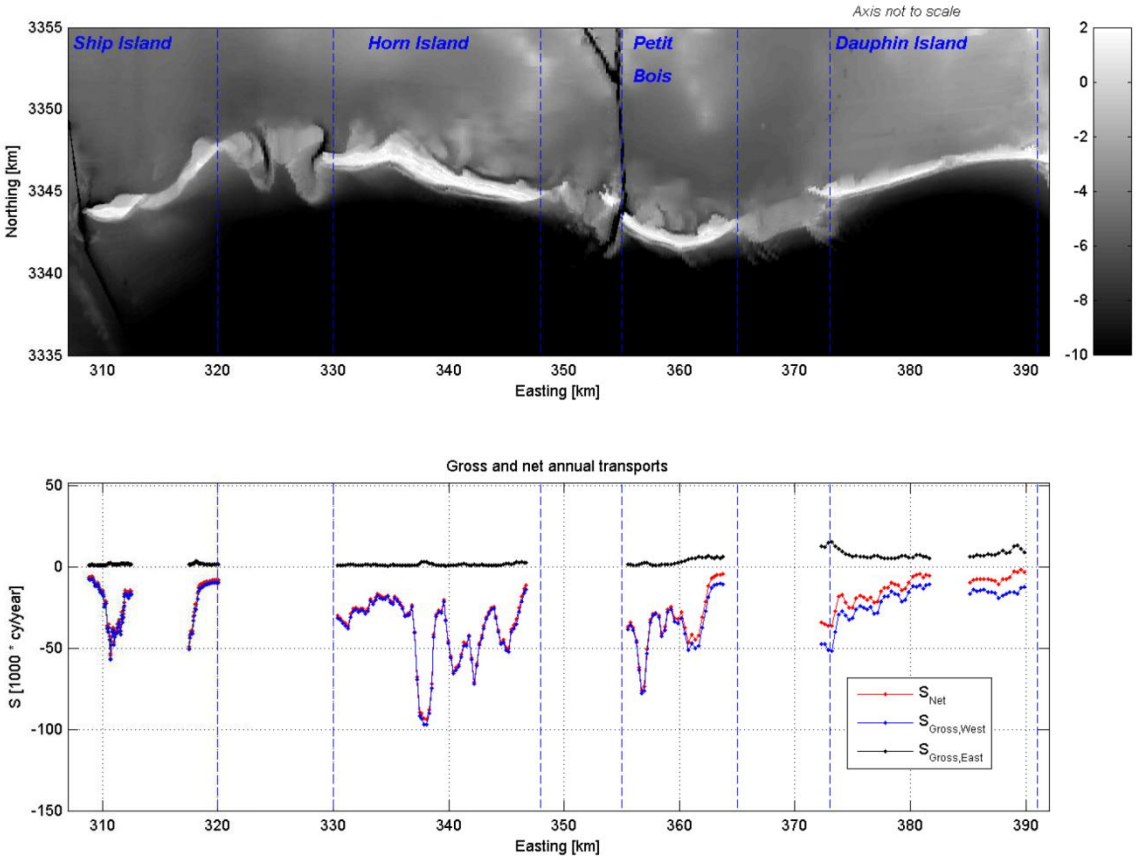

Figure 6.4 Upper Panel: MCC area with locations of transects. Lower Panel: Annual net and gross littoral transport along Gulf side barrier islands for average wave conditions.

6.2.3 Relative importance of individual wave conditions

The year-averaged conditions cover a broad range of wind and wave conditions including storm events and (mild) daily conditions. To obtain more insight into the dominant wave conditions, the littoral transport for the year-averaged conditions has been studied in more detail. Figure 6.5 shows the littoral transport as a function of the offshore wave direction (central plot) and offshore wave height (lower plot). In these plots westward contributions to the transports are indicated with blue, eastward contributions with yellow/red.

It can be concluded that the largest contribution to the transport is caused by wave angles from the southeast (the shoreline orientation is indicated by the red line in the central plot), thus generating a westward transport. The largest contribution to the annual transport is made by wave conditions with an angle between 100° and 180°N. The effect of each wave direction depends on the local shoreline orientation as was also mentioned in Section 6.2.2.

By analyzing the net littoral transport as a function of the incident wave height it is found that (10 of the 165) wave conditions with Hs > 3.75m (non-hurricane events with high waves) with a low probability of occurrence substantially contribute to the yearly net sediment transport. Smaller wave heights (1.00m < Hs < 3.75m) have a relatively small contribution to the net littoral transport.

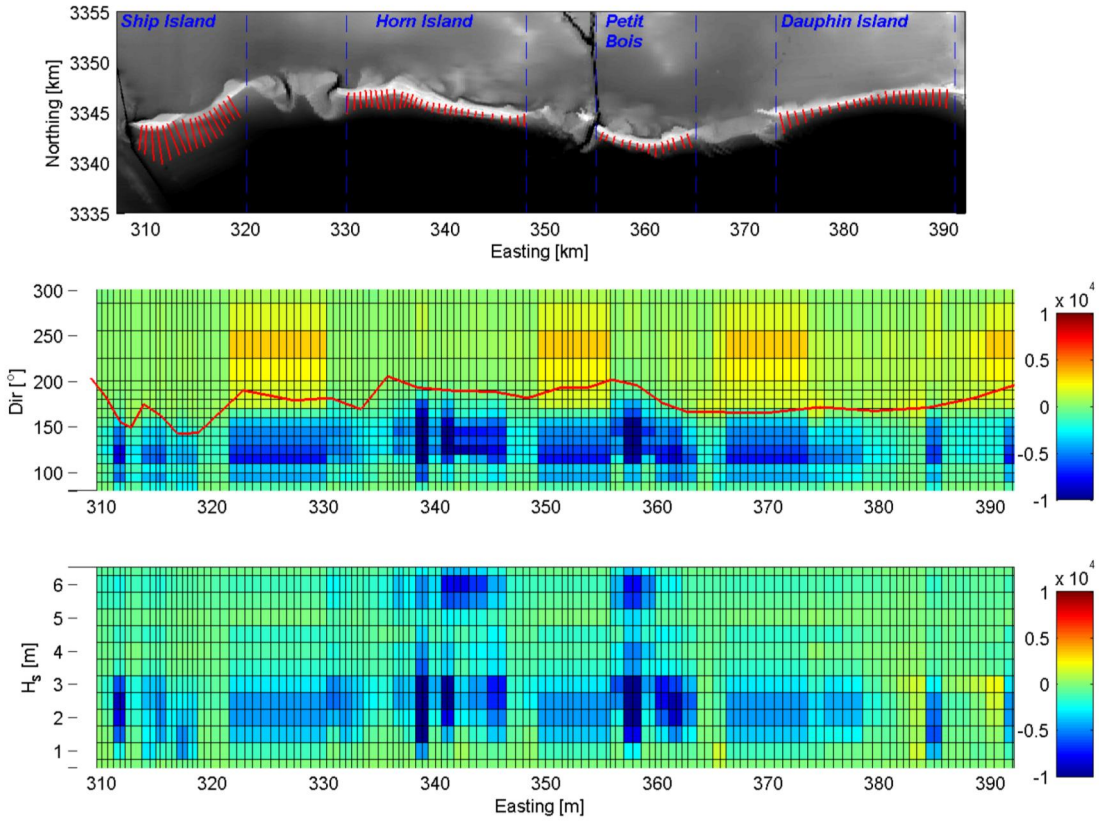

Figure 6.5 Upper Panel: MCC area with locations of transects. Middle Panel: Annual littoral transport along barrier islands as function of the wave direction. Lower Panel: Annual littoral transport along barrier islands as function of the wave direction.

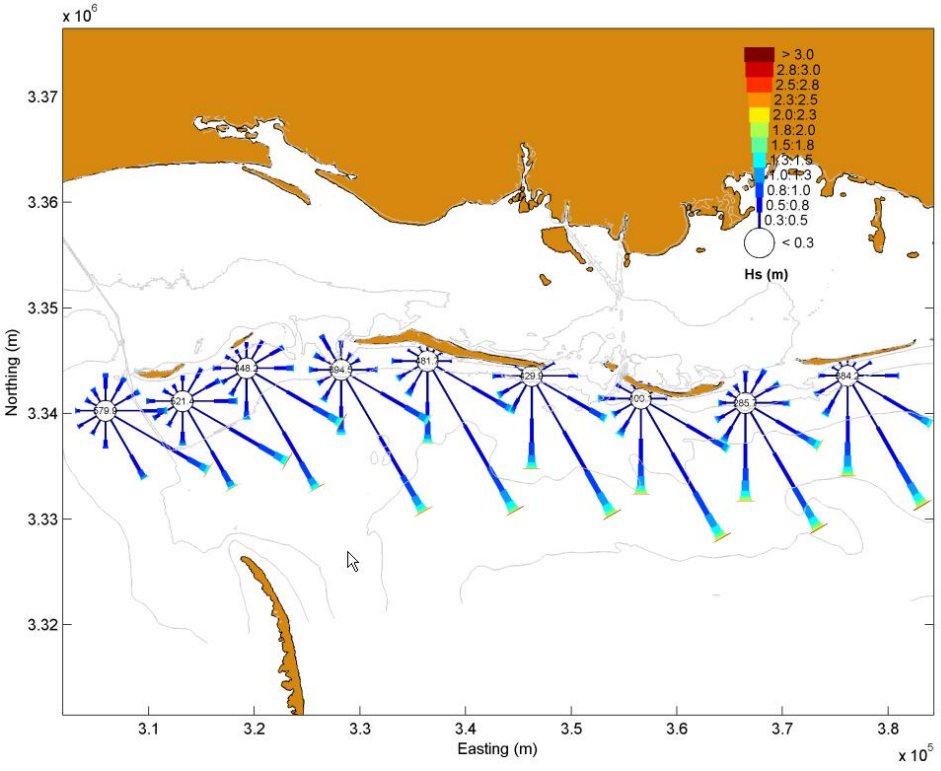

Figure 6.6 Computed nearshore wave roses.

The relative importance of wave conditions depends on the coastline orientation. For Dauphin Island, East-Petit Bois and Ship Island, with a shoreline that is primarily facing the southeast, smaller wave height conditions (Hs < 3.75m) have a relatively large contribution to the annual transport. The highest waves approach these coastlines under a relatively small angle, and thus do not contribute substantially to the longshore transport, see Figure 6.6. For Horn Island and West-Petit Bois, with coast-normals oriented towards the south-southwest, the highest 10 wave conditions (Hs>3.75m) have a significant contribution to the annual net littoral transport.

The relatively large angle of wave incidence is the primary reason for the large longshore transports at West-Petit Bois and Horn Island.

6.3 Modeling of transport due to hurricanes

6.3.1 Approach

6.3.1.1 Introduction

In contrast to the average conditions, the highly dynamic and unique character of hurricanes inhibits the definition of representative hurricanes that can act as reference conditions to establish the morphological impact or the contribution to a sediment budget. In the present study we have overcome this problem by adopting an approach in which all hurricanes relevant for the MCC sediment budget are considered. To be consistent with earlier studies, the same analysis period from 1917 to 2010 as also applied in Byrnes et al. (2011) is used. The contribution of hurricanes to the long-term sediment budget is determined by evaluating all the historic hurricanes relevant for the MCC-area in a number of steps:

1. Selection of all category 4 and 5 hurricanes in the Gulf of Mexico and hurricanes or tropical storms with a wind speed higher than 39 Mph within a circle of 500 km around Ship Island (see Section 3.8).
2. The resulting 208 hurricanes from Step 1 are imposed on the GoM and PAN-models to estimate their contribution to the sediment budget by applying the CERC transport formula as a proxy for their transport potential.
3. The hurricanes with the largest transport potential that together encompass the bulk of the total hurricane transports are considered for the detailed transport calculations with the MCC-model.

6.3.1.2 Model cascade for hurricane modeling

6.3.1.3 Model area, bathymetry and grid

For the hurricane modeling the same models were used as applied for the averaged conditions, however wave growth due to wind is now already included in the largest (GoM) scale. The following model domains, consecutively nested, are used for the hurricane modeling: Gulf of Mexico (GoM), Panhandle (Pan), Mississippi Coastal Cell (MCC). Detailed model descriptions can be found in Chapters 2 and 4.

Figure 6.7 presents a flow chart illustrating how each of the model domains and modules are linked, including the processes and parameters that are communicated. The blue boxes represent the boundary conditions forcing the different model domains included in the hurricane modeling train. The colors of the model domains match with the colors of the model grids presented in Figure 2.1. The arrows in combination with the red colored text labels

indicate which parameters are communicated to the different domains/modules. Radiation stresses are communicated from the Wave module to the Flow module, though not indicated in Figure 6.7.

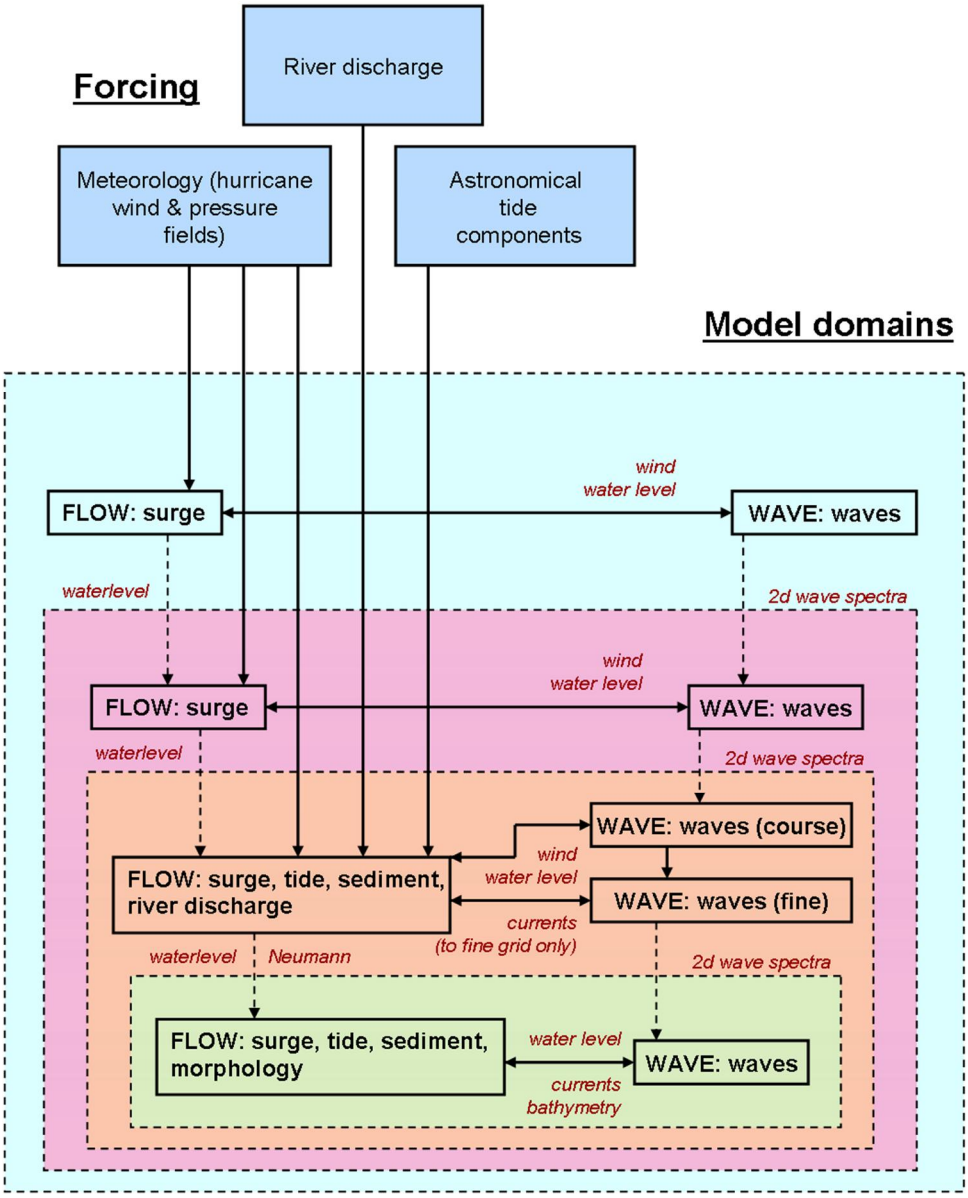

Figure 6.7 Flow diagram of the hurricane model procedure

Chen et al. (2010) found that in hurricane conditions the development of the waves requires the inclusion of water level changes due to storm surges, especially in shallow water. To account for this process, the two-way coupling between the Flow and Wave modules is activated in Delft3D, implying water levels and current velocities from the Flow module are used in the Wave module and that the wave characteristics are incorporated in the Flow module. Hindcast simulations with and without accounting for storm-induced water level confirmed the findings of Chen et al. (2010).

6.3.1.4 Hurricane boundary conditions

The hurricane forcing conditions are imposed on the model as space and time varying wind and atmospheric pressure fields. Identical hurricane forcing is imposed on each of the models and the hydrodynamic boundary conditions are taken from the next largest model. The hurricane data is submitted on a fixed and equidistant rectangular grid covering the entire Gulf of Mexico (Figure 6.8). For the modeling assignment, the hurricane data is projected onto a spiderweb grid format. The spiderweb grid reflects the circular wind patterns associated with hurricane winds, allowing for a better interpolation of the wind vectors in time. During the simulation the spiderweb grid moves along with the hurricane propagation. The hurricane eye, represented by the lowest pressure point in the time instant atmospheric pressure field, coincides with the spiderweb center. The spiderweb grid has a radius of 2.000 km (to cover the entire Gulf of Mexico as soon as the hurricane enters the model domain), has 36 directional bins (1/10ºdeg) and 400 radial bins (1/5km).

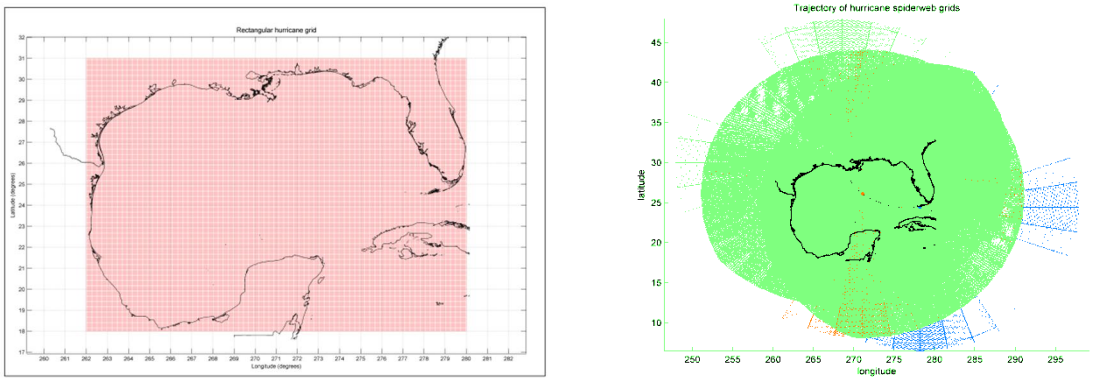

Figure 6.8 Rectangular, equidistant grid of the submitted synthetic hurricane wind and pressure fields (left pane). Spiderweb grid on which the submitted wind and pressure fields are interpolated on for modeling purposes (right pane).

As the influence of the tide is considered to be minimal on the hurricane-induced surge propagation in the offshore areas, tide was ignored in the GoM and PAN-models. In the smaller models (MCC and smaller) tide was included by imposing tidal astronomical components on the model boundaries (see Chapter 4). The hurricane induced surge level is added to the tidal water levels boundaries of the MCC-model.

River discharges from the rivers arriving at the Mississippi coastline are also accounted for in the MCC domain by a time constant inflow of water at the model domain boundaries (see Section 3.7).

6.3.1.5 Hurricane model settings

The majority of the model settings used for the normal conditions has been adopted in the hurricane model train as well, with the exception of some key parameters associated with extreme wind and atmospheric pressure gradients.

The wind drag has a major impact on predicted surge levels. The wind drag coefficient, describes the roughness of the water surface with as a function of the wind speed; Figure 6.9 presents a number of relations commonly used in coastal modeling applications.

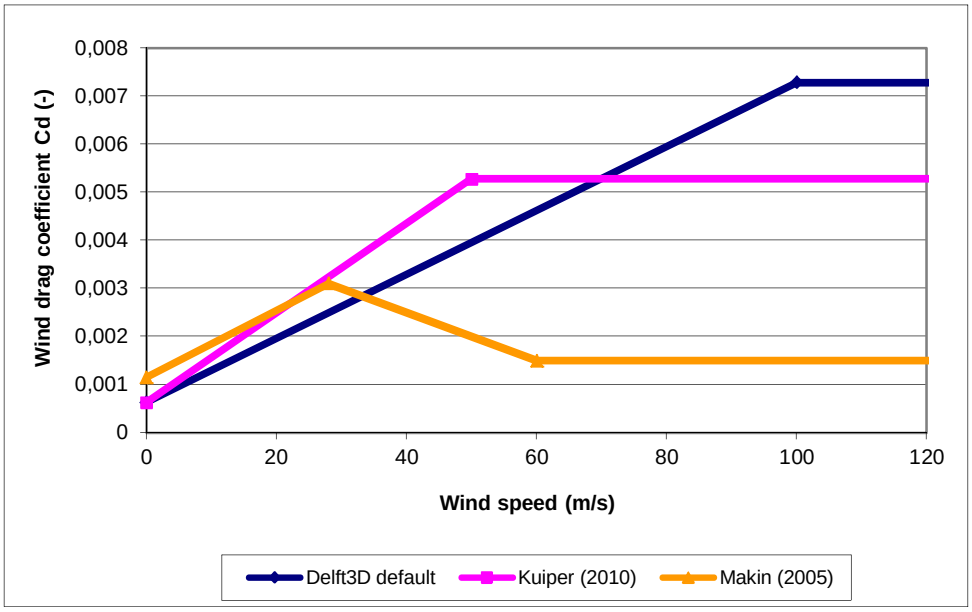

Figure 6.9 Diagram showing wind drag vs. wind speed relations.

The blue line represents the Delft3D default relation and is a linear increasing relation of the wind drag coefficient with the wind speed. This relation is applied to simulate the 'normal' conditions. Powell et al. (2003) speculate that due to actively breaking waves, the foam coverage at the air-sea interface is enhanced, leading to a reduction of the surface drag for hurricane wind speeds. Makin (2005) suggested that for wind speeds exceeding 30m/s a thin boundary layer at the sea surface develops that reduces the surface drag and acceleration of the air flow. It is apparent that the choice of wind drag formulation has a major impact on the predicted surge levels. For the hurricane simulations the Makin (2005) formulation was applied as previous in-house model calibrations have shown that this formulation resulted in the best agreement with nearshore water level observations.

For the hurricane modeling the SWAN wave model was applied in instationary mode which is another difference with the averaged conditions where SWAN was applied in stationary mode.

Table 6.1 provides an overview of other hurricane specific settings for the MCC-model.

Parameter	Value
FLOW simulation time step	**0.5 min**
Coupling interval FLOW-WAVE	**10 min**
WAVE simulation time step	**5 min (instationary)**
WAVE whitecapping scheme	**Komen et al. (1984)**

Table 6.1 Overview of the relevant hurricane model settings

Selection of hurricanes for detailed computations

The predicted maximum surge levels and wave heights for the selected 208 hurricanes show that a large majority (about 130-140) only induce maximum surge levels of 1 m and wave heights of 0.5 m and less (see Figure 6.10 and Figure 6.11).

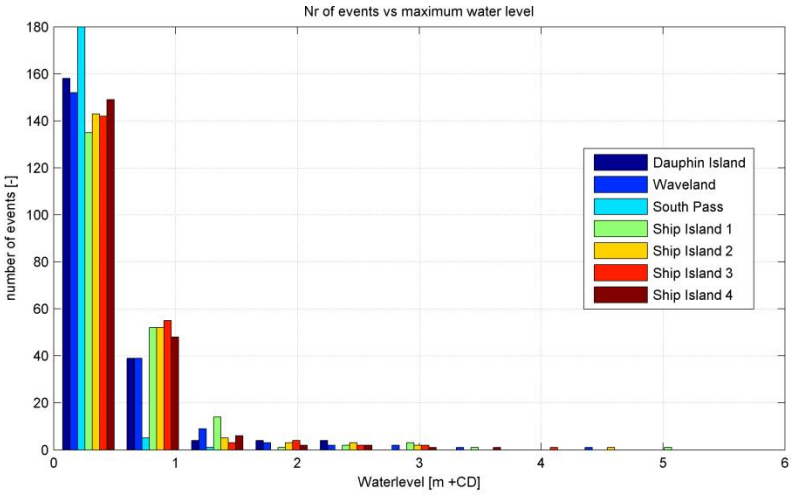

Figure 6.10 Grouping of hurricanes according to the predicted maximum water levels (see Figure 6.12 for locations).

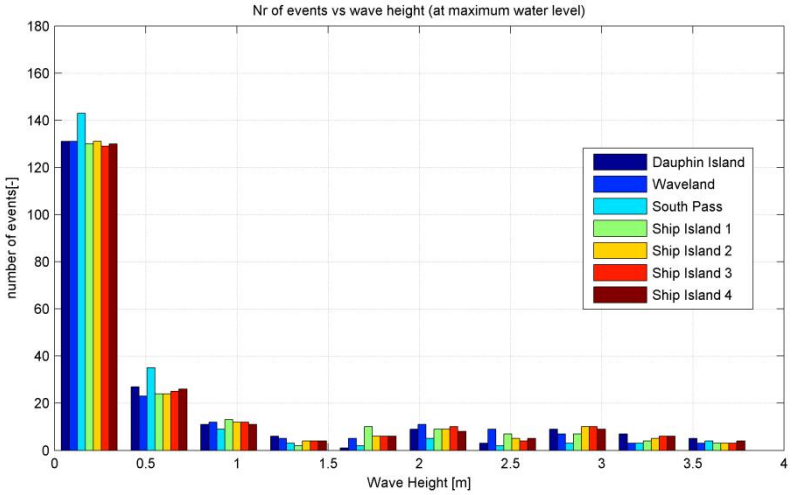

Figure 6.11 Grouping of hurricanes according to the predicted maximum wave heights (see Figure 6.12 for locations).

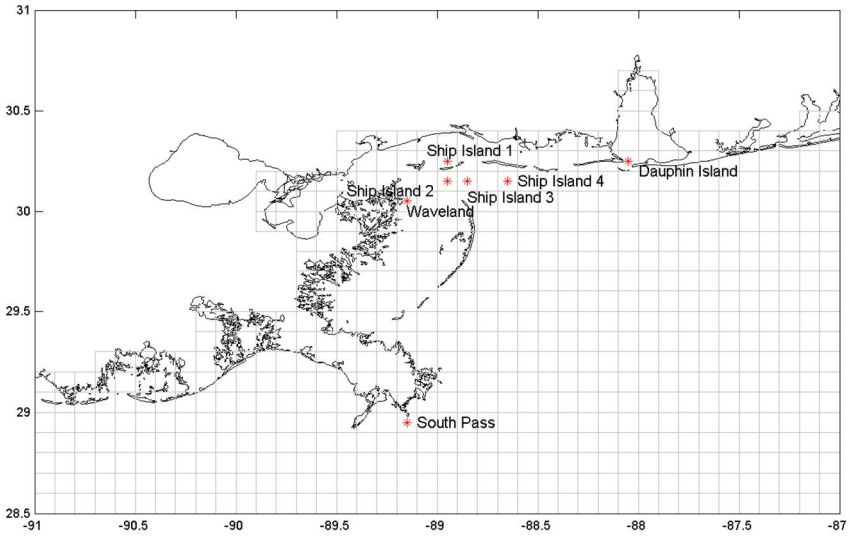

Figure 6.12 Locations used in the evaluation of the hurricanes.

The (longshore) transport potential of the hurricanes is estimated by applying the CERC formula. The CERC formula was applied, since the PAN-model-grid does not resolve the littoral zone. Therefore transports have to be estimated using a 'bulk formula' (a comparison between CERC and the Van Rijn 1993/2004 formulations can be found in Appendix C.3) using the predicted offshore wave characteristics at location "Ship Island 3" shown in Figure 6.12 considering the Gulf side coastal orientations at Ship Island. The results of this exercise are summarized in Figure 6.13 in which the hurricanes are grouped in transport classes along the horizontal axis. The top plot shows that for lower transports the majority of the hurricanes (80%) are classified in the collision regime some in the overwash and inundation regimes. As the transports become larger (i.e. hurricanes become more energetic) the number of hurricanes in the inundation regime increases and for the three largest transport classes all hurricanes are in this regime. The somewhat discrete changes in the regimes are caused by the relative small number of hurricanes that induce the larger transports (2nd plot Figure 6.13). It can be seen that about 85% of the hurricanes only contribute about 30% to the total hurricane transport load (4th plot Figure 6.13). Therefore, the transport contribution is determined with the MCC-model for the largest 15% (32) of the hurricanes (see Figure 6.14 and Table 6.2). From Table 6.2 it becomes apparent that most tropical storms are excluded and that milder hurricanes are only included if they make landfall in the vicinity of Ship Island. Larger hurricanes (H4 and H5 categories) making landfall at larger distances induce a large enough effect to still be included (e.g. Lily, Rita and Ike).

To account for the excluded tropical storms and hurricanes, the hurricane contribution derived from the considered (32) hurricanes is scaled to estimate the total hurricane contribution (208 hurricanes) to the sediment budget (see Chapter 7). The selected hurricanes contribute 71% to the longshore transport potential, therefore a scaling factor of 1.41 (1/0.71) is used to estimate the total hurricane transport contribution.

In the next sub-section the results of the transport simulations with the MCC-model are further discussed.

Year	Month	Name	Category	Minimum Distance Ship Island (km)
1917	9	No Name	H4	117
1918	8	No Name	H3	382
1919	9	No Name	H4	416
1920	9	No Name	H2	227
1926	8	No Name	H3	209
1926	9	No Name	H4	29
1947	**9**	**No Name**	**H5**	**84**
1950	8	BAKER	H3	110
1953	9	FLORENCE	H3	204
1955	7	BRENDA	TS	69
1960	9	ETHEL	H5	31
1964	9	HILDA	H4	75
1965	8	BETSY	H5	189
1969	**8**	**CAMILLE**	**H5**	**87**
1974	8	CARMEN	H4	248
1979	7	BOB	H1	160
1979	8	FREDERIC	H4	80
1985	8	ELENA	H3	7
1985	10	JUAN	H1	97
1985	11	KATE	H3	286
1988	9	FLORENCE	H1	96
1992	8	ANDREW	H5	243
1995	9	OPAL	H4	169
1997	7	DANNY	H1	52
1998	**9**	**GEORGES**	**H5**	**28**
2002	9	ISIDORE	H3	103
2002	9	LILI	H4	332
2004	**9**	**IVAN**	**H5**	**93**
2005	**8**	**KATRINA**	**H5**	**102**
2005	9	RITA	H5	426
2008	8	GUSTAV	H4	205
2008	9	IKE	H4	463

Table 6.2 Hurricanes considered for transport calculation with MCC-model ("H": hurricane category, TS: tropical storm).

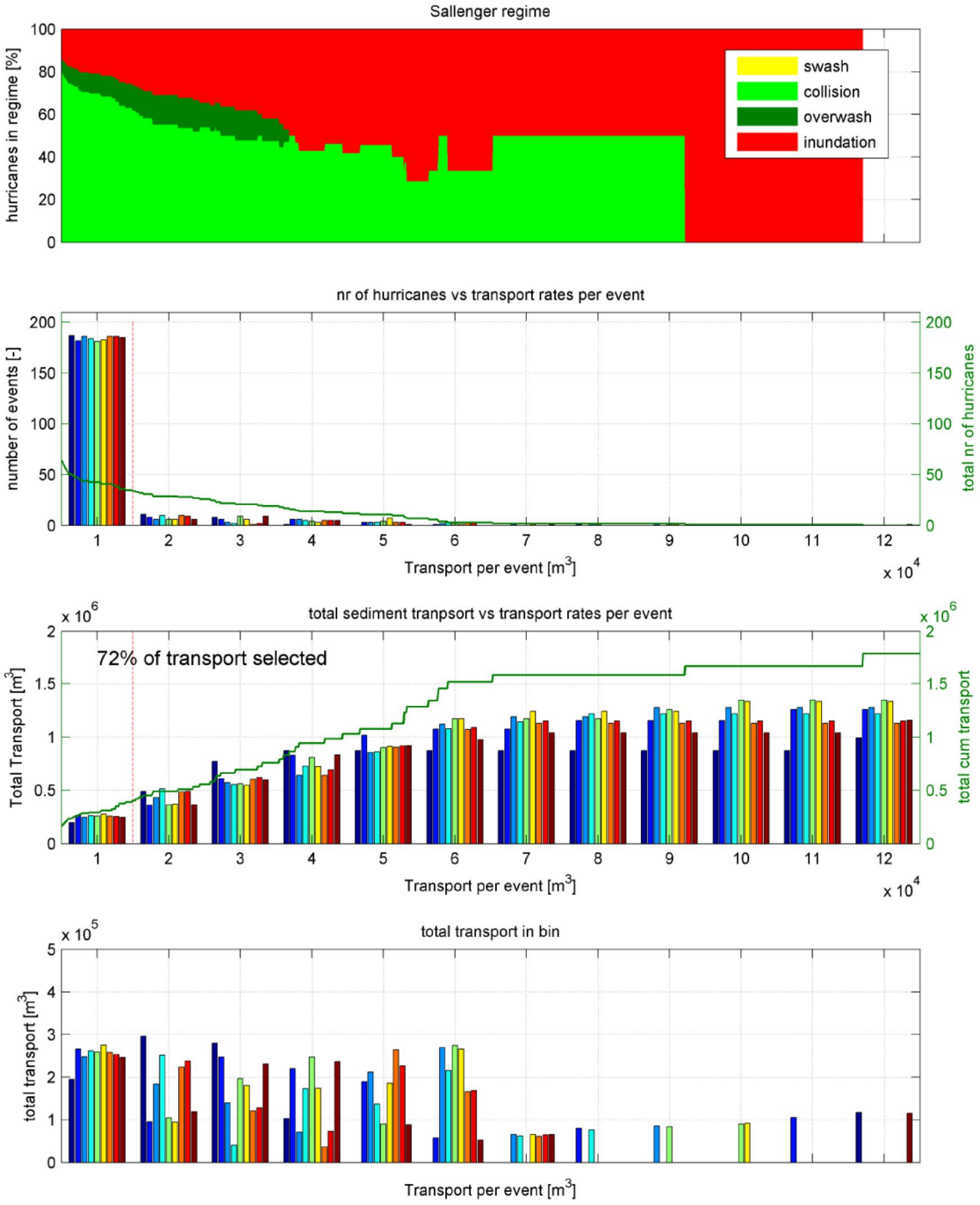

Figure 6.13 Summary of hurricane regimes and transport potential based on GoM and PAN-models at Ship Island, colors in histograms represent the different coastal orientations at Ship Island.

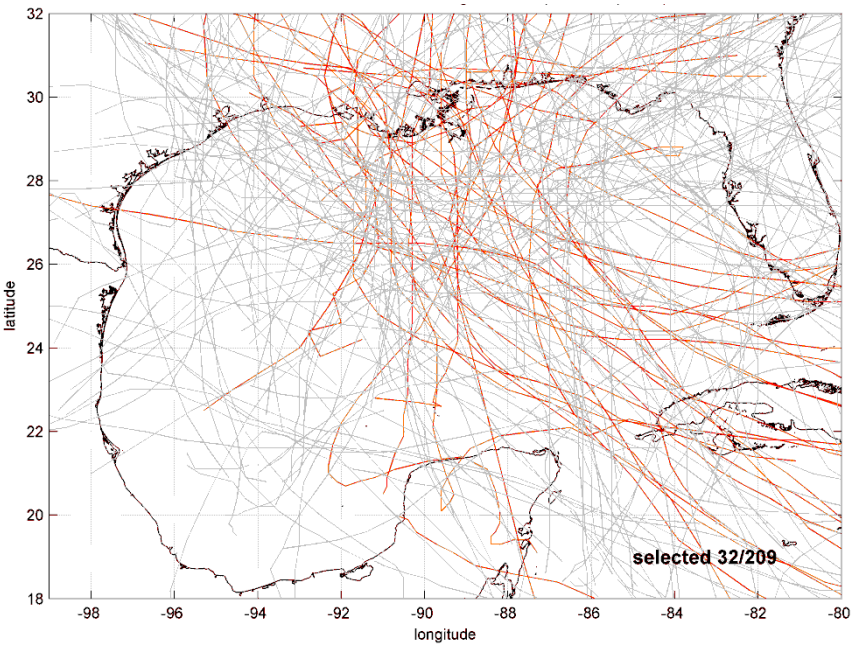

Figure 6.14 Selected hurricanes (red) for detailed transport calculations with the MCC-model.

6.3.2 Hurricane induced transports on MCC-scale

The blue line in Figure 6.15 shows the contribution of all hurricanes in the period 1917-2011 translated to an annual transport. For this purpose the total cumulative computed longshore transport caused by all hurricanes in this period has been averaged over 94 years. For comparison, also the annual transport caused by the year-averaged conditions has been presented in the graph (red line, referred to as 'Sannual'). Figure 6.16 shows the computed sediment balance due to hurricanes.

The figure shows that the contribution of the hurricanes to the longshore transport along the Gulf oriented shorelines is of a similar order of magnitude as the contribution of the year-averaged waves. For Dauphin Island the contribution of the hurricanes to the long term longshore transport is slightly larger than that of the year-averaged conditions. Along Petit Bois, Horn Island and Ship Island the contribution of hurricanes is overall somewhat smaller than the contribution of the year-averaged conditions. The overall alongshore pattern of the hurricane transport is similar to that for the year-averaged conditions, implying that the hurricanes tend to re-enforce erosive and accreting shoreline trends generated during year-averaged conditions.

As will be discussed in more detail in Section 6.3.3, along Dauphin Island, Petit Bois and Horn Island all considered hurricanes generate a net westward directed transport. Along Ship Island the presented net transport is the result of westward and eastward components.

It is noted that the impact of hurricanes on the morphology of the islands is considerably larger than suggested by Figure 6.15, which only shows the computed net longshore transport along the islands. During hurricanes considerable cross-shore transports are generated, which are included in the sediment balance presented in Figure 6.16. These cross-shore effects may result in significant bathymetry changes during the event, which may also affect the sediment transport in the period after the event.

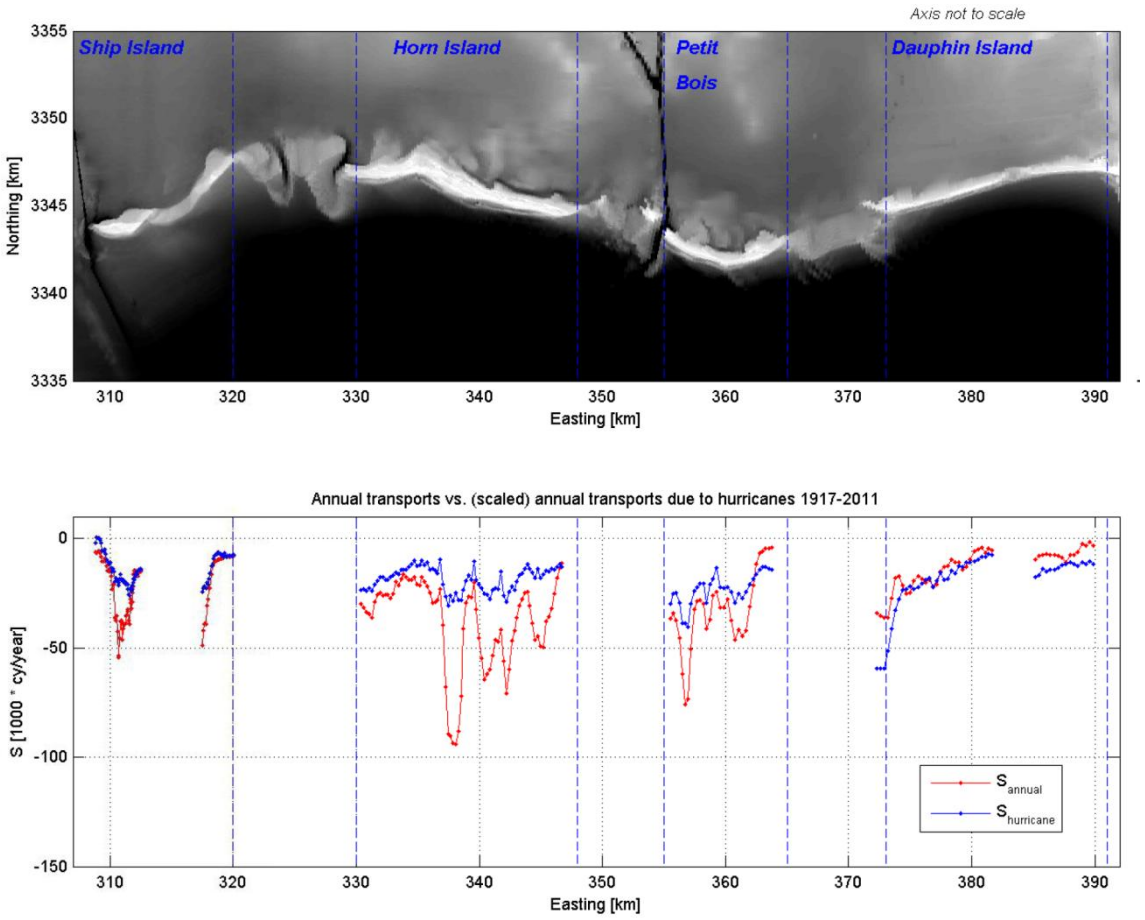

Figure 6.15 Scaled longshore transport due to hurricanes (blue) compared to annual transport due to year-averaged conditions (red).

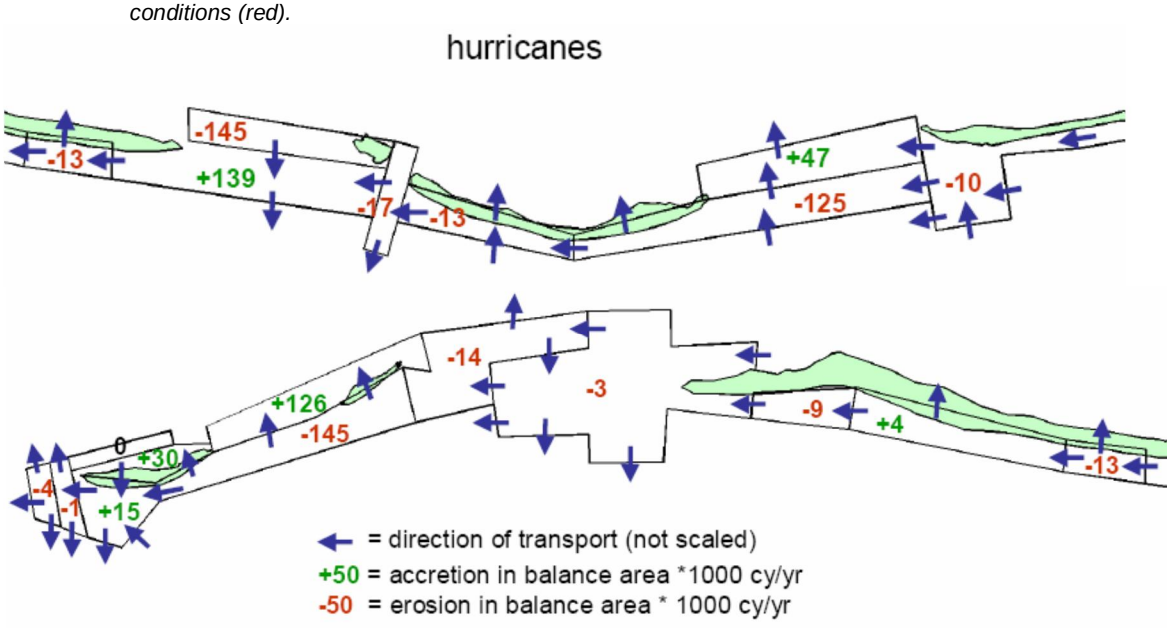

Figure 6.16 Computed sediment balance due to hurricanes.

6.3.3 Relative importance of individual hurricanes

Consistent with Byrnes et al. (2011) this investigation has integrated the transports along cross-shore transects limited by the -30ft depth contour and the center of the islands. The net longshore transports for the five hurricanes with the largest contributions (bold in Table 6.2) at Ship Island are summarized in Figure 6.18 in which also the annual net transport for the averaged wave conditions are shown as a reference (the latter are further discussed in Chapter 7). For the selected hurricanes the net transports are significantly larger or comparable to the annual transports for the averaged wave conditions. The unnamed 1947 hurricane and Georges (1998) result in the net largest longshore transport at Ship Island, which is primarily due to the proximity of the landfall locations. This is a consistent finding for the other hurricanes as well and is also causing the changes in the magnitude of the longshore transports between the islands (e.g. Ivan which made landfall at Fort Morgan peninsula and induces the largest longshore transports at Dauphin Island). The large longshore transports towards the western tips of the islands are mainly caused by the currents flowing through the adjacent inlets and should be considered with care.

Interestingly, not all hurricanes induce a net westward transport at Ship Island, viz. Camille and Katrina result in significant eastward directed transports at Ship Island but westward transports for the other islands. This was further investigated by separating the transports into a flooding phase (from the start of hurricane to maximum surge level) and an ebbing phase (from maximum surge level to the end of a hurricane) for the five hurricanes shown in Figure 6.14. Comparison of the net and gross transports for a number of hurricanes (Figure 6.19 to Figure 6.23) reveals that in most cases the gross transports are significantly larger than the net transports. Although, the magnitude of the transports varies between Camille and Katrina, the transport patterns of both hurricanes are very similar (compare Figure 6.20 and Figure 6.23). For example at the Gulf-side of West Ship Island nearshore transports are dominated by the flooding phase, whereas further offshore ebbing is dominant. As both Camille and Katrina passed west of Ship Island along an approximately south-north track the ebb flows were enhanced by strong eastward winds as the hurricanes move north. For both hurricanes the emptying of Lake Ponchartrain and Lake Borgne primarily occurs through the inlets surrounding Ship Island causing the ebb phase to dominate over the flooding phase at Ship Island. This is confirmed by the water level gradients across Ship Island (Figure 6.17) which had the largest positive water level gradients (i.e. water level higher in Sound than in Gulf) across Ship Island.

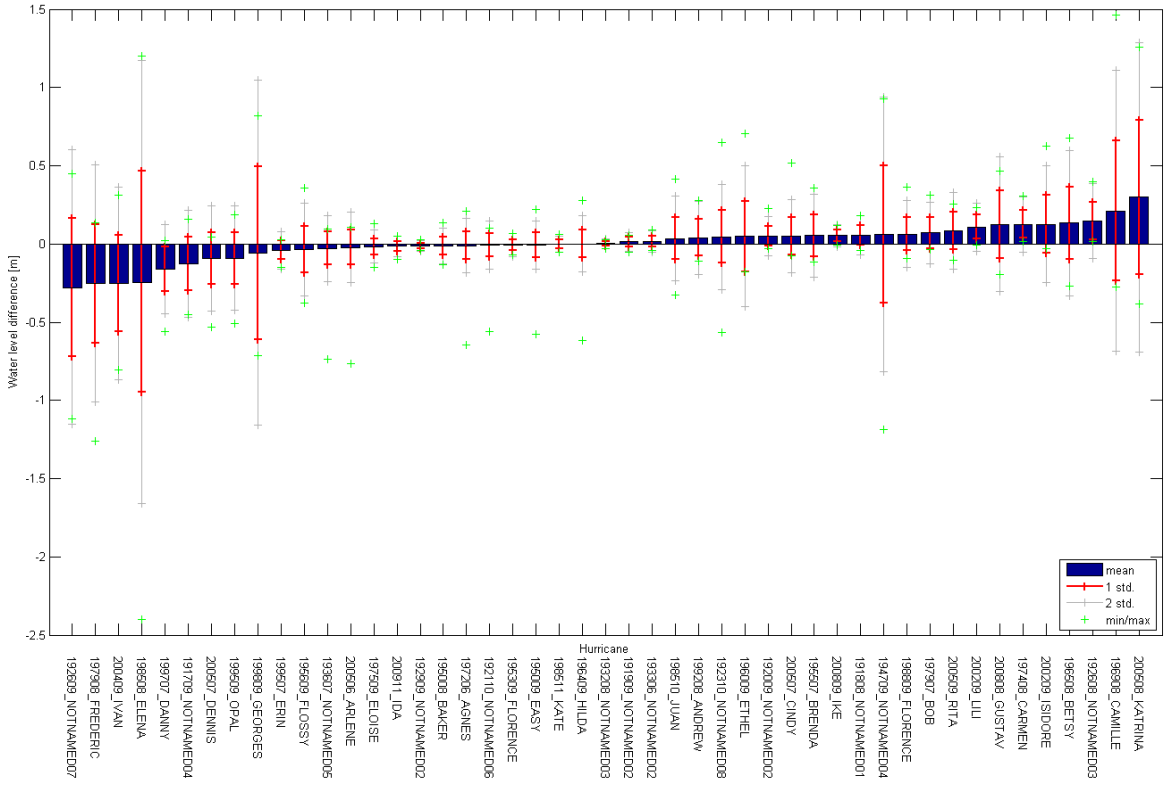

Figure 6.17 Time-averaged water level differences across Ship Island derived from the MCC model. Standard deviations are obtained from the 72 hours around the peak of the storm.

For the unnamed 1947 hurricane the ebbing phase is relatively unimportant (Figure 6.19) causing the net transport patterns to be dominated by the flooding phase. As this hurricane crossed the Chandeleur Islands about 80 km south of Ship Island along an east-west track, the flooding was enhanced by the prevailing wind directions being predominantly westward and northward directed as it passes the MCC and moves further westward, respectively. The ebb flows are therefore not being accelerated by the hurricane winds resulting in relatively low transports during the ebbing phase.

Georges (1998) passed just east of Ship Island causing the second largest net longshore transports at Ship Island of the considered 32 hurricanes (again Figure 6.18). As surge levels in Lake Ponchartrain were significantly lower compared to Katrina and Camille, the ebb phase resulted in relatively low transports. The fact that the (westward) transports during the flooding phase are significantly larger for Katrina compared to Georges (compare Figure 6.21 and Figure 6.23) highlights the importance of separating both phases and the large potential impact of the ebbing phase on the net transports.

The sediment transport along the Sound side of the island is usually significantly lower than the Gulf side, but is still of relevance for the sediment budget (discussed in the next chapter). Furthermore, the hurricanes have the ability to induce significant transports through the inlets as well. The transport direction mainly depends on the characteristics of the hurricane and may also vary from inlet to inlet.

Although the analysis is not specifically aimed at understanding or explaining some of the distinct morphological features in the area, the results provide some insight. For example, the relatively deep area just north of the western tip of West Ship Island is likely to be maintained

by the hurricane induced ebb flows. Furthermore, only the ebb flows (and the associated wave action) have the capacity to induce major changes to Cat Island. The spit at the northern tip of Cat Island is probably the result of hurricane generated ebb flows.

A limited analysis of the model results for the ebbing phase is presented in Figure 6.24 highlighting the relevance of the hurricane track as this is the determining factor for the associated winds and waves to amplify or damp the hurricane ebb flows. As hurricane Ivan passed east of Ship Island the maximum ebb flows coincide with high winds and (wind generated) waves in approximately the same direction (left column of plots in Figure 6.24). This results in relative high waves (H_s is approximately 1.5 to 2 m) at the Sound side of Ship Island which will results in significant transports around the western tips of West Ship Island. For Katrina even stronger ebb flows are present, but as Katrina passed west of Ship Island the wind and (wind-generated) waves are still landward directed resulting in significantly lower waves at the Sound shoreline of West Ship Island (right column of plots in Figure 6.24).

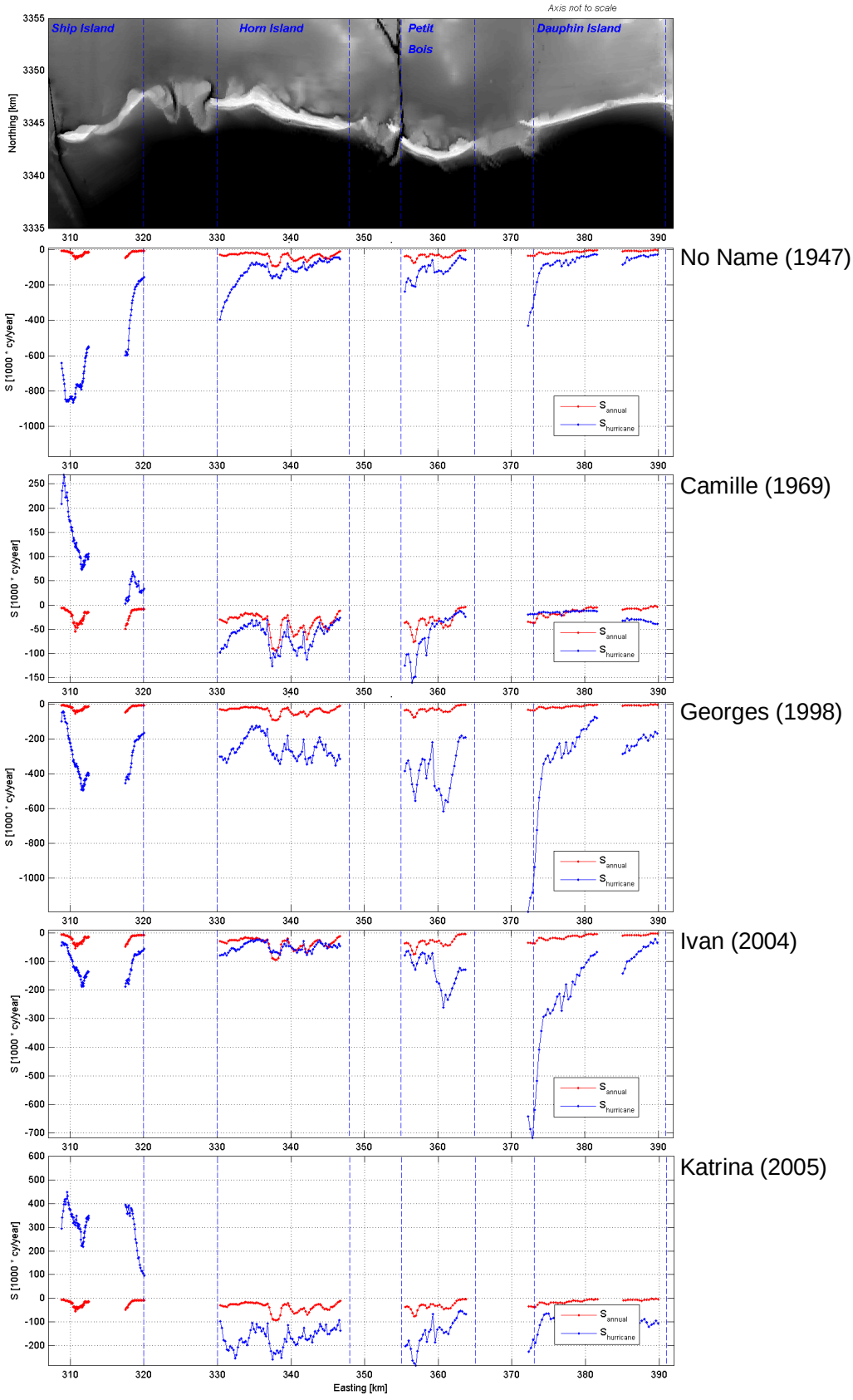

Figure 6.18 Averaged conditions (red) and hurricane (blue) induced net longshore sediment transports.

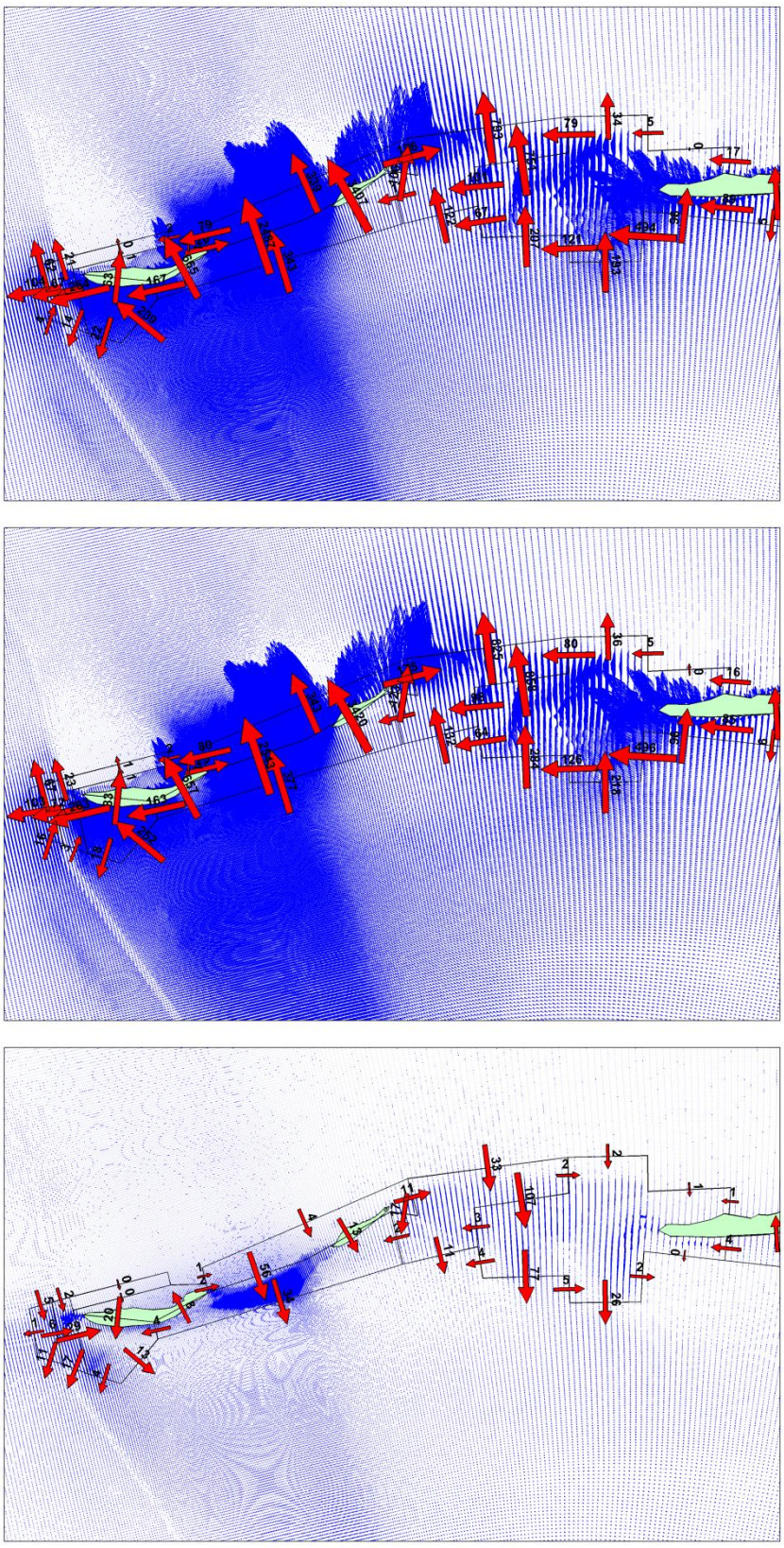

*Figure 6.19 Transports (1000*cy/yr) for Unnamed-1947 hurricane (Top plot: net transports, Middle plot: averaged transports during flooding phase, bottom plot: averaged transports during ebbing phase).*

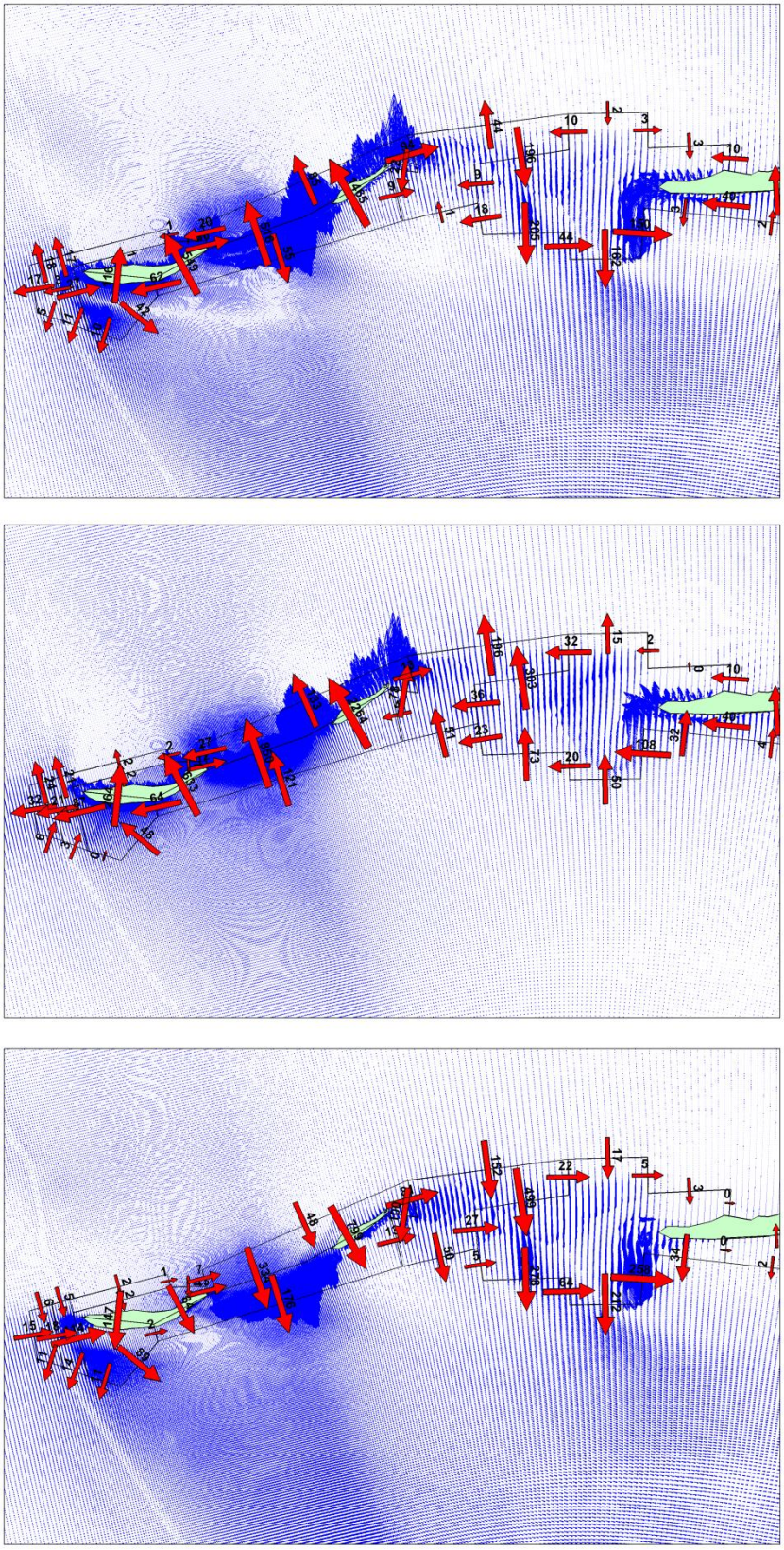

*Figure 6.20 Transports (1000*cy/yr) for hurricane Camille-1969 (Top plot: net transports, Middle plot: averaged transports during flooding phase, bottom plot: averaged transports during ebbing phase).*

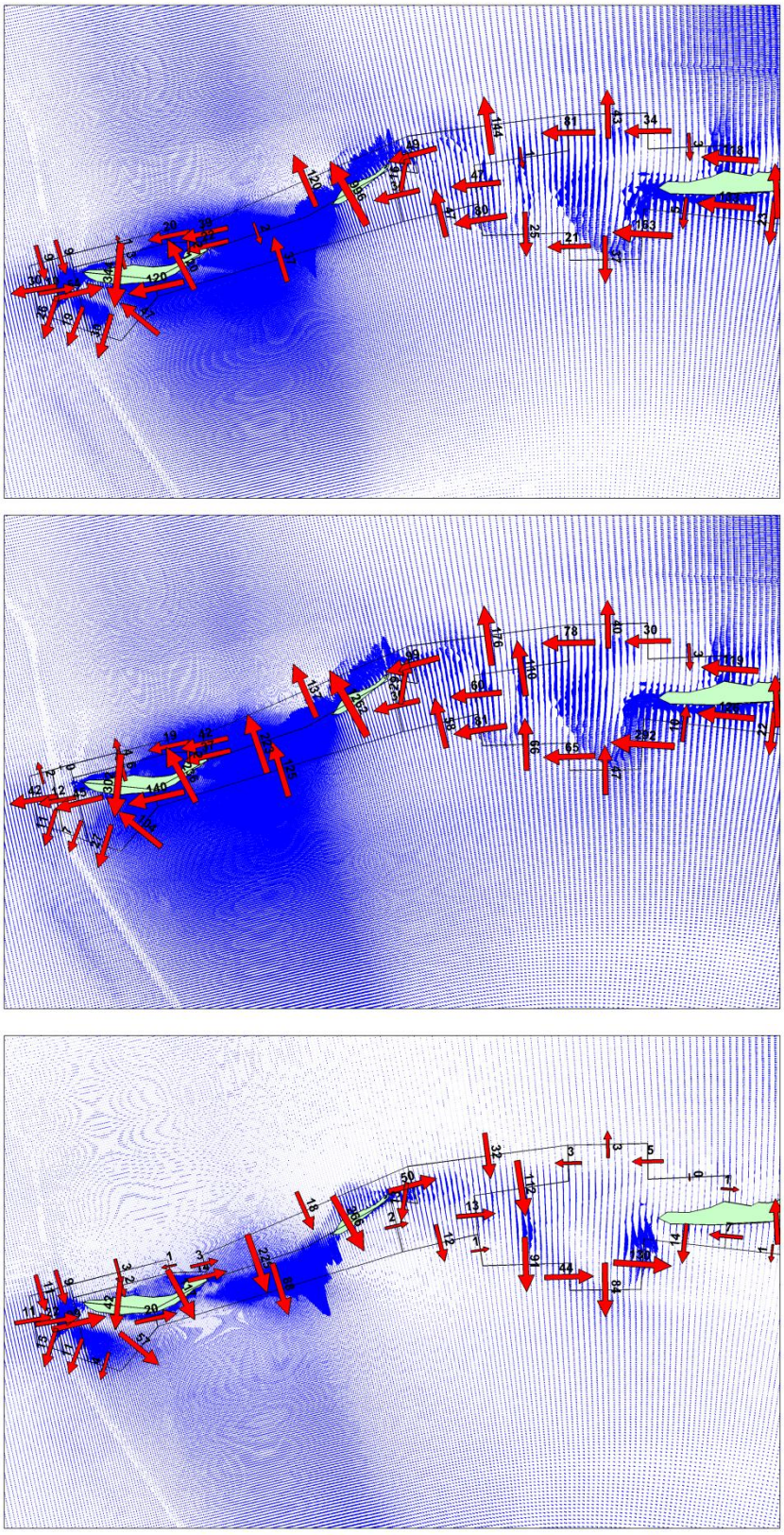

*Figure 6.21 Transports (1000*cy/yr) for hurricane Georges-1998 (Top plot: net transports, Middle plot: averaged transports during flooding phase, bottom plot: averaged transports during ebbing phase).*

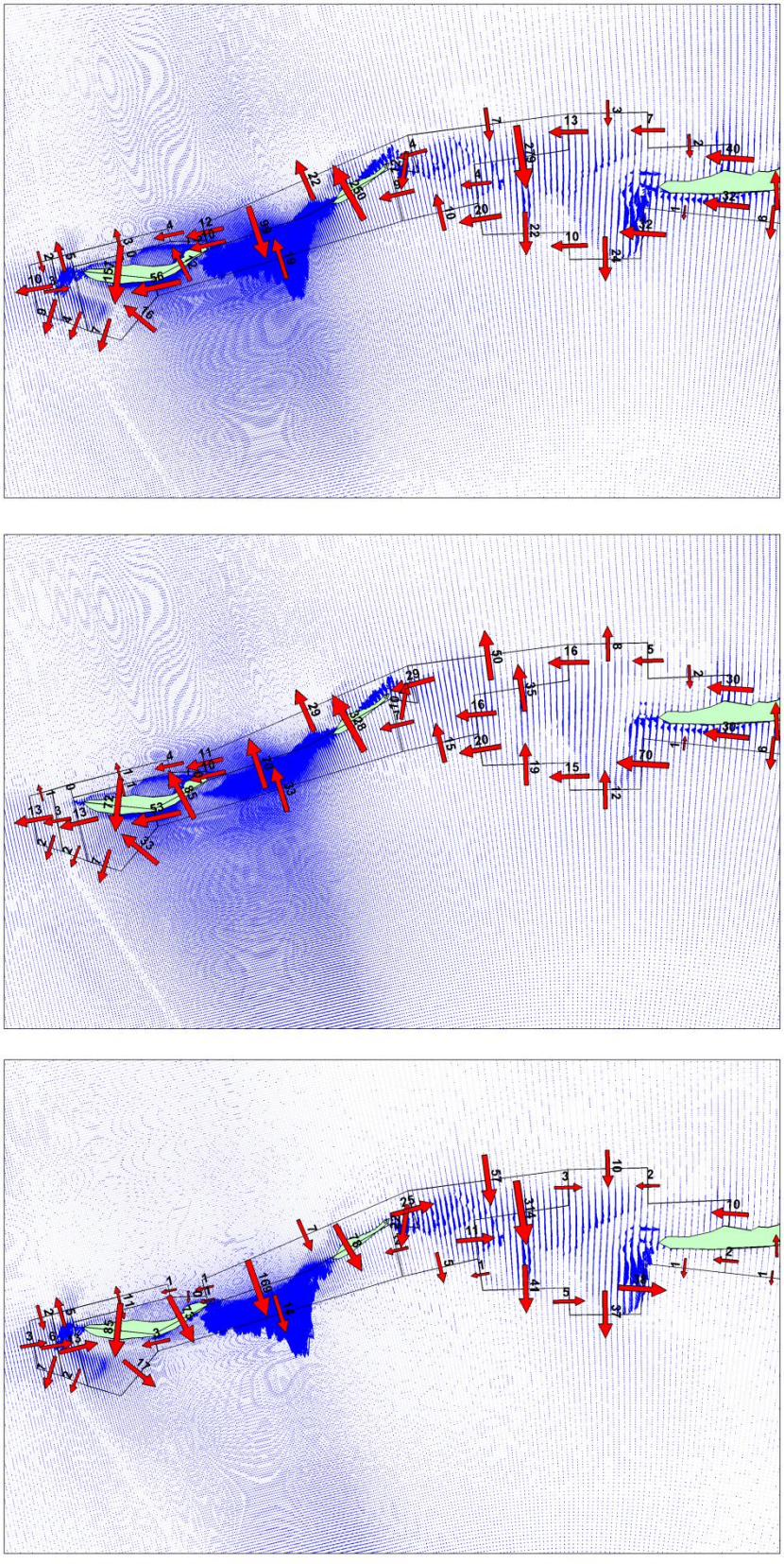

*Figure 6.22 Transports (1000*cy/yr) for hurricane Ivan-2004 (Top plot: net transports, Middle plot: averaged transports during flooding phase, bottom plot: averaged transports during ebbing phase).*

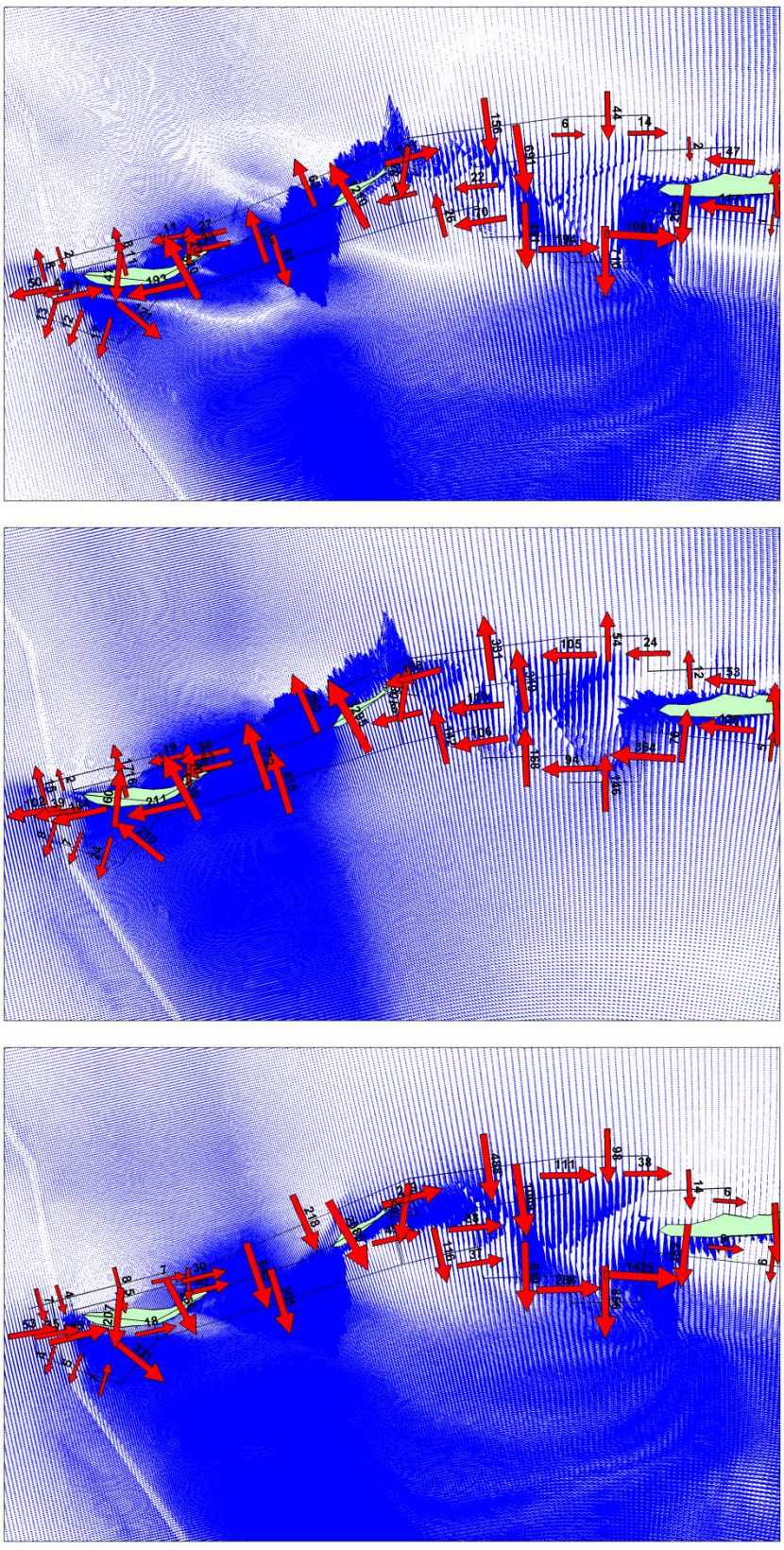

*Figure 6.23 Transports (1000*cy/yr) for hurricane Katrina-2005 (Top plot: net transports, Middle plot: averaged transports during flooding phase, bottom plot: averaged transports during ebbing phase).*

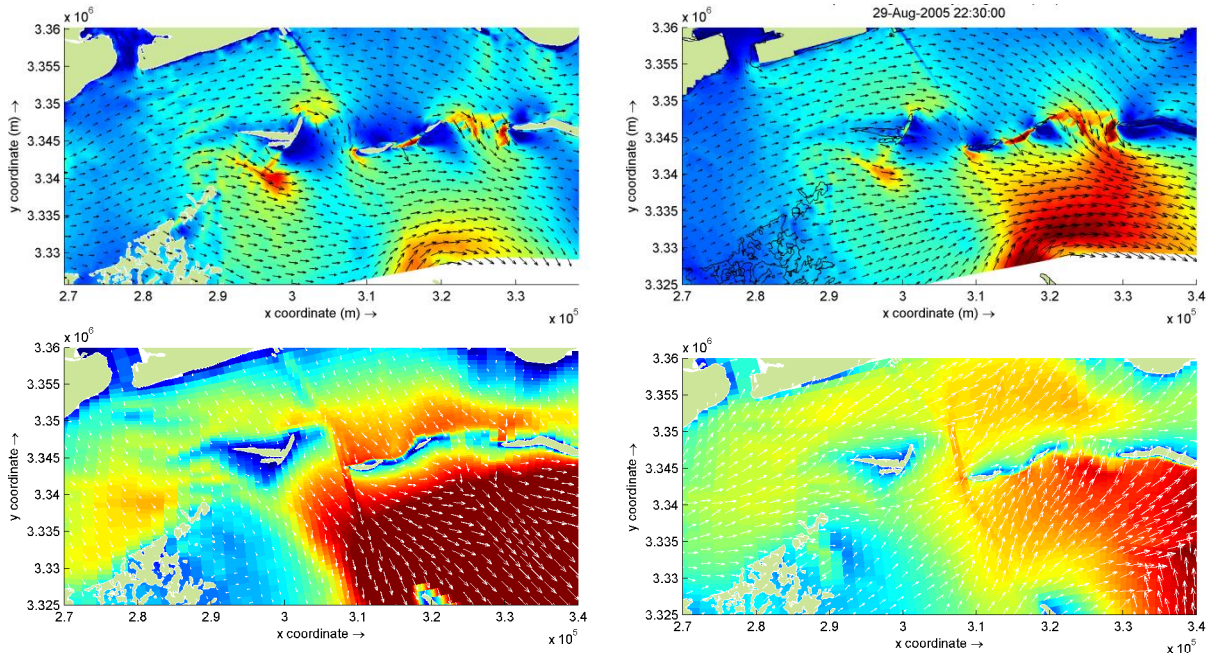

Figure 6.24 Velocities (top row) and wave heights (bottom row) for Hurricanes Ivan during maximum ebb flows (left column) and Katrina (right column) (for relative purposes only, red = high velocity/wave height, blue = low velocity/wave height)

6.4 Modeling of transport due to cold fronts

6.4.1 Approach

For the contribution of the cold fronts a different approach has been adopted, since during cold front events the wave heights remain relatively small. The breaker zone created by these low waves is too narrow for accurate sediment transport computations with the MCC model. Therefore, the contribution of the cold fronts on the transport along the Sound-oriented shoreline has been computed with the model Unibest-CL+. For a description of this modeling software reference is made to Annex E. Cold front modeling has been applied for West Ship island (so not for all barriers).

With the model the longshore transport was computed in nine (9) rays along West Ship Island as indicated in Figure 6.25.

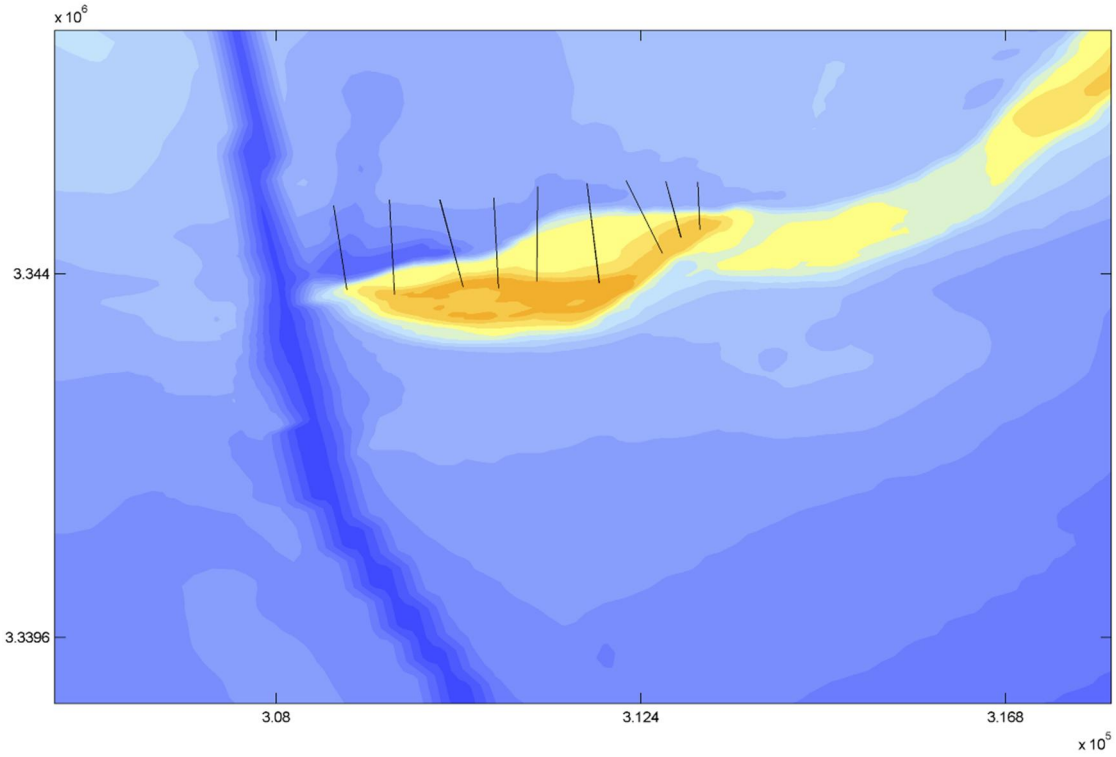

Figure 6.25 Rays for cold front transport modeling (left: ray 1, right: ray 9).

The waves have been hindcasted on the basis of wind data from the meteorological stations at Dauphin Island, Gulfport and Gulfport Outer Range, see Figure 6.13. From the time series of wind speed and –direction three events have been selected, all three with a typical wind direction. Event 1 represents a cold front with wind blowing predominantly from the North (N)), Event 2 from the North-West (NW), and Event 3 from the North-East (NE) as represented in Figures 6.26 thru 6.28, respectively.

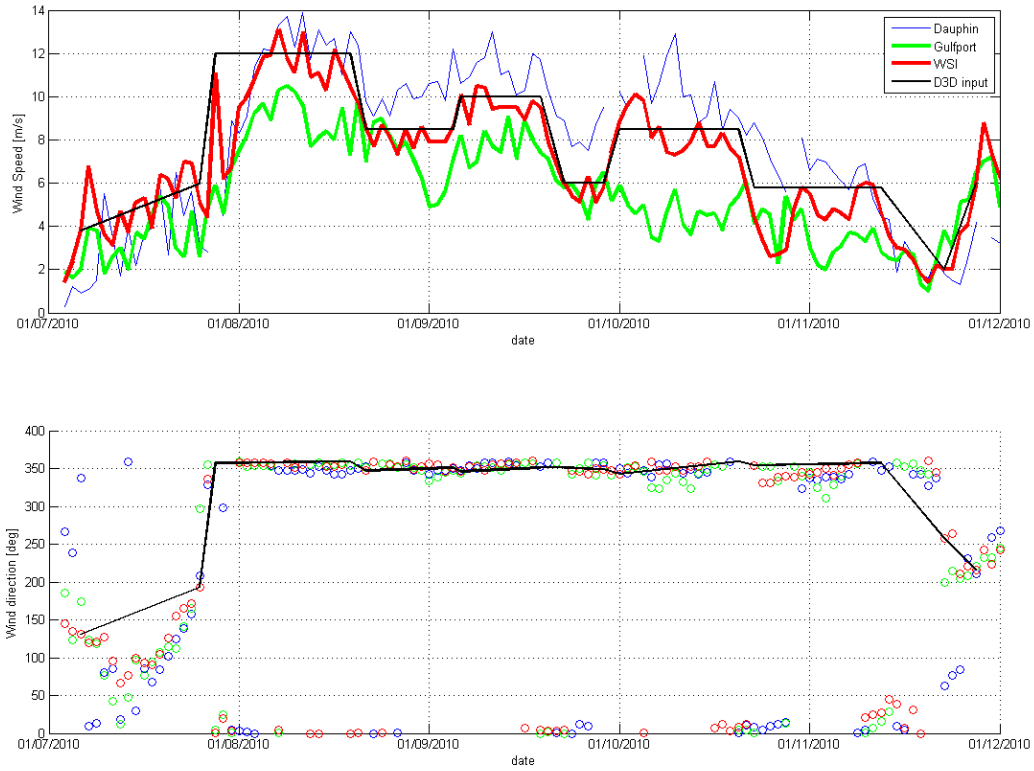

Figure 6.26 Event 1: Measured and schematized (black line) wind conditions. Above: wind speed, below: wind direction.

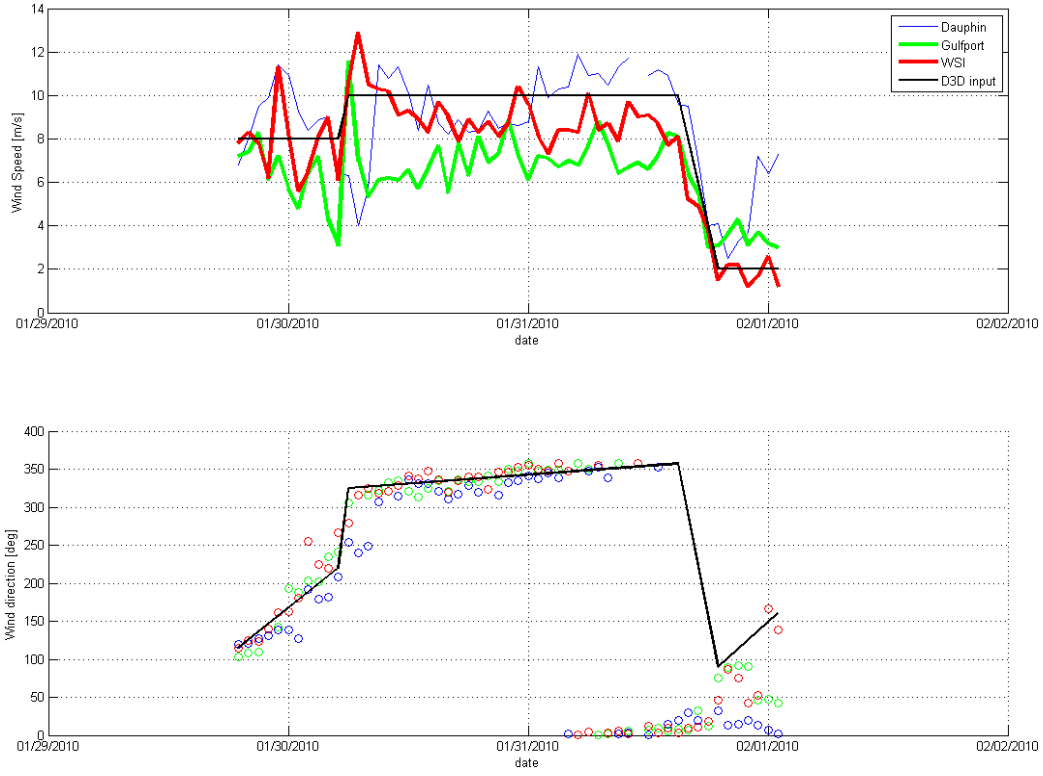

Figure 6.27 Event 2: Measured and schematized (black line) wind conditions. Above: wind speed, below: wind direction.

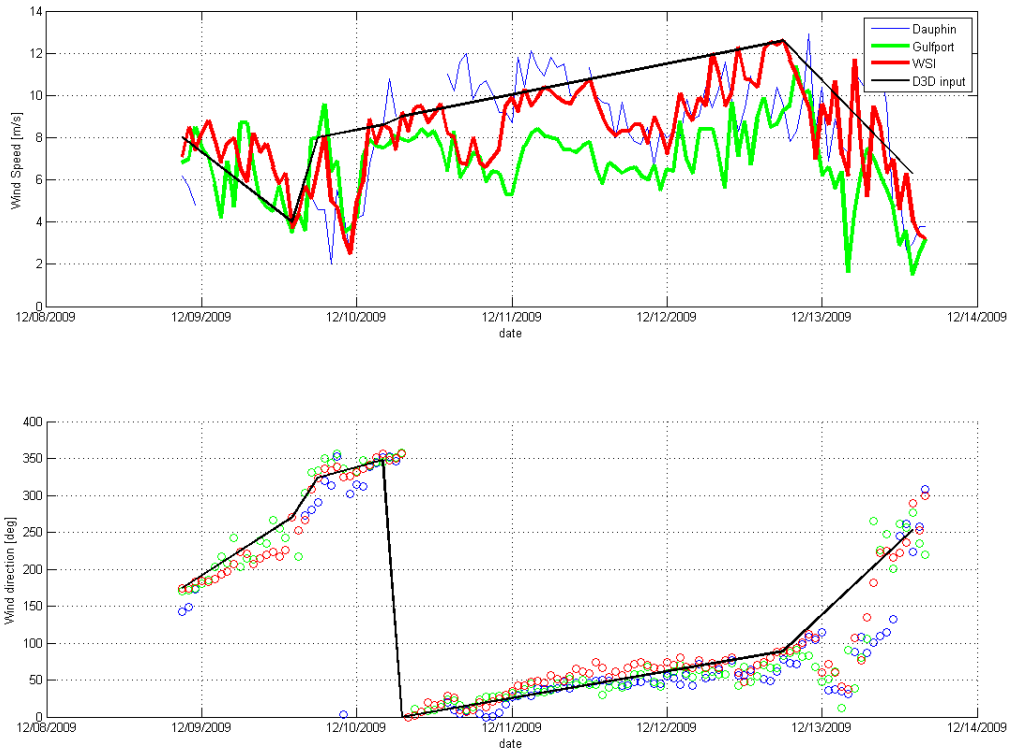

Figure 6.28 Event 3: Measured and schematized (black line) wind conditions. Above: wind speed, below: wind direction

On the basis of the wind speed and fetch length in the Sound the waves near Ship Island were computed with the Bretschneider formula. This resulted in a time series for the nearshore wave conditions at the Sound side of West Ship island as presented in Figure 6.29. These waves were used as input for the modeling. The wave-induced currents were computed with the model Unibest-CL+.

For the tide a typical spring and a typical neap tide was considered, for which the currents (depth-averaged current velocities) were computed with the MCC model and used as input for Unibest-CL+. These currents were the combined effect of tidal and wind forcing. The flow velocities during spring and neap for the considered locations are presented in Figure 6.31 (for the location of the observation points in flow model, see Figure 6.30). The figure shows that for the evaluated cold fronts the wind forcing dominates the tide at the considered locations.

With the above input the longshore transport was computed for the three (3) selected events at the nine (9) selected locations, using the Van Rijn 2004 formula and a median sediment diameter D_{50} = 0.3 mm. On the basis of an analysis of all cold fronts in the measurement period Jan 2007-Jan 2011 (which included 144 cold fronts with a duration larger than 1 day) the results for the three (3) events were translated to an annual transport.

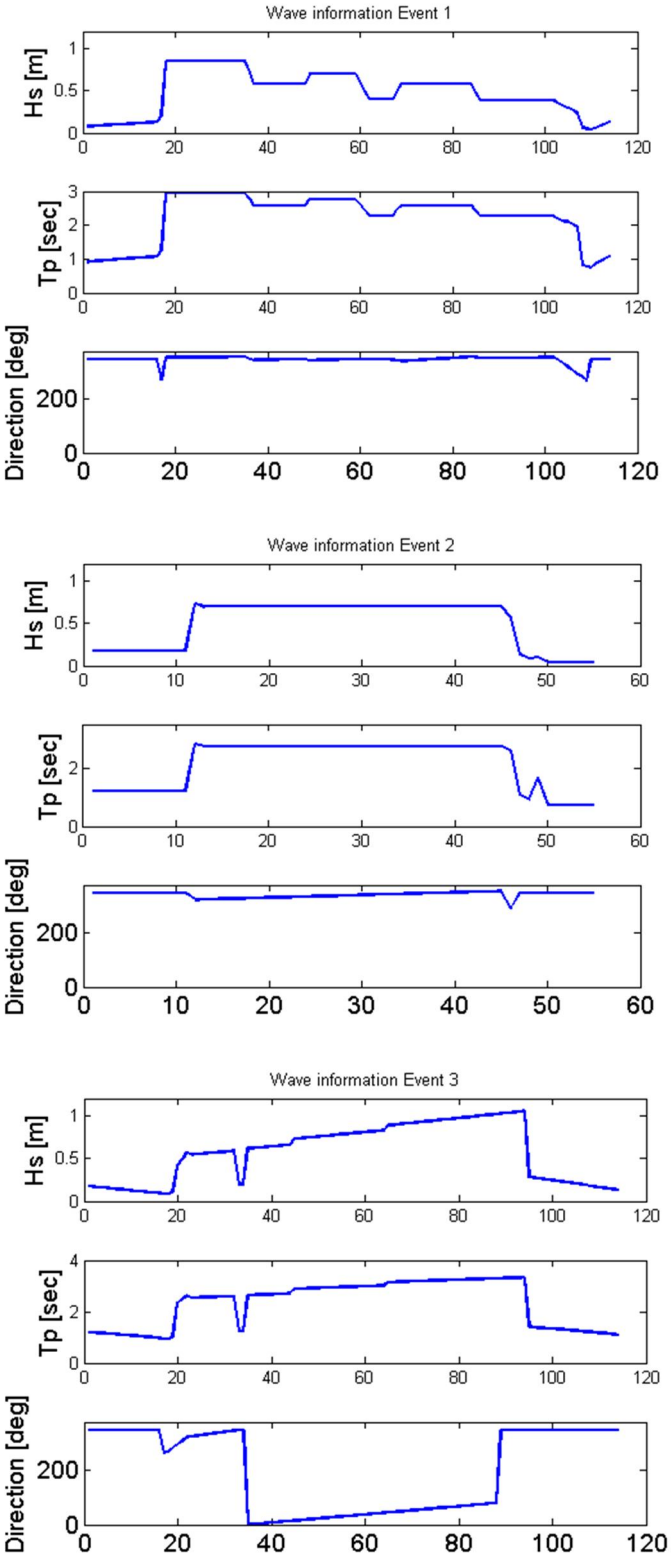

Figure 6.29 Computed nearshore wave conditions cold fronts for events 1, 2 and 3.

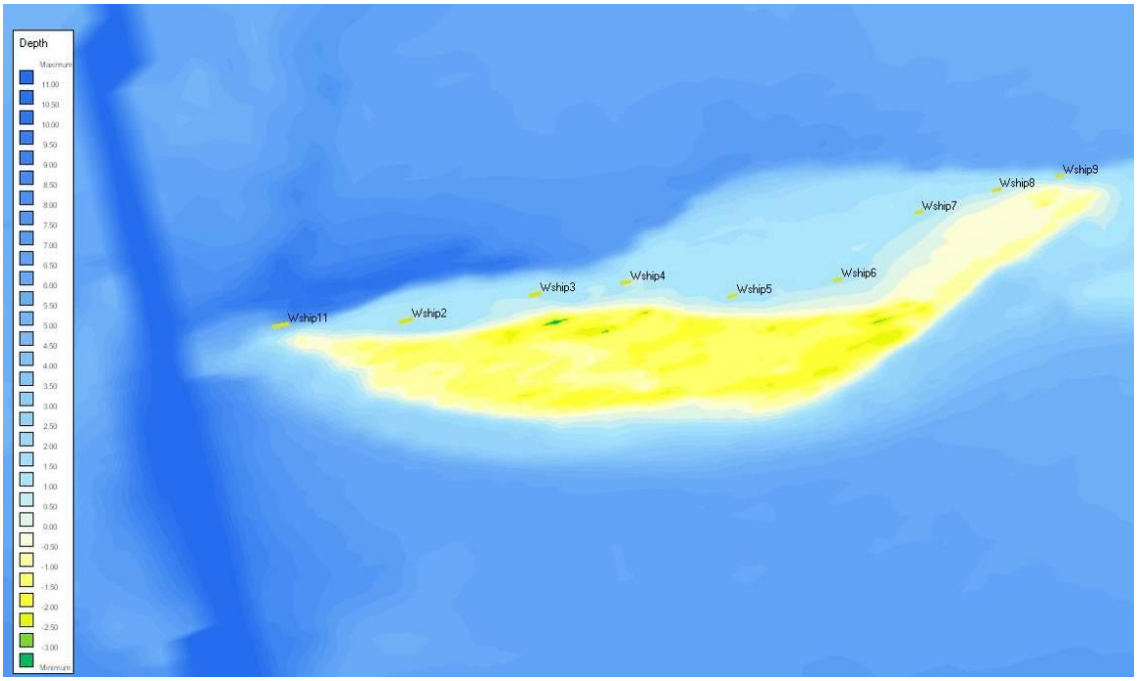

Figure 6.30 Observation points in flow model.

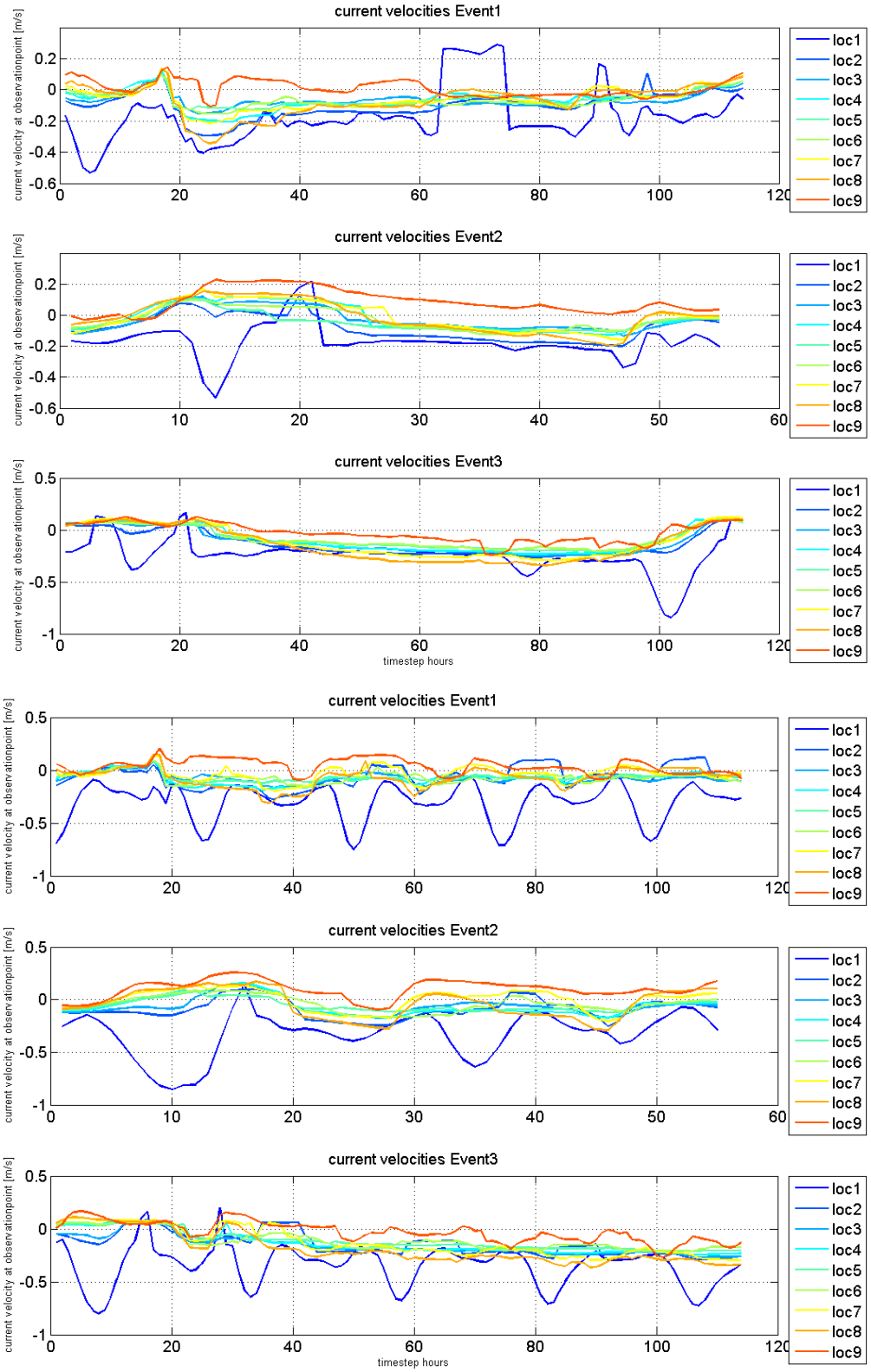

Figure 6.31 Flow velocities derived form flow model for events 1 to 3, upper: neap, lower: spring.

6.4.2 Transport caused by cold fronts

Cold fronts occur 30 to 40 times per year. The computed annual net transport pattern at the Sound side of West Ship Island due to cold fronts is presented in Figure 6.32. The transports are westward directed and vary between about 2,000 and 9,000 cy/yr. The computed gradient suggest a tendency of accretion along the central section and a tendency of erosion along both ends of West Ship Island.

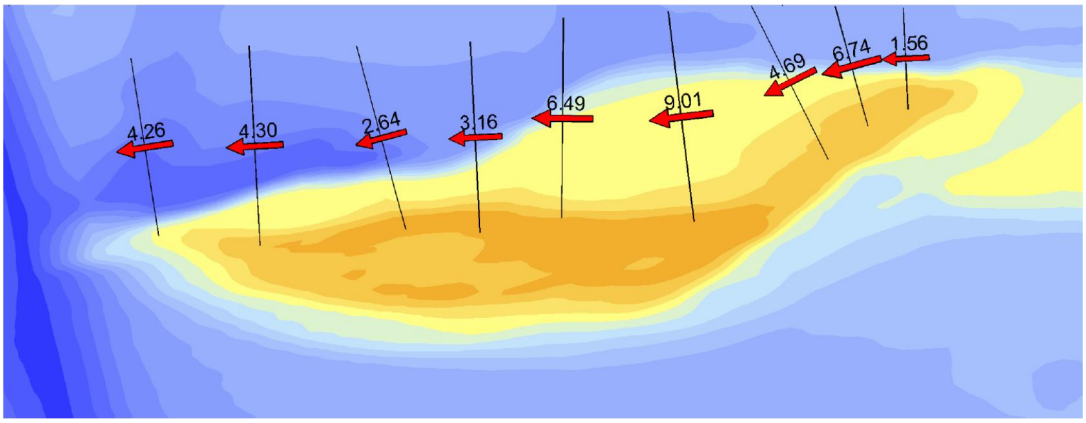

*Figure 6.32 Computed net longshore transports due to cold fronts (*10^3 cy/yr) along West Ship Island.*

6.4.3 Relative importance of individual events

In Figure 6.33 the contributions of the evaluated wind directional sectors is presented. The red line represents the computed total annual transport due to cold fronts, the blue bars represent the contribution of the directional sectors (upper: NW, central: N, lower: NE) to this total transport. The results indicate that the cold fronts with wind from the directional sector NE are dominant in terms of resulting longshore transport.

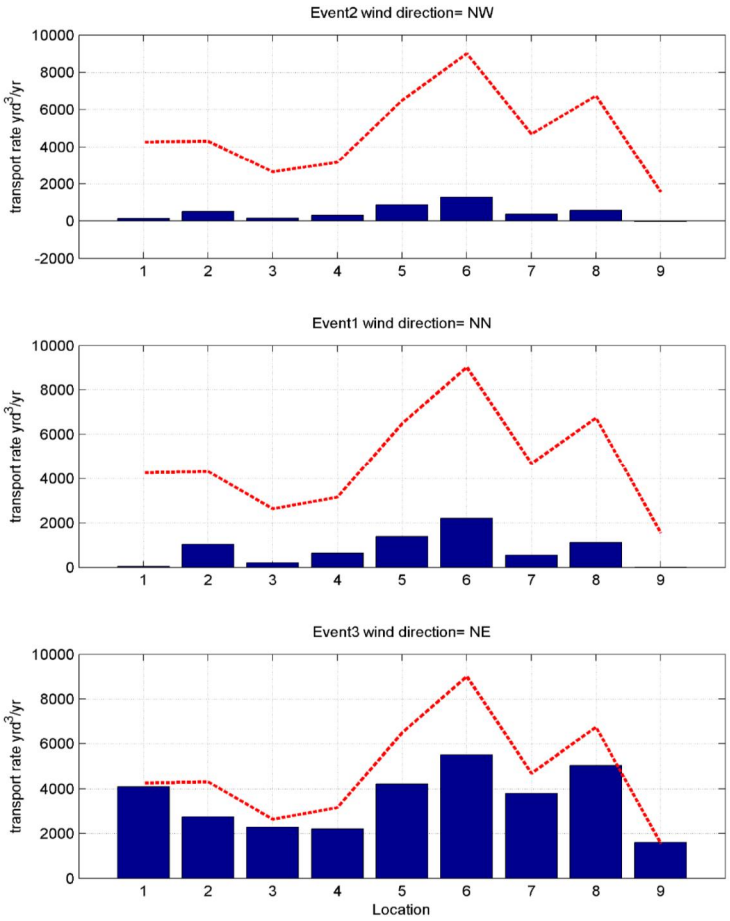

Figure 6.33 Contributions of different wind sectors to cold front transport (red line = total computed annual transport).

7 Sediment balance

7.1 Introduction

In this chapter the computed sediment transports for year averaged conditions and hurricanes are combined. Reference is made to Section 7.2.

Uncertainties related to the numerical modeling are discussed in Section 7.3, with the objective to assess a confidence interval for interpretation of the results. The uncertainties are partly caused by physical (e.g. grain size or salinity) and model parameter (e.g. choice of transport formulation or bed shear stress formulation) settings, and partly by the adopted modeling approach.

Next, in Section 7.4, the computed sediment balance is evaluated, based on a comparison with a large-scale and long-term sediment balance presented by Byrnes et al. (2011). This balance was derived from historical shoreline and bathymetric survey data.

Maintenance dredging records are available for Pascagoula Ship Channel and Gulfport Ship Channel. In Section 7.5 the local transports are evaluated based on these dredging data, taking into consideration the transport at the Gulf side due to year averaged conditions, transport due to hurricanes, transport at the Sound side due to cold fronts, and the effect of a disposal area close to the channel.

Various other studies have been carried out for the area. In Section 7.6 the main results of these studies are briefly summarized and compared with the results of the current study.

This chapter is concluded with discussion on the results in Section 7.7.

7.2 The computed sediment balance

Figure 7.1 shows the computed total longshore transport (see green line, S_{tot}) in which the contribution of the year averaged conditions and the hurricanes (both presented in Chapter 6) are combined. The longshore pattern of both contributions is similar, so the considerations presented in Section 6.2.2 for the year-averaged conditions also apply to the total transport.

It is noted that the computed values presented should be interpreted as ‘best estimates’ with a considerable range.

Figure 7.2 shows the computed sediment balance based on the combined effect of the year-averaged conditions and the hurricanes (both presented in Chapter 6). In Section 7.3 this balance is compared with the sediment balance presented by Byrnes at al. (2011).

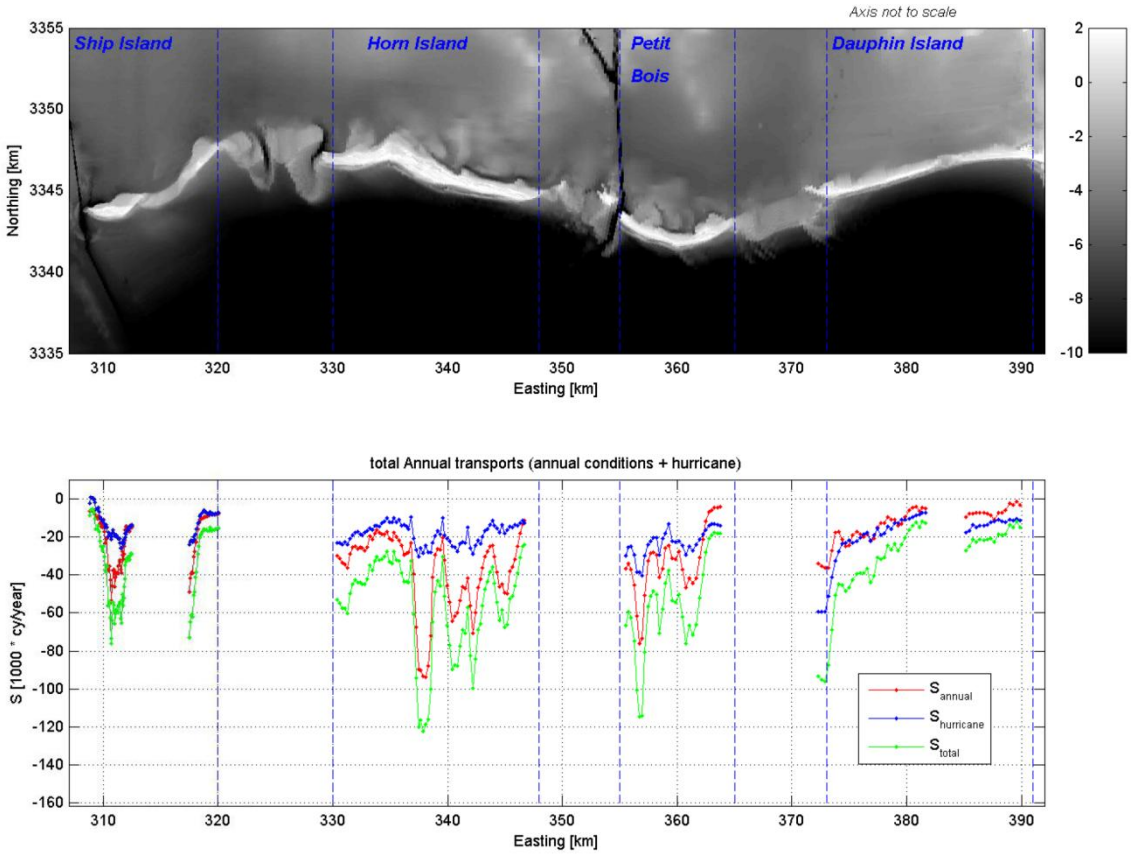

Figure 7.1 Computed total transport along Gulf side of barrier islands (green line) due to combined effect of year-averaged conditions (red line) and hurricanes (blue line).

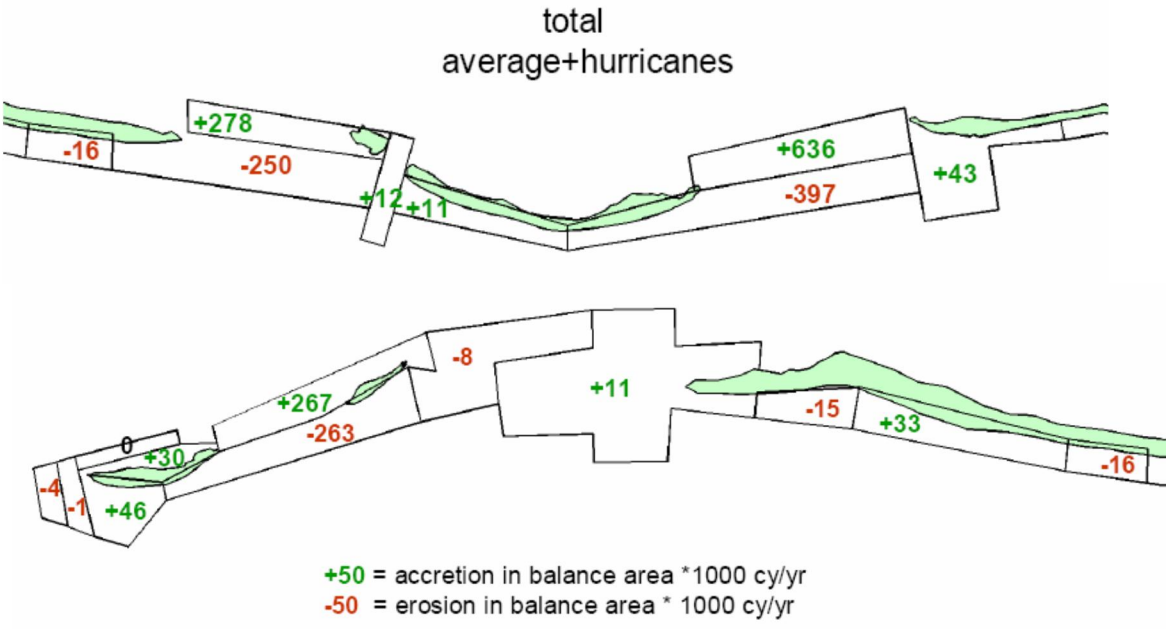

Figure 7.2 Computed sediment balance due to combined effect of year-average conditions and hurricanes.

7.3 Uncertainties

A detailed sensitivity analysis is presented in Appendix B where parameters to which the model is potentially most sensitive are varied. Both physical parameters (e.g. grain size or salinity) and model parameters (e.g. choice of transport formulation or bed shear stress formulation) are considered. The model parameters and the physical parameters are varied within the appropriate ranges for the study area. The parameters are subdivided into four groups for which the longshore transports along the barrier island are evaluated (default settings are underlined):

- Group A: Hydrodynamics
  - Bed shear stress formulation under waves (Fredsoe, 1984; Van Rijn, 2007)
  - Density (ρ), salinity (S) and temperature (T) of the sea water (1025 kg/m3, 31 ppt, 15°C; 1020 kg/m3, 31 ppt, 30°C; 1000 kg/m3, 10 ppt, 30°C)
  - Background diffusivity and viscosity (0.5, 0.5; 0.2, 0.2; 1, 1)
- Group B: Wave conditions
  - Breaker parameter (γ=0.73; Ruessink, 1998; Battjes and Stive, 1985):
  - Increase of 10% of all wave heights
- Group C: Sediment properties
  - Median sediment grain size (D_{50} = 200, 250, 300, 400 μm):
- Group D: Sediment transport formula
  - Van Rijn (1993)
  - Van Rijn (2004)

The results of the sensitivity analysis are shown as transport envelops for each group in Figure 7.3. Group A only has a minor effect on the magnitude of the alongshore sediment transport rates and hardly impacts the overall alongshore patterns (i.e. the spatial trends and gradients remain more or less the same). Also Group B had a relatively small effect as the overall patterns did not change. However, both the sediment properties (Group C) and the sediment transport formula (Group D) have a significant impact on the computed sediment transports. A larger D_{50} increases the critical shear stress of the sediment at which the grains may become suspended and increases the particle fall velocity. Under the same hydrodynamic conditions, this results in decreased mobility of the sediment (i.e. decreasing sediment transport rates). Although both the Van Rijn (1993) and (2004) sediment transport formulations are widely applied in sediment transport modeling, the differences in the alongshore sediment transport rate are large.

Based on the outcomes of the sensitivity analysis, overall factors of 0.8 and 3.5 on the default longshore transports are defined as the lower and upper ranges of the predictions. As the longshore transport distribution patterns are mostly unaffected (implying that only the response rates are affected, not the morphological response itself) Van Rijn 1993 was selected as the default transport formula for the sediment budget since it requires less computational time.

Surveys (USGS, 2011) showed a large spatial variability in the grain size distribution on the shoreface (active part of the profile just seaward of the surf zone). If it is assumed that a similar variability in sediment characteristics is also present in the entire littoral zone, a large part of the uncertainty also originates from the sediment characteristics.

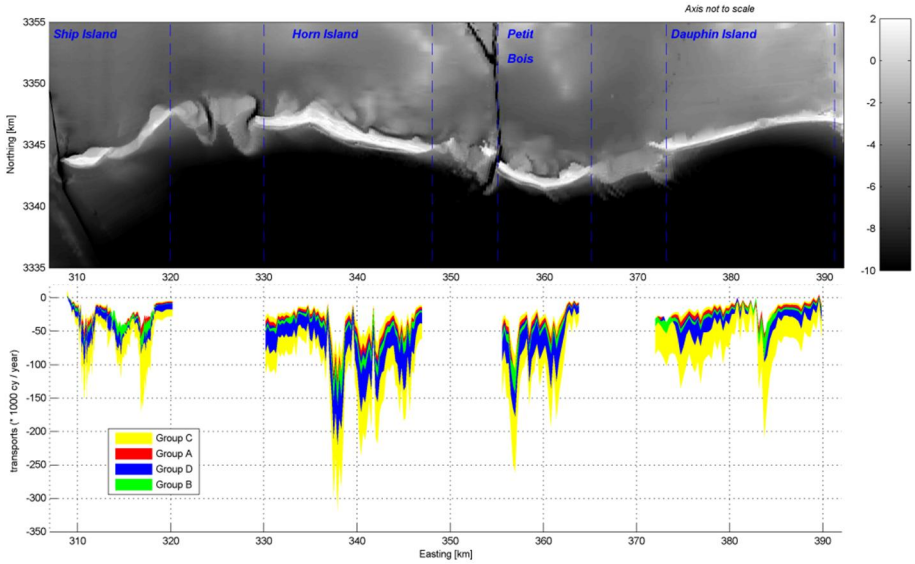

Figure 7.3 Envelope of longshore transports due the variations in each of the groups.

Besides the investigated model parameters, the adopted approach also introduces uncertainties. The most significant of these are discussed below:

- Not all wave conditions are considered, in stead the conditions are aggregated in wave height and direction bins and the wave period is based on the weighted averaged (based on the occurrence probability) of the conditions in each bin. Since a detailed wave climate was utilized it is expected that the wave schematization for the sediment budget study does not introduce major uncertainties.
- The sediment transports are derived from so-called initial model simulations in which no bed change was included. Although this usually does not influence the larger scale sediment transport distributions (e.g. island scale), it may result in irregular transports which can cause local deviations of typically 50% to 100%. This effect was accounted for in the derivation of the sediment budget; however, in the longshore transport distributions it is believed that the observed small scale irregularities originate from this.
- A single post-Katrina bathymetry was used to calculate the sediment transports. However, the MCC has experienced considerable changes over the past century: islands have re-aligned and some have completely disappeared. It is expected that these morphological changes have a major influence on the sediment budget and especially on the sediment bypass across the inlets. The single bathymetry approach induces the largest uncertainties of the discussed “approach uncertainties”. Unfortunately it was not possible to quantify the uncertainty due to the significant associated computational effort. It is expected that significant local deviations may result from this (O(100%)). Furthermore the local transport patterns across the inlets are likely to be affected.

A straightforward summation of all listed uncertainties would result in ranges exceeding 50% to 500%. However, based on previous experience, ranges of 0.5 to 3.5 times the default transport calculations are considered a good measure for the confidence intervals.

7.4 Comparison with Byrnes study

The sediment budget study carried out by Byrnes *et al*. (2011) is based on historical shoreline and bathymetric survey data over a period of about 90 years between 1917 and 2005. In this

study, sediment transports have been derived from observed volume changes (corrected for dredging) between consecutive surveys.

In Figure 7.4 the MCC model results are compared with the macro-scale sediment budget of Byrnes. Byrnes considers five (5) boxes for which the sediment exchange with the surrounding area was determined. In this section, the study focuses on the longshore transport. In the figure, the black arrows indicate the total transport in the littoral zone above -30ft (along the Gulf side plus the Sound side, in cy/yr) derived by Byrnes.

The Byrnes study clearly shows that for boxes 1 to 3 the littoral transport over the box edges is substantially larger than the sediment losses offshore and to the Sound. However, in box 4 and 5 the littoral transport rapidly decreases whereas cross-shore sediment losses offshore and to the Sound increase, making these relatively more important.

According to the Byrnes sediment balance, at the eastern edge of box 1, the littoral transport is about 300,000 cy/yr. At the western edge of box 1, the littoral transport increases to more than 400,000 cy/yr and remains more or less constant until the western edge of box 3. From this point to the west, the littoral transport decreases to zero at the western boundary of box 5.

The total transports computed with the MCC-model have been added in Figure 7.4, for the reference computation (Van Rijn, 1993) in red. The magnitude of the littoral transport estimated by Byrnes is substantially larger than the computed transports. As discussed in Section 7.3 the model results should be interpreted with a range of 0.5 – 3.5 around the computed value.

In Figure 7.5 the computed large scale longshore transport (red line in central graph) is compared with that presented by Byrnes (black line). The figure illustrates that the large-scale patterns of the longshore transport are in fair agreement, but (as discussed earlier above) that the computed longshore transport with Van Rijn 1993 is considerably smaller. With the exception of box 4, the volume changes (red versus black bars in the lower graph) resulting from the transport gradients show a fair agreement (factor 1 to 2 difference).

The red dotted lines in Figure 7.5 show the inaccuracy range around the model results. It is concluded that the results of Byrnes are at the higher end of the model accuracy range.

In Table 7.1 we compare the volume changes based on gradients in the longshore transport generated along the Gulf-facing shores[8]. These transports are only slightly smaller than the total transport (Gulf plus Sound). The table indicates that on a large scale and in a qualitative sense the computed gradients are in fair agreement with those presented by Byrnes. With the exception of box 4, also in a quantitative sense there is a fair similarity.

8. *The longshore transports indicated by Byrnes in Figure 7.14 include the combination of longshore transport generated along the Gulf-facing plus the Sound-facing shore. On the basis of the more detailed balances presented in Figure 3.18 we have derived the longshore transport along the Gulf shores as presented in Table 7.1.*

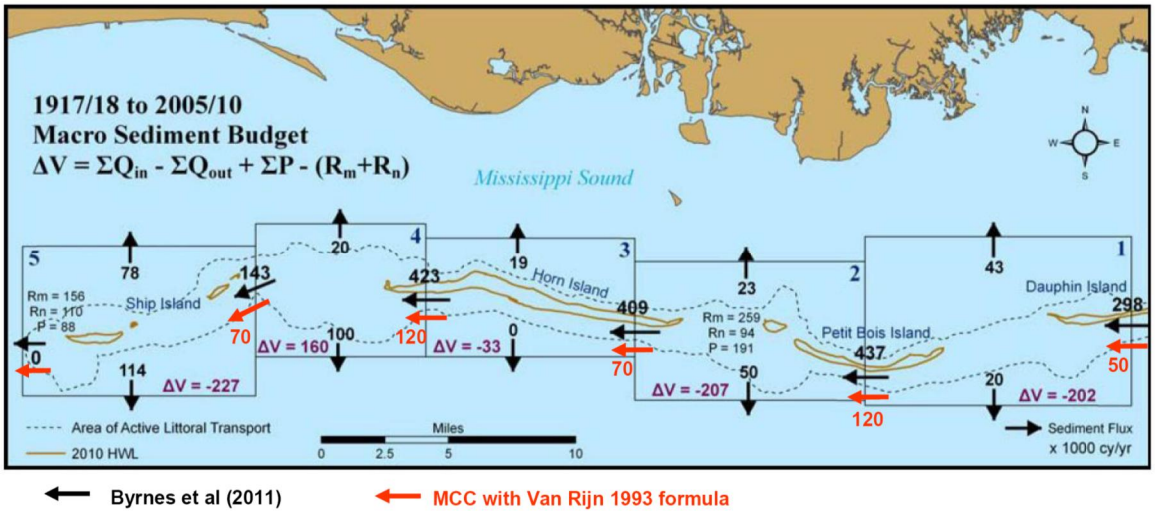

Figure 7.4 Macro scale sediment budgets according to Byrnes (black arrows and numbers, in cy/yr). Red arrows and numbers indicate macro scale sediment budgets based on simulation result from Delft3D MCC-model with D50 of 0.3 mm with formula Van Rijn (1993). For an explanation of P, Rm and Rn reference is made to Section 3.9.2.

Box	ΔS (cy/year)	
	Byrnes	Model, Van Rijn 1993
1	-143,000	-70,000
2	+57,000	+50,000
3	-33,000	-50,000
4	+260,000	+50,000
5	+143,000	+70,000

Table 7.1 Comparison of longshore transport 'gradients' ΔS (ΔS = Sin - Sout, where S = longshore transport).

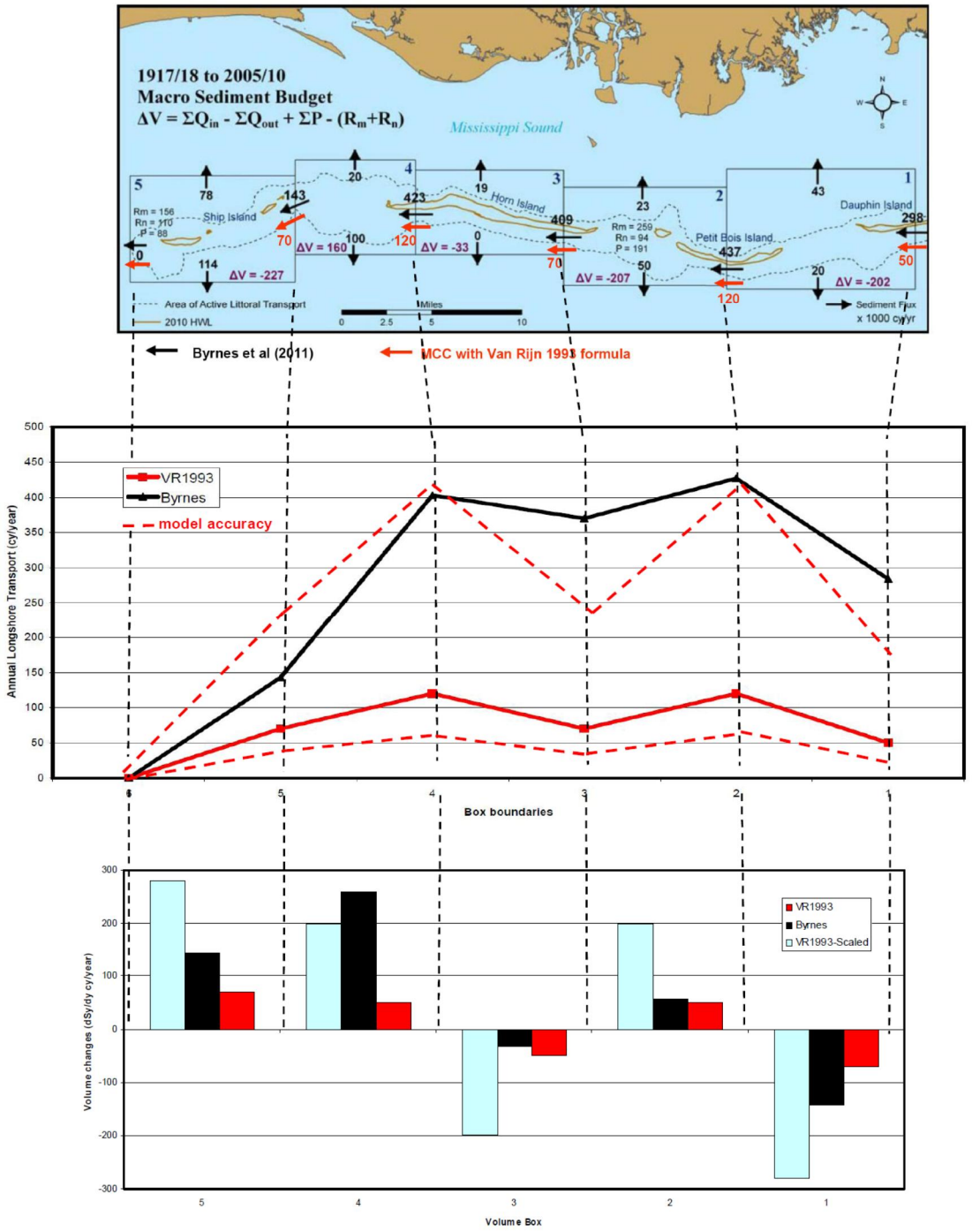

Figure 7.5 Comparison of sediment balance of Byrnes, MCC with Van Rijn 1993 and scaled Van Rijn 1993.

The MCC model results for year-averaged and hurricane conditions have also been compared with the more detailed sediment balances presented by Byrnes et al (2011), as presented in Figure 3.20. For this purpose the Balance Area presented in Figure 7.2 has been chosen approximately similar to the accretion and erosion areas presented in Figure 3.20. On the basis of the computed net transports in and out of these Balance Areas the volume changes have been determined and compared with the volume change rates presented by Byrnes, see Figure 7.6. In the figure the volume changes presented by Byrnes

have been corrected to account for dredging and dumping, so they represent the effect of the natural processes only.

Qualitatively the overall erosion – accretion pattern computed with the model is in fair agreement with the pattern presented by Byrnes. Quantitatively, in some Balance Areas the deviations between the model results and the volume changes presented by Byrnes are considerable.

Figure 7.6 shows that at the western end of Dauphin Island (area 1) the model and Byrnes both indicate accretion. Byrnes indicates a considerably higher accretion rate than the model. This may be (partly) due to the fact that the Byrnes balance includes the effect of the migration of the island into this area (compare in Figure 3.20 the location of the HWL in 1917 and the HWL in 2010) which may not only be affected by the longshore transport along the island, but also by the balance of Petit Bois Pass. This is illustrated by the balance of area 2, where the model shows considerable accretion in the area where further migration of Dauphin Island is expected in the future. For the Balance Areas 1 and 2 combined the computed accretion is in fair agreement with the balance of Byrnes. In Balance Area 3 the computed trend is similar to that presented by Byrnes.

Along Petit Bois Island (Balance Areas 3 and 4) the computed pattern is similar to that presented by Byrnes. However, in area 4 the computed accretion is considerably smaller than the rate presented by Byrnes. This may be explained in a similar way as discussed above for Balance Area 1. For Balance Area 5 the model indicates slight accretion, where Byrnes (corrected for dredging) indicates significantly more accretion than the model. Balance Area 5 represents the Pascagoula Ship Channel, so the computed accreting tendency in this area is as to be expected for the present situation. In the areas 6 and 7 in Horn Island Pass the computed accretion and erosion are in fair agreement with the balance presented by Byrnes.

Along Horn Island the computed accretion and erosion pattern (areas 8, 9 and 10) is in fair agreement with the Byrnes balance, though overall the computed values are somewhat smaller. In areas 11 and 12 in Dog Keys Pass the model indicates similar to Byrnes accretion and erosion, though with considerably smaller rates than Byrnes. It is not clear how the temporary existence of Dog Island has affected the long term balance of Byrnes, but the dynamics of this island may have contributed to relatively large volume changes derived from the maps and surveys.

The computed accretion and erosion along East Ship Island and Camille Cut (areas 13 and 14) are in reasonable agreement with that presented by Byrnes. The areas 15 and 16 combined and area 17 show a fair similarity between the computed accretion and that presented by Byrnes. Balance Area 18 is located at the present Ship Island navigation channel location, after re-alignment of the channel around 1993. Until that time, this section of the channel was located more eastward. In the Byrnes balance (corrected for dredging), in area 18 accretion is indicated in the navigation channel. The model shows a more or less neutral balance, but it is noted that the balance of this complex area depends largely on the exact position of the balance boundaries, since small shifts may change the balance considerably. In Section 7.4 this area is evaluated in more detail. This detailed evaluation shows that the model indicates accretion in area 18. The model indicates that area 19 is slightly erosive, with a smaller rate than the erosion indicated by Byrnes (corrected for sand placement). Also this small area is very sensitive for the exact position of the area boundaries.

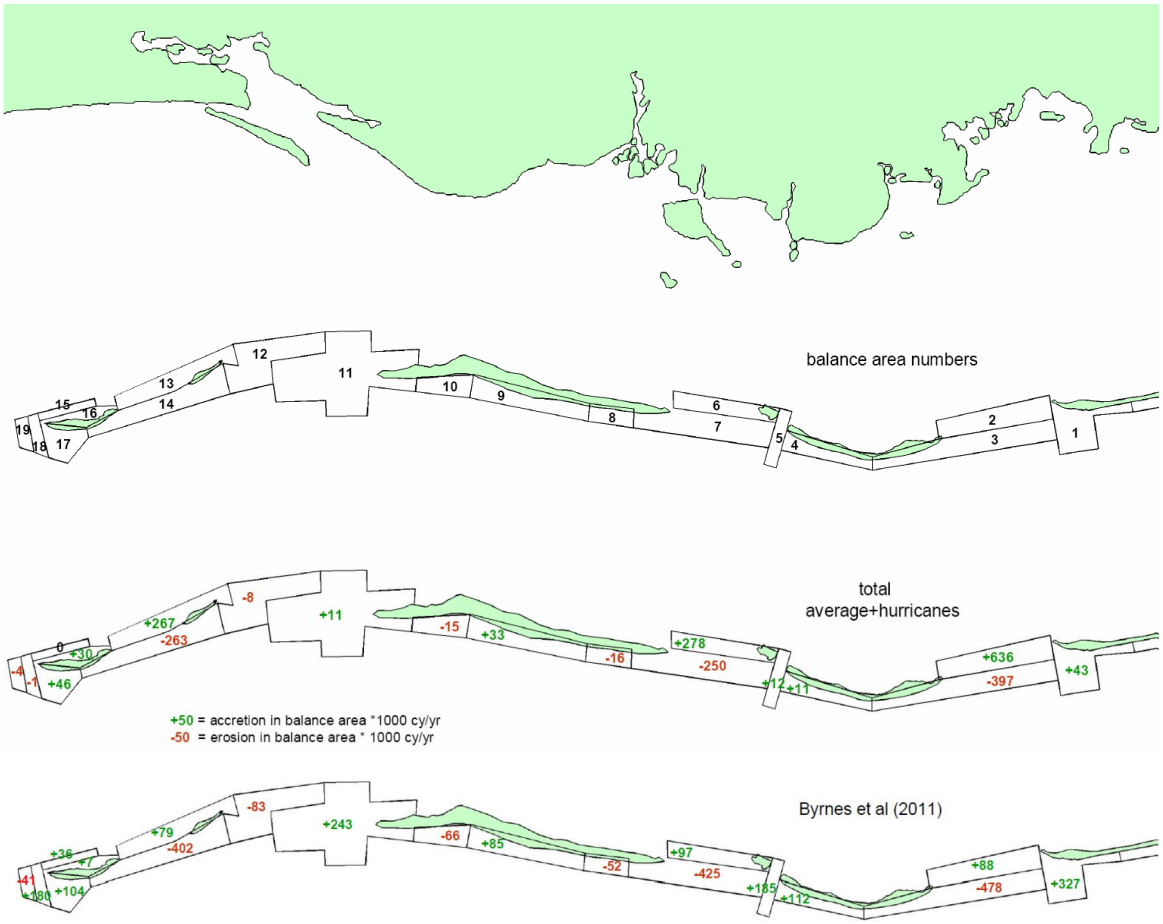

Figure 7.6 Comparison of detailed sediment balance MCC model and Byrnes at al (2011) (Byrnes volumes in areas 5, 18 and 19 have been corrected to account for sand dredging and placement)

7.5 Comparison with dredging records and contributions to channel sedimentation

The Mississippi Sound contains several navigation channels. Two channels cross the littoral system, i.e. Pascagoula Ship Channel (located west of Petit Bois Island) which runs through Horn Island Pass and Gulfport Ship Channel (located west of Ship Island), which runs through Ship Island Pass, see Figure 7.7. The maintenance dredging records for these two passes are presented in Figure 7.8 (source: Byrnes et al. (2011)). The figure shows maintenance dredging only (no new work dredging). The composition of the dredged material (percentage sand and silt) was not available during the study. Therefore an analysis of this aspect could not be addressed in this report. This data has recently become available, but it was not addressed in this report since it was not available when the investigation was conducted. It is recommended to investigate the relevance for the sediment balance.

Figure 7.8 shows that in the past (1905-1955) about 40,000 cy/yr was dredged in Horn Island Pass. Recent dredging rates between 1995 and 2009 for Horn Island Pass are in the order of 390,000 cy/yr.

For Ship Island Pass in the past (1900-1950) about 43,000 cy/yr was dredged over a channel length of about 4,000 ft. The recent dredging rate representative for the period after

realignment of the channel to the west (1992-2009) is about 175,000 cy/yr over an assumed channel length of 8 miles[9].

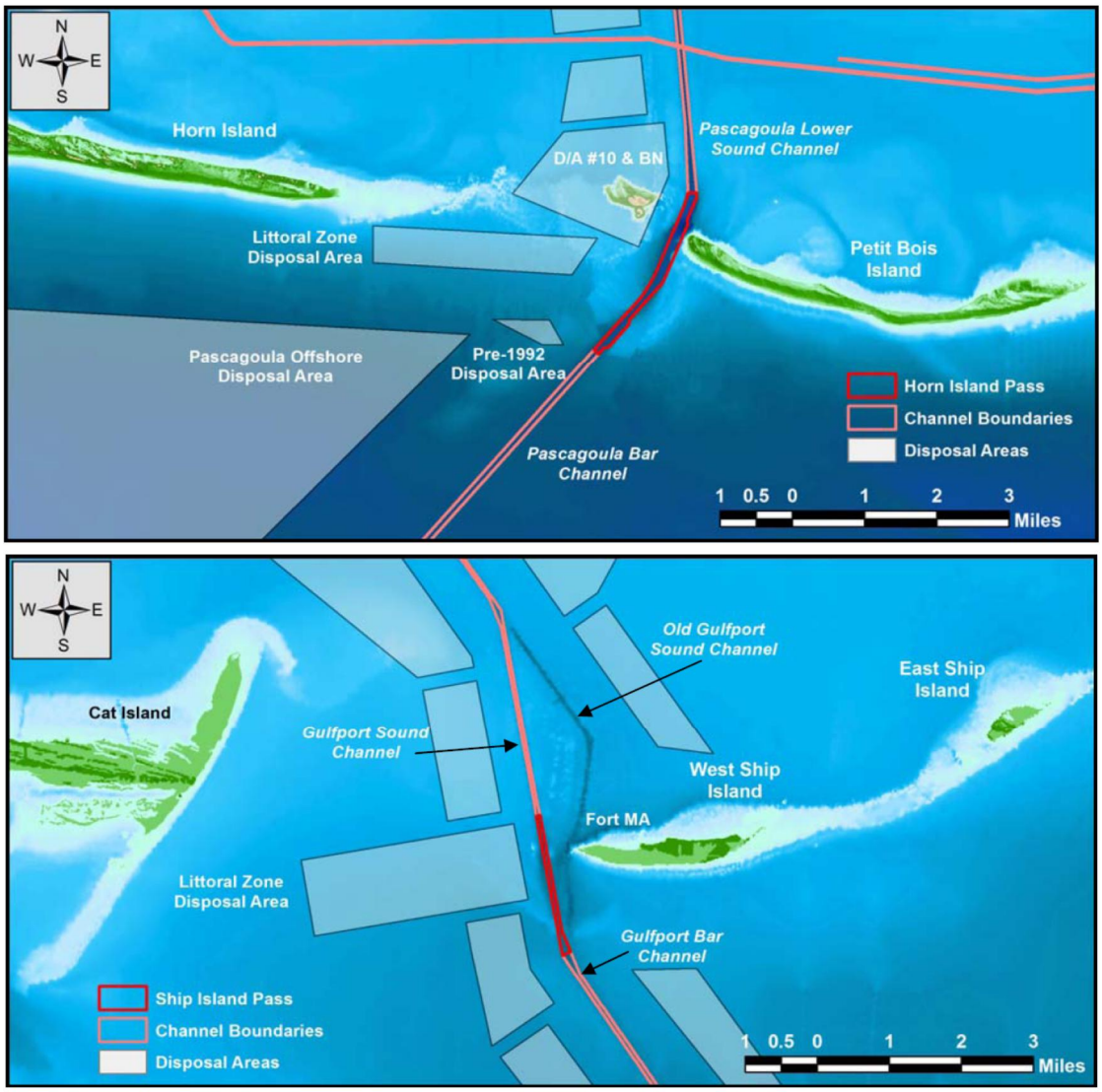

Figure 7.7 Location of Horn Island Pass and Ship Island Pass, and location of disposal areas (source: Byrnes et al., 2011).

9. *For the period 1992-2009 the length of the dredged section is not reported in the data source. However, in the preceding period 1949-1991 it is reported that dredging was carried out over a length of 8 miles. This has therefore been assumed also for the period 1992-2009.*

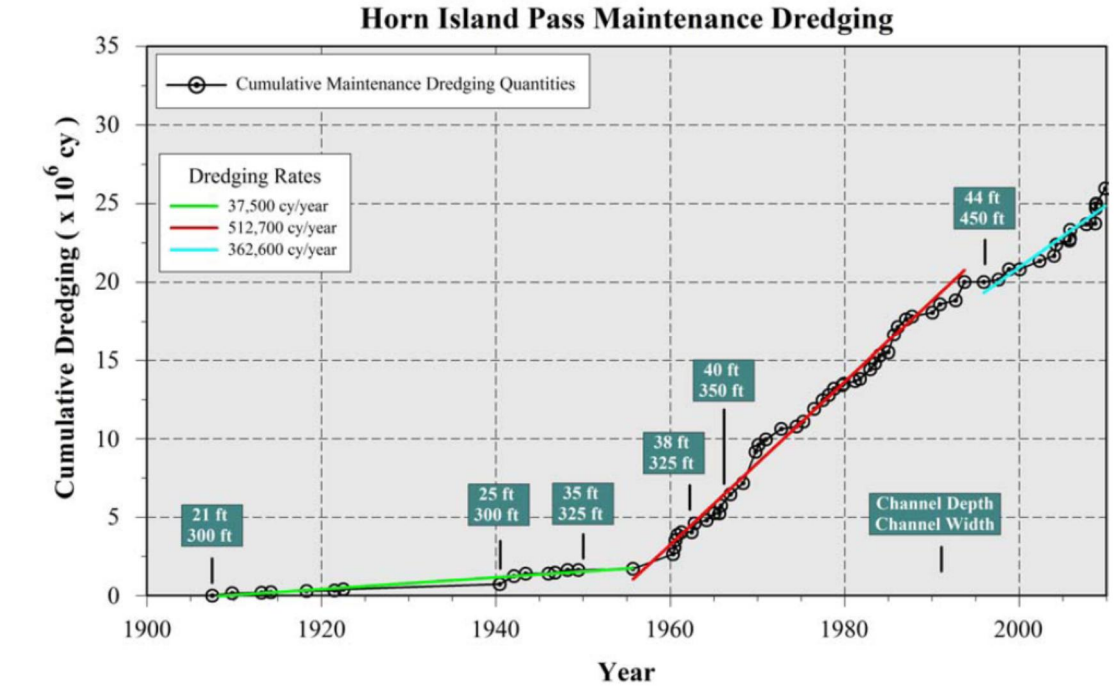

.

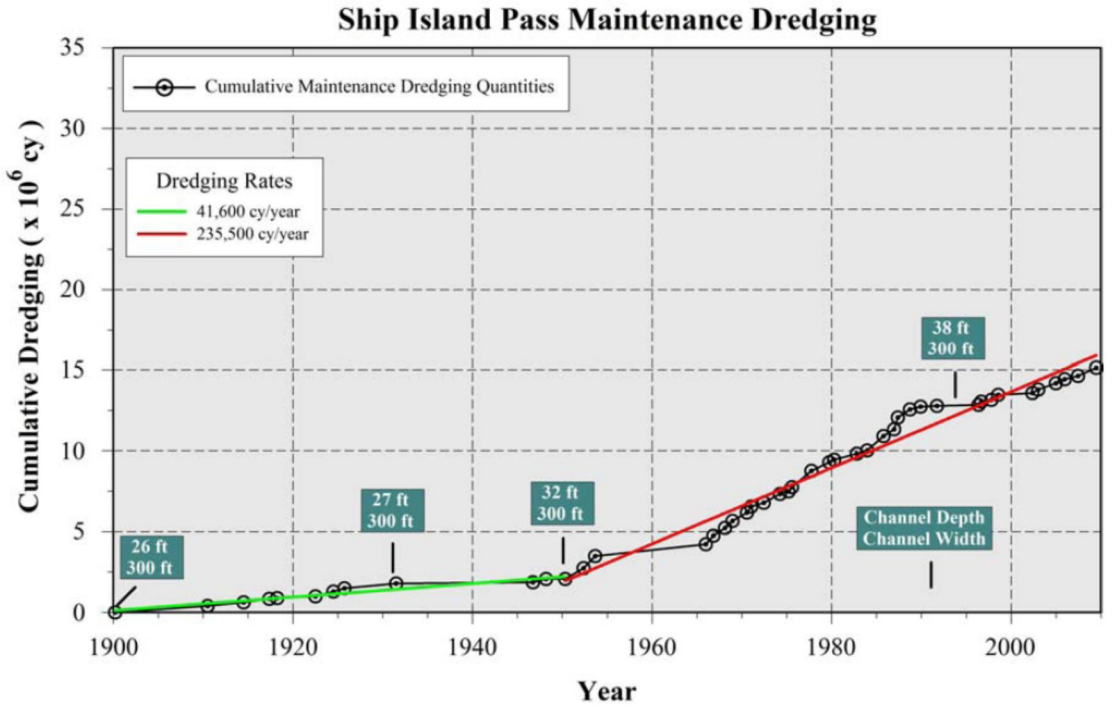

Figure 7.8 Dredging records at Horn Island Pass (Pascagoula channel) and Ship Island pass (Gulfport Ship channel) (source: Byrnes et al., 2011).

Changes in the dredging rates can partly be attributed to manmade modifications to the channel cross-section (deepening and widening of the channel), and partly to changes in the length of the dredged channel section. For example, it is our understanding that for Ship Island Pass the sudden increase in dredging quantities in 1950 is not only due to the deepening of the channel, but also due to an extension of the dredged channel section from 4,000 ft to 8 miles. In the 8 miles long channel section a considerable part of the

sedimentation can be expected to be related to transport not generated along or around the barrier islands but to transport in the deeper region by the tide and by hurricanes. Moreover, at some distance from the islands, the percentage of fines may increase. Information on the distribution of the dredged volume along the 8 miles section was not available.

It is remarkable that for both passes there are several periods longer than 10 years in which no or negligible maintenance dredging has been carried out.

As discussed above, it is likely that part of the dredged material since 1950 originates from other sediment sources than the littoral drift along the barrier islands. In the period 1900-1950 dredging was carried out over a length of 4,000 ft, which is assumed to be the section through the littoral zone. In that period the average dredging rate was about 43,000 cy/yr.

Given above discussed uncertainty on the distribution of the dredging along the channel and the composition of the dredged material, in the littoral part of Ship Island Pass (Balance Area 1 in Figure 7.9) an indicative range for sedimentation due to sand was assumed to be in the range of 40,000 to 180,000 cy/yr. This is in good agreement with Byrnes (2011), who estimated the rate of material dredged from the littoral zone to be 156,000 cy/yr. In the entire 8 miles dredging zone, the sedimentation is about 180,000 cy/yr. In the following a comparison of our model result with the dredging records is presented.

Various contributions to the channel sedimentation will be discussed separately, i.e.:
- Transport at Gulf Side due to year-averaged conditions
- Transport due to hurricanes (incl. the effect of ebb surges)
- Transport at Sound side due to cold fronts
- The effect of disposal area close to channel

All transports are presented as best estimates, which should be interpreted with a considerable range (as discussed in Section 6.2.2).

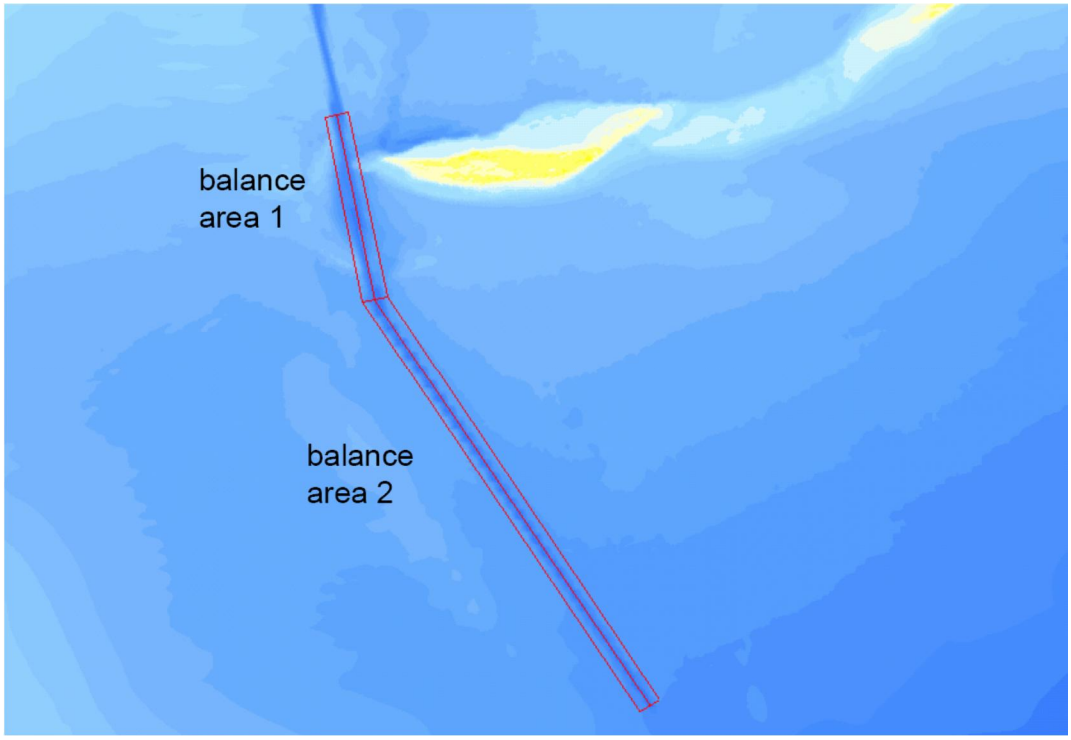

Figure 7.9 Considered Balance Area for channel sedimentation assessment, littoral zone (area 1) and 8 miles zone (area 1 plus area 2).

Transport at Gulf Side due to year-averaged conditions

The computed maximum littoral drift (Gulf side) at some distance from the western end of Ship Island is 80,000 cy/yr, but at the most western end it drops to about 10,000 cy/yr (see Figure 7.1). Therefore, the transport in the littoral zone near the channel is small.

The sedimentation in Ship Island Pass has been evaluated by considering the gross transport directed towards the channel during year-averaged conditions for Balance Area 1 as presented in Figure 7.9. Results are presented in Table 7.3 (see 'year-averaged'). In the table the total gross transport towards the Balance Area is presented and the volume that is indicated by the model to remain trapped in the channel. This 'trapped in area' rate should be used with some caution, since the accuracy of the computed trapping percentage is limited given the model grid size relative to the channel width. The 'transported towards area' rate would be the sedimentation in case that 100% of the sand is trapped in the Balance Area.

The results indicate that under the considered conditions about 15,000 cy/yr is transported towards the channel. It has been roughly estimated that about 10,000 cy/yr is trapped in the Balance Area.

As discussed in Chapter 8, due to the oblique wave attack at the western end of Ship Island it is expected that the sand transport at the western tip exceeds the 10,000 cy/yr computed at that location. Averaged over a longer period, the actual transport may be closer to 80,000 cy/yr but the sand reaches the tip in more or less periodic shoreline features. Thus, the presented 15,000 and 10,000 cy/yr should be considered as a low estimate.

- **Transport due to hurricanes (incl. the effect of ebb surges)**

The contribution of all hurricanes in the period 1917-2011 has been computed for Balance Area 1[10]. All contributions were combined and translated to average annual sedimentation rates in a similar way as discussed for the overall balance in Section 6.3.1. The result is presented in Table 7.3, see 'hurricanes' (for Balance Area 1).

The results indicate that under the considered conditions about 20,000 cy/yr is transported towards the channel. It has been roughly estimated that about 10,000 cy/yr is trapped in the Balance Area.

The rates presented in Table 7.3 are averaged over time. In years of occurrence of a hurricane, the event will largely affect the sedimentation in the considered Balance Area. This is illustrated in Table 7.2, which shows the results for some hurricanes in cy/event. For these hurricanes also values for Balance Area 2 (see Figure 7.9) are presented in Table 7.2.

Condition	Balance Area 1 (littoral zone)		Balance Area 1 plus area 2 (8 miles zone)	
	transported towards area (cy/event)	trapped in area (cy/event)	transported towards area (cy/event)	trapped in area (cy/event)
Katrina	90,000	45,000	860,000	420,000
Notnamed 1947	105,000	45,000	440,000	205,000
Camille	60,000	25,000	230,000	105,000
Georges	60,000	25,000	345,000	185,000
Ivan	35,000	25,000	140,000	90,000
Betsy	25,000	10,000		

Table 7.2 Computed sedimentation in Balance Area in Figure 7.9, contribution of selected hurricanes, values per event.

- **Transport at Sound side due to cold fronts**

From Section 6.4.3 it is concluded that about 5,000 cy/yr is generated along the Sound side due to cold front at the most western tip of Ship Island, see Figure 6.33. This value has been added to Table 7.3, see 'cold fronts'.

- **The effect of disposal area close to channel**

In order to obtain insight into the potential relevance of a disposal area close to the Balance Area, a hurricane simulation has been carried out with the model. On the basis of data presented in Byrnes et al. (2011) a disposal area has been chosen at the location presented in Figure 7.10, at a depth of about MSL -5m to -8 m. Of all disposal areas this one is located closest to the relevant part of the navigation channel, and it therefore potentially has the largest effect on sedimentation in the channel. At the disposal site bed levels have been raised by 1 m. The disposed material was assumed to have the same sediment

10. *For 'Balance Area 1' the contribution of all hurricanes in the period 1917-2011 has been computed and the total volume has been averaged over the considered period to obtain the average annual sedimentation. For 'Balance Area 1 + 2' the annual sedimentation has been estimated in a more indicative way. First from Table 7.2 it was derived that for the considered individual hurricanes, the sedimentation in 'Balance Area 1 + 2' was a factor 4 to 5 larger than in 'Balance Area 1'. Then, in Table 7.3 this factor was applied to the computed value for 'Balance Area 1' to obtain the estimate for 'Balance Area 1 + 2'.*

characteristics as applied for all other model runs (so median sand diameter D_{50} = 0.3 mm, no fines). The simulation was carried out for a hurricane with a return period of about 1/10 yr. The model indicated no significant effect on the sand transport in and around the channel. Given this result, the effect of other disposal areas was not considered further.

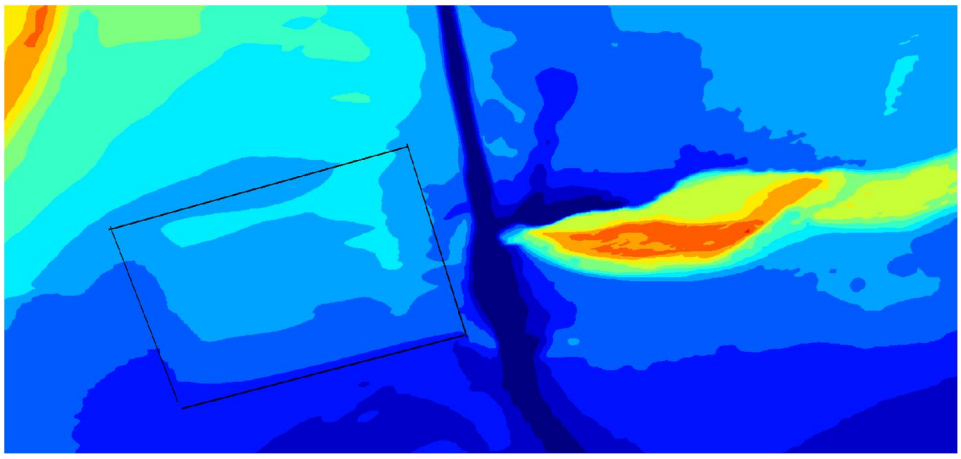

Figure 7.10 Location of disposal area.

Total effect considered contributions

Table 7.3 shows the combined result of the contributions discussed above. The best estimate for the sedimentation in Balance Area 1 is 25,000 to 40,000 cy/yr (for about 60 % resp.100% trapping of sand in the channel). The upper limit of the computed range lies close to the lower limit of the range derived from the dredging quantities (which was 40,000 to 180,000 cy/yr). As discussed above, there may be some under-estimation of the year-averaged contribution, since periodically waves of sand are expected to reach the tip of the island. During such periods the transport towards the channel is expected to exceed the computed 15,000 cy/yr.

Condition	Balance Area 1 (littoral zone)		Balance Area 1 plus area 2 (8 miles zone)	
	transported towards area (cy/yr)	trapped in area (cy/yr)	transported towards area (cy/yr)	trapped in area (cy/yr)
year-averaged	15,000*	10,000*	20,000*	15,000*
hurricanes	20,000	10,000	80,000	40,000
cold fronts	5,000	5,000	5,000	5,000
disposal area	nihil	nihil	nihil	nihil
total	40,000	25,000	105,000	60,000

* *As discussed under the header 'Transport at Gulf Side due to year-averaged conditions' these values are expected to under-estimate the effect of the year-averaged conditions, due to phenomena which can not be derived directly from the initial transport computations*

Table 7.3 Computed annual sedimentation rate in Balance Area, best estimates, to be interpreted with a range.

For Balance Area 1 plus 2 combined the computed sedimentation is 60,000 to 105,000 cy/yr (assuming about 60% and100% trapping of sand in the channel).

According to the model results, for Balance Area 1 the contribution of the year-averaged conditions and the hurricanes are similar. For Balance Areas 1 and 2 combined, the contribution of the hurricanes becomes dominant.

As discussed in Section 6.2.2 the reported computed values are best estimates which should be interpreted with a range.

7.6 Comparison with model results other studies

The order of magnitude of the computed longshore transports in the MCC-model are in fair agreement with computational results presented by Cipriani and Stone (2001). These computations were based on a CERC-type of longshore transport formula. The computations were forced with the year-averaged wave conditions derived from WIS data for the period 1956-1975. The maximum transport rate computed by Cipriani and Stone (2001) is 60,000-65,000 m^3/yr (80,000-85,000 cy/yr), found at the western end of Dauphin Island and at sections of Horn Island. Similar to the MCC-model results, the longshore transport pattern found by Cipriani and Stone (2001) is rather irregular alongshore. The effect of hurricanes is not discussed in the paper.

In ERDC/CHL (2009), the computed longshore transports are presented. For Dauphin Island the values range between about 0 and 95,000 cy/yr, for Petit Bois between -30,000 (eastward) and 160,000 (westward) cy/yr, for Horn Island between 20,000 and 200,000 cy/yr, and for Ship Island between -80,0000 (eastward) and 200,000 (westward) cy/yr. In ERDC/CHL (2011) transports have been computed with the model GENESIS, based on WIS wave data. The study computed a net westward transport between 0 and about 250,000 m^3/yr at West Ship Island, which is considerably larger than the transport computed with the MCC-model.
In ACRE (1999) computed transports along Morgan Peninsula are presented. Values between 50,000 and 100,000 m^3/yr are presented. In ACRE (2008) computed values along Morgan Peninsula between 100,000 and 250,000 cy/yr are presented and values between 50,000 and 250,000 cy/yr along Dauphin Island.

It is concluded that the order of magnitude of the transport computed with the MCC model is in fair agreement with some of the previous studies, while compared to some others the computed transports are somewhat smaller.

7.7 Discussion

In this chapter the computed sediment balance has been presented and compared with readily available data and other studies of the area.

The long-term sand balance of Byrnes at al. (2011) was assumed to provide the most comprehensive information as it is based on an elaborate study of the historic bathymetry surveys and dredging volumes. The transport computed with the MCC model tends to be considerably smaller than that presented by Byrnes. However, for large parts of the study area, the large-scale computed longshore transport gradients are in fair agreement with Byrnes, see Table 7.1 and Figure 7.5. On a smaller scale the computed erosion and accretion pattern shows a fair agreement with the pattern of Byrnes, see Figure 7.6, though at some locations the quantitative resemblance is poor. Beforehand deviations between the

computations and the Byrnes balance were expected, given that the current study only considered one bathymetry. Reference is made to the discussion on uncertainty in Section 7.3. The MCC model shows initial patterns based on the present situation, whereas the Byrnes balance is based on long term averaged patterns over a long period of time (period 1917-2010) in which islands have partly migrated in and out of Balance Areas or have breached. At some locations, small islands have even disappeared (Dog Island).

Based on the discussion on uncertainties in Section 7.3 it is concluded that the model results should be interpreted with a range of 0.5 to 3.5 times the default transport calculations. The results presented by Byrnes are at the upper limit of this range. Considering an accuracy range of the Byrnes' study, the agreement between both approaches is considered fair.

The order of magnitude of the transport computed with the MCC model is in fair agreement with some earlier studies in the area, while compared to some others the computed transports are somewhat smaller.

In conclusion, compared to all published transport data, our basic computation, carried out with the formula of Van Rijn (1993), is near the lower end of the range in the published data.

In Appendix C some computations with other modeling tools are presented, which have been made as a verification of the computed order of magnitude of the transport in the MCC model. These confirm the computed transport rates. On the basis of the sensitivity analysis and Appendix C, and given the low wave energy under normal conditions, we consider the order of magnitude of the transport computed with the MCC-model realistic.

As discussed in Section 6.2.2, on the basis of several considerations, it is possible to upscale the computed transport. However, as discussed above, given several uncertainties and difficulties in comparing the results with the other data, such up-scaling has not been carried out. Moreover, the transport pattern and morphological response (erosion-accretion pattern) are considered satisfactory. Therefore, time scale of the morphological response is the main uncertainty.

8 Morphological evaluation of the restored Ship Island

8.1 Introduction

The morphological evolution of the restored Ship Island and the associated impact on its surroundings is discussed in this chapter. The impact of the restoration design is addressed by evaluating the predicted sediment transports and morphodynamic development relative to the baseline case (i.e. pre-restoration situation). To separate the impact of the different elements of the restoration (i.e. closure of Camille cut, additional sand placements and borrow areas), a number of cases have been defined in which several combinations of the restoration elements are separately considered (see Table 8.1).

Case	Camille Cut closure	SE sand placement	Offshore borrow area	Ship Isl. Pass borrow source	Widened Gulf Port channel	north sand placement
1a	no	no	no	no	yes	yes
1b	no	no	no	yes	yes	yes
2a	yes	yes	no + yes	no	yes	yes
2b	yes	yes	no	yes	yes	yes

Table 8.1 Summary of baselines and restoration designs to be studied (see also Section 1.1).

The restored Ship Island is morphologically evaluated for three distinct scenarios:

1. Medium-term – post-construction: The medium term, 4 year, morphological development under averaged conditions (excluding cold fronts) just after construction for all cases listed in Table 8.1.
2. Hurricane impact – Post-construction: the impact for six (6) different types of hurricane as defined by the Sallenger (2000) classification just after construction for the Cases 1a and 2a (with offshore borrow area).
3. Medium-term – Post-hurricane: the post-hurricane recovery potential under averaged conditions of the restored Ship Island for three of the predicted post-hurricane bathymetries from Step 2 (i.e. repeating Step 1 with the final bathymetries from Step 2).

Furthermore, a limited number of additional medium-term simulations for an alternative transport formulation and different D_{50} grain sizes were performed as these parameters were identified by the sensitivity analysis in the previous chapter.

In the following section the modeling approach is further detailed, followed by Section 8.2.4 in which the predicted morphological developments for the three scenarios outlined above are discussed.

8.2 Modeling Approaches

8.2.1 General

In this section the focus is on the models that are relevant for the evaluation of the restored Ship Island. This is the smallest scale in the cascade of the models that has been set-up for the present study. Details of the larger scale models can be found in the previous chapters (Chapter 4: hydrodynamic modeling, Chapter 5: wave modeling). A Delft3D model of Ship Island (labeled SPI-model) is used to determine the medium term morphodynamic evolution

of Ship Island whereas an XBeach-model that covers the same domain is applied to estimate the hurricane impact. Both models are forced with the hydrodynamic and wave forcing boundary conditions derived from the MCC-model (see Chapters 4 and 5).

8.2.2 Medium-term morphodynamic modeling of the restored Ship Island

The Delft3D SPI-model is a local cut-out of the MCC grid around Ship Island with an identical resolution as the MCC-model. The SPI-grid consists of 325 by 330 grid cells (Figure 8.1). The boundary conditions for the SPI are derived from the MCC-model. To enable multi-annual morphodynamic simulations a number of input reduction and morphological acceleration techniques have been applied. These techniques are aimed at increasing the computational efficiency of the simulations without affecting the quality of the predictions. The input conditions for both the tide and the wave conditions have been reduced. Furthermore, the morphodynamic simulations were sped up by using the parallel-"Delft3D-Online" or MorMerge approach which combines a morphological acceleration technique with a parallelization of the simulation.

The morphodynamic modeling therefore requires the application of the following methods:

1. An elongated tide approach in which a single tide represents a full neap-spring tidal cycle was used. The concept was first introduced by Latteux (1995) for which van Rijn (1993) proposed a relative simple approximation which is adopted in the present study (see Section 6.2.1.2 for details).
2. The full wave climate (139 discrete wave height, period and direction combinations) was reduced by ensuring the wave driven initial transports of the full and reduced wave climate result in near identical transport patterns over the entire model domain (this is further detailed below). In this case the in-house developed 'Opti'-method was used to derive the representative wave climate (see e.g. Roelvink and Reniers, 2011).
3. The morphological acceleration concept inspired by Latteux (1995) was incorporated in Delft3D by Lesser et al., (2004) as the MorFac-approach and utilizes the differences between the hydrodynamic and morphological response time. Typically upscaling factors of O(10) to O(100) can be used for high-energy and moderate events, respectively. A significant further computational efficiency increase was obtained by simulating the separate wave conditions in parallel but simultaneously upscaling and coupling the modeled bathymetry each flow time step. This so-called MorMerge-approach allows for relatively high MorFac upscaling factors as (among others) the updated bathymetry is the weighted net result of all wave conditions, see Roelvink (2006) for details.

The representative tide is already discussed in Section 6.2.1.2, the remaining steps are discussed further below.

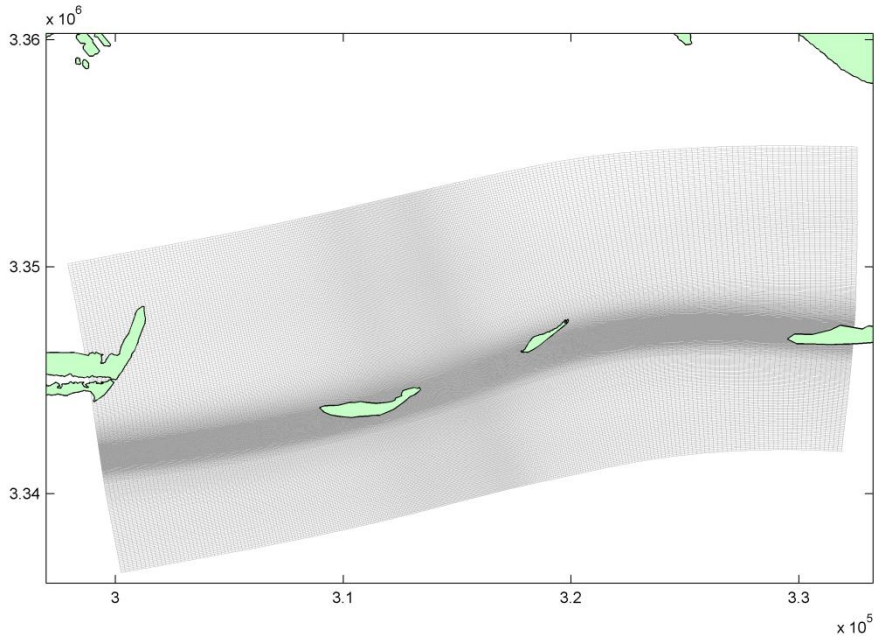

Figure 8.1 computational grid for the SPI model

Morphological wave climate

The aim is to represent the full wave climate with a reduced set of conditions which result in a similar morphodynamic response. Because a morphodynamic simulation based on the full wave climate is not possible due to the unacceptably long computational time, the residual transports obtained with initial transport calculations were used for the full wave climate as a proxy. To schematize the wave climate, the Opti-method (Roelvink and Reniers, 2011, WL|Delft Hydraulics, 2007) was applied. As a target the full climate based transports integrated over a number of transects along East and West Ship Island was used. The defined transects and the integrated transports that act as the target for the Opti-method are shown in Figure 8.2. The considered transects are chosen such that they capture the relevant (both cross-shore and longshore) sediment pathways around East and West Ship Island.

Through an iterative process, the Opti-method eliminates the wave condition that contributes least to the target and recalculates the probability of occurrence of the remaining conditions. As a result the Opti-method provides insight to what extent the remaining conditions reproduce the target for each iteration step (i.e. model performance as a function of the number of selected wave conditions). For the present application it was possible to represent transports resulting from the full wave climate with 16 wave conditions with sufficient accuracy (RMS error < 6%). The weighted net transports from the reduced wave climate show very good agreement with the full set (compare Figure 8.2 and Figure 8.3).

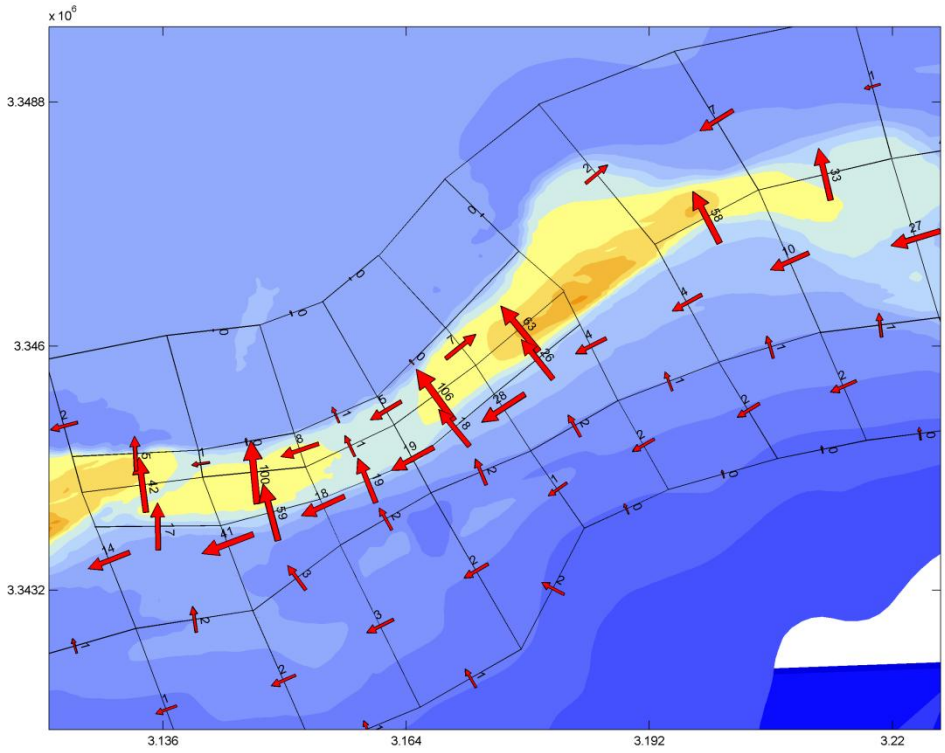

Figure 8.2 Annual sediment transports around Ship Island based on 139 wave conditions

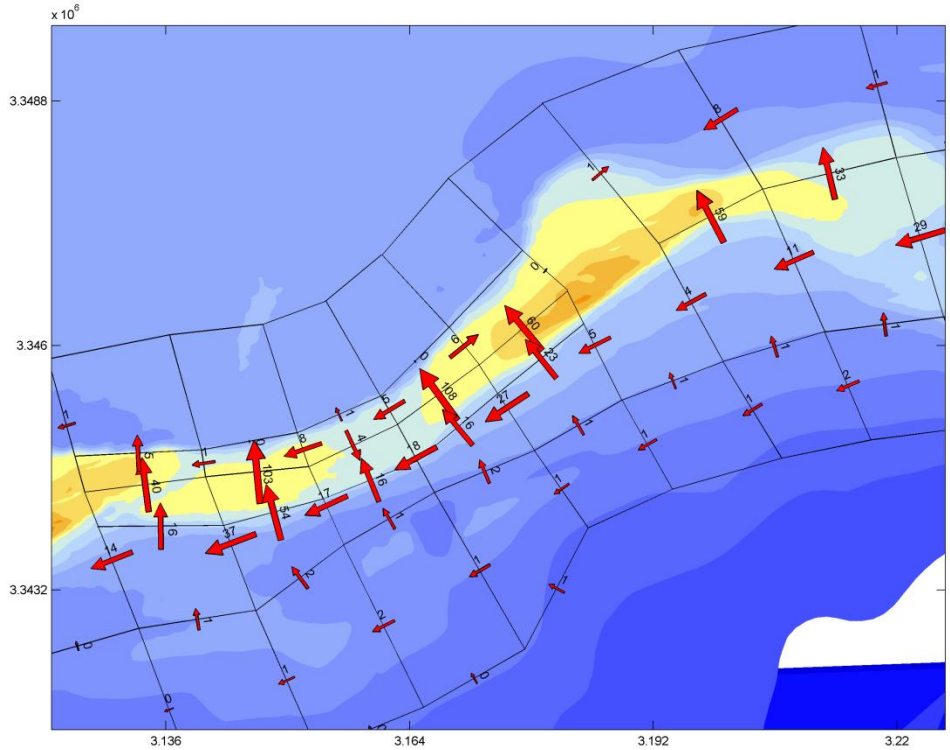

Figure 8.3 Annual sediment transports around Ship Island based on 16 wave conditions after OPTI reduction of the full wave climate

Morphodynamic modeling (MorMerge-approach)

For the medium-term morphological modeling we utilize the MorMerge-approach (Roelvink, 2006) which is schematically shown in Figure 8.4. For all 16 wave conditions, the sediment

transports and bed change under the combined wave and tidal action are simultaneously computed (each wave condition is combined with the representative tide). At every flow time step (i.e. each 12 seconds), the calculated bed change for each wave condition (weighted with its probability of occurrence) is used to determine an updated model bathymetry which is fed back into individual morphodynamic simulations.

Besides the increased computational efficiency due to the parallelization, the MorMerge approach also allows for a larger morphological acceleration factor. The maximum upscaling is typically limited by the relative short period during which the transports are the largest, which is usually the case during maximum ebb or flood. By starting the morphodynamic simulations at different times, the tidal phasing is also shifted. This causes the resulting bed changes to be evenly spread over the tidal cycle and as a result the tidal influence is removed from the merged (and upscaled) bathymetry which allows for an enhanced upscaling factor. This enhanced upscaling factor is typically one order of magnitude larger for the MorMerge-approach. In the present simulations a factor (*MorFac*) of 473 was used. A 4-year prediction was made for the configurations listed in Table 8.1. More information regarding the upscaling and Mormerge-approach and morphodynamic upscaling can be found in Roelvink (2006) and Ranasinghe *et al*. (2011).

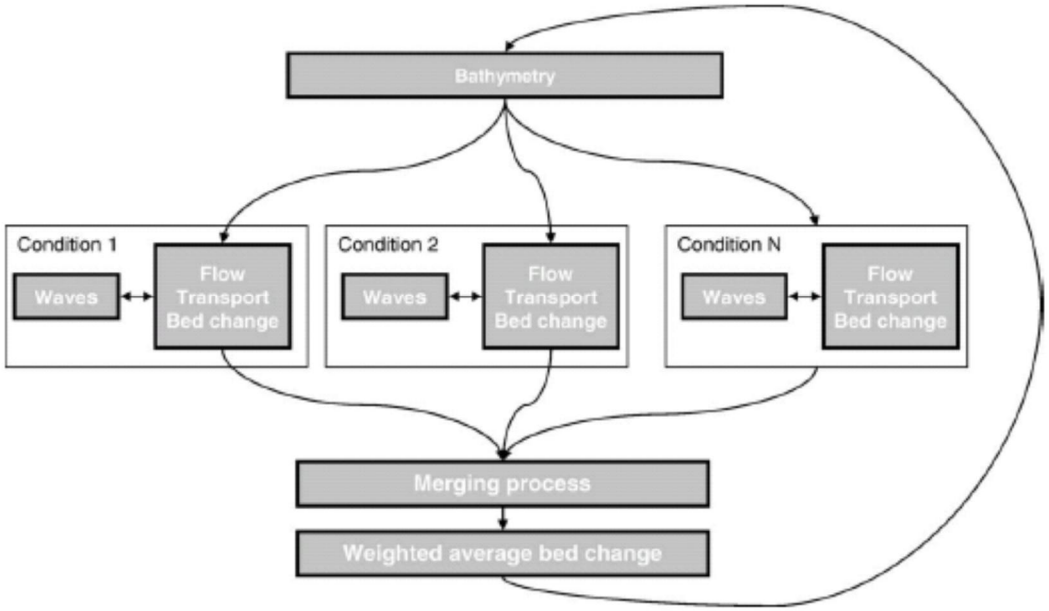

Figure 8.4 Flow diagram of the morphodynamic MorMerge-approach (Roelvink, 2006).

Model settings

Apart from the grid and domain, the setup of the SPI-model is identical to the MCC-model. The SPI-model is used to perform morphodynamic simulations (based on the representative wave climate) whereas the MCC-model is used to calculate the sediment transports without bed-updating (for all 139 wave conditions).

The most relevant model parameter settings for the three different modules of Delft3D (FLOW, WAVE and 3DMOR) for the MCC were described in Section 7.3.3. Unless discussed below, the model settings for the SPI model are similar.

As discussed in Section 7.7, on the basis of the sensitivity analysis with the large scale MCC-model, it was found that Van Rijn (2004) resulted in the best agreement with the

measurements. Therefore the basic runs in the SPI model were carried out with the Van Rijn (2004) formula. Choosing Van Rijn (2004) in-stead of Van Rijn (1993) also implies the activation of a roughness predictor. Therefore, the roughness no longer needs to be prescribed (a constant Manning value was used in the MCC-model with Van Rijn, 1993). The bed roughness computes the space- and time-varying bed form roughness heights based on the sediment diameter (D_{50}), flow conditions and wave conditions.

The nesting of the SPI-model was verified by comparing hydrodynamics (water levels and current velocities) with predictions from the MCC-model. The modeled water levels and current velocities and directions for the MCC- and SPI-models for a storm wave condition at two observation points are compared in Figure 8.13. Based on the near-perfect agreement between both models, it was assumed the SPI-model could be used for the medium-term morphodynamic predictions.

8.2.3 Medium term post-hurricane recovery potential

The medium term simulations of 4 years were initialized with the post-hurricane bathymetries predicted with XBeach for the “collision+”, “overwash+” and “inundation+” hurricanes. The model settings and modeling approach is identical to the medium term modeling of the restored Ship Island (see Section 8.2.2).

8.2.4 Hurricane impact modeling

The morphological hurricane impact is assessed with the XBeach model that covers the same domain as the smallest scale Delft3D (SPI) model. The model set-up, a small validation and the selection of six (6) characteristic hurricanes according to the Sallenger (2000) classification are described here.

8.2.4.1 Set-up of the hurricane impact model (XBeach)

Domain and Grid

The XBeach model covers the entire Ship Island and parts of the adjacent barrier islands (Cat and Horn Island) to ensure the inlets surrounding Ship Island are included (Figure 8.5). The domain is about 20x30km^2 in size with approximately 600,000 cells (~1000x600 cells). The resolution in cross-shore direction gradually decreases from 5 m on and around Ship Island to 30 m at the distal model boundaries. The longshore resolution is 20 m at Ship Island and decreases to 75 m at the lateral model boundaries.

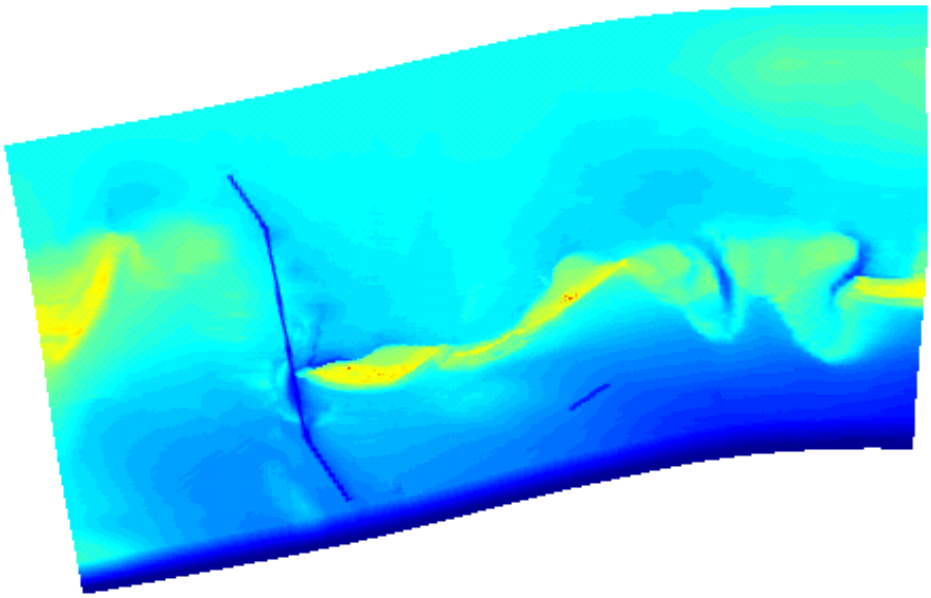

Figure 8.5 XBeach model domain for Ship Island.

Boundary conditions
Boundary conditions are derived from the MCC-model at the four corners of the XBeach domain. The model is forced with time series of water level and wave characteristics (height, period and direction). The water levels are directly imposed on the model boundaries. The wave time series from the MCC-model are used to determine an hourly average wave spectrum. The JONSWAP spectrum shape is used. Directional spreading (s=20) and seven (7) directional bins are used.

8.2.4.2 Validation using Katrina

Model settings, bathymetry and topography data
The XBeach model of Ship Island for the MsCIP project is validated using the observed morphological changes due to hurricane Katrina (2005). The pre-Ivan topography was used to initialize the model as this was the latest high resolution bathymetry measurement available before Katrina struck. The pre-Ivan and post-Katrina topography is mainly based on topography data obtained from NOAA with the LIDAR Data Retrieval Tool (http://www.csc.noaa.gov/ldart). Absent data points are filled using the baseline Delft3D bathymetry. The pre-Ivan and post Katrina data sets cover a major part of the topography of Ship Island (Figure 8.6). At the seaward boundary a plane sloping bed (1/10) to about -15 m is introduced to avoid disturbances related to the prescription of the combined long-short wave boundary conditions (see also Figure 8.5).

The model was applied with default settings which are primarily based on a calibration of the XBeach model on the impact on Santa Rosa Island due to hurricane Ivan (see McCall et al., 2010).

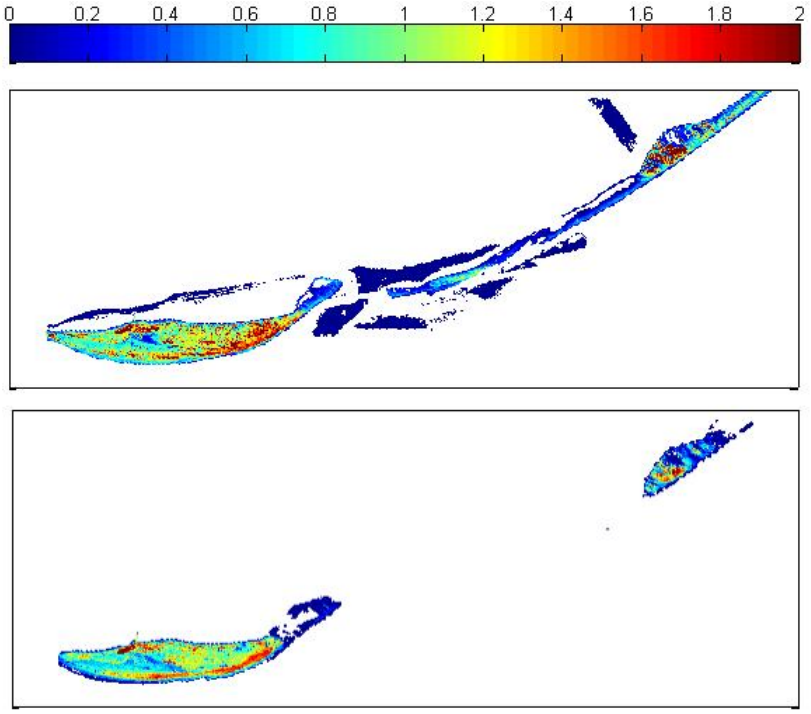

Figure 8.6 Topographic lidar data of pre-Ivan (2004, Top) and post-Katrina (2005, bottom).

Model performance

In accordance with the observations, the predicted largest impact of Katrina is on Camille Cut and East Ship Island. West Ship Island is affected to a lesser extend, but also suffered severe erosion (Figure 8.7). Comparison of predicted and observed topographic contour lines (-0.5m, 0.0 and 1.0 m, see Figure 8.8) confirms that the model is capturing the morphological response. This is especially the case for the most impacted higher parts (+1 m) of the island. For the lower parts of the island some deviations are present, but the general agreement is still good. In general, the sound side of the barrier islands show good resemblance with the measurements and also is the northward migration of the eastern tip of West Ship Island is represented.

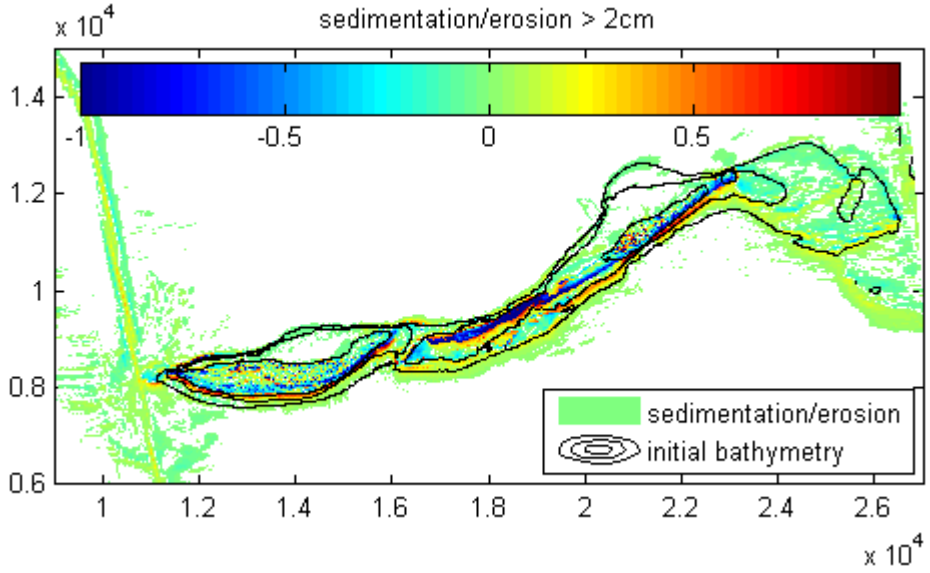

Figure 8.7 Predicted sedimentation-erosion due to hurricane Katrina with XBeach (blue: erosion, yellow-red: sedimentation).

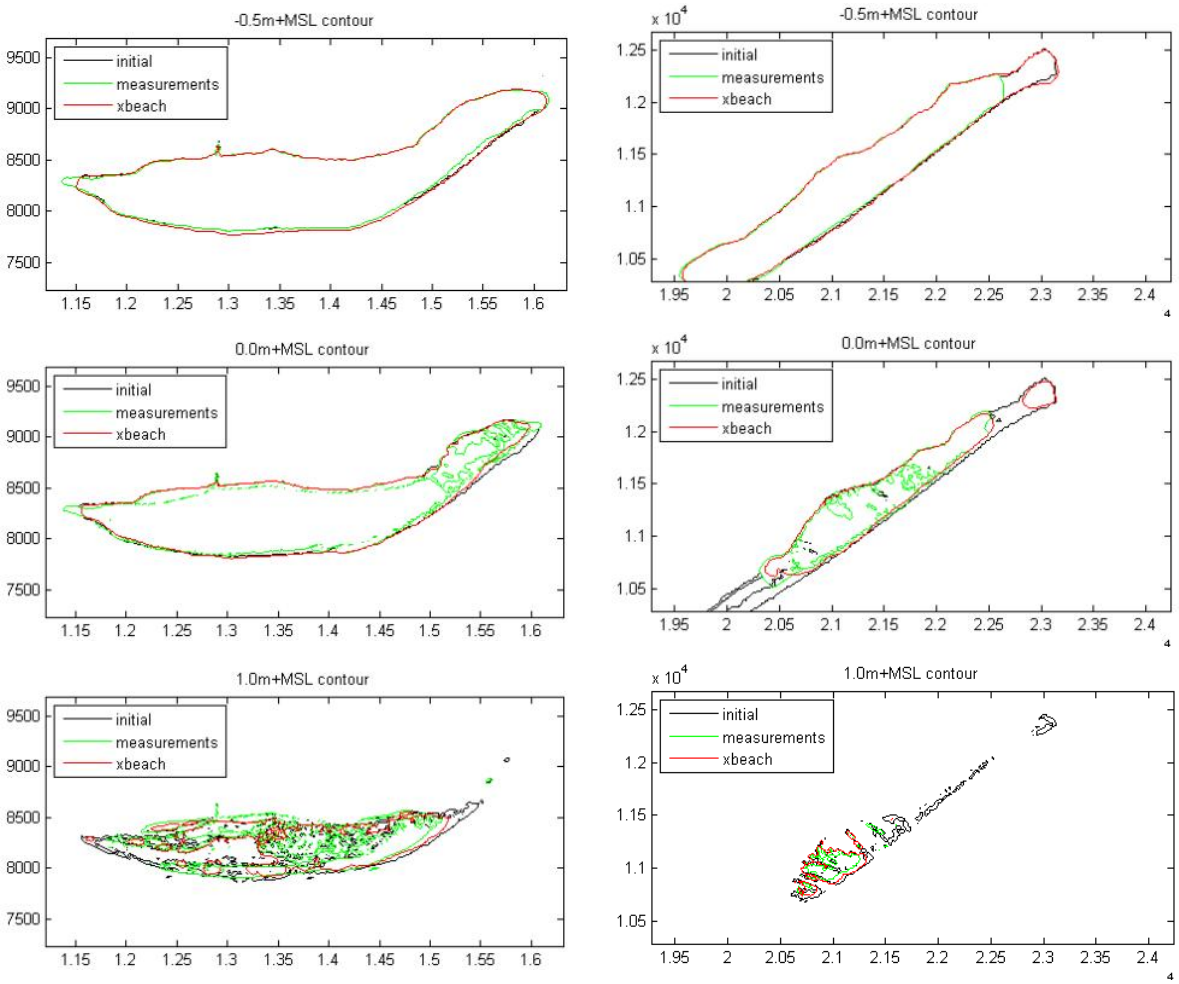

Figure 8.8 Comparison of initial and final observed and computed contour lines for West Ship Island (left) and East Ship Island (right).

Figure 8.9 plots the measured and predicted bed level change and the colors indicate the density of the points (i.e. indication of number of grid points). It can be seen that the model is slightly less erosive than the measurements, since the gravity center of the plot is slightly below the diagonal symmetry line. The model tends to enhance erosion and deposition slightly with respect to the measurements, since the cloud of points is slightly tilted with respect to the diagonal symmetry line.

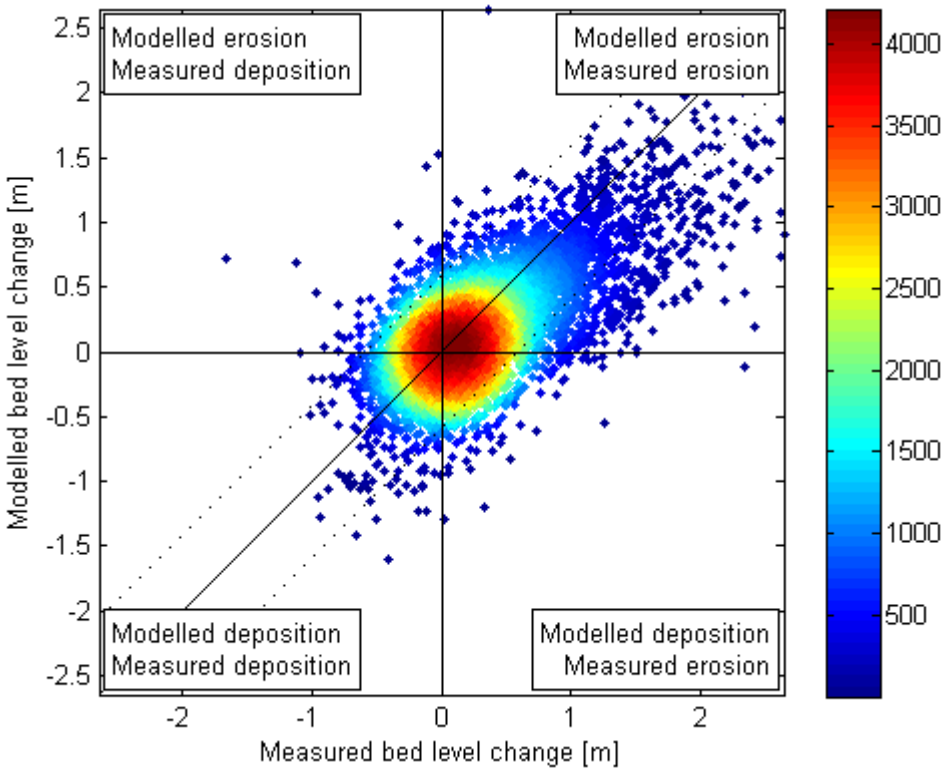

Figure 8.9 Point-by-point correlation between measured and calculated erosion and deposition. Diagonal solid line indicates a perfect match; the dashed lines indicate one standard deviation from a perfect match in terms of measured erosion.

Eighty-nine percent (89%) of the points are located within the bandwidth of one standard deviation of the measured bed level change. The remaining 11% that are outside this bandwidth are indicated in Figure 8.10 and Figure 8.11 and are categorized depending on whether the point is more erosive (red) or more accretive (green) than in the measurements. More erosive, is in this case, the same as less accretive, so it indicates the difference in bed level change with respect to the measurements. In these two categories, the points where erosion is measured, but deposition is modeled or vice versa, the color intensity is higher. This is the case for 8% of all points, but as can be seen in Figure 8.9, the bed change for the fast majority of these points is relatively small.

Considering the fact that the model has been applied with default parameters settings, we consider the general performance of the XBeach model sufficient for a further application in the present study.

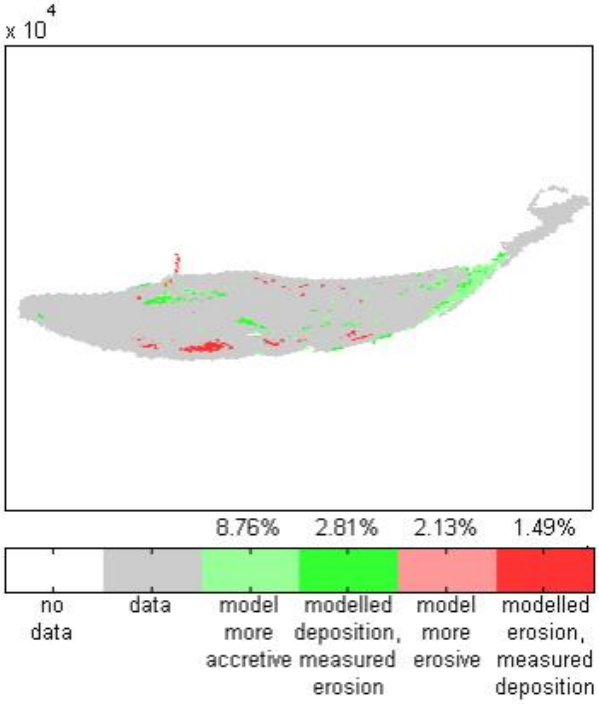

Figure 8.10 Locations and categorization of points for West Ship Island where the bed level change is outside the one standard deviation of the measurements bandwidth for the southern part of the island

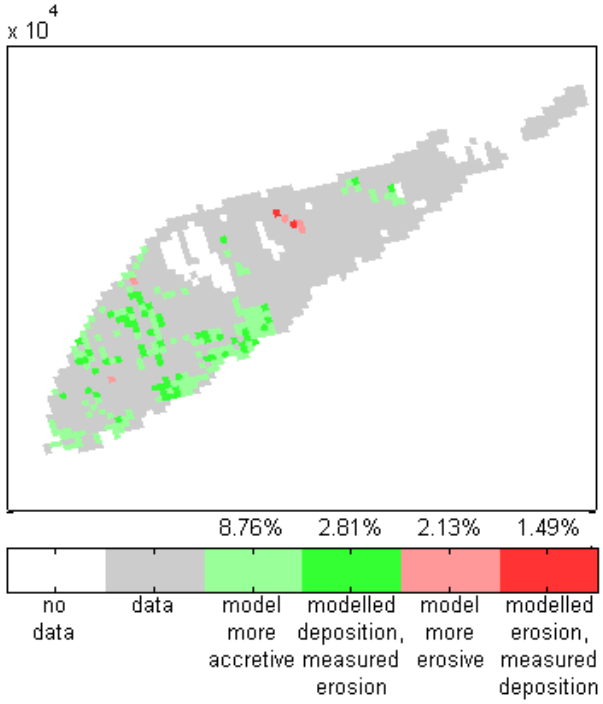

Figure 8.11 Locations and categorization of points for East Ship Island where the bed level change is outside the one standard deviation of the measurements bandwidth for the northern part of the island

8.2.4.3 Selection of characteristic hurricanes following the Sallenger (2000) classification

The same model set-up was used to investigate the morphological response for the three Sallenger (2000) hurricane regimes. A collection of recent hurricanes (after 1994) is categorized according to these Sallenger regimes. For each regime an average and an

extreme event was considered, based on three parameters: maximum surge level, significant wave height and peak wave period. For each regime the mean and standard deviation of these parameters is determined. The hurricanes that agree best with the mean values and the mean values plus twice the standard deviation are selected as the average and extreme events respectively. This resulted in the following hurricanes, listed in Table 8.2, to be considered with XBeach.

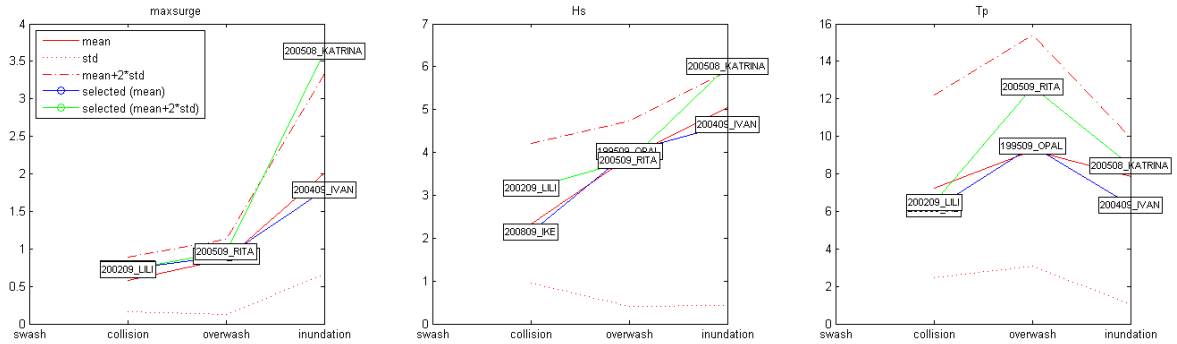

Figure 8.12 Selection of the hurricanes according to the Sallenger (2000) regimes, vertical axis in m.

Hurricane	Regime	Max. Surge (m)	Hs (m)
Ike (2008)	Collision	0.7	2.0
Lilly (2002)	Collision+	0.7	3.2
Opal (1995)	Overwash	0.9	3.5
Rita (2005)	Overwash+	1.0	3.7
Ivan (2004)	Inundation	1.7	4.3
Katrina (2005)	Inundation+	3.5	6.0

Table 8.2 Selected hurricanes according to the Sallenger classification.

The forcing conditions for each hurricane were derived from the MCC-model on the four corner points of the XBeach model domain resulting in both cross-shore and longshore water level gradients induced flows. However, conceptually the differences in the morphological response between the hurricane regimes primarily originate from the cross-shore processes across Ship Island. Therefore the evaluation removed longshore water level gradients by imposing the longshore averaged forcing conditions for both the Gulf and Sound Side on the XBeach model boundaries.

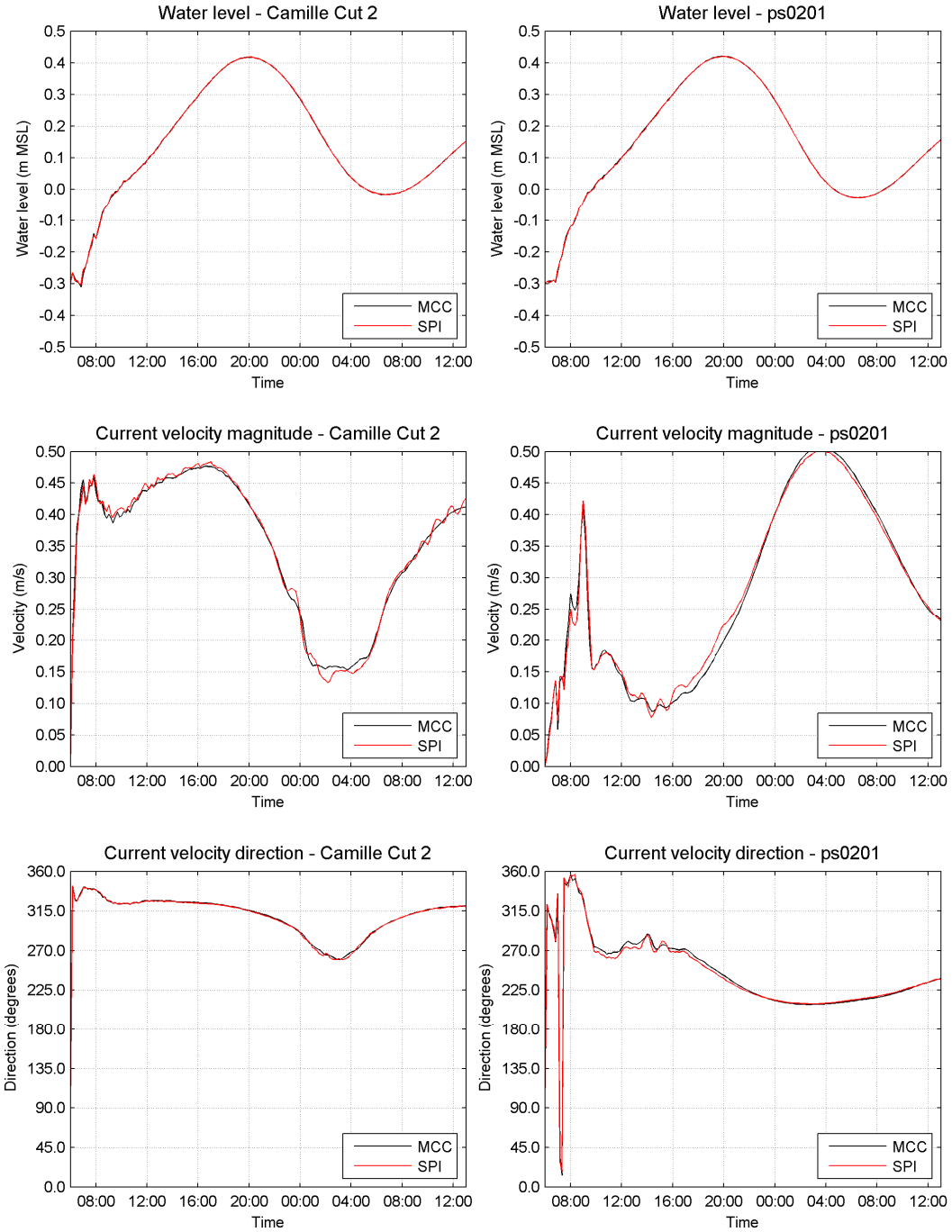

Figure 8.13 Comparison of modeled water levels, flow velocities and flow directions with the MCC and the SPI-model.

8.3 Morphological predictions of the restored Ship Island

8.3.1 Medium-term morphodynamic modeling under averaged conditions (excluding cold fronts)

Baseline, Case 1a: Baseline without borrow area in Ship Island Pass

Figure 8.14 and Figure 8.15 show the morphological changes and the transport patterns along Ship Island for the Baseline Case 1a, after 2 and 4 years, respectively. The transport pattern and erosion-accretion pattern for the two periods are quite similar. The observed

erosion-accretion pattern is dominated by cross-shore transport through Camille Cut. This causes erosion at the Gulf side and accretion at the Sound side in the cut.

Along East Ship Island the model shows erosion along the Gulf side; this is caused by the gradient in the net longshore transport along the barrier. At the eastern end the erosion is strongly increased by a cross-shore transport, moving sand form the Gulf side to the Sound side. As a result of this balance the eastern end of East Ship Island is eroding and moving landward. This trend is in qualitative agreement with the long-term tendency shown in Figure 3.20.

For West Ship Island the overall sand balance of the Gulf shore is more or less neutral, with about 30,000 to 40,000 cy/yr entering at the eastern end and moving out at the western end. This would imply a more or less stable overall position of the Gulf shoreline of West Ship Island, which is confirmed by the long-term trend presented in Figure 3.20. Along West Ship Island the model indicates erosion along the eastern section and accretion along the western section of the Gulf shore, which is caused by the gradient in the net longshore transport. This would imply some reshaping of the shore. Along the submerged part of the western tip sand is transported from the Gulf side to the Sound side.

As discussed in Chapter 7, the computed gradient can be explained by the shoreline orientation and curvature. The decrease in transports due to an increase of the coast orientation with respect to the dominant wave conditions can cause so-called longshore instabilities. Large-scale examples of these are the cuspate spits at the Sea of Azov and the Capes of the Carolinas. Both these coasts are subject to wave climates in which a predominance of the deep-water wave energy approaches from high angles relative to the overall coastline orientation (Ashton et al., 2001). At West Ship Island the high incident wave angles results in the development in alongshore sand waves (i.e. of small scale areas with alternating erosion and deposition of sediment). These sand waves gradually migrate westward as can be inferred from a comparison of the sedimentation erosion patterns after 2 and 4 years. This implies that at least part of the sediment passing along the island is captured in these deposition areas and is not gradually being transported along the island. Inspection of the aerial photographs (Figure 8.16) of the West Ship Island reveals that its Gulf coastline frequently shows some alongshore variations that could be a manifestation of this process. However, after a hurricane these small scale features will erode again (this is also observed in the aerial photographs: compare top plot with 2nd plot in Figure 8.16).

The western tip of West Ship Island is also heavily impacted by hurricanes. In Figure 8.16 it can be seen that the tip is completely eroded after Hurricane Katrina, but gradually re-appears in the following year. The deposition of sediment at the tip is also predicted under averaged conditions. Interestingly, the distal part of the tip curves seaward which implies that ebb flow (possibly in combination with cold fronts) are dominant in this area.

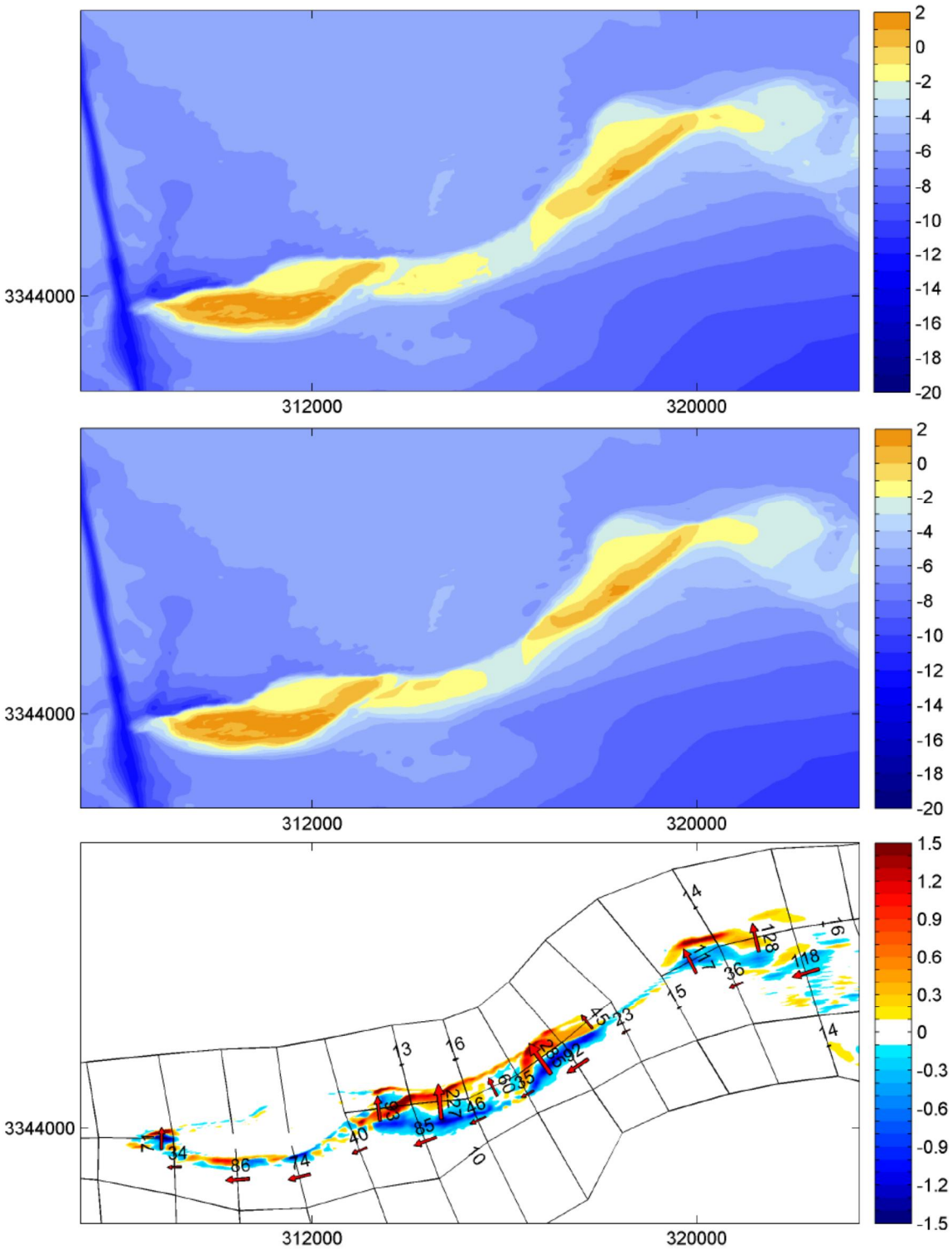

Figure 8.14 Baseline, Case 1a for 0-2 yrs, Upper: Bottom level at start of simulation (m with respect to MSL), Middle: Bottom level after 2 yrs (m with respect to MSL), Lower: erosion and accretion (m in considered period) and net longshore transport (cy/yr).

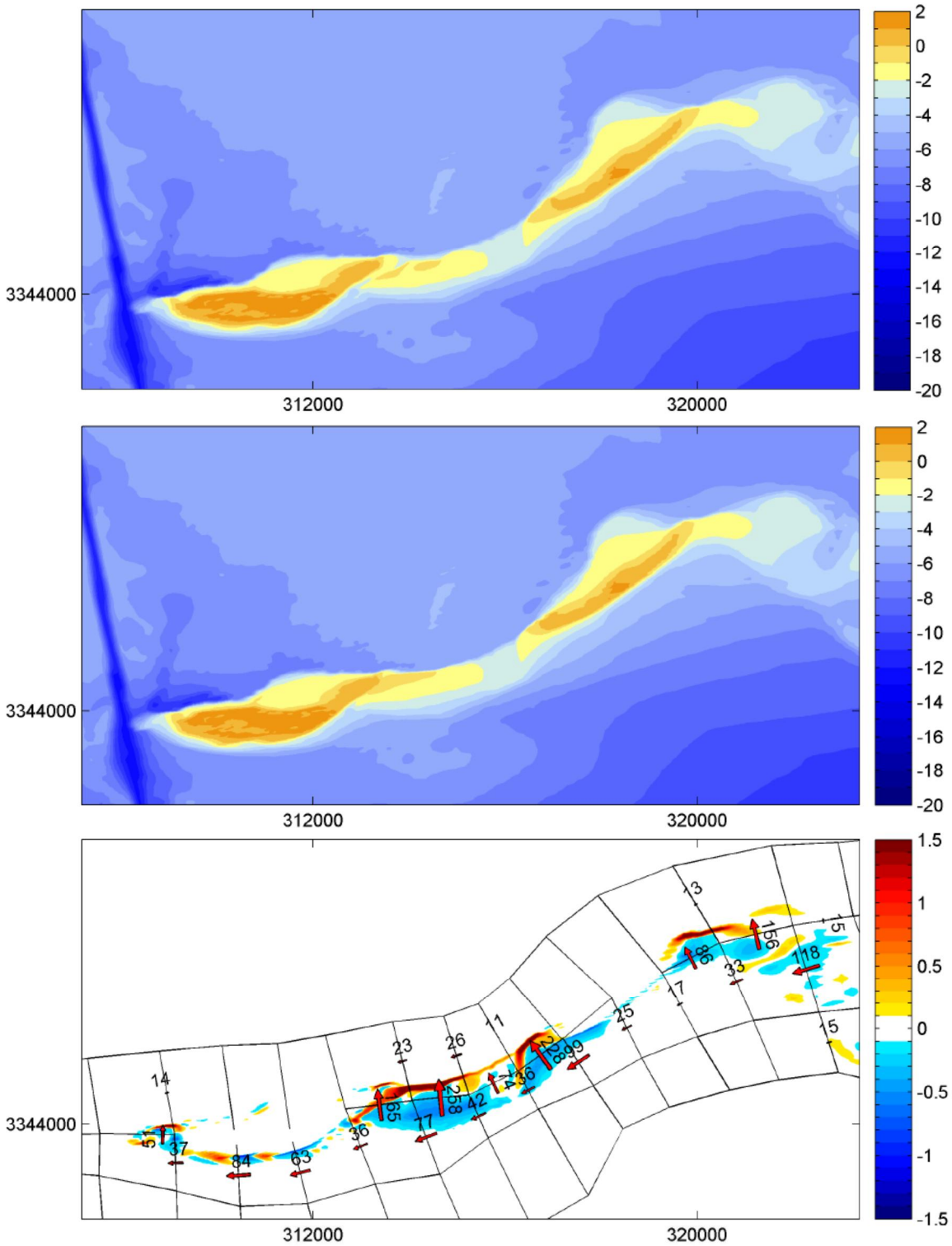

Figure 8.15 Baseline, Case 1a for 2-4 yrs, Upper: Bottom level after 2 yrs (m with respect to MSL), Middle: Bottom level after 4 yrs (m with respect to MSL), Lower: erosion and accretion (m in considered period) and net longshore transport (cy/yr).

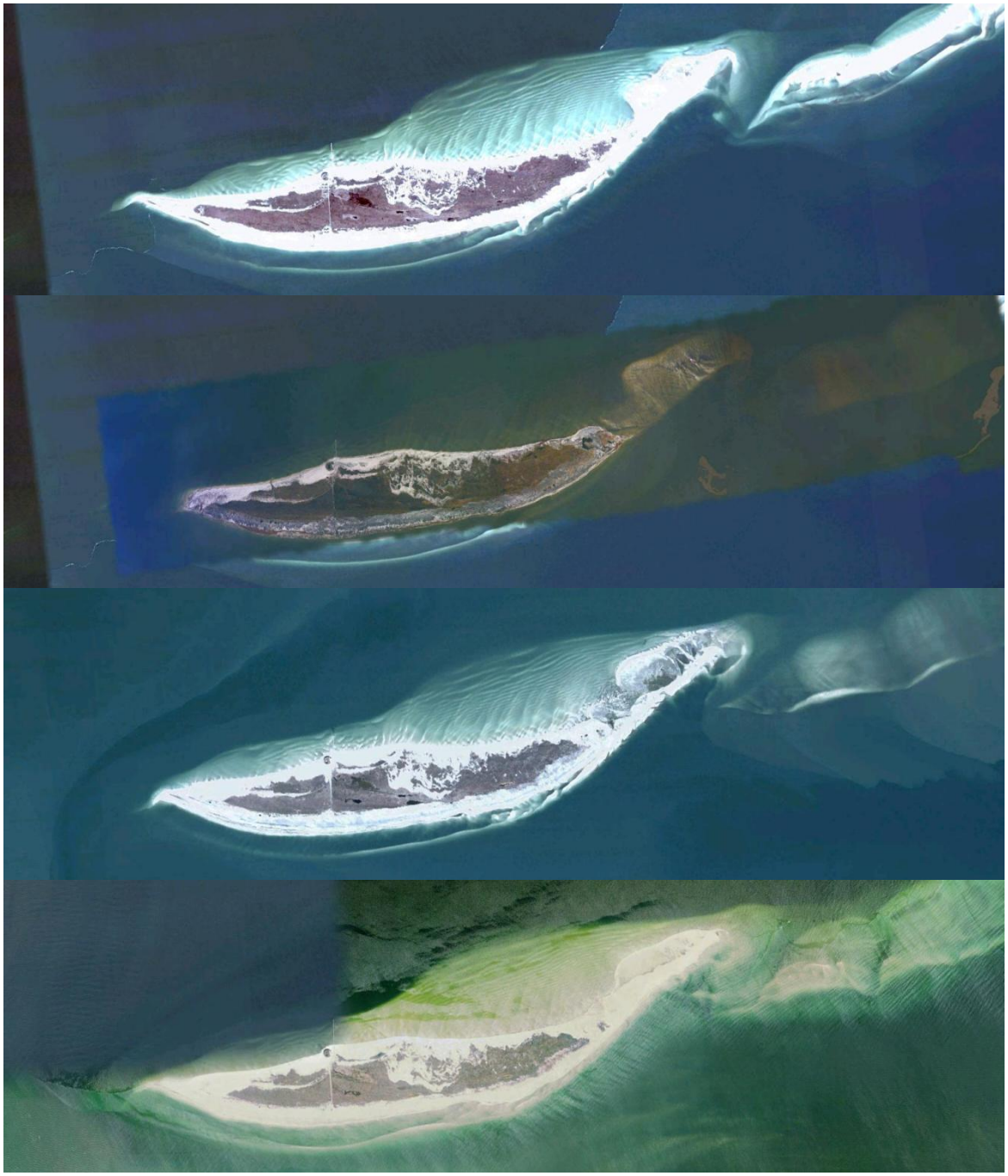

Figure 8.16 Aerial photographs of West Ship Island (Top: 1-25-2005, 2nd: 9-1-2005, 3rd: 11-22-2005 and bottom: 6-7-2006). Source Google Earth.

Baseline, Case 1b: Baseline with Ship Island Pass borrow area

Figure 8.17 and Figure 8.18 show the morphological changes and the transport patterns along Ship Island for the Baseline Case 1b, for the period 0-2 yr and 2-4 yr respectively. The transport pattern and erosion-accretion pattern for the two periods are quite similar.

In the period 0-2 yr the sediment transport are similar to that for Baseline Case 1a, compare Figure 8.17 with Figure 8.14. In the period 2-4 yr the effect of the borrow source in Ship Island Pass is somewhat more noticeable in the transport magnitude at the western tip. However, the overall erosion-accretion pattern is very similar to that for Baseline Case 1a, compare Figure 8.18 with Figure 8.15.

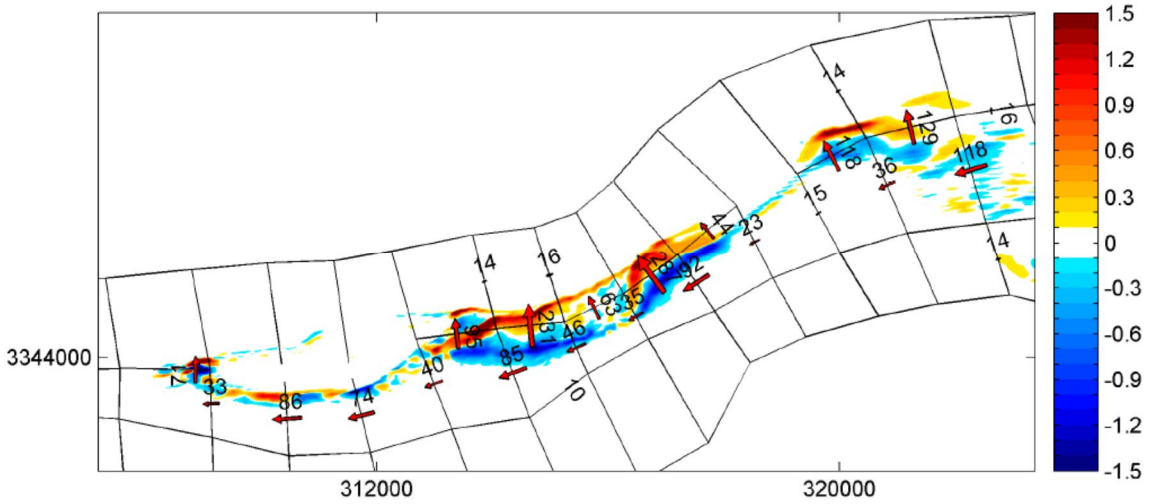

Figure 8.17 Baseline Case 1b for 0-2 yrs: erosion and accretion (m) and net longshore transport (cy/yr)

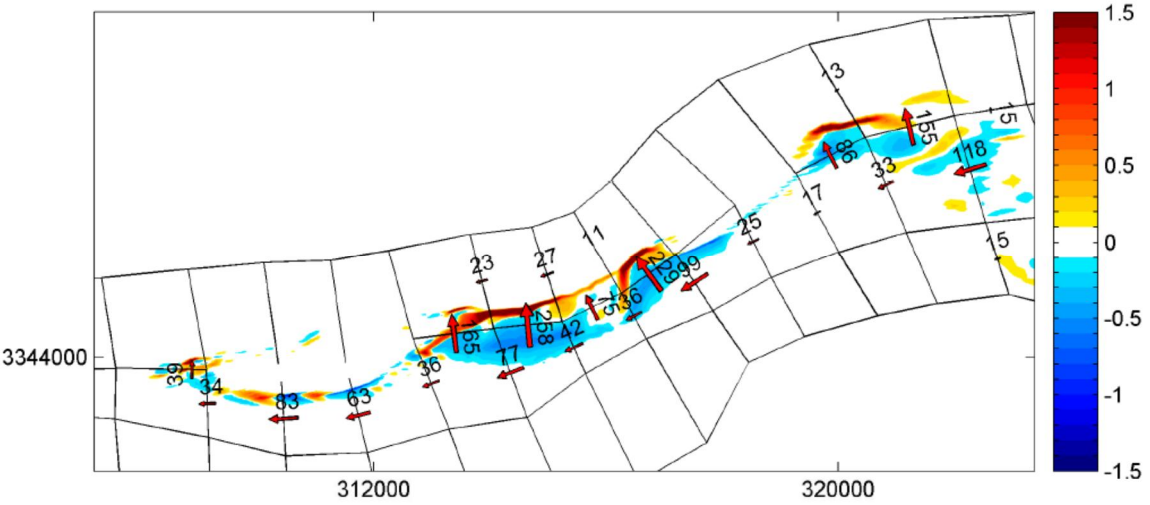

Figure 8.18 Baseline Case 1b for 2-4 yrs: erosion and accretion (m) and net longshore transport (cy/yr).

Case 2a: Closed Camille Cut with SE sand placement, without and with the Ship Island Pass borrow area

Case 2a-1: Case 2a without the offshore borrow area

Figure 8.19 and Figure 8.20 show the morphological changes and the transport patterns along Ship Island for the Case 2a-1, for the period 0-2 yr and 2-4 yr respectively. The transport pattern and erosion-accretion pattern for the two periods are quite similar.

Erosion is found along the eastern section of the island, which can be explained by the gradient in the net longshore transport. As discussed in Chapter 7 this gradient is caused by the curvature in the shoreline. Along the western end the net transport decreases again, since at this section the angle of wave incidence is very oblique. The sand waves that result from these high incident wave angles are also found for the Baseline Case 1a. The transports along West Ship Island are not significantly affected by the Camille Cut closure for the considered period.

Figure 8.21 and Figure 8.22 compare the Baseline Case 1a and Case 2a-1, for the periods 0-2 yrs and 2-4 yrs respectively. As expected, the main changes occur along the Camille Cut section. Along a considerable stretch west of Camille Cut, the longshore transport is affected significantly. In that area, after closure of the cut the transport rate is predicted to increase significantly as the littoral drift can now fully develop from East to West Ship Island.

At the western tip, near Ship Island Pass, some additional changes are predicted, but the effect of the Camille Cut closure appears to be relatively small. However, the closure has caused additional sediment to deposit along the eastern part of West Ship Island. This deposition gradually grows westwards (comparing the deposition after 2 and 4 years). It is likely that this deposition area gradually migrates westward along shoreline. This potentially could cause an increased sedimentation at the tip and in Ship Island Pass about 10-20 years after closure. As the effect of hurricanes is not incorporated in these simulations, it is very likely that the additional sand is diffused. The diffusion of the depositional area(s) will cause some additional sedimentation of Ship Island Pass and the Bar channel under hurricane conditions. However, compared to the typical overall hurricane-induced morphological changes, the additional sedimentation due to the closure are expected to be minimal.

The interaction of the closure for hurricane conditions is discussed in the following section.

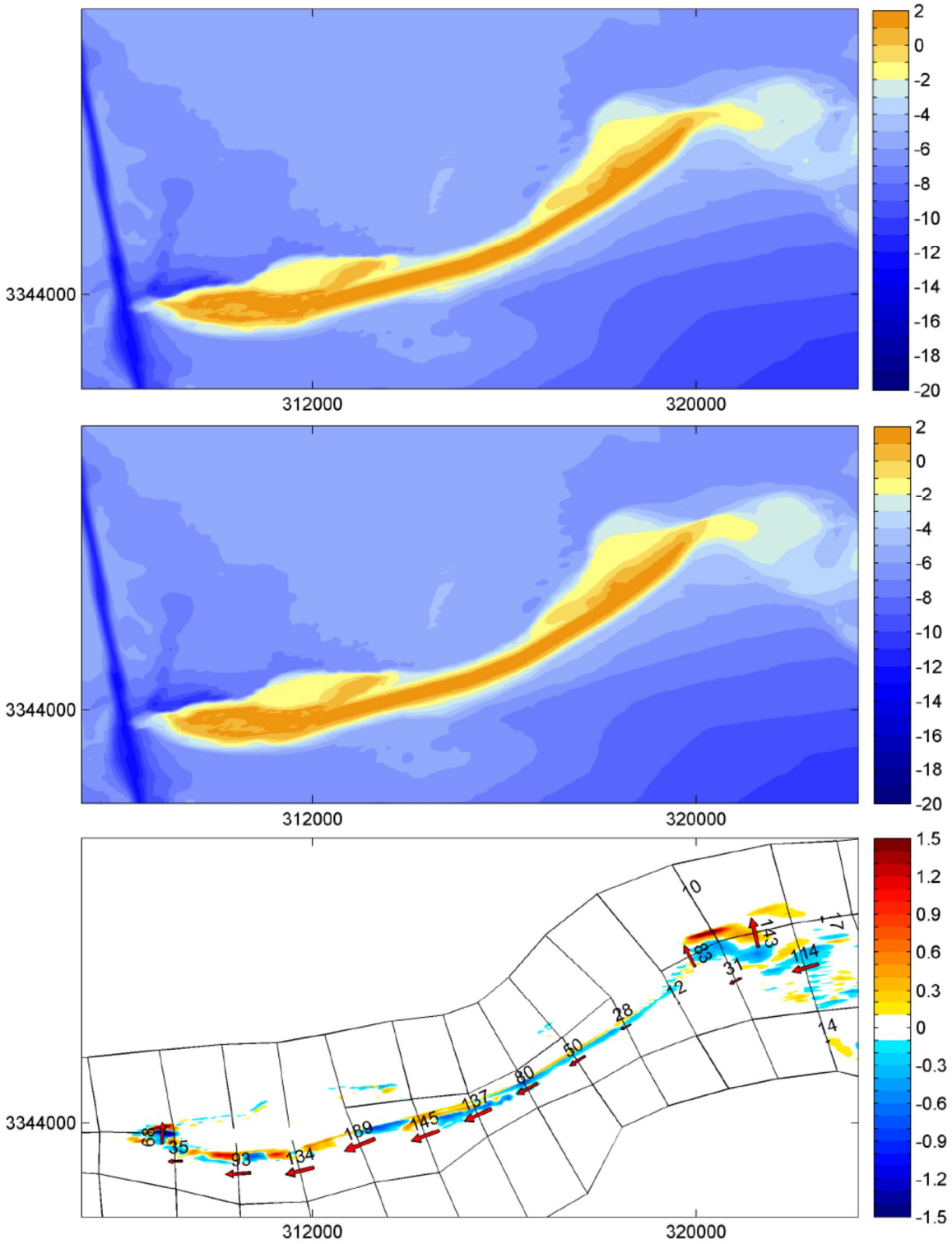

Figure 8.19 Design 2a-1 for 0-2 yrs, Upper: Bottom level at start of simulation (m with respect to MSL), Middle: Bottom level after 2 yrs (m with respect to MSL), Lower: erosion and accretion (m in considered period) and net longshore transport (cy/yr).

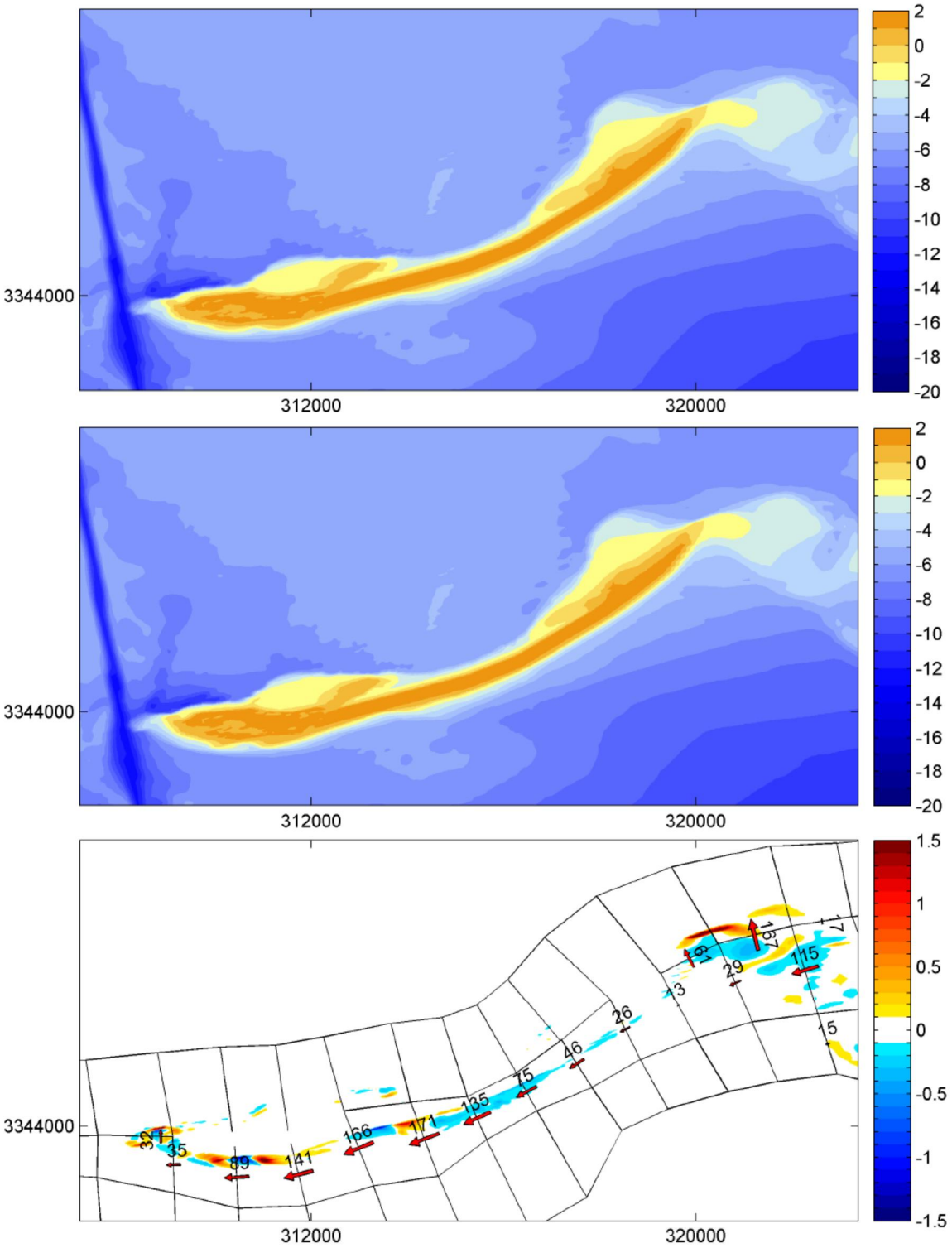

Figure 8.20 Design 2a-1 for 2-4 yrs, Upper: Bottom level after 2 yrs (m with respect to MSL), Middle: Bottom level after 4 yrs (m with respect to MSL), Lower: erosion and accretion (m in considered period) and net longshore transport (cy/yr).

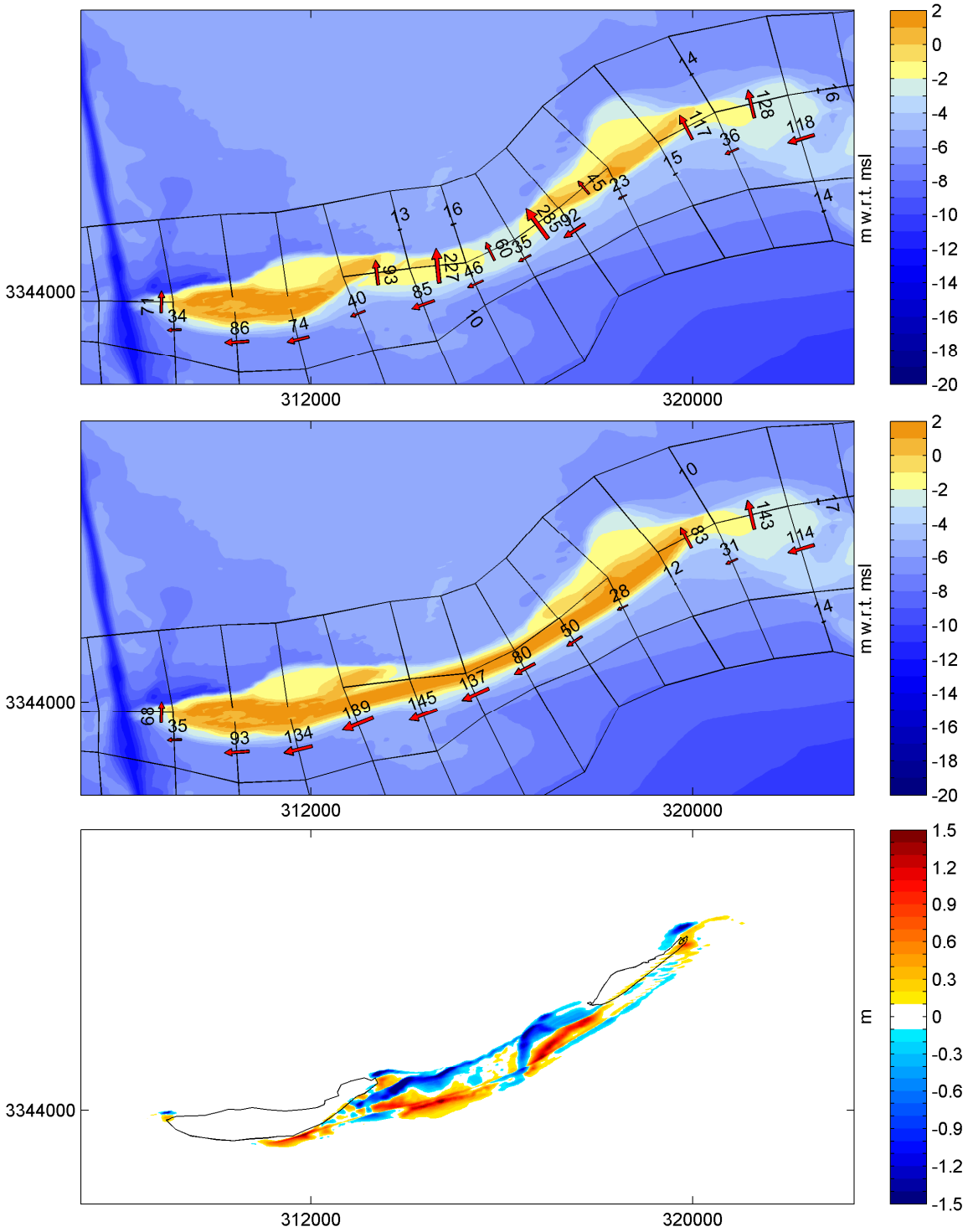

Figure 8.21 Relative effect of Design 2a for 0-2 yrs, Upper: Baseline Case 1a after 2 years (m with respect to MSL), Middle: Case 2a-1 after 2 yrs (m with respect to MSL), Lower: relative erosion and accretion (m in considered period).

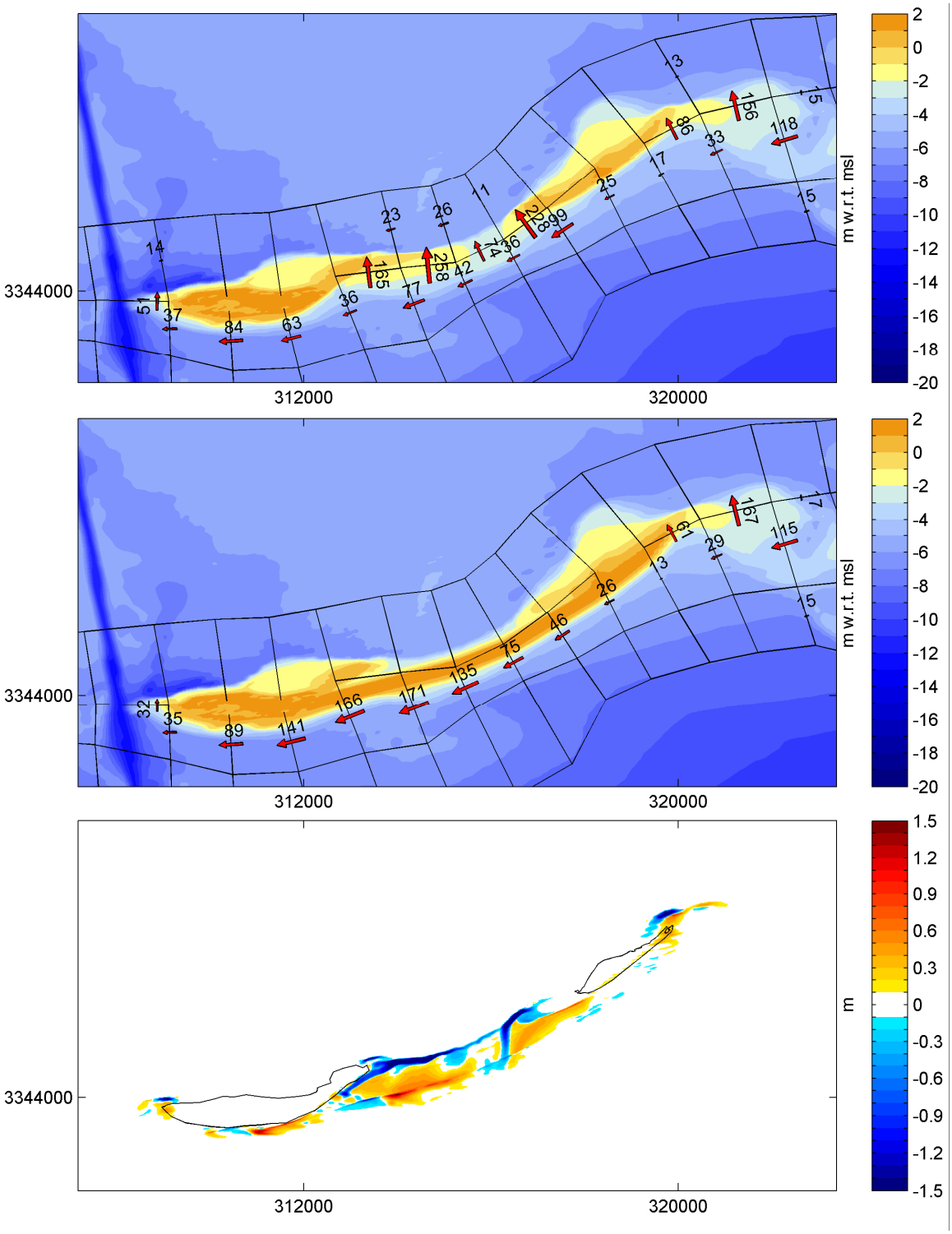

Figure 8.22 Relative effect of Design 2a for 2-4 yrs, Upper: Baseline Case 1a after 2 years (m with respect to MSL), Middle: Case 2a-1 after 2 yrs (m with respect to MSL), Lower: relative erosion and accretion (m in considered period).

Case 2a-2: Case 2a with the offshore borrow area

Figure 8.23 and Figure 8.24 show a comparison between the simulations with and without the offshore borrow area, for the periods 0-2 yrs and 2-4 yrs respectively. Compared to the erosion-sedimentation caused by the Camille Cut closure and the sand placement the predicted effect of the borrow pit is insignificant after both 2 and 4 years. It is anticipated that for longer periods the effect of the offshore borrow area decreases as it gradually diffuses and back fills.

The negligible effect of the offshore borrow area can be explained by its small dimensions (horizontal and vertical) and its location at a relatively large depth. As a result its effect on the waves, the main driving force of the transport along the gulf oriented shorelines, is relatively small.

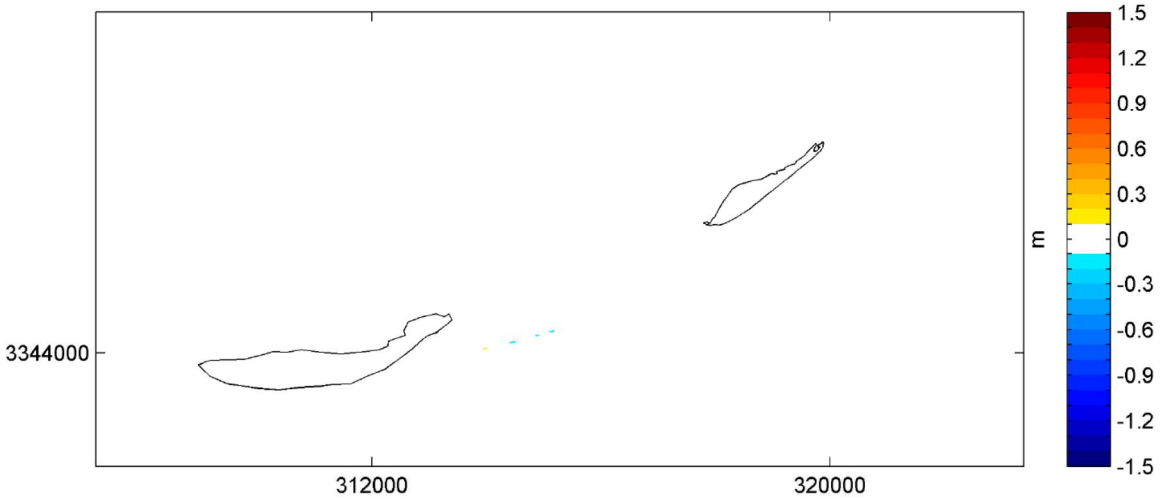

Figure 8.23 Relative erosion and accretion (m) for Case2a-1 (no borrow area) and Case 2a-2 (with borrow area) after 2 years.

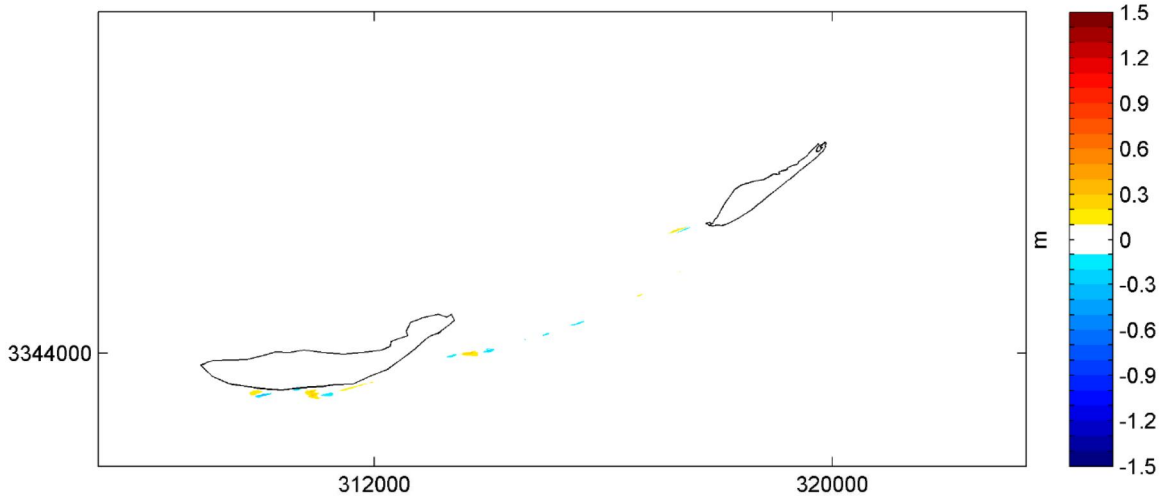

Figure 8.24 Relative erosion and accretion (m) for Case2a-1 (no borrow area) and Case 2a-2 (with borrow area) after 4 years

Case 2b: Closed Camille Cut with SE sand placement with the Ship Island Pass borrow area

For Case 2b the transport and erosion-accretion patterns are presented in the Figure 8.25 and Figure 8.26, for the periods 0-2yrs and 2-4 yrs respectively. Comparing Figure 8.21 and Figure 8.22 with the Figure 8.25 and Figure 8.26 it is apparent that the results are very similar implying the borrow area at Ship Island Pass only has a small effect.

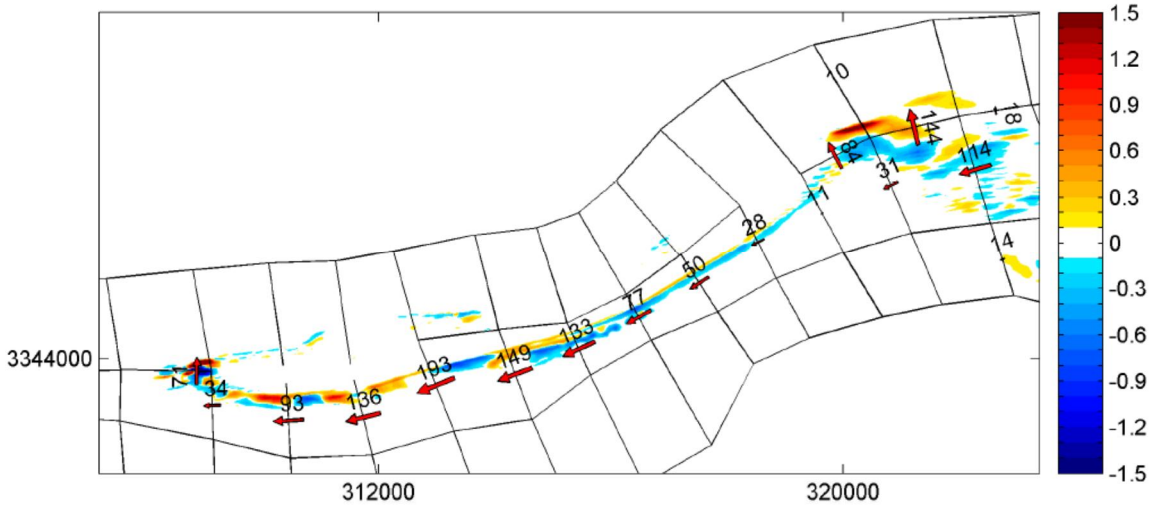

Figure 8.25 Design 2b for 0-2 yrs, erosion and accretion (m in considered period) and net longshore transport (cy/yr)

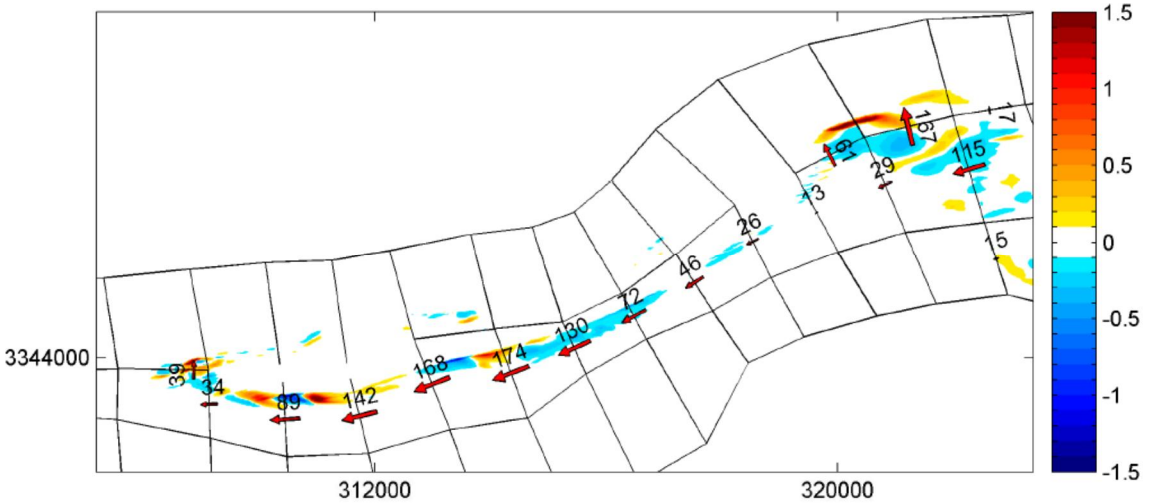

Figure 8.26 Design 2b for 2-4 yrs, erosion and accretion (m in considered period) and net longshore transport (cy/yr)

Testing the sensitivity to changes in sediment size and transport formulation

The sediment around the barrier islands is characterized as fine to medium sand. Based on sediment sample data (see also Chapter 3) a mean sediment diameter (D_{50}) of 300 µm has been used in the sediment transport calculations. In reality, the D_{50} varies significantly around the barrier islands, which has not been taken into account in the model. In Chapter 7 it was shown that the choice of sediment size and transport formulation resulted in the largest variation in the predicted transports. As a follow up to the extensive sensitivity analysis

presented in Chapter 7 both aspects were considered in a number of medium term morphodynamic simulations. In the sensitivity simulations increased and decreased sediment sizes (D_{50} = 0.2 mm and D_{50} = 0.4 mm) have been considered. Furthermore, an additional simulation has been performed in which the Van Rijn (1993) transport formula was selected. All sensitivity simulations were conducted for Case 2b.

Figure 8.27 shows the effect of the applying D_{50} = 0.2 mm instead of the default D_{50} = 0.3 mm, and Figure 8.28 when using D_{50} = 0.4 mm. These sensitivity runs confirm the sensitivity of the model outcomes as already concluded in the previous chapter. For D_{50} = 0.2 mm the transports are significantly larger than for D_{50} = 0.3 mm. As a result the erosion-accretion pattern along the Gulf shore is also amplified. For both sand diameters the transport patterns are similar, though for D_{50} = 0.2 mm some more deposition of sand at the Sound side of the western tip is predicted. As expected, for D_{50} = 0.4 mm the transports are smaller and the erosion-accretion pattern is less pronounced.

Figure 8.29 compares the van Rijn (1993) and van Rijn (2004) transport formulas, instead of the Van Rijn 2004 formula (used in the medium term simulations). The net longshore transport along the barrier computed with the van Rijn (1993) formula is significantly smaller than the transport computed with van Rijn (2004). Use of the van Rijn (1993) formula to some extent also affects the transport patterns. At the eastern tip of Ship Island the sediment balance is affected significantly, due to a smaller sand supply from the delta and a larger cross-shore transport towards the Sound. As a result the Gulf oriented shoreline of the eastern tip erodes faster for the van Rijn (1993) simulation. Along the Gulf shoreline the cross-shore distribution of erosion and deposition is somewhat different for the van Rijn (1993) computation. The overall sedimentation-erosion patterns agree fairly well between both transport formulations. This implies that the magnitude of the response varies, but not the type of response.

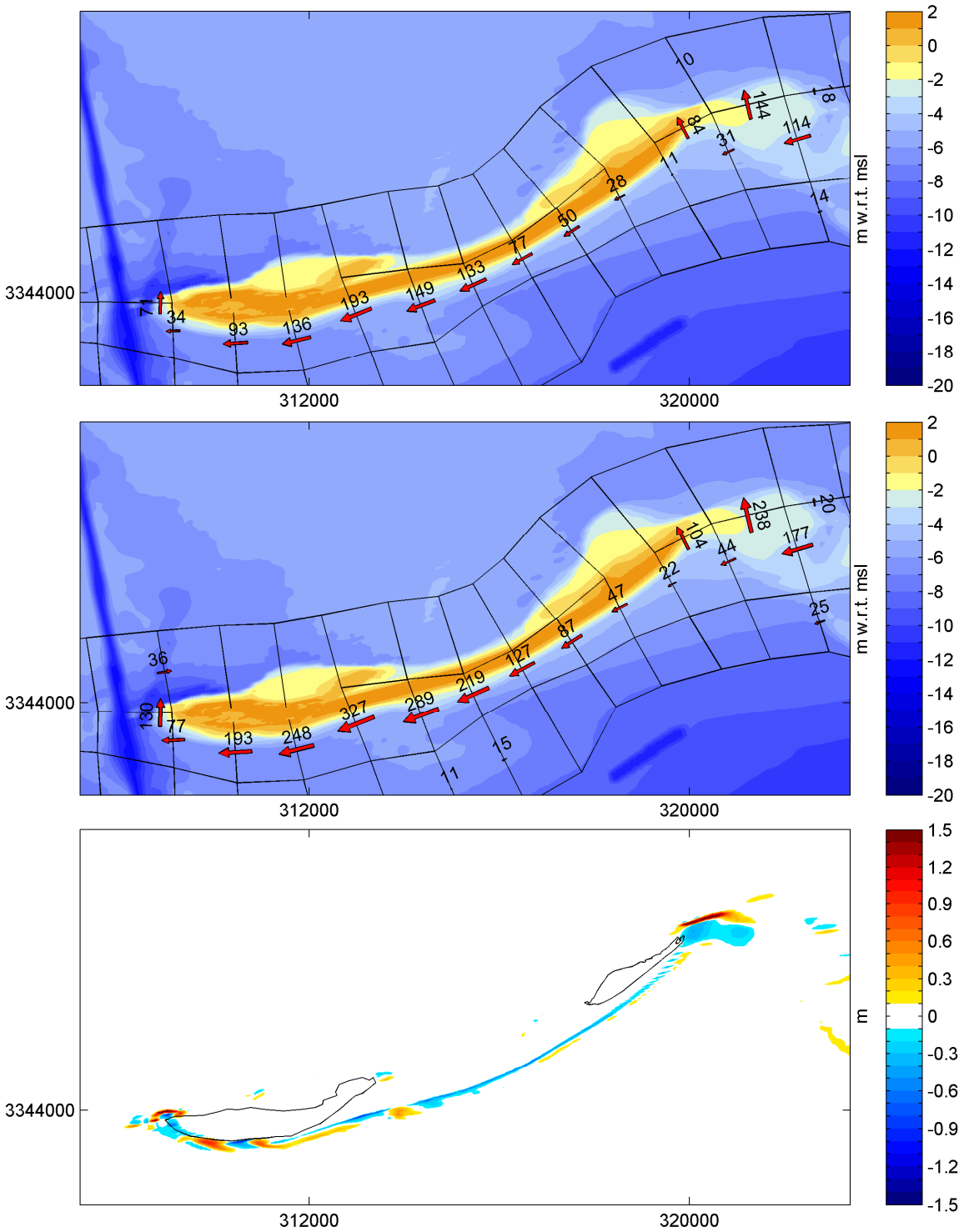

Figure 8.27 Sensitivity run with smaller D50, Upper: Transport (cy/yr) for D50=0.3 mm, Middle: Transport (cy/yr) for D50=0.2 mm, Lower: Difference in erosion-accretion pattern.

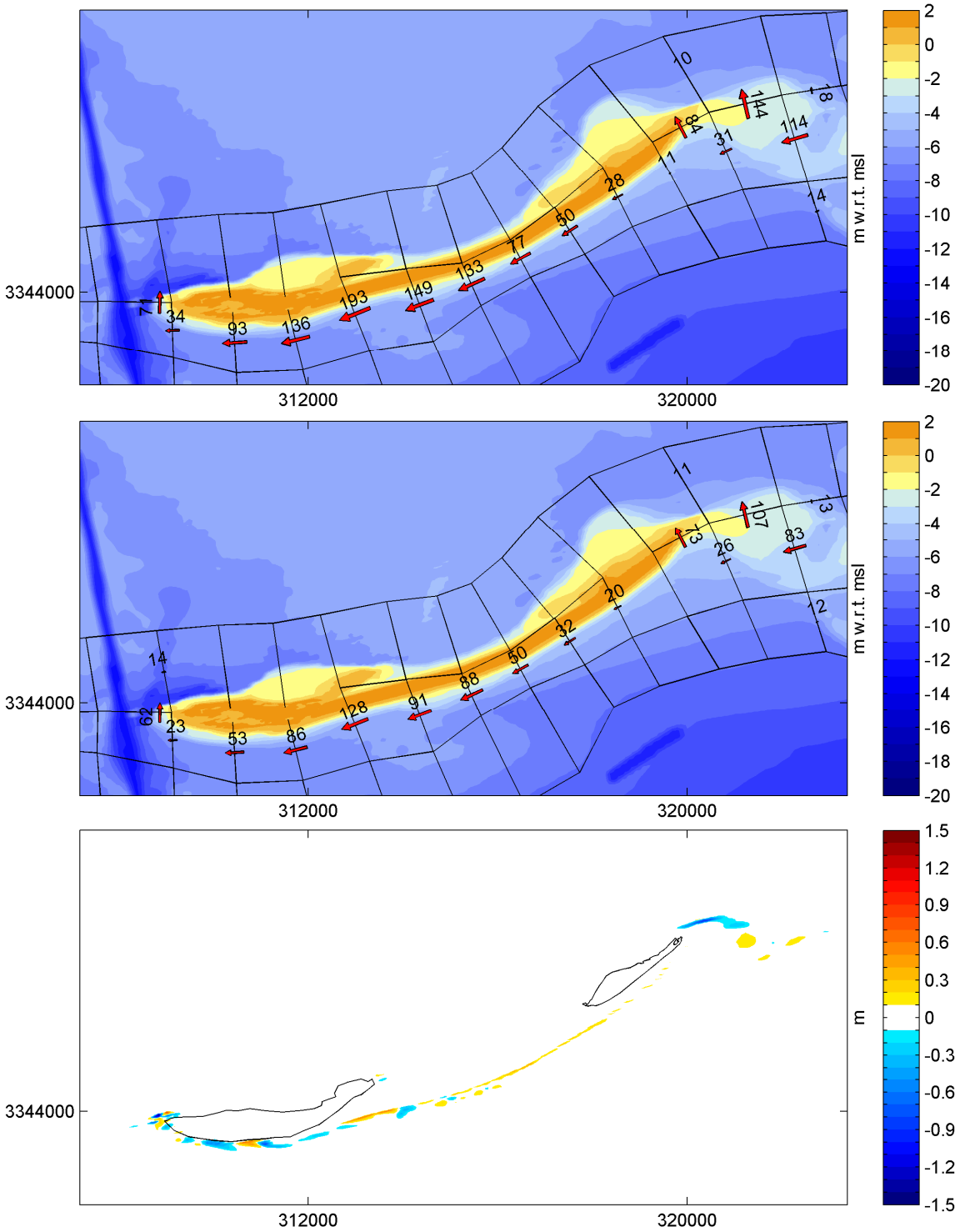

Figure 8.28 Sensitivity run with larger D50, Upper: Transport (cy/yr) for D50=0.3 mm, Middle: Transport (cy/yr) for D50=0.4 mm, Lower: Difference in erosion-accretion pattern.

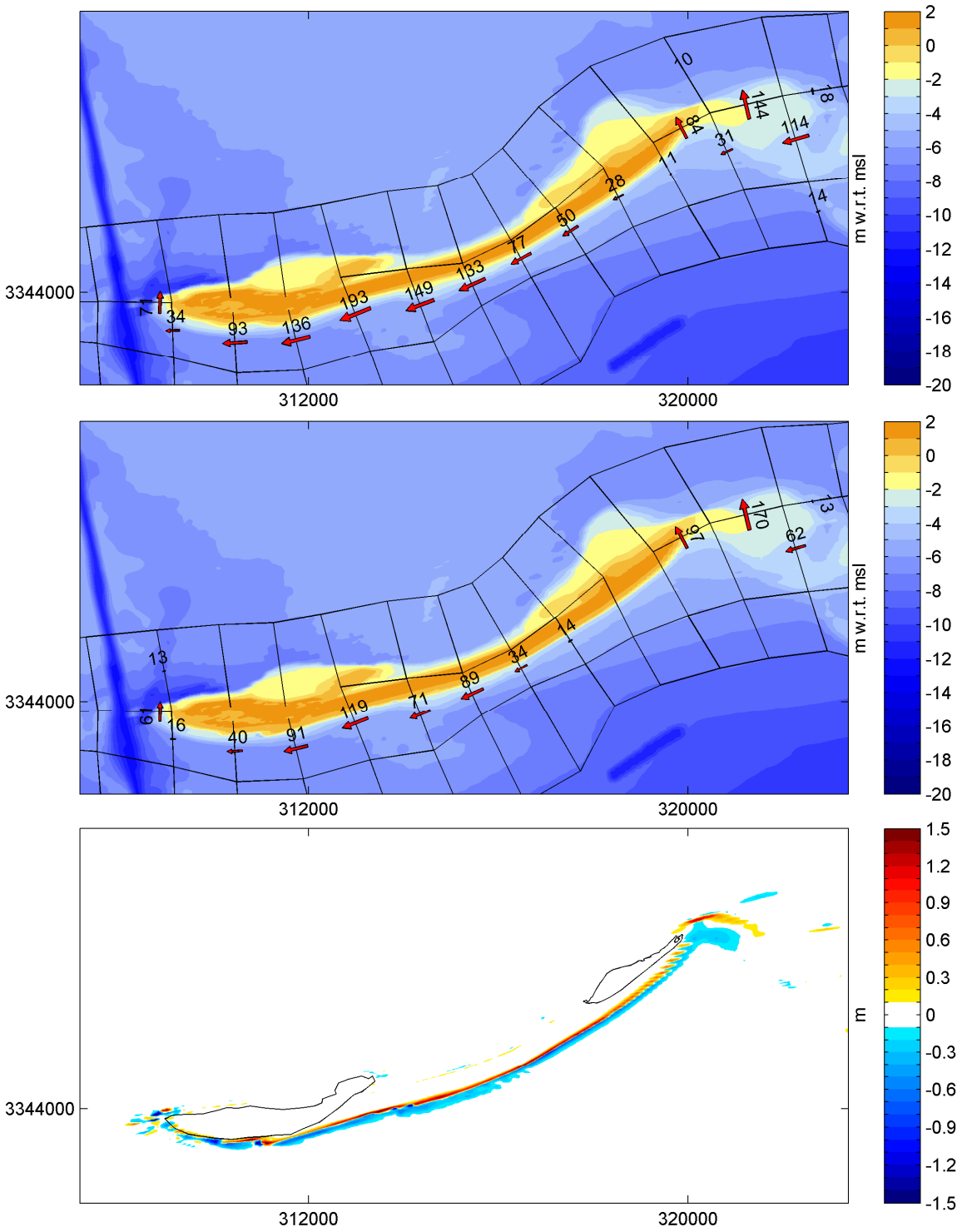

Figure 8.29 Sensitivity run with formula Van Rijn 1993, Upper: Transport (cy/yr) for Van Rijn 2004, Middle: Transport (cy/yr) for Van Rijn 1993, Lower: Difference in erosion-accretion pattern.

8.3.2 Morphological evaluation of the restored Ship Island due to Hurricanes

8.3.2.1 Morphological impact for the collision, overwash and inundation hurricane regimes

The predicted impact for hurricanes in the collision, overwash and inundation regimes are summarized in Figure 8.30 ignoring wind-driven flows. In the inundation regimes the central part of the island suffers from the most erosion, the sediment that is eroded from central parts of the island is primarily deposited just seaward and landward of the island. For the milder hurricanes the sediment eroded from the dunes and upper part of the beach is deposited lower in the profile.

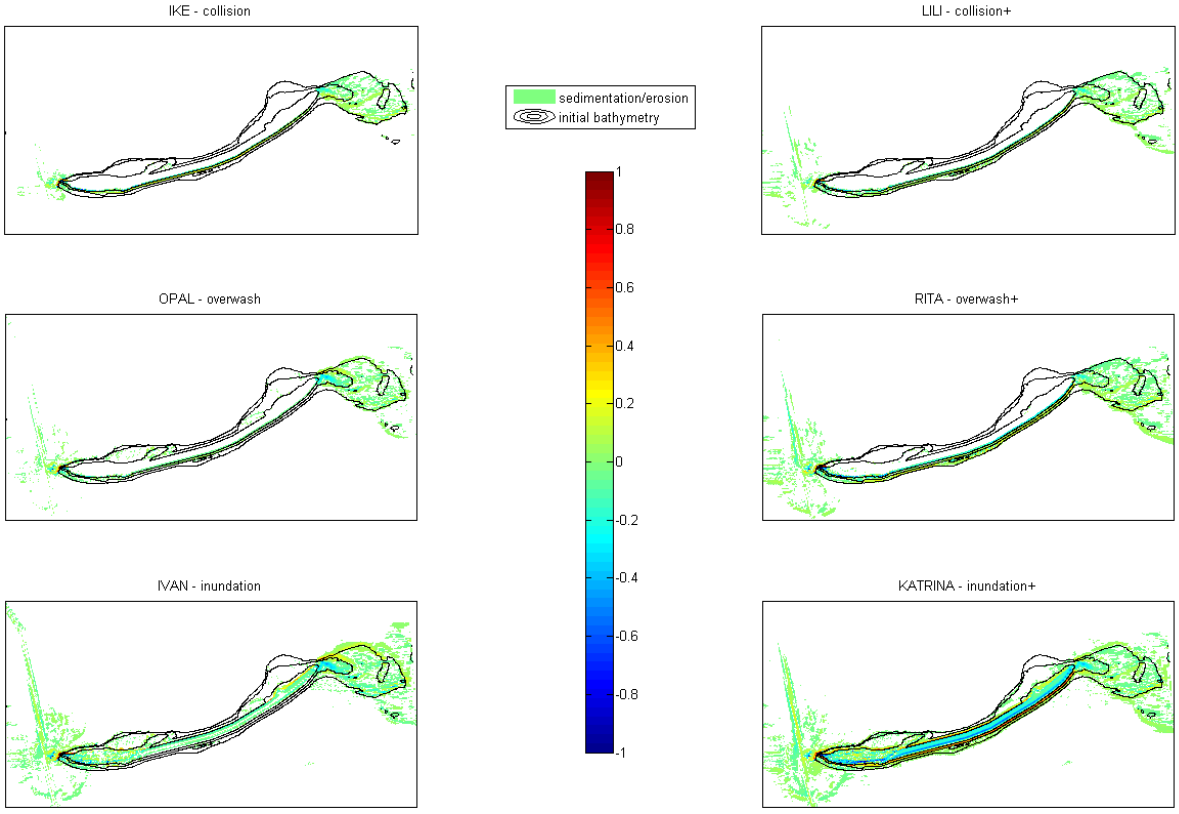

Figure 8.30 Predicted morphological change after hurricane impact (top row: collision regime, middle row: overwash regime and bottom row: inundation regime).

The resulting sediment net transports and the transports during the flooding phase, ebbing phase for the "+"-hurricane scenarios are shown in Figure 8.31 to Figure 8.33. Consistent with the findings in Section 6.3 (where the MCC-model was used to estimate the initial sediment transports), the net transports are usually considerably smaller than the transports during the flooding or ebbing phases of the hurricanes. Interestingly, for all the selected hurricanes the net cross-shore transports across the tips of the Ship Island are ebb dominated. The results further highlight the importance of the alongshore water level gradients. In the XBeach simulations the alongshore water level gradient was removed, resulting in net westward directed transports along Ship Island. This is further addressed in the next section.

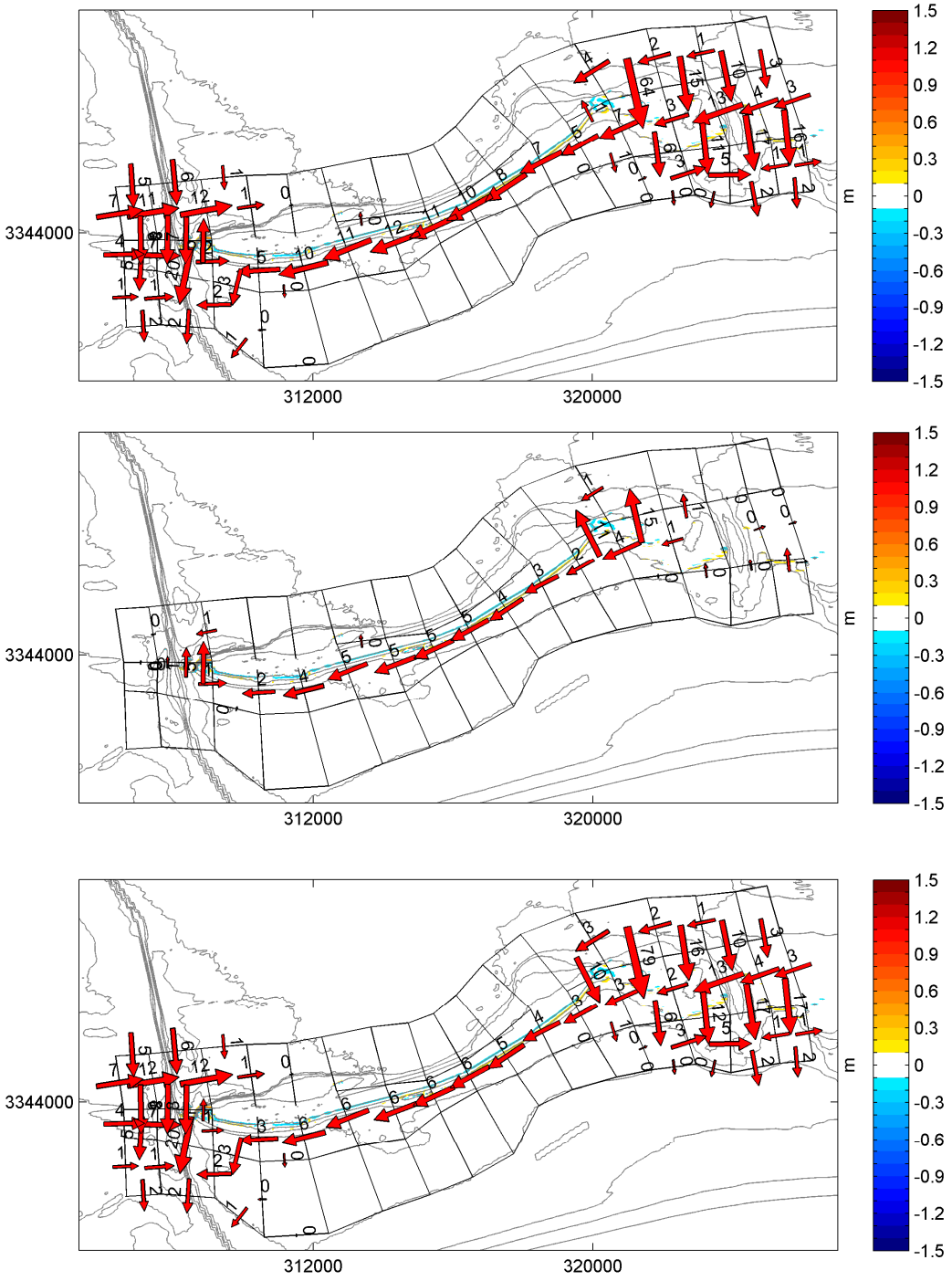

Figure 8.31 Predicted sediment transports for the collision+ (Lili) hurricane scenario. Top: net transports, middle transports during flooding phase, bottom: transports during ebbing phase (colors indicate the total sediment-erosion in m).

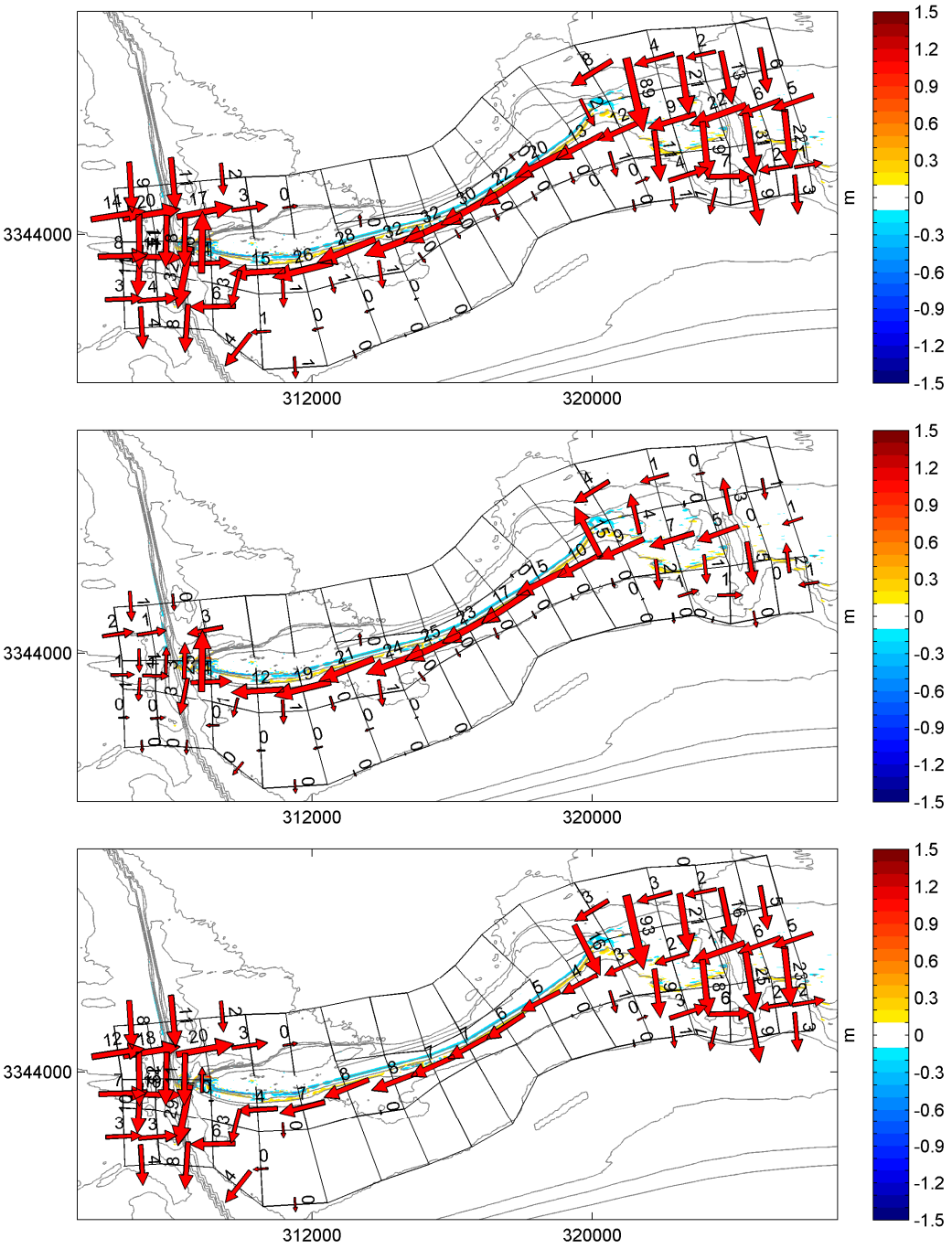

Figure 8.32 Predicted sediment transports for the Overwash+ (Rita) hurricane scenario. Top: net transports, middle transports during flooding phase, bottom: transports during ebbing phase (colors indicate the total sediment-erosion in m).

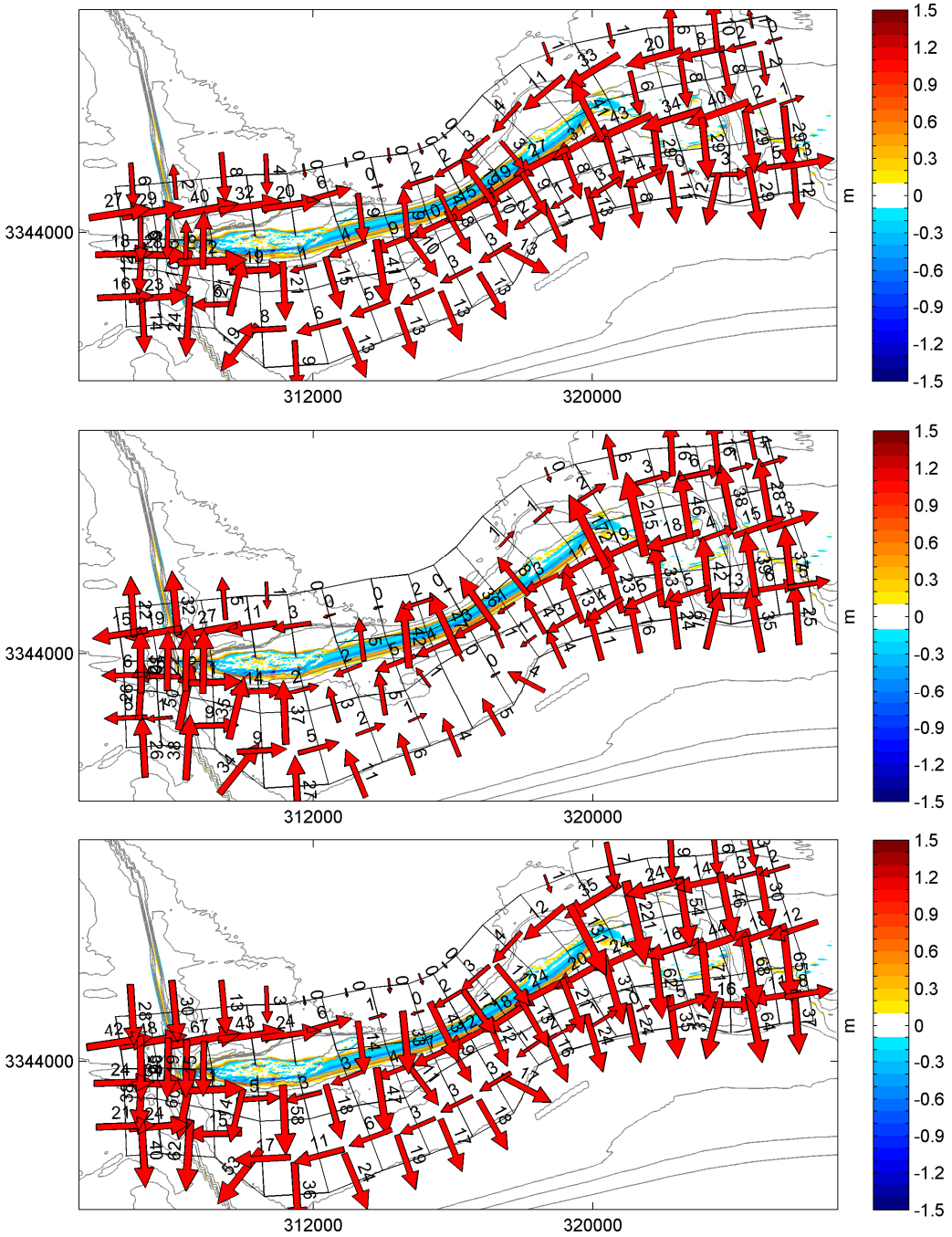

Figure 8.33 Predicted sediment transports for the inundation+ (Katrina) hurricane scenario. Top: net transports, middle transports during flooding phase, bottom: transports during ebbing phase (colors indicate the total sediment-erosion in m).

8.3.2.2 Relative influence of the restored Ship Island

The relative influence of the restoration effort is established by comparing the morphodynamic evolution of the pre- and post-restoration situations (Cases 1a and 2a). The differences between both cases are shown in Figure 8.34 for the three "+" -hurricane regimes. For all hurricanes the influence of the restoration is primarily present at Ship Island itself. Differences induced by the restoration at larger distance from the island are limited. At the passes some changes are predicted, but no obvious trends (e.g. increased sedimentation in the passes) are visible. As could be expected, the largest impact is predicted for Hurricane Katrina. For the other hurricanes the impact is smaller at both the island and in the passes. For Katrina the central and eastern part of the restored Ship Island are experiencing more erosion then was the case for the existing situation, which can be explained by the increased elevations. This also causes the increased sedimentation in the adjacent areas. The relative changes at West Ship Island are mainly due to a reduced erosion/sedimentation after the restoration.

The presented results clearly show that the influence of the restoration is restricted to the direct surroundings of the restored Ship Island for hurricane impact. However, here focus has been on the cross-shore water level gradients. In Section 6.3 MCC-model simulations revealed the importance of ebb flows which are also driven by alongshore water levels gradients generated by the hurricane forcing itself and the draining of the Lake Ponchartrain and Lake Borgne. The draining of both lakes results in additional momentum which can not be captured by the SPI model if it is only driven by water levels. A first indication of the relevance of alongshore water level gradients (excluding the momentum effect) is provided by comparing the XBeach validation simulation based on the unfiltered Katrina forcing derived from the MCC-model and "+"-inundation Katrina simulation which only accounts for cross-shore water level gradients (see Figure 8.35). The relative sedimentation-erosion patterns (i.e. difference between both model predictions) highlights the potential importance of the alongshore water level gradients. Increased ebb flows cause an additional erosion of the upper parts of the island and the eroded sand is deposited on the Gulf side of the island. Furthermore additional deposition is present in the Ship Island Pass and Gulf Port Channel.

Although, the alongshore water level gradients impact the morphological development of Ship Island itself, its influence on the adjacent passes and access channels is probably more relevant. It is expected that the longshore water level gradients could result in additional sedimentation in the passes and channels as more sediment is being mobilized and transported over larger areas. As this is a potentially important aspect, it was considered through additional simulations with the MCC-model in which both the longshore and cross-shore water level gradients and the momentum flux due to the draining of Lake Ponchartrain and Lake Borgne are included by definition. This is investigated further in the following sub-section.

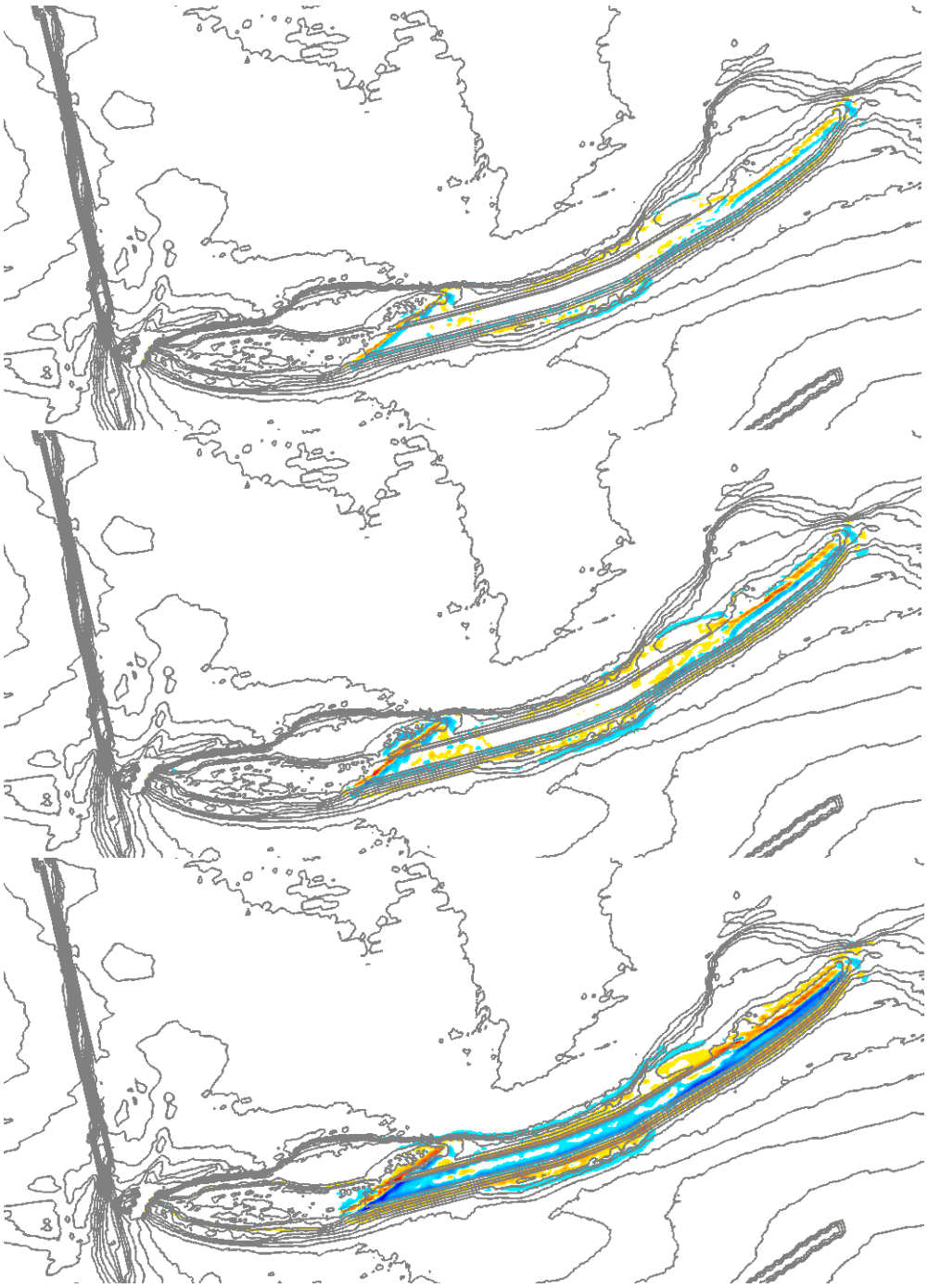

Figure 8.34 Relative bed changes for the pre- and post-restoration bathymetries due to hurricane impact. Top: Lili, middle: Rita, bottom: Katrina. Colors indicate relative sediment-erosion (m); positive values: increased sedimentation (or reduced erosion) due to restoration, negative values: increased erosion (or reduced sedimentation) due to restoration.

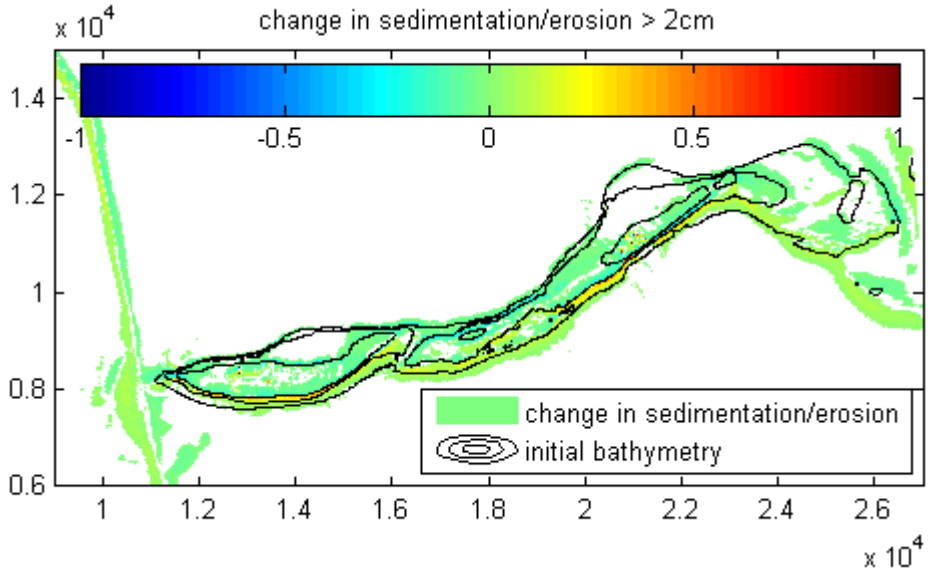

Figure 8.35 Relative bed changes for Katrina forced with unfiltered water levels and for Katrina with only cross-shore water gradients included.

8.3.2.3 *Interaction between the restored Ship Island and Ship Island Pass*

The influence of the restored Ship Island on the sedimentation rates of Ship Island Pass is investigated by comparing MCC-model simulations results with and without the restoration at Ship Island for Hurricanes Katrina and Georges. Also, the effect of the Ship Island Pass borrow source was investigated. The sedimentation in Ship Island Pass is estimated according to the method described in Section 7.5 and the results are summarized in Table 8.3 (the Balance Areas 1 and 2 are shown in Figure 7.9).

The upper two lines in the table show the computed pre-restoration volumes. It is noted that according to information presented in Byrnes (2011) shortly after Hurricane Katrina approximately 250,000 cy was dredged from the channel and shortly after Hurricane Georges approximately 300,000 cy. The computed volume for Georges in Balance Areas 1 + 2 is in fair agreement with the volume presented by Byrnes. However, on the basis of the computed sedimentation for Katrina, significantly more dredging would be expected than presented by Byrnes. It is noted that for Katrina more sedimentation would be expected than for Georges, so the computed trend is considered more logical than the trend suggested by the actual dredging records. The low dredged volume could be partly due to large maintenance dredging in 2004 (shortly before the occurrence of Katrina).

The closure of Camille Cut has a relatively large effect on the sedimentation of Ship Island Pass for both hurricanes for Balance Areas 1 and 2. Furthermore, the Ship Island Pass borrow source appears to have a major impact on the sedimentation volumes for Balance Area 1 for Hurricane Georges as the trapping is even predicted to decrease with 10,000 cy after closure. A further analysis on this aspect showed that this was mainly caused by altered ebb flows during this hurricane due to the closure of Camille Cut. However, it also reveals the limitations of the adopted analysis which may be sensitive to the exact location of the Balance Area locations. Especially for Balance Area 1 this can have a major impact on the results because the occasional large transports along the western tip of Ship Island can influence the results considerably. The estimated sedimentation volumes for Balance Area 2 are believed to be less sensitive to this aspect.

So although it is emphasized the sedimentation numbers should be interpreted with care, it is clear that especially the closure of Camille Cut has a relatively large impact resulting in a 10% to 30% increase of the sedimentation rates for both hurricanes. This is mainly caused by the closure of Camille Cut which induces larger flows across and through the access channels and passes. The backfilling of the access channel (Balance Area 2) is mainly affected by hurricane Katrina which mobilized sediment over large areas. This indicates that the increase of transport towards the channel dominates over the possible effect of changes in the trapping efficiency. For milder hurricanes the access channel is likely to be less affected by the closure.

Combining these results with the XBeach simulations presented in the previous sub-section, it is likely that the vast majority of the sediment trapped in the access channel and pass is not originating from the sand placements, but is transported from the surrounding areas.

Condition	Balance Area 1	Balance Area 2	Balance Areas 1 + area 2 (8 miles zone)	
	trapped in area (cy/event)	trapped in area (cy/event)	trapped in area (cy/event)	transported towards area (cy/event)
Katrina (pre-restoration)	45,000	375,000	420,000	860,000
Georges (pre-restoration)	25,000	160,000	185,000	345,000
Katrina (post-restoration)	70,000	485,000	555,000	1,150,000
Georges (post-restoration)	60,000	195,000	255,000	500,000
Katrina (post-restoration + SIP borrow source)	55,000	480,000	535,000	1,120,000
Georges (post-restoration + SIP borrow source)	17,000	190,000	210,000	415,000

Table 8.3 Computed sedimentation in Balance Areas defined in Figure 7.9, contribution of selected hurricanes, values per event (the Balance Areas 1 and 2 are shown in Figure 7.9).

8.3.2.4 Impact of multiple hurricanes

To further investigate the longevity of the restored Ship Island the resulting post-hurricane bathymetries were subjected to another Hurricane Katrina. The bed change due to the 2nd Hurricane Katrina impact is shown in Figure 8.36. The morphological response is very similar for all cases, but somewhat less for the case "1st" Katrina case (bottom right plot).

Comparison of the total erosion volumes confirms that the successive hurricanes more or less have the same impact and is approximately independent of the pre-hurricane bathymetry. As can be seen in Figure 8.37 (and Table 8.4) even a 3rd Hurricane Katrina only results in small decrease of the total erosion volumes (i.e. erosion volumes above MSL). Furthermore, these additional simulations have also shown that the restored Ship Island can also endure three (3) consecutive Katrina-type hurricanes without breaching (see also Figure 8.38). However, it has to be noted that in these simulations the alongshore variation of crest of the fill is very

limited. Small variations in the crest height could induce a local scour which could lead to breaching of the fill.

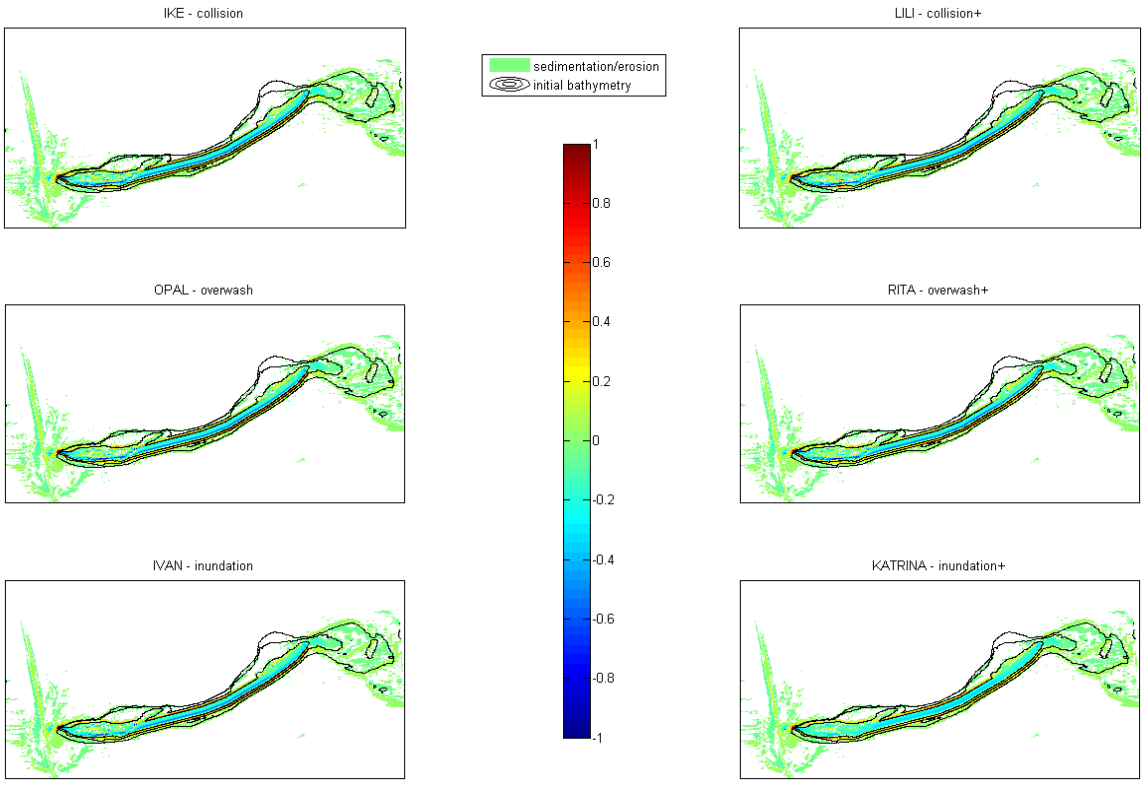

Figure 8.36 Predicted relative morphological change after hurricane Katrina is imposed on the predicted post-hurricane bathymetries (top row: collision regime, middle row: overwash regime and bottom row: inundation regime).

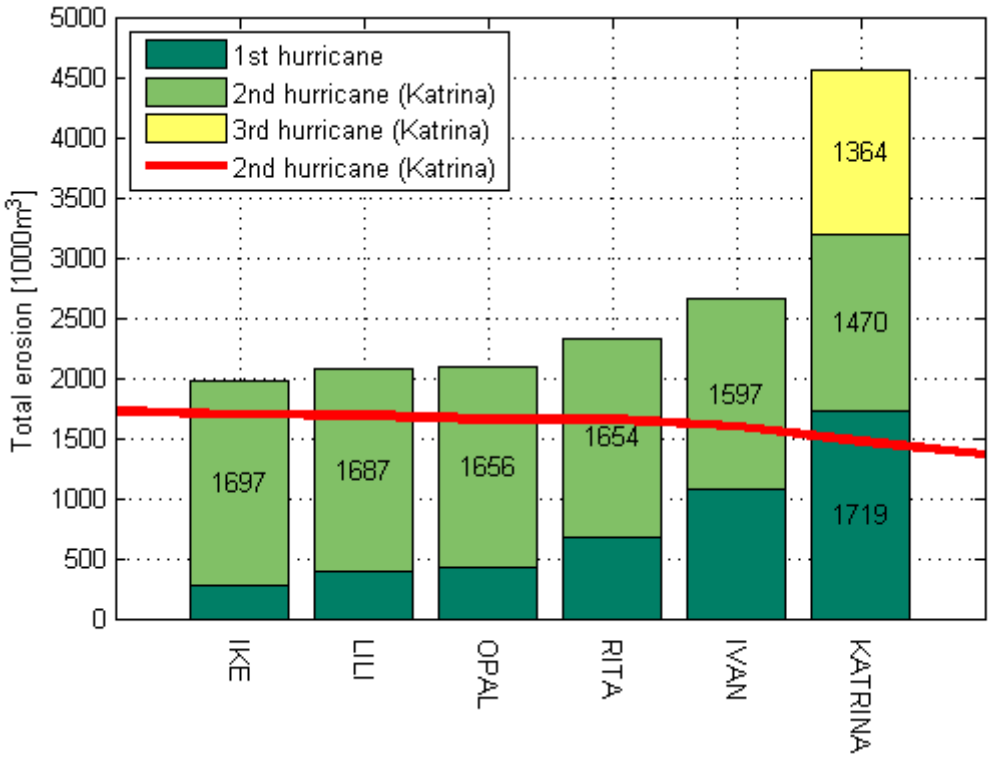

Figure 8.37 Predicted total erosion volumes after for multiple hurricane impacts.

	actual	2nd (Katrina)	3rd (Katrina)
Ike	278	1697	-
Lili	389	1687	-
Opal	430	1656	-
Rita	676	1654	-
Ivan	1067	1597	-
Katrina	1719	1470	1364

Table 8.4 Computed erosion volumes in millions m^3 for the actual hurricane (1st column) and the compound impact in case of an additional Katrina hurricane (2nd and 3rd column).

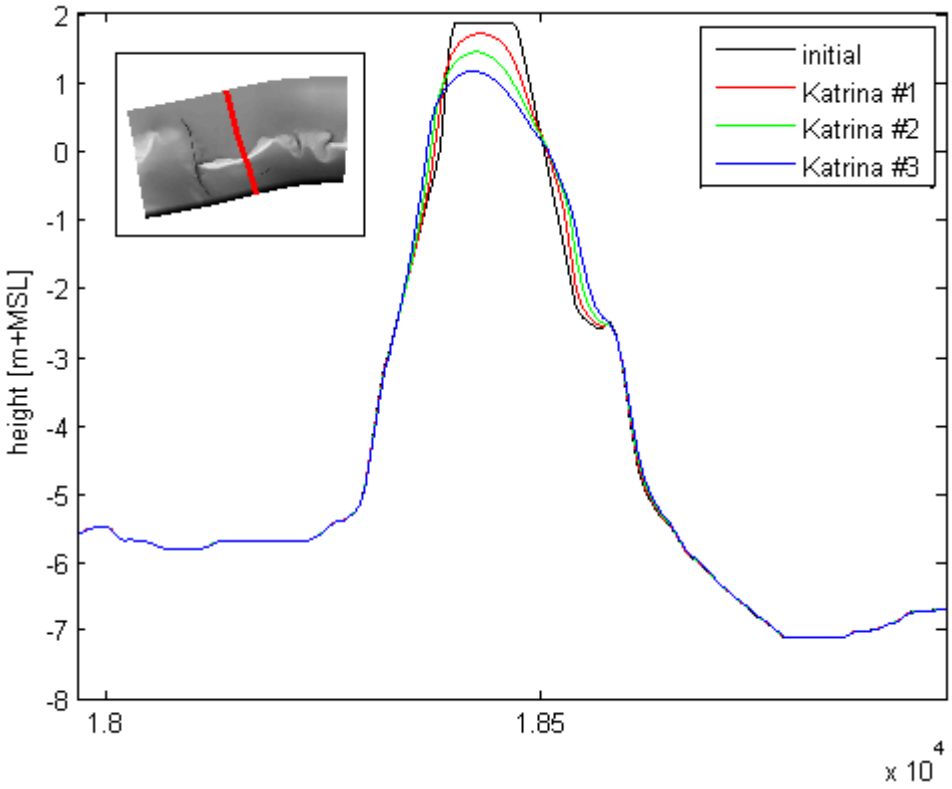

Figure 8.38 Initial and post-hurricane cross-shore transects across the closed Camille cut.

8.3.3 Medium term post-hurricane recovery potential

The predicted post-hurricane medium term development of the restored Ship Island after 4 years is shown in Figure 8.39. The post-hurricane bathymetries for the “collision+”, “overwash+” and “inundation+” were used to initialize the medium simulations. The bed changes and the net transports for the three post-hurricane bathymetries are very similar. Furthermore, the development is also in close agreement with the considered post-restoration predictions (compare Figure 8.39 with Figure 8.20).

On the considered time scales (4 years), the restored Ship Island remains stable and does not breach for the considered hurricanes. The fact that the island is able to resist the hurricanes is the primary reason the morphological changes under averaged conditions after 4 years are not significantly influenced by the hurricane impact.

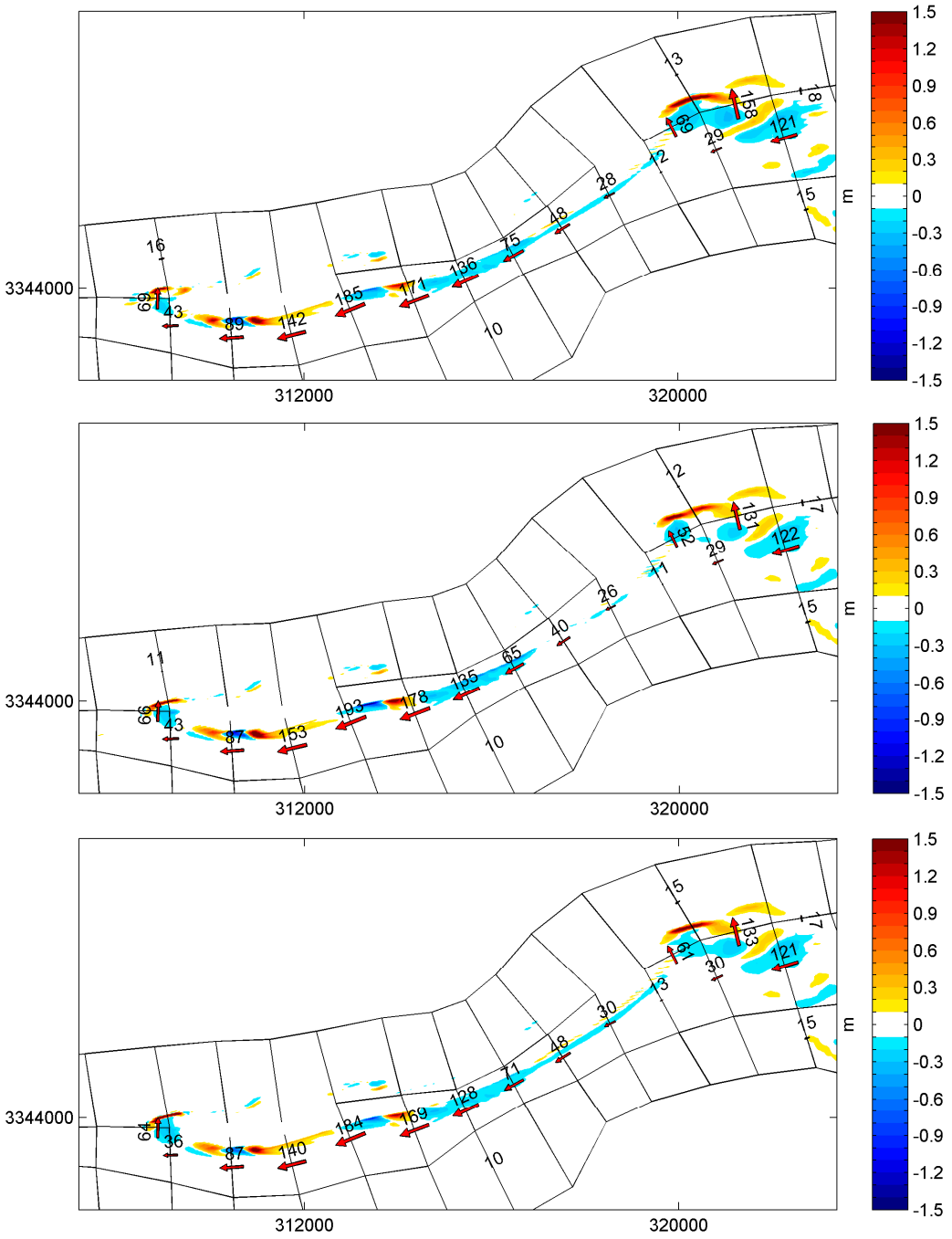

Figure 8.39 Bed change(m) for the medium term post-hurricane recovery of the restored Ship Island (Case 2a) after 4 years for the different hurricane impact scenarios (Top plot: collision regime, middle plot: overwash regime, bottom: inundation regime).

9 Addressing the key questions

9.1 Introduction

The main findings of the study are briefly summarized in Sections 9.2 and 9.3.
In Section 9.4 the key questions are addressed.

9.2 The sediment balance

Numerical modeling has been carried out to obtain insight into the sediment balance of the barrier islands Dauphin Island, Petit Bois, Horn Island and Ship Island, to such extent that predictions of impacts of the closure of Camille Cut and the planned south-eastern nourishment can be made.

Contributions to the sediment balance have been assessed for year-averaged conditions, hurricanes and cold fronts. Each contribution required a different modeling setup, but by making consistent modeling choices comparison of the various contributions is considered to be justified. All contributions have been combined to assess the total sediment balance.

It was found that for the long term average net longshore transport at the Gulf sides of the barriers, the contribution of year-averaged conditions and hurricanes are of a similar order of magnitude, although the mean annual percentage of hurricanes is no more than about 3%. Along the Sound side the transport is considerably smaller (approximately 10% of the transport at the Gulf side), and here cold fronts and hurricanes contribute more or less evenly.

For the year-averaged conditions a westward directed net transport is found, while also the net effect of the historic hurricanes is westward directed. It is noteworthy that for some hurricanes the resulting transport along Ship Island was eastward directed, while at all other barrier islands all evaluated hurricanes resulted in a westward transport. This can be explained by the relatively stronger effect of ebb surge at Ship Island.

For all islands except Ship Island the computed net transport at the western end is larger than the transport at the eastern end. This would indicate overall erosion of the Gulf-orientated shorelines, which is confirmed by observations. The observed net erosion along Ship Island seems to be caused by cross-shore transport through Camille Cut rather than the longshore transport gradient.

The computed longshore transport pattern along all barriers can be explained by the individual island geometries, and at most locations observed shoreline behavior seems to confirm the computed pattern.

For all islands the net transport at their eastern end is 3 to 5 times smaller than the net transport at the western end of the updrift (eastward) located island. This may be an indication that a significant part of the sediment is not crossing the passes to feed the next island in the chain.

The overall effect of the year-averaged conditions and the hurricanes at the Gulf side of the islands is a net westward directed transport with a computed magnitude varying

between 10,000 and 120,000 cy/yr. At the Sound side the computed net transport is less than 10,000 cy/yr.

The computed large-scale sediment balance along the islands and in the passes has been compared with the long-term sand balance presented by Byrnes et al. (2011). The computed erosion and accretion pattern shows a fair qualitative agreement with this balance. In a quantitative sense the deviations are within uncertainty ranges identified in Section 7.3.

Sedimentation in Gulfport Ship Channel (located just west of Ship Island) has been considered with the model for the stretch running through the littoral zone and the more offshore located stretch. For the littoral part of the channel the computed contributions of the year-averaged conditions and the hurricanes are similar, while for the offshore part the effect of the hurricanes is dominant.

Model results of sediment transport and coastal morphology should inevitably be interpreted with an uncertainty range. The computed values for the sediment transport, erosion and accretion presented in this report are ‘best estimates’ which should be interpreted with a considerable range. A sensitivity and uncertainty analysis have indicated that the computed transport can be up- or down-scaled with a factor of 0.5 to 3.5.

Compared to published transport data for the area, the transports computed with the MCC-model are near the lower end of the range in these data. The actual transport, erosion and accretion rates may therefore be somewhat larger than computed with the model. This would imply that the time scale of the predicted impact may be somewhat different than suggested by the model. The transport pattern and morphological response (erosion and accretion) are considered satisfactory. The uncertainty is in the time scale.

9.3 The predicted impact of the restored Ship Island

The restoration of Ship Island is made up of sand placements and borrow areas. The impact of the sand placements for averaged conditions (i.e. closure of Camille Cut and southeast sand placement) and the borrow areas possibly affecting Ship Island (borrow area just offshore of Ship Island and Ship Island Pass borrow source) have been identified by evaluating a number of cases from which the effect of these restoration components could be isolated. For the hurricane conditions, the primary focus was on the sand placements.

For averaged conditions the closure is eliminates the flows through Camille Cut. As a consequence, the littoral drift can now fully develop along the Gulf shoreline of the restored Ship Island. A comparison between the reference case and the restored Ship Island revealed that the largest differences occur in the closure area. However, more interestingly, the littoral drift causes additional sedimentation along the central part of West Ship Island. The alongshore location of this accumulation is governed by the updrift supply and the local shoreline orientation. Looking westward, the shoreline orientation at West Ship Island is gradually changing from southeast to south to southwest causing a decrease in the littoral drift and consequently an accumulation of sediment. The 4 year prediction period is too short to directly establish whether the additional sedimentation will result in additional sedimentation of Ship Island Pass. The sediment accumulation gradually migrates westward which implies that additional sedimentation at the pass is to be expected after some time. Based on the migration rates over the 4 year period (and

ignoring tropical storms and hurricanes) it is estimated that additional sedimentation of the Ship Island Pass could occur after 10 to 15 years. However, the interaction between averaged conditions and hurricanes has not explicitly been considered. Given the fact that the MCC is impacted by hurricanes every five years on average, it is unlikely the described scenario will occur. In stead, hurricanes will diffuse the sediment accumulation, but it is expected that this will have only a negligible effect on Ship Island Pass, given the large morphological changes induced by hurricanes.
The impact of the hurricanes on the post-restoration bathymetry was mainly confined to the restored Ship Island itself. This assessment was based on six hurricanes representing an averaged and severe condition in each of the three Sallenger (2000) hurricane regimes. For the collision and overwash regimes (respectively hurricanes Lily and Rita), the impact on the central and eastern part of Ship Island is comparable. For the inundation regime (Katrina) the southeast sand placement is slightly more impacted. However, the overall performance of the Camille Cut closure and the southeast sand placement is comparable. The relative performance depends primarily on the characteristics of the hurricane.

Multiple hurricane impact was established by imposing the severe ("+") inundation (Katrina, 2005) regime on the final post-hurricane bathymetries. It was found that the impact of the second hurricane was more or less independent from the first hurricane. To test the residual strength of the restored Ship Island it was also impacted by three successive Katrina hurricanes. Although a continued decrease in crest height was predicted after each hurricane, Ship Island did not breach. However, it can not be certain that due to small initial alongshore variations in crest height breaching could occur. In the simulations the study assumed an initial alongshore constant crest height. Furthermore, the hurricane regimes focused on the combined effects of waves and water levels gradients across Ship Island. For some hurricanes considerable water level gradients along the islands were also present which could substantially increase the sediment losses from the central parts of Ship Island as eroded sand is transported towards the tips of the island. Sediment transport calculations using the MCC-model confirmed the relevance of the longshore water level gradients. These are potentially important during both the build up (or flooding) phase of the hurricane and during the ebbing phase (ebb surge) as water is draining from Lake Ponchartrain, Lake Borgne and the Mississippi Sound through Ship Island Pass and Dog Keys Pass.

The relative contribution of both phases especially depends on the hurricane track. For example, both Camille and Katrina resulted in large storm surges in Lake Ponchartrain which caused the transport patterns around Cat and Ship Island to be dominated by the ebbing phase. The relative large influence of the ebbing phase for these hurricanes also explains the large morphological impact which is primarily resulting from the gross transport (i.e. Ship Island is impacted two times). Hurricanes for which the draining of the back barrier basins coincides with eastward directed winds tend to have relative large ebbing phase transports. Depending on the exact wind direction this can either impact the transports at the Sound or Gulf side shorelines. During Katrina the wind was northeastward directed during the ebbing phase, therefore enhancing the eastward directed transports along the Gulf shoreline of Ship Island. In contrast, the southeastward directed winds during Hurricane Ivan resulted in relative large transports at the Sound shoreline during the ebbing phase.

The impact of the restoration on the transport and flow patterns around Ship Island is limited. The closure of Camille Cut causes increased flow rates along the island tips and

through the inlet to occur as water can no longer flow through the cut. The associated sediment transports also increase which results in somewhat enhanced transports through and along the passes. The sediment transport calculations indicate that the Camille Cut closure results in slightly (5-30%) enhanced sedimentation rates for Ship Island Pass during hurricane conditions.

The post-hurricane recovery potential for the three considered hurricane regimes did not show significant differences. This was primarily due to the fact that the restored Ship Island did not breach. The medium-term (4 year) post-hurricane predictions show a large overall agreement with the post-restoration predictions. Only the western tip of Ship Island is experiencing some additional erosion for the post-hurricane simulation which is also reflected by an increase of the transports across the western tip towards the Mississippi Sound.

The effect of the offshore borrow area was very small and could hardly be distinguished from the model simulations. The relative small size and especially the limited excavation (cut) depth help to minimize the impact on Ship Island. Moreover the predicted changes are expected to diminish over time as the borrow area gradually backfills.

For averaged conditions the Ship Island Pass borrow source has no noticeable impact on the medium-term (0-10 yrs) morphological development. However, for hurricane conditions the borrow source appears to somewhat act as a sediment trap resulting in a reduction in the Ship Island Pass back fillings rates. The impact of the borrow source diminishes as it back fills and it is not expected to have a major impact on the longer term maintenance dredging. However, it does reveal that the borrow source is able to trap sediment reducing the backfilling rates of the pass. Further research on this was beyond the scope of the present study, but it could be an efficient method to reduce future maintenance dredging cost.

9.4 Addressing the key questions

9.4.1 **Key Question 1**: How will closing of Camille Cut and the nearshore sand placement at the southeast end of Ship Island impact sediment transports?

- **Morphological development of the restored Ship Island**

The closure of Camille Cut reconnects East and West Ship Island and consequently enables the littoral drift along Gulf shoreline to fully develop. Furthermore, cross-shore tidal, wave and wind-driven flows through Camille Cut are not present anymore. Due to the changing shoreline orientation of Ship Island, transports first increase along the southeast sand placement and central part of the island and decrease along western end. For averaged conditions the medium term (4 year) simulations predict a local accumulation of sediment which prevents the sand reaching the western tip of West Ship Island and Ship Island Pass. This accumulated sediment gradually migrates westward and it is expected to reach the pass after about 10 to 15 years excluding the effect of hurricanes. Although the interaction between the medium term development and hurricanes was beyond the scope of the present study, it is expected that hurricanes will diffuse the accumulated sediment which will result in a minimal increase (0-10%) of sedimentation in Ship Island Pass.

The post-restoration configuration just after construction primarily has a local effect under hurricane impact and most of the sand used in the restoration effort will remain in the active

parts of Ship Island. The model does not indicate deposition of sand from the fill in the channel just after construction.

- **Transports around the restored Ship Island**

The overall sediment transport patterns are primarily affected by the closure of Camille Cut. This results in slightly increased transports along the tips of Ship Island (0-10% under year averaged conditions) to compensate for the closure of Camille Cut.

The influence of the restored Ship Island is confined to the island itself and the adjacent passes (which is further addressed in Key Question 3). No interaction with the neighboring islands could be identified. This conclusion holds for both averaged conditions and hurricanes.

9.4.2 **Key Question 2**: Will sand extracted from offshore borrow sites negatively impact erosion and deposition on the barrier islands?

Due to its small size and the limited excavation depth the borrow area just south of Ship Island will not negatively impact the overall morphological development of the restored Ship Island. Comparison of 4 year morphological simulations under averaged conditions (excluding tropical storms and hurricanes) with and without the borrow area showed negligible differences which were only present along parts of the coast directly behind the borrow area. Potentially local adjustments of the shoreline could occur during specific conditions, but the magnitude of these adjustments is expected to be insignificant. Furthermore, the impact on Ship Island will gradually disappear when the borrow slopes flatten and the borrow area backfills over time.

9.4.3 **Key Question 3**: How will closing of Camille Cut and nearshore sand placement at the southeast end of Ship Island impact operation and maintenance at Ship Island Pass?

The sand used to restore Ship Island will only result in a limited increase of the sedimentation of Ship Island Pass (see also Key Question 1) which is primarily caused by hurricanes. With an assumed averaged hurricane return period of 5 years, it is expected that the averaged conditions do not result in increased sediment transport into Ship Island Pass. Furthermore, the restoration decreases the cross-sectional flow area which consequently increases the flows and transports along the tips of Ship Island and the flows and transports across and through the access channels and passes. Although this effect is minimal for the averaged conditions, as tidal flows through the passes are relatively small and waves are generally low, its residual effect could be a small reduction of the sedimentation in Ship Island Pass. However, hurricanes have the potential to induce large flooding and ebbing velocities through the passes which are noticeably increased by the closure of Camille Cut. In combination with large waves that stir up the sediment this causes additional sedimentation of the Gulfport Ship Channel and Ship Island Pass. For Hurricanes Katrina and Georges the closure of Camille Cut resulted in an estimated 10% to 30% increased sedimentation in Ship Island Pass and the Ship Channel. For milder hurricanes this effect will be not as noticeable and is estimated to be between 0% and 10%. The increase in sedimentation is due to a slight increase of the discharge through the passes at both sides of Ship Island, caused by a diversion of the present flow through Camille Cut. As a result more sediment is transported through the passes and more sedimentation occurs in the channel (increased transport dominates over possible effect of changes in the trapping efficiency). The model does not indicate additional deposition of sand originating from the fill in the channel.

References

ACRE (Applied Coastal Research and Engineering, Inc.), 1999. Environmental Survey of Identified Sand Resource Areas Offshore Alabama, Vol. 1: Main text.

ACRE (Applied Coastal Research and Engineering, Inc.), 2008. Evaluation of channel dredging on shoreline response at and adjacent to Mobile Pass, Alabama.

Ashton A, Murray AB, Arnoult O, 2001. Formation of coastline features by large-scale instabilities induced by high-angle waves. Nature, 414: 296-300.

Murray, A.B., Ashton, A., 2004. Extending a 1-line modeling approach to explore emergent coastline behaviors. 29th ICCE, pp. 2035-2047

Byrnes, M.R., Rosati, J.D., Griffee, S.F., Berlinghoff, J.L., 2011. Littoral Sediment budget for the Mississippi sound barrier islands, Final report, October 2011.

Chaney, P.L., Stone, G.W., 1996. Soundside erosion of a nourished beach and implications for winter cold front forcing: West Ship Island, Mississippi, Shore and beach, Vol. 64, 27-33.

Cipriani, L.E. and Stone, G.W., 2001. Net longshore sediment transport and textural changes in beach sediments along the southwest Alabama and Mississippi barrier islands, U.S.A. Journal of coastal research, vol. 7, no. 2, pp. 443-458

Deltares, 2011a, Mississippi Barrier Island Restoration, Progress Report 1, Desk Top Study, Report 1204473-000-HYE-0003.

Deltares, 2011b, Mississippi Barrier Island Restoration, Progress Report 2, Setup and Calibration of the Mississippi Coastal Cell Model, Report 1204473-000-HYE-0007.

Deltares, 2011c. WES; Wind Enhance Scheme for cyclone modeling. User Manual (version: 3.00, revision: 15423, 18 May 2011).

ERDC/CHL, 2009. Mississippi Coastal Improvement Program, Regional sediment budget for Mississippi mainland and barrier island coasts.

ERDC/CHL, 2011. Mississippi Coastal Improvement Program, Barrier island restoration numerical modeling, Draft report.

ERDC, 2012. Chapter 4: Nearshore wave modeling, Draft Report

Hasselmann, K., T. P. Barnett, E. Bouws, H. Carlson, D. E. Cartwright, K. Enke, J. Ewing, H. Gienapp, D. E. Hasselmann, P. Kruseman, A. Meerburg, P. Mueller, D. J. Olbers, K. Richter, W. Sell and H. Walden, 1973. Measurements of wind wave growth and swell decay during the Joint North Sea Wave Project (JONSWAP)." Deutsche Hydrographische Zeitschrift 8 (12).

Hsu, S.A. and Zhongde Yan. 1999. A Note on the Radius of Maximum Wind for Hurricanes, Journal of Coastal Research, Vol. 14, No. 2, pp 667-668.

Komen, G., S. Hasselmann and K. Hasselmann, 1984. On the existence of a fully developed

wind-sea spectrum. Journal of Physical Oceanography 14, pp 1271-1285.

Kuiper, S., 2010, Cross-shore morphological response on Chaland Headland due to hurricanes Gustav and Ike, MSc Thesis, Delft University of Technology

Latteux, B., 1995. Techniques for long-term morphological simulations under tidal action Marine Geology, 126(1-4), 129-141.

Makin, V.K., 2005. A note on the drage of the sea surface at hurricane winds, Boundary Layer Meteorology, 115: 169-176.

McCall, R.T., Van Thiel de Vries, J.S.M., Plant, N.G., Van Dongeren, A.R., Roelvink, J.A., Thompson, D.M., Reniers, A.J.H.M., 2010. Two-dimensional time dependent hurricane overwash and erosion modeling at Santa Rosa Island. Coastal Engineering 57, pp 668-683.

Morton, R.A., 2007. Historical changes in the Mississippi-Alabama barrier islands and the roles of extreme storms, sea level, and human activities. USGS report 2007-1161.

Powell, M.D., Vickery, P.J., Reinhold, T.A., 2003. Reduced drag coefficient for high wind speeds in tropical cyclones. Nature 422. Doi: 10.1038/nature01481.

Ranasinghe, R., C. Swinkels, A. Luijendijk, J.A. Roelvink, J. Bosboom, M.J.F. Stive, D.J.R Walstra, 2011. Morphodynamic upscaling with the morfac approach: dependencies and sensitivities. Coastal Engineering, Vol. 58, Issue 8, 806-811.

Roelvink, J.A., Reniers, A.J.H.M., 2011. A guide to modeling coastal morphology. Advances in Coastal and Ocean Engineering. World Scientific Pub. Co. Inc.

Roelvink, J.A., 2006. Coastal morphodynamic evolution techniques. Coastal Engineering 53,177–187.

Rogers, W.E., P.A. Hwang, and D.W. Wang. 2003. Investigation of wave growth and decay in the SWAN model: three regional-scale applications, J. Phys. Oceanogr., Vol. 33, 366-389.

Rosati, J.D., Byrnes, M.R., Gravens, M.B., Griffee, S.F., 2009. Mississippi Coastal Improvement Project Study, Regional Sediment Budget for Mississippi Mainland and Barrier Island Coasts, July 2009.

Sallenger, A.H., 2000. Storm impact for barrier islands. Journal of Coastal Research, Vol. 16, No. 3, 890-895.

Sheng, Y.P., Zhang, Y., Paramygin, V.A., 2010. Simulation of storm surge, wave, and coastal inundation in the Northeastern Gulf of Mexico region during Hurricane Ivan in 2004, Ocean Modeling, Vol. 35, Iss. 4, 314-331, ISSN 1463-5003, 10.1016/j.ocemod.2010.09.004.

Stone, G.W., Liu, B., Pepper, A.P., Wang, P., 2004.The importance of extratropical and tropical cyclones on the short-term evolution of barrier islands along the northern Gulf of Mexico, USA. Marine Geology, Vol. 210, 63-78.

USACE, 2009a. Comprehensive Plan and Integrated Programmatic Environmental Impact Statement, Mississippi Coastal Improvements Program (MsCIP) Hancock, Harrison, and

Jackson Counties; Comprehensive Plan and Integrated Programmatic Environmental Impact Statement. Volume 1: Main Report, June 2009

USACE, 2009b. Mississippi Coastal Improvement Program (MsCIP) Hancock, Harrison, and Jackson Counties, Mississippi. Appendix H, Barrier Islands, June 2009

USACE, 2010. Results of Sand Borrow Investigation Mississippi Barrier Island Restoration Plan. MsCIP, November 2010 (file: GeoTechRptDraftV8.1_Dec2010.pdf)

USACE, 2011?. ERDC/CHL TR-11-x, Chapter 2, Field Data Collection

Van Os, J. and S. Caires, 2011: How to Carry out metocean studies. Proc. 30th Int. Conf. on Offshore Mechanics and Arctic Eng. (OMAE2011-49066).

Van Rijn, L.C., 1993. Principles of sediment transport in rivers, estuaries and coastal seas. Aqua publications, Amsterdam, the Netherlands.

Van Rijn, L.C., 2007a. Unified view of sediment transport by currents and waves, I: initiation of motion, bed roughness and bed-load transport. Journal of Hydraulic Engineering, ASCE 133 (6), 649–667.

Van Rijn, L.C., 2007b. Unified view of sediment transport by currents and waves, II: suspended transport. Journal of Hydraulic Engineering, ASCE 133 (6), 668–689.

Van Rijn, L.C., 2007c. Unified view of sediment transport by currents and waves, III: graded beds. Journal of Hydraulic Engineering, ASCE 133 (7), 761–775.

A Hurricanes in the Gulf of Mexico (1917-2010)

id	Year	Month	Name	Category	Minimum Distance Ship Island	Sallenger regime
1	1917	9	NOTNAMED04	H4	117	inundation
2	1918	8	NOTNAMED01	H3	382	collision
3	1919	9	NOTNAMED02	H4	416	collision
4	1920	9	NOTNAMED02	H2	227	collision
5	1921	10	NOTNAMED06	H4	590	collision
6	1923	10	NOTNAMED08	TS	22	collision
7	1926	8	NOTNAMED03	H3	209	collision
8	1926	9	NOTNAMED07	H4	29	collision
9	1929	9	NOTNAMED02	H5	269	collision
10	1932	8	NOTNAMED03	H1	68	collision
11	1933	6	NOTNAMED02	H2	469	collision
12	1936	7	NOTNAMED05	H1	196	collision
13	1947	9	NOTNAMED04	H5	84	inundation
14	1950	8	BAKER	H3	110	collision
15	1950	9	EASY	H3	456	swash
16	1953	9	FLORENCE	H3	204	collision
17	1955	7	BRENDA	TS	69	collision
18	1956	9	FLOSSY	H1	73	collision
19	1960	9	ETHEL	H5	31	overwash
20	1964	9	HILDA	H4	75	collision
21	1965	8	BETSY	H5	189	inundation
22	1969	8	CAMILLE	H5	87	inundation
23	1972	6	AGNES	H1	320	collision
24	1974	8	CARMEN	H4	248	collision
25	1975	9	ELOISE	H3	246	collision
26	1979	7	BOB	H1	160	collision
27	1979	8	FREDERIC	H4	80	collision
28	1985	8	ELENA	H3	7	overwash
29	1985	10	JUAN	H1	97	collision
30	1985	11	KATE	H3	286	collision
31	1988	9	FLORENCE	H1	96	collision
32	1992	8	ANDREW	H5	243	collision
34	1995	7	ERIN	H1	139	collision
35	1995	9	OPAL	H4	169	inundation
36	1997	7	DANNY	H1	52	overwash
37	1998	9	GEORGES	H5	28	inundation
38	2002	9	ISIDORE	H3	103	collision
39	2002	9	LILI	H4	332	collision
40	2004	9	IVAN	H5	93	overwash
41	2005	6	ARLENE	TS	130	collision
42	2005	7	CINDY	H1	72	collision
43	2005	7	DENNIS	H4	186	collision
44	2005	8	KATRINA	H5	102	inundation

45	2005	9	RITA	H5	426	collision
46	2008	8	GUSTAV	H4	205	inundation
47	2008	9	IKE	H4	463	collision
48	2009	11	IDA	H2	46	collision
49	1919	7	NOTNAMED01	TS	175	collision
50	1919	9	NOTNAMED04	TS	311	swash
51	1920	9	NOTNAMED05	H1	383	collision
52	1922	10	NOTNAMED05	TS	103	collision
53	1923	6	NOTNAMED01	TS	117	collision
54	1923	10	NOTNAMED06	H1	233	collision
55	1924	9	NOTNAMED05	H1	210	collision
56	1924	9	NOTNAMED08	H1	394	collision
57	1924	10	NOTNAMED09	TS	383	swash
58	1924	10	NOTNAMED10	H5	796	collision
59	1926	7	NOTNAMED01	H4	316	collision
60	1928	8	NOTNAMED01	H2	428	collision
61	1928	8	NOTNAMED02	H1	354	swash
62	1928	9	NOTNAMED04	H5	668	collision
63	1930	8	NOTNAMED02	H2	617	collision
64	1931	7	NOTNAMED02	TS	240	collision
65	1932	8	NOTNAMED02	H4	545	collision
66	1932	9	NOTNAMED05	TS	260	collision
67	1932	9	NOTNAMED06	TS	271	collision
68	1932	10	NOTNAMED08	TS	89	collision
69	1933	7	NOTNAMED04	TS	381	collision
70	1933	7	NOTNAMED05	H1	305	collision
71	1933	8	NOTNAMED06	TS	476	collision
72	1933	8	NOTNAMED12	H4	516	collision
73	1934	6	NOTNAMED02	H1	211	collision
74	1934	7	NOTNAMED03	H1	228	collision
75	1934	8	NOTNAMED05	H1	340	swash
76	1934	10	NOTNAMED09	TS	63	collision
77	1935	8	NOTNAMED02	H5	522	swash
78	1935	10	NOTNAMED06	H1	305	swash
79	1936	7	NOTNAMED04	TS	159	collision
80	1936	8	NOTNAMED07	TS	340	swash
81	1936	8	NOTNAMED09	TS	29	swash
82	1937	8	NOTNAMED03	TS	224	swash
83	1937	9	NOTNAMED06	TS	128	swash
84	1937	9	NOTNAMED09	TS	284	swash
85	1938	8	NOTNAMED02	H2	413	collision
86	1938	10	NOTNAMED05	TS	327	collision
87	1938	10	NOTNAMED07	TS	328	collision
88	1939	6	NOTNAMED01	TS	86	collision
89	1939	8	NOTNAMED02	H1	196	collision
90	1939	9	NOTNAMED03	TS	145	swash
91	1940	8	NOTNAMED02	H1	255	collision
92	1940	9	NOTNAMED06	TS	174	swash
93	1941	9	NOTNAMED01	TS	238	swash

94	1941	9	NOTNAMED02	H1	460	collision
95	1941	10	NOTNAMED05	H3	400	swash
96	1942	8	NOTNAMED01	H1	287	collision
97	1943	7	NOTNAMED01	H1	231	collision
98	1943	9	NOTNAMED06	H2	343	swash
99	1944	9	NOTNAMED06	TS	74	collision
100	1945	6	NOTNAMED01	H3	417	collision
101	1945	8	NOTNAMED05	H4	697	collision
102	1945	9	NOTNAMED07	TS	74	collision
103	1945	9	NOTNAMED09	H4	698	swash
104	1946	6	NOTNAMED01	TS	163	collision
105	1946	10	NOTNAMED05	H4	621	collision
106	1947	8	NOTNAMED03	H1	428	swash
107	1947	9	NOTNAMED05	TS	63	collision
108	1947	10	NOTNAMED07	TS	390	collision
109	1947	10	NOTNAMED08	H1	390	collision
110	1948	7	NOTNAMED02	TS	176	collision
111	1948	9	NOTNAMED05	H1	114	collision
112	1948	10	NOTNAMED08	H4	975	collision
113	1949	9	NOTNAMED05	TS	189	collision
114	1949	9	NOTNAMED10	H4	512	collision
115	1950	10	HOW	TS	442	collision
116	1950	10	KING	H3	459	collision
117	1950	10	LOVE	H1	350	collision
118	1953	5	ALICE	TS	294	collision
119	1955	8	NOTNAMED05	TS	81	collision
120	1956	6	NOTNAMED01	TS	166	collision
121	1957	6	NOTNAMED01	TS	336	collision
122	1957	8	BERTHA	TS	292	collision
123	1957	9	DEBBIE	TS	198	swash
124	1957	9	ESTHER	TS	161	collision
125	1959	5	ARLENE	TS	244	swash
126	1959	7	DEBRA	H1	492	swash
127	1959	9	GRACIE	H4	827	swash
128	1959	10	IRENE	TS	120	collision
129	1960	7	BRENDA	TS	543	swash
130	1960	8	DONNA	H5	718	collision
131	1960	9	FLORENCE	TS	132	swash
132	1961	9	CARLA	H5	626	collision
133	1964	8	ABBY	TS	350	collision
134	1964	8	CLEO	H5	727	collision
135	1964	8	DORA	H4	393	swash
136	1965	6	NOTNAMED01	TS	169	collision
137	1965	9	DEBBIE	TS	17	collision
138	1966	6	ALMA	H3	413	collision
139	1966	9	INEZ	H4	810	collision
140	1967	9	BEULAH	H5	951	swash
141	1969	9	SUBTROP1	TS	238	collision
142	1969	10	JENNY	TS	295	collision

143	1969	10	LAURIE	H2	427	collision
144	1970	7	BECKY	TS	341	collision
145	1970	9	FELICE	TS	272	collision
146	1971	9	EDITH	H5	209	collision
147	1971	9	FERN	H1	72	collision
148	1972	5	ALPHA	TS	402	collision
149	1973	9	DELIA	TS	456	collision
150	1976	5	SUBTROP1	TS	332	collision
151	1977	8	ANITA	H5	349	swash
152	1977	9	BABE	H1	153	swash
153	1978	8	DEBRA	TS	433	swash
154	1979	7	CLAUDETTE	TS	487	collision
155	1979	8	DAVID	H5	747	swash
156	1979	8	ELENA	TS	454	swash
157	1979	9	HENRI	H1	466	swash
158	1980	7	ALLEN	H5	750	collision
159	1980	9	DANIELLE	TS	315	collision
160	1982	9	CHRIS	TS	444	swash
161	1983	8	ALICIA	H3	389	collision
162	1984	9	DIANA	H4	818	swash
163	1985	8	DANNY	H1	354	collision
164	1986	6	BONNIE	H1	399	collision
165	1986	8	CHARLEY	H1	471	collision
166	1987	8	NOTNAMED01	TS	186	collision
167	1988	8	BERYL	TS	73	collision
168	1988	9	GILBERT	H5	930	collision
169	1989	6	ALLISON	TS	476	collision
170	1989	7	CHANTAL	H1	459	collision
171	1989	9	HUGO	H5	891	collision
172	1994	6	ALBERTO	TS	209	collision
173	1994	8	BERYL	TS	171	swash
174	1995	6	ALLISON	H1	365	collision
175	1996	10	JOSEPHINE	TS	351	collision
176	1998	8	EARL	H2	185	collision
177	1998	9	HERMINE	TS	145	collision
178	1998	10	MITCH	H5	715	swash
179	1999	8	BRET	H4	836	swash
180	1999	9	FLOYD	H5	940	swash
181	1999	9	HARVEY	TS	429	collision
182	2000	9	HELENE	TS	175	collision
183	2001	6	ALLISON	TS	81	collision
184	2001	8	BARRY	TS	241	collision
185	2002	8	BERTHA	TS	100	collision
186	2002	9	EDOUARD	TS	332	collision
187	2002	9	HANNA	TS	17	collision
188	2003	6	BILL	TS	142	collision
189	2003	9	HENRI	TS	287	collision
190	2004	8	BONNIE	TS	281	collision
191	2004	8	CHARLEY	H4	741	collision

192	2004	8	FRANCES	H4	397	collision
193	2010	7	BONNIE	TS	123	collision
194	2004	9	JEANNE	H3	486	swash
195	2004	10	MATTHEW	TS	199	collision
196	2005	7	EMILY	H5	866	collision
197	2005	10	TAMMY	TS	313	swash
198	2005	10	WILMA	H5	805	collision
199	2006	6	ALBERTO	TS	444	collision
200	2007	9	HUMBERTO	H1	311	swash
201	2008	8	EDOUARD	TS	230	swash
202	2008	8	FAY	TS	152	collision
203	2008	11	PALOMA	H4	344	swash
204	2009	8	CLAUDETTE	TS	198	collision
205	1949	8	NOTNAMED02	H4	573	collision
206	1951	8	CHARLIE	H4	992	collision
207	1953	9	NOTNAMED07	TS	201	collision
208	1954	7	BARBARA	TS	287	collision
209	1957	6	AUDREY	H4	430	collision

B Sensitivity analysis longshore transport in MCC

B.1 Introduction

In this appendix a sensitivity analysis is presented for the longshore sediment transport under year-averaged conditions computed with the MCC model, as described in Chapter 7.

This analysis is based on the baseline transport pattern as computed during Phase 1 of the study, which differs slightly from the baseline pattern discussed in Chapter 7 (due to different transport transect used for post-processing in Phase 1 and Phase 2). However, the conclusions derived on sensitivity also apply to the Phase 2 results.

B.2 Sensitivity parameters

The numerical model requires input of several model parameters. These may be directly related to physical quantities (such as sediment grain size) or to specific coefficients in process formulations (such as in the sediment transport formula). Since in general measured sediment transport data in the field are scarce, there is some uncertainty in the validity of these model settings. Also variations in hydrodynamics and wave conditions are a (natural) source of uncertainty in sediment transport computations.

To obtain more insight into these uncertainties, a sensitivity analysis has been carried out. The following parameter settings have been varied within a physically realistic range around their default value (where the settings used in the reference run are considered as the default).

The parameters were subdivided into four groups:

- Group A: Hydrodynamics
- Bed shear stress formulation under waves:
    1. Van Rijn (2004) (default)
    2. Fredsoe (1984)
- Density(ρ), salinity(S) and temperature(T) of the sea water:
    1. ρ = 1025 kg/m^3, S = 31 ppt, T = 15°C (default)
    2. ρ = 1020 kg/m^3, S = 31 ppt, T = 30°C
    3. ρ = 1000 kg/m^3, S = 10 ppt, T = 30°C
- Background diffusivity (diff) and viscosity (visc):
    1. Diff = 0.5,visc = 0.5 (default)
    2. Diff = 0.2,visc = 0.2
    3. Diff = 1,visc = 1
- Group B: Wave conditions
- Breaker parameter (γ):
    1. γ = 0.73 (uniform) (default)
    2. γ based on bi-phase breaking of Ruesink (1998)
    3. γ based on formulation of Battjes and Stive (1985)
- Incorporation of uncertainty in simulated yearly averaged wave conditions:
    1. increase of 10% of all wave heights
- Group C: Sediment properties
- Median sediment grain size (D_{50}):
    1. D_{50} = 200 μm

2. D_{50} = 250 µm
3. D_{50} = 300 µm (default)
4. D_{50} = 400 µm

- Group D: Sediment transport formula
- Sediment transport formula:
    1. Van Rijn (1993) (default)
    2. Van Rijn (2004)

B.3 Uncertainty range sediment budget

In Figure A.1 the alongshore sediment transport rates of the base run are plotted together with results of the Group A sensitivity simulations. The results indicate that different parameter settings to some extent affect the magnitude of the alongshore sediment transport rates, but hardly impact the overall alongshore pattern (i.e. the spatial trends and gradients remain more or less the same). Variations of the background diffusivity and viscosity did not significantly affect the results and are not presented in the figure.

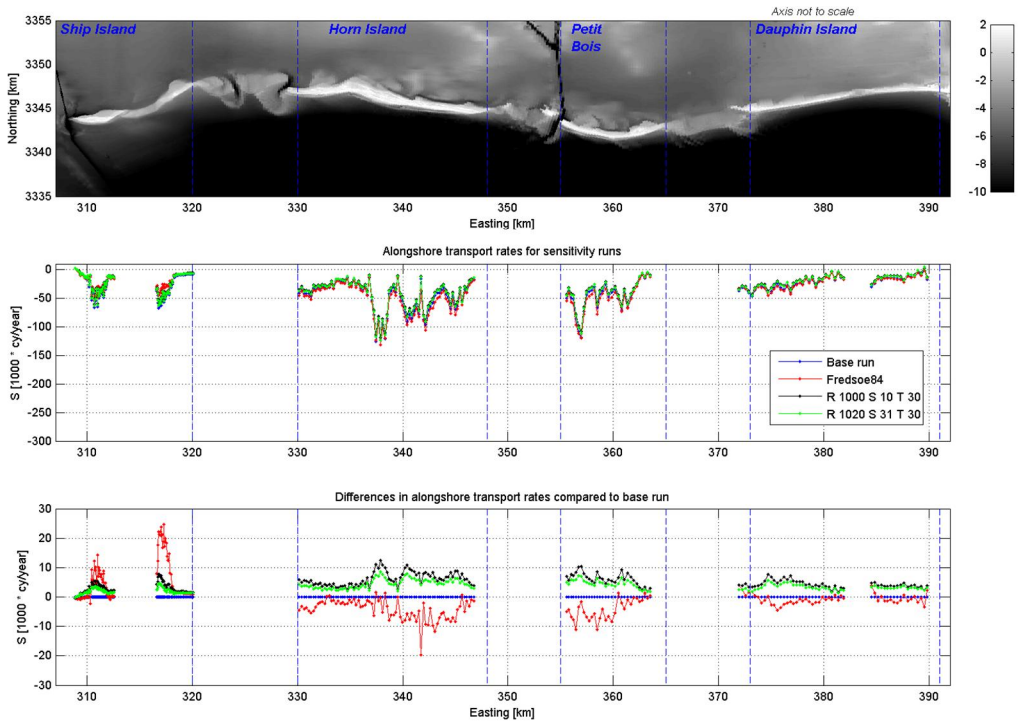

Figure B.1 Model sensitivity for hydrodynamic parameters (Group A)

Figure A.2 shows the results for the Group B sensitivity runs, related to wave conditions. The largest effect is found for the 10% increase of the wave heights. As discussed in Chapter 5, the computed nearshore wave heights tend to be slightly (up to about 10%) lower than nearshore wave height measurements. The sensitivity runs indicate that the effect of this on the computed transports is relatively small and sediment transport patterns remain comparable.

Figure A.3 shows the Group C sensitivity runs, related to the D_{50} of the sand. The results show that the computed transport values are rather sensitive for the input parameter D_{50}.

Figure A.4 shows that application of the Van Rijn (2004) formula results in considerably larger sediment transport than the Van Rijn (1993) formula, for D_{50} = 0.3 mm. Also for this formula, the sensitivity for the D_{50} is considerable. The relatively large difference between the transport computed with van Rijn (2004) and van Rijn (1993) may be due to a difference in the criterion for incipient motion for both methods. Given a high percentage of occurrence of very low waves in the study area, this criterion may be relatively important.

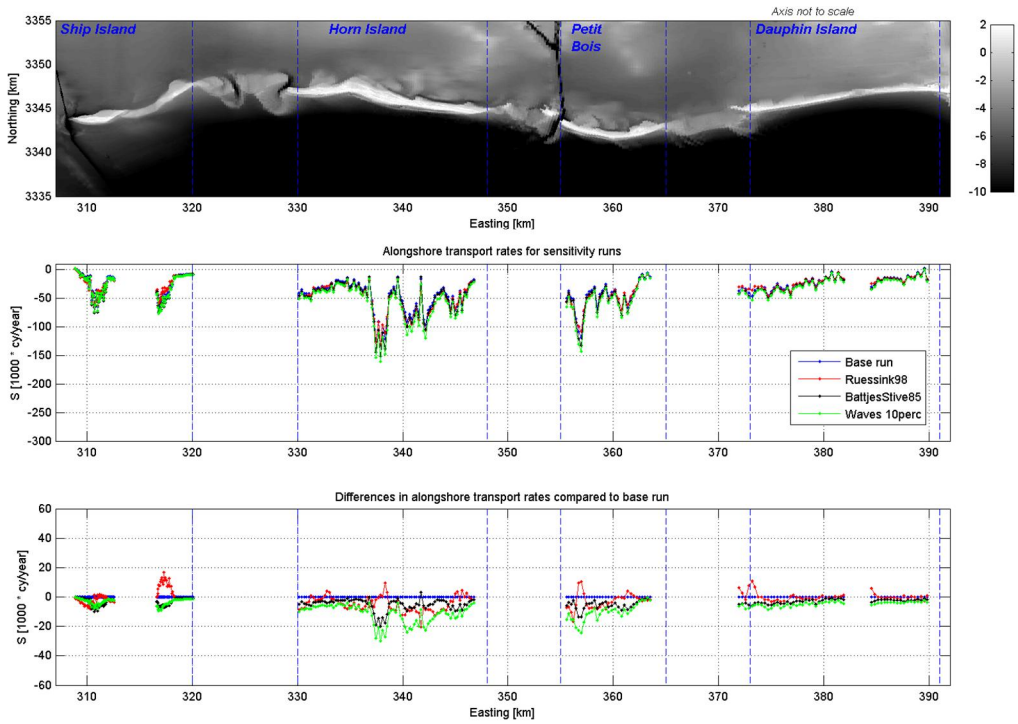

Figure B.2 Model sensitivity for parameters related to wave breaking and wave conditions (Group B)

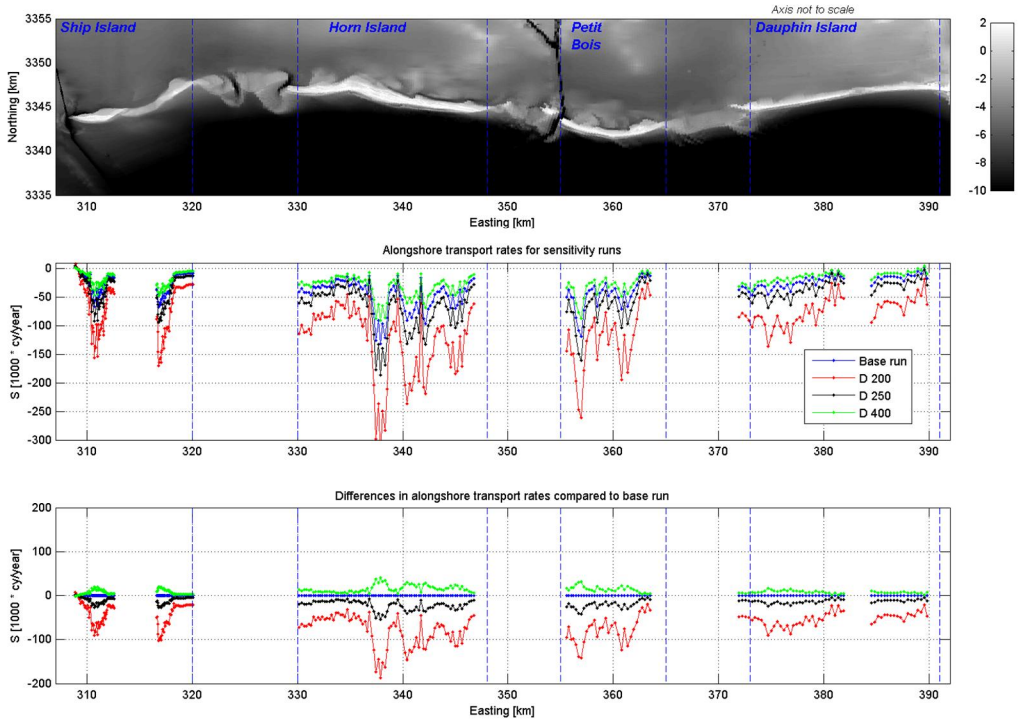

Figure B.3 Model sensitivity for sediment properties (Group C)

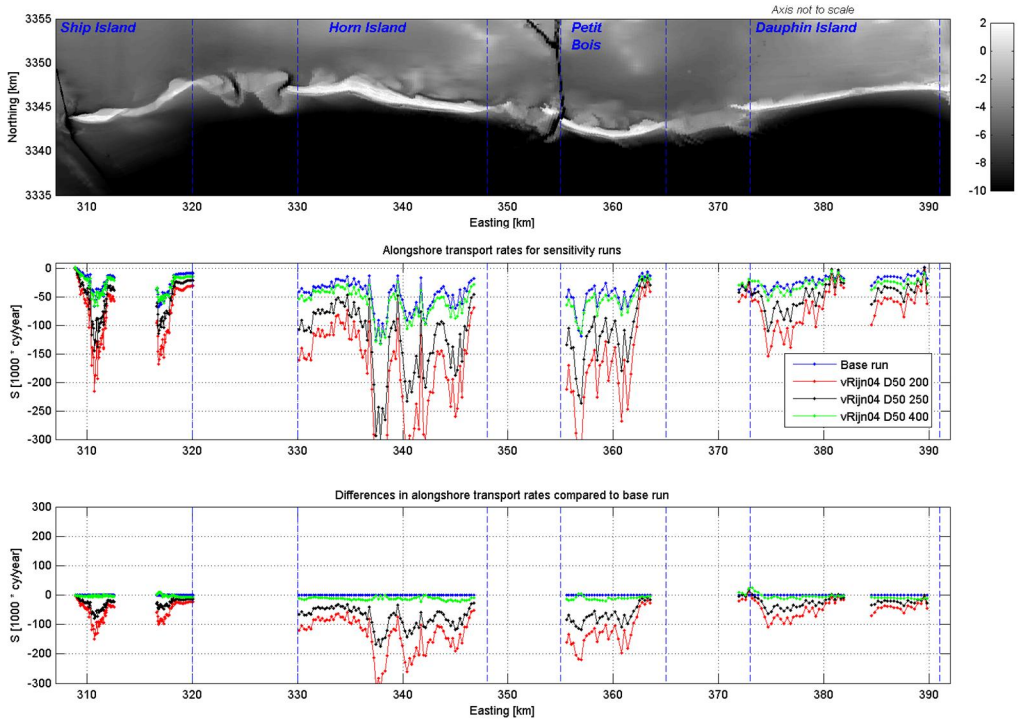

Figure B.4 Model sensitivity for transport formula (Group D)

If the tested ranges for all considered parameters are considered to be realistic, band widths around the computed transports can be estimated, as presented in Figure A.5.

Based on above sensitivity runs it is concluded that the alongshore transport rate is especially sensitive to the sediment diameter and sediment transport formulation. An increased D_{50} increases the critical shear stress of the sediment at which the grains may become suspended and increases the particle fall velocity. Under the same hydrodynamic conditions this results in decreased mobility of the sediment (decreasing sediment transport rates). Although both the Van Rijn (1993) and (2004) sediment transport formulation are widely applied in sediment transport modeling, the differences in the alongshore sediment transport rate is rather large.

The other model settings that have been investigated have a minor impact on the resulting sediment transport rates. The main findings are listed below:

- The shear stress formulation of Fredsoe (1984) result in slightly lower transport rates than the Van Rijn (2004) formulation in the base run.
- The sediment transport rates generally decrease with decreasing water density, which is related to the decrease in shear stress (i.e. for the same sediment characteristics a decreased shear stress implies a decrease in sediment transport capacity of the flow).
- Different formulations for the wave breaker parameter generally show a slight increase in transport rates compared to the base run, whereas the transport rates are hardly sensitive to changes in eddy diffusivity and viscosity.

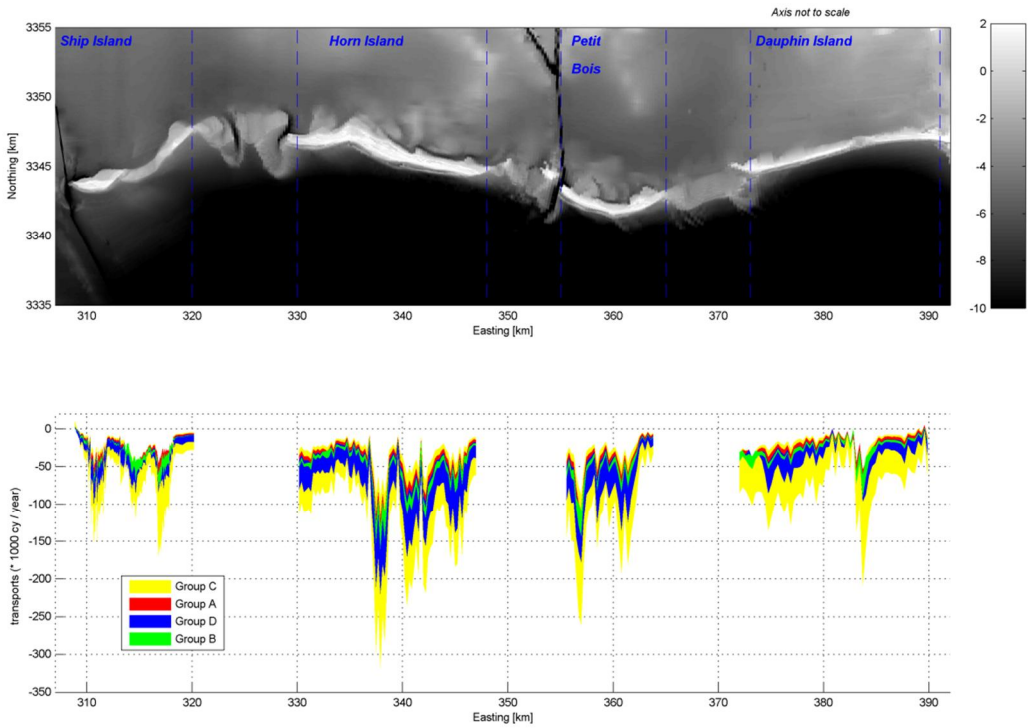

Figure B.5 Band widths related to the 4 different groups

C Verification of longshore transport computations

C.1 Introduction

In order to verify the longshore transports computed with the MCC model, verification computations have been carried out with two numerical modeling tools ('Unibest-CL+' and 'Littoral') which are relatively easy to set up and require little computational time.

The results are summarized below. *It should be noted that in this annex the presented transports are in m^3/yr whereas in the main report the transports are presented in cy/yr (conversion factor: 1 m^3 = 1.32 cy)*

From the results it is concluded that these numerical models - based on the same wave climate as applied in the MCC model – result in a similar order of magnitude of the net longshore transport as in the MCC model.

C.2 Model: Unibest-CL+

From the wave model described in Chapter 5 of the main report wave climates (consisting of 95 wave conditions) were derived at a depth of MSL -8 m seaward of Ship Island, Horn Island and Dauphin Island. With these wave climates computations were made with Unibest CL+, with the formulae of Van Rijn1993 and Bijker.

With Unibest-CL+ so-called S-ϕ curves are computed, where S is the net longshore transport and ϕ the orientation of the seaward-directed shore-normal. Examples of S-ϕ curves are presented below, in which:

Horizontal axis:	orientation ϕ in ºN
Vertical axis:	S in 10^3 m^3/yr (+ = westward directed)
Dashed green line	equilibrium orientation (for which S=0)
Solid green line	actual orientation at the location for considered location

Due to the curvature in the barrier shorelines the orientation ϕ varies strongly alongshore. This results in the gradients which were also found with the MCC model, as discussed in Section 6.2.2.
For Ship Island the S-ϕ curves - given the local wave climate – a maximum net transport of about 50,000 m^3/yr (Van Rijn 1993) to 80,000 m^3/yr (Bijker), at an orientation of the shore-normal of about 180ºN.
For Horn Island the S-ϕ curves - given the local wave climate – a maximum net transport of about 80,000 m^3/yr (Van Rijn 1993) to 110,000 m^3/yr (Bijker), at an orientation of the shore-normal of about 200ºN.
For Dauphin Island the S-ϕ curves - given the local wave climate – a maximum net transport of about 100,000 m^3/yr (Van Rijn 1993) to 140,000 m^3/yr (Bijker), at an orientation of the shore-normal of about 200ºN.

Ship Island

Van Rijn 1993:

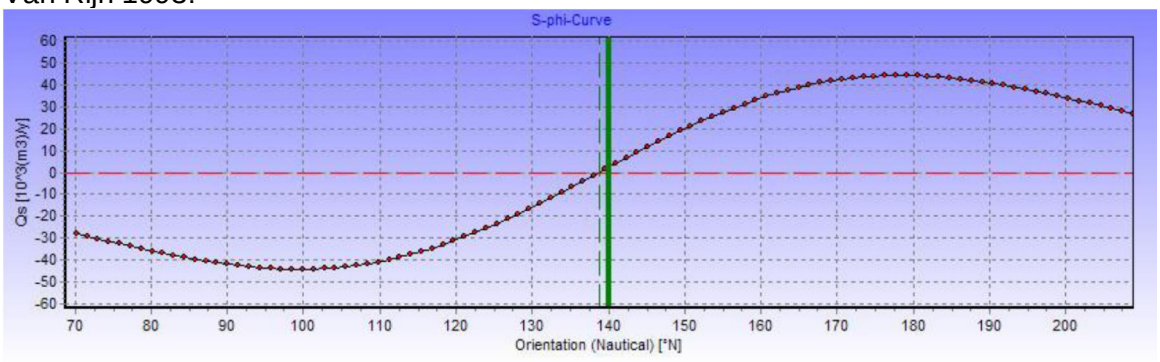

Bijker:

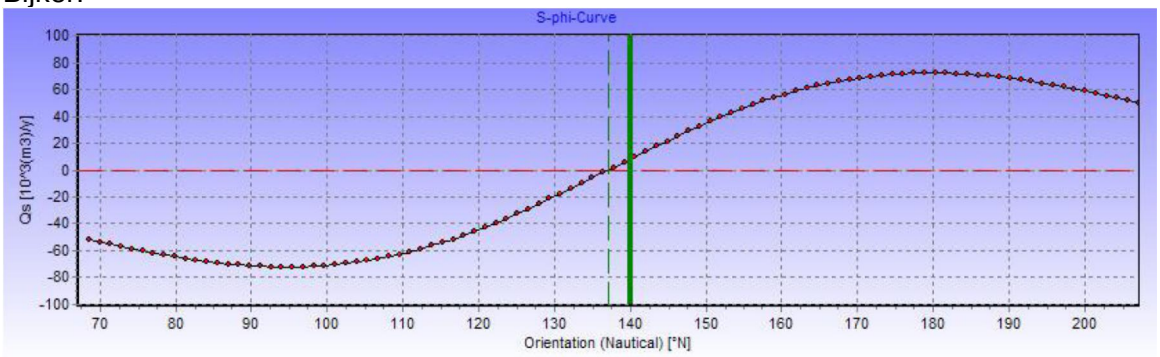

Horn Island

Van Rijn 1993:

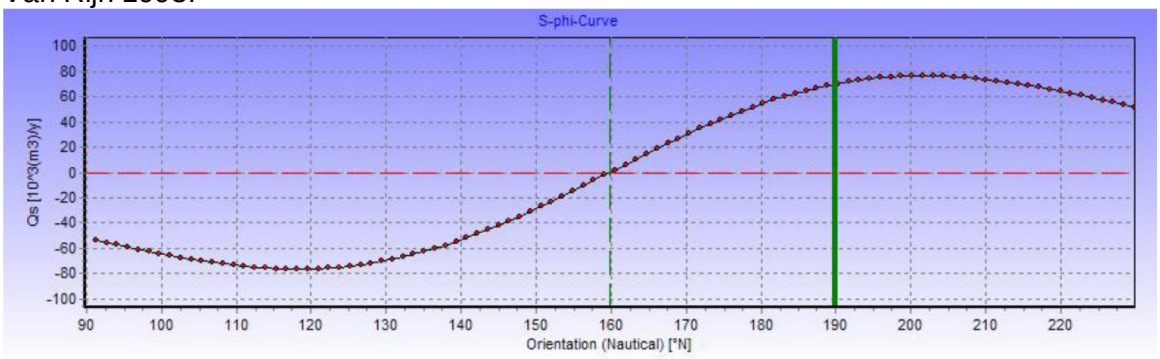

Bijker:

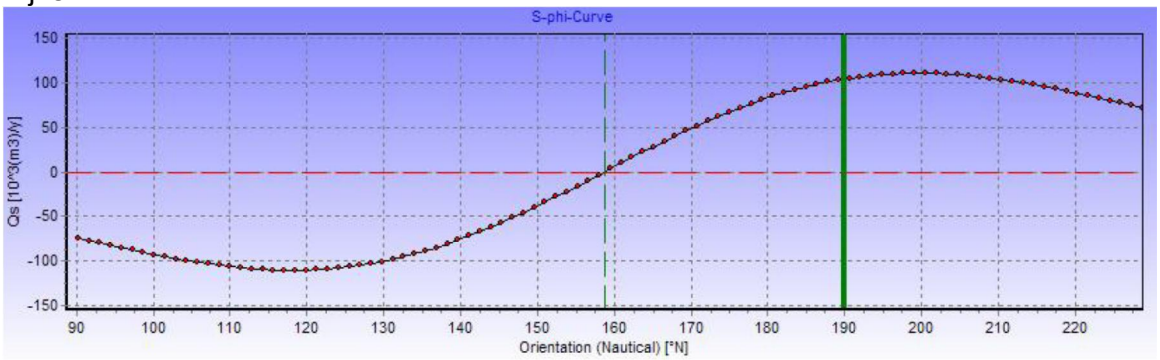

Dauphin Island

Van Rijn 1993:

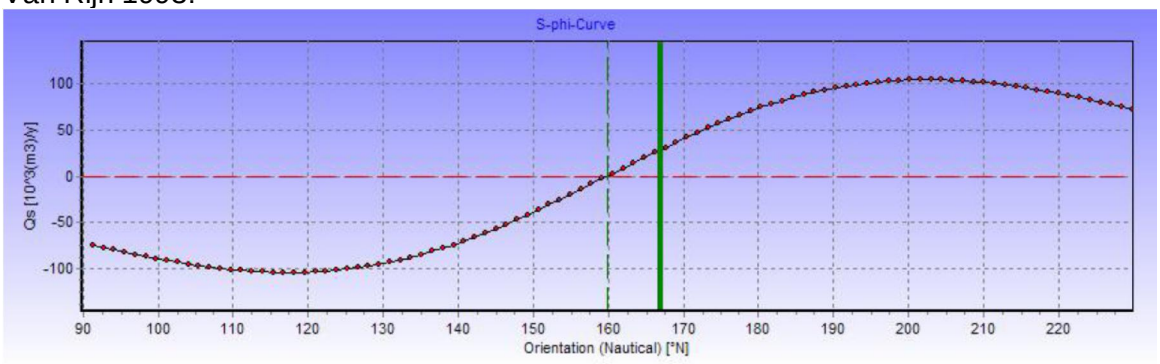

Bijker:

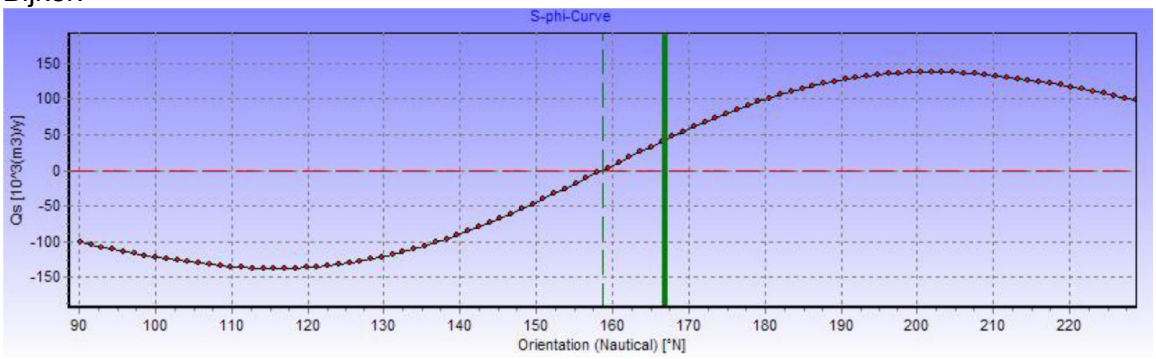

C.3 Model: Littoral

Excel model LITTORAL has been used to estimate LT at Ship island with various formulae and 2 sediment sizes. The annual wave heights in deep water (assumed to be20 m) are given in Table 1.
Wave breaking coefficient= 0.6
Bed slope in surf zone is 1 to 50.
Shore normal= 330^{o} to 355^{o} to North (see Figure C.1).
d_{50}=0.2 and 0.3 mm

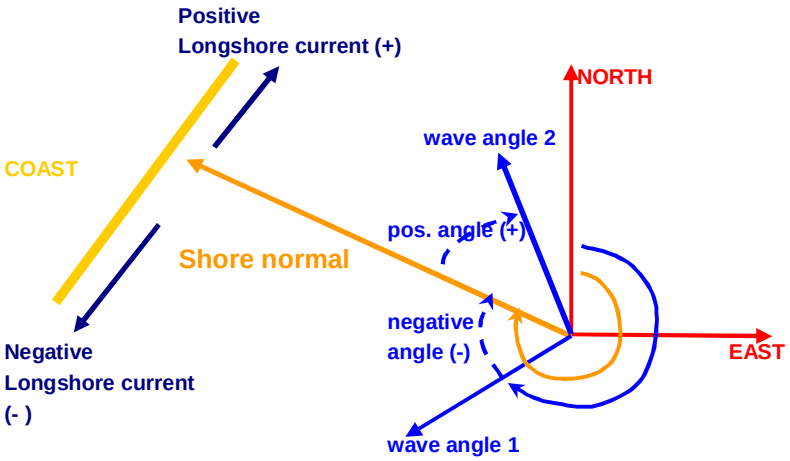

Figure C.1 Definitions of shore normal and wave directions

Wave height H_s (m)	Wave period T_p (s)	Wave direction to North (degrees)	Percentage of occurrence (days)
0.2	2	75	52
0.45	3.5	285	33
0.48	5.5	315	62
0.44	5.4	325	20
0.75	6.3	315	20
0.68	6.5	325	8
0.96	5	305	14
0.78	3.5	325	13
1.35	5.8	305	1.5
1.30	6.1	315	5
1.25	6.7	315	1
1.43	6.1	305	3
1.55	7.7	315	0.3
1.30	8	325	1.4
0.77	3.1	145	2.7
2.38	8	315	0.6
<0.2	0	0	127
Total			365 days

Table C.1 Wave data in deep water

Figure C.2 shows the computed longshore transport values as function of the coastline angle, which is varied between 330 (west of Ship island) and 355 (east) degrees to North. Three formulas have been used: CERC, Kamphuis and Van Rijn 2004. The formulae of Kamphuis and Van Rijn yield approximately the same LT-values for d_{50}=0.3 mm. The effect of sediment size is larger for the Van Rijn formulae. The CERC formula has no sediment size effect.
The longshore transport is almost exclusively to the west for the wave climate from Table 1.

Figure C.3 shows the effect of wave height increase on longshore transport. All wave heights of Table 1 have been multiplied by a linear factor in the range of 1 to 2. A wave height increase by a factor factor of 1.5 leads to an increase of LT from about 50.000 to 175.000 m^3/year (factor 3.5).

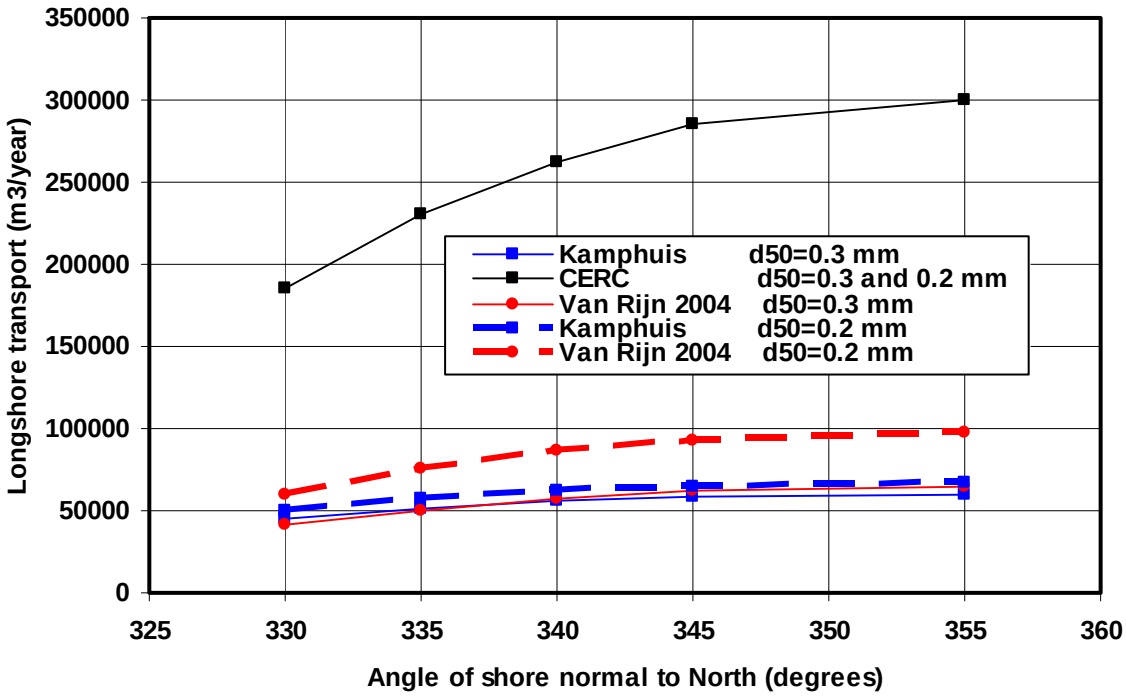

Figure C.2 Longshore transport as function of coastline angle and d50

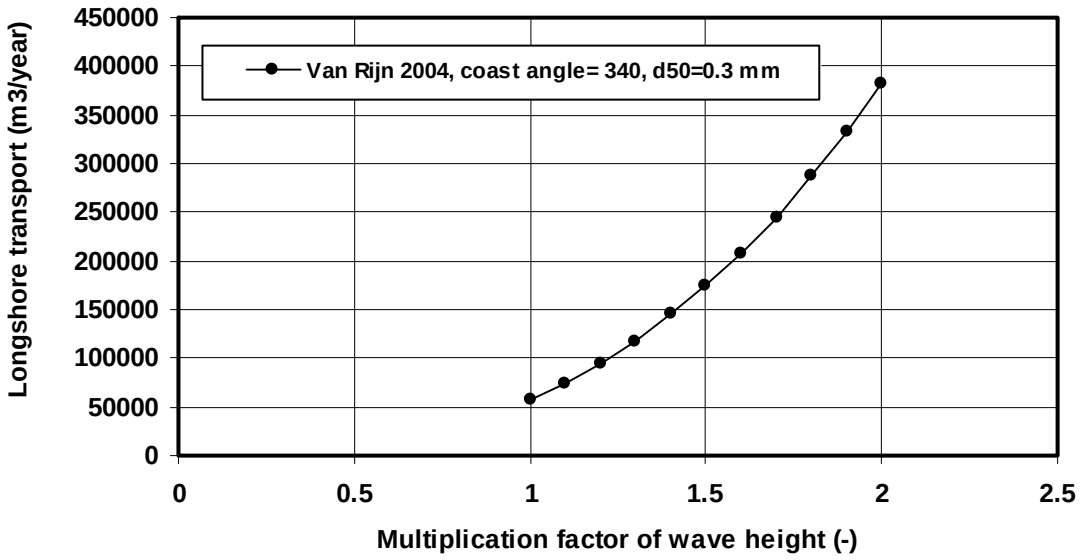

Figure C.3 Effect of wave height increase on longshore transport

D Wind-driven currents

During set-up and calibration of the Delft3D-FLOW model for the Mississippi Barrier Island Restoration project (MsCIP), various sets of measured water levels, currents and wind were analysed and compared with model results.

This section gives a brief description of the wind-induced currents in the study area. As wind-induced currents are not only related to the wind speed, but also (importantly) to the direction of the wind, duration of wind events and air pressure, the analysis focused on the local wind climate as well as residual water levels and currents.

All measured datasets presented in this memo have been downloaded from NOAA's Center for Operational Oceanographic Products and Services (*www.tidesandcurrents.noaa.gov)*.

Data used for analysis

Analysis of 5-years of measured wind speeds and directions at Dauphin Island (NOAA station 8735180) shows that the wind is variable in direction with relatively low wind speeds (Figure B.1). The wind climate is presented as joint-occurrence table in Figure B.2. Box plots of daily and yearly wind variations (Figure B.3) show that on average:

1) winds with average speeds of 5m/s from N during day and from S during night;
2) dominant wind from N to NE during winter and from SE to SW during summer months

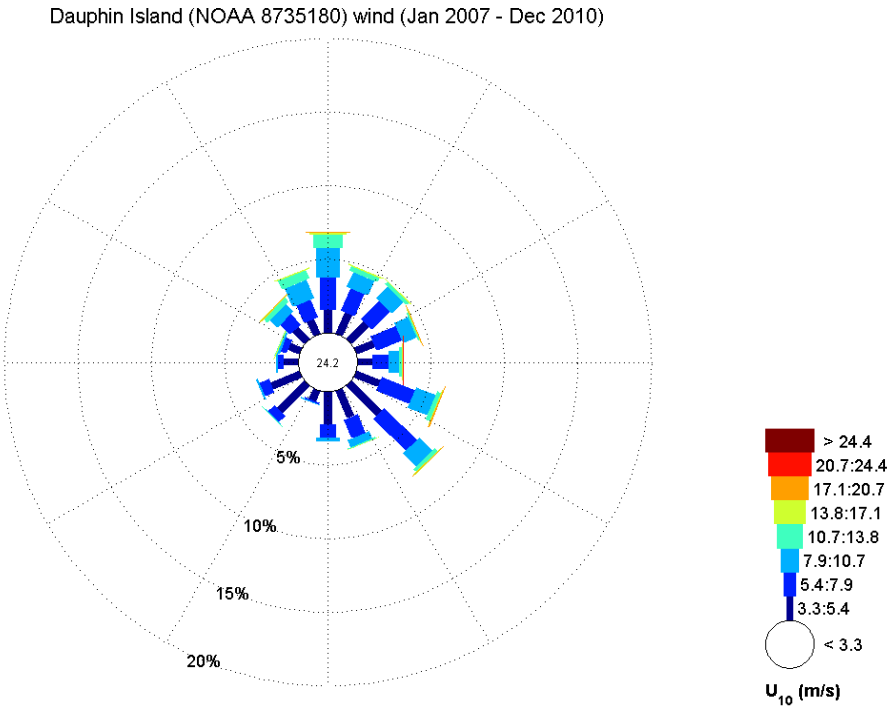

Figure D.1 Wind rose at Dauphin Island for period 2007 - 2010

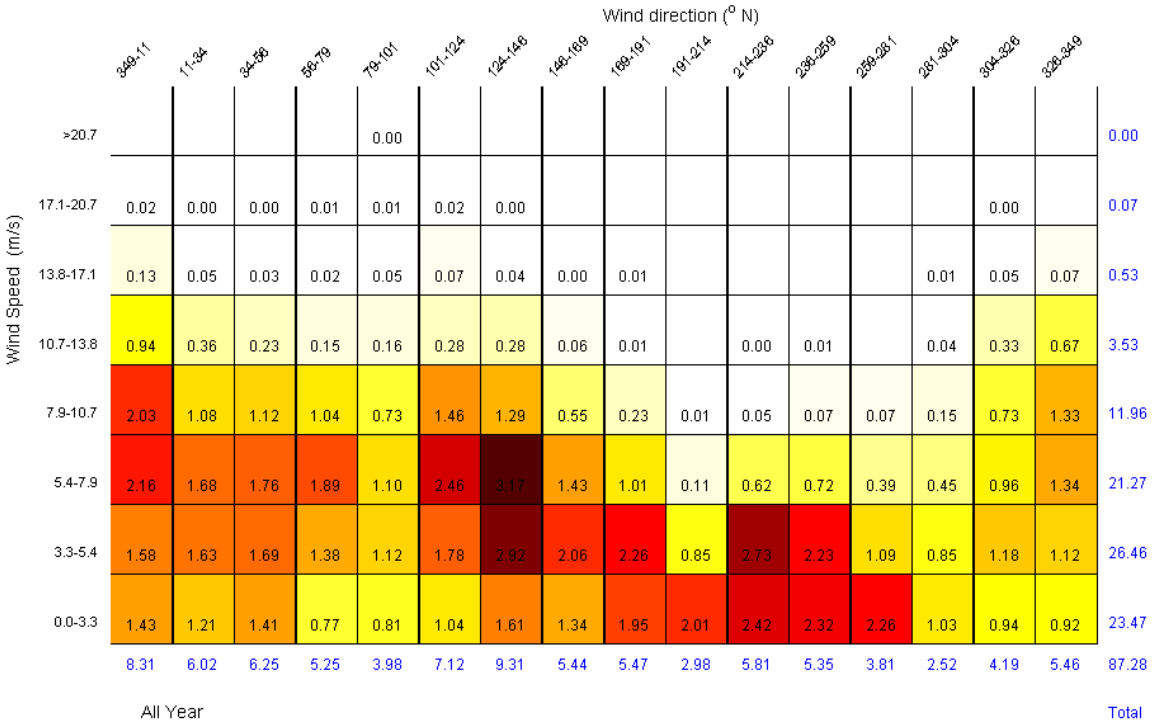

Figure D.2 Joint-occurrence table of wind at Dauphin Island for period 2007 - 2010

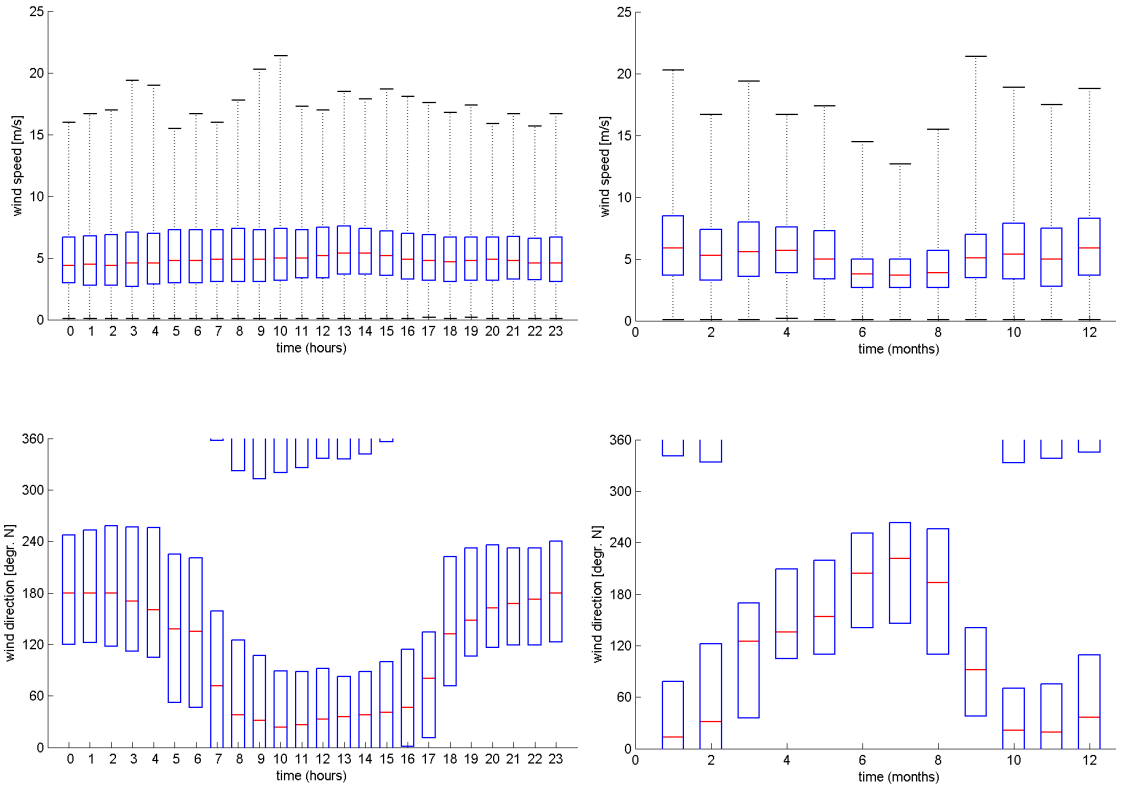

Figure D.3 Box plots of daily (left, in GMT) and yearly (right) wind variations

Wind-induced water levels

Multi-year measurements of water levels have been analyzed for the following stations:

New Canal Station	NOAA 8761927	Period: 2006 – 2010
Shell Beach	NOAA 8761305	Period: 2008 – 2010
Bay Waveland Yacht Club	NOAA 8747437	Period: 2006 – 2010
Coast Guard Sector Mobile	NOAA 8736897	Period: 2007 – 2010

The tidal component was separated from the total observed water levels by means of harmonic analysis. An example of observed, hindcast and residual water levels from Bay Waveland Yacht Club measurements is presented in Figure B.4 and for New Canal Station in Figure B.5. These figures show the following:

	Bay Waveland Yacht Club	**New Canal Station**
Tide range (m, MSL)	-0.5 – 0.5	-0.1 – 0.1
Residual water level range (m)	-0.5 – 0.5 (average) -0.9 – 2.8 (hurricanes)	-0.5 – 0.5 (average) -0.8 – 1.2 (hurricanes)

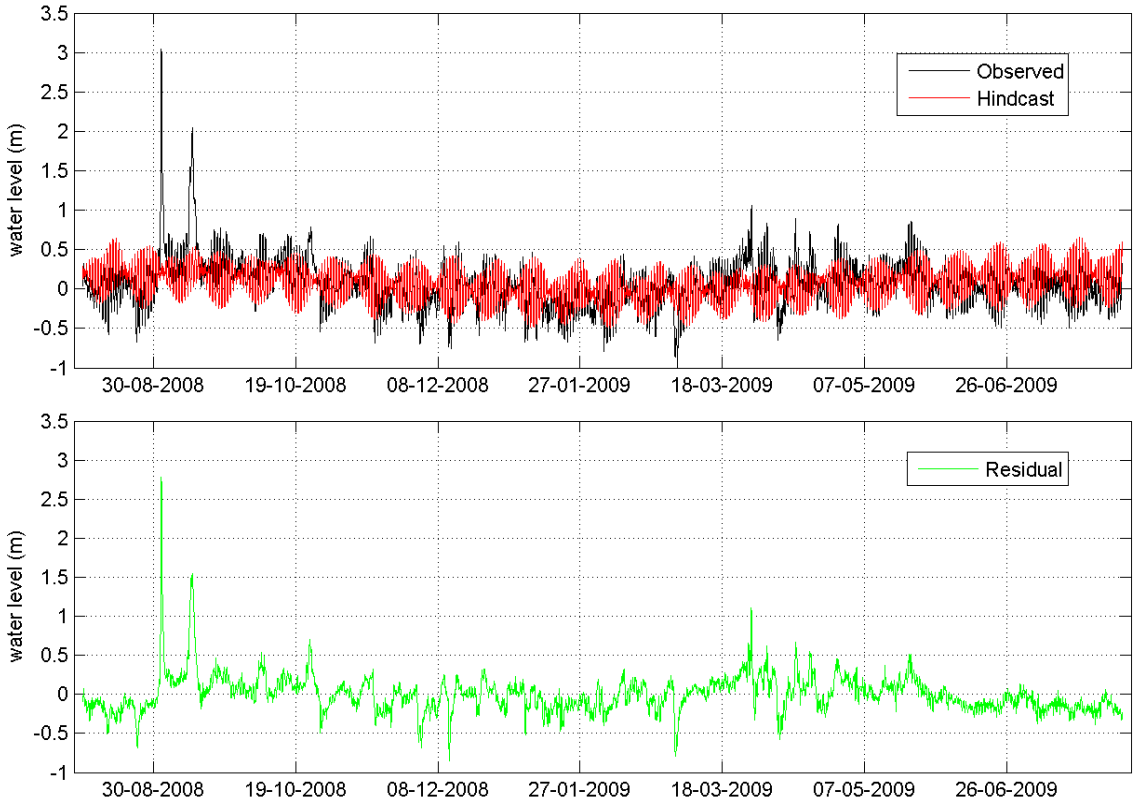

Figure D.4 Observed, hindcast and residual water levels based on Bay Waveland Yacht Club measurements

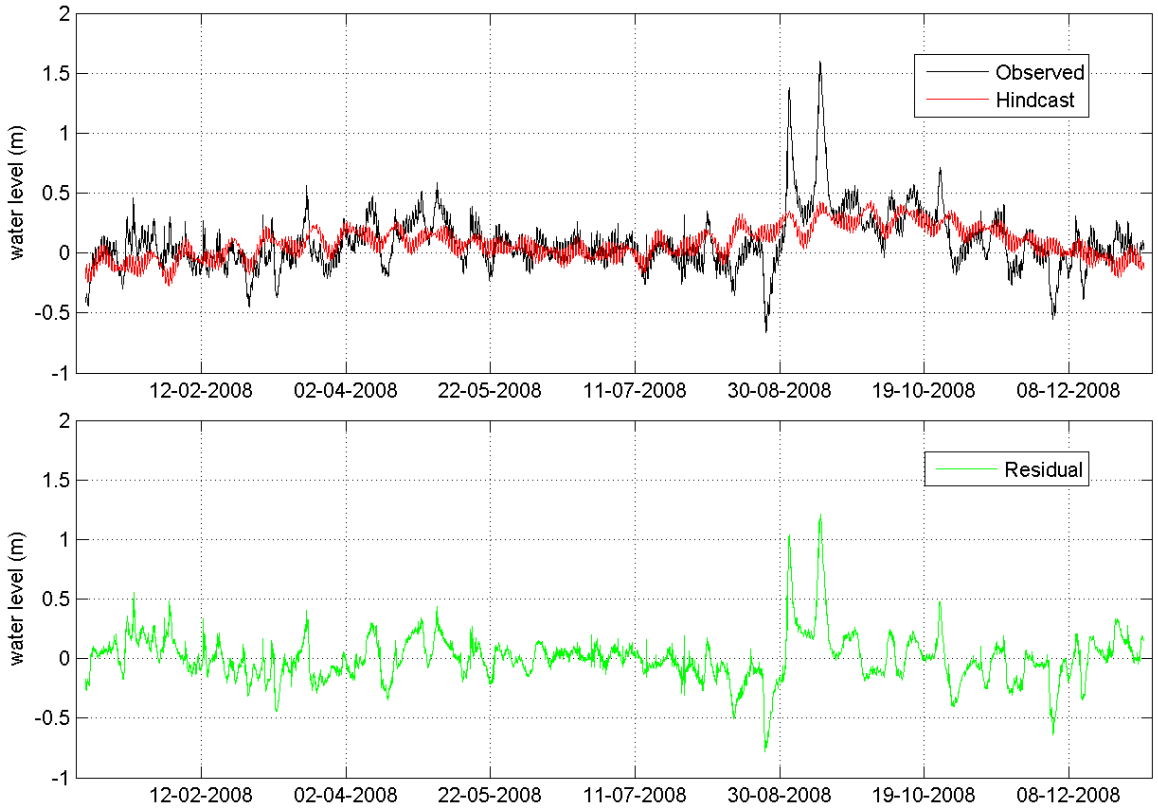

Figure D.5 Observed, hindcast and residual water levels based on New canal Station measurements

Extreme value analysis was performed on the residual water levels resulting from the harmonic analysis (period 2006 – 2010) for the considered stations. Rreturn value plots for Bay Waveland Yacht Club and New Canal Station are presented in Figure B.6. These plots show that once per year residual water levels are reached in the order of 0.8m at Bay Waveland Yacht Club and approx. 1.1m at New Canal Station. Residual water levels on a monthly basis are respectively in the order of 0.5m and 0.7m.

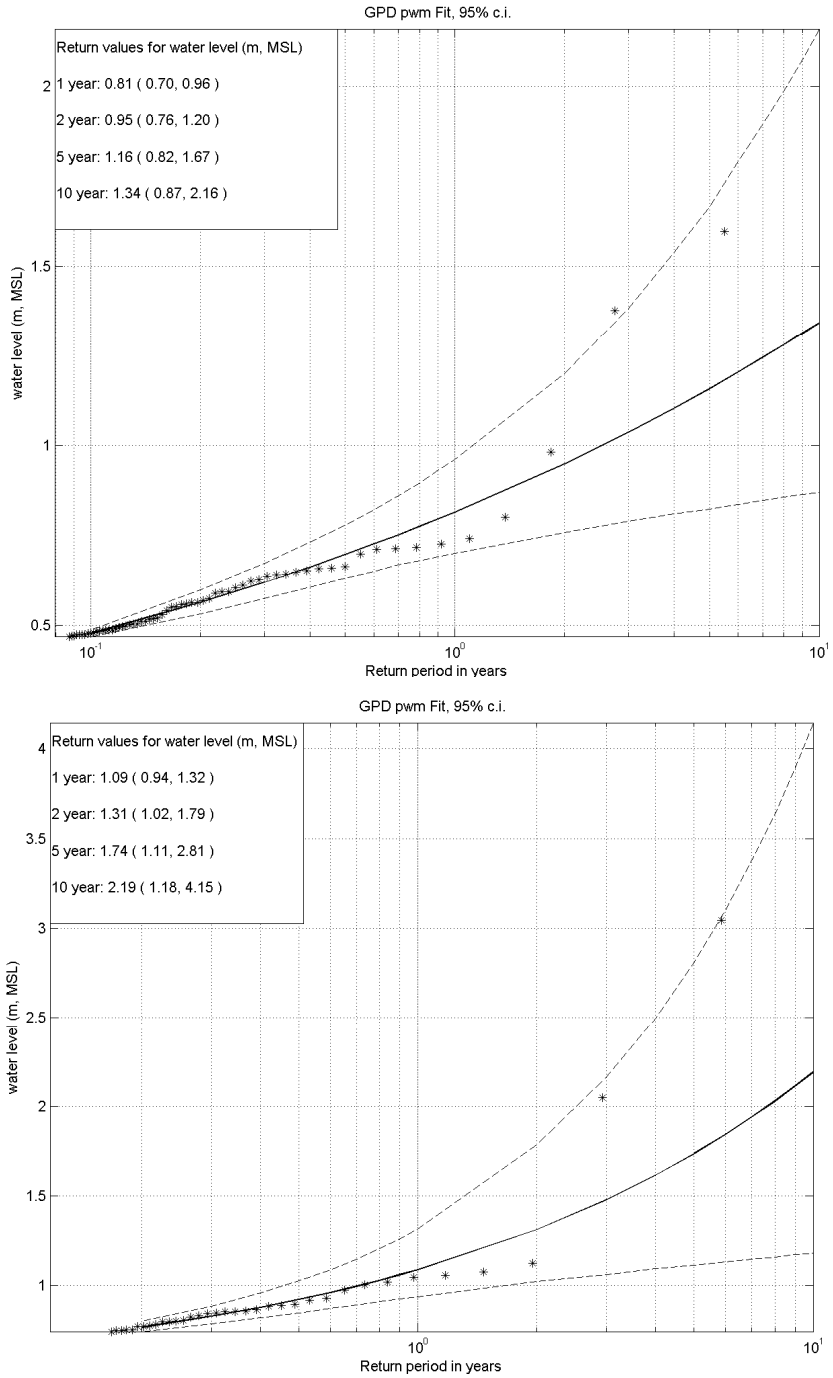

Figure D.6 Return value plots of residual water levels at Bay Waveland Yacht Club (top) and New Canal Station (bottom)

Wind-induced currents

No long duration (mid-depth) current measurements exist in the area of interest. Therefore, an analysis of wind-induced currents is presented simulated with the MCC model (*Test33a*) for a simulation with only wind as forcing and no tide. Time-varying water level variations at the open boundaries of the MCC model were derived from a simulation with the PAN model. The modeling applied uniform wind conditions based on the Dauphin Island wind measurements.

Figure B.7 presents time-series of:
Top plot: water levels as computed at Bay Waveland and a shallow-water location just south of Ship Island (Ship Island 1)
Middle plot: computed depth-averaged current magnitude and direction at Ship Island 1
Bottom plot: measured wind speed and direction at Dauphin Island

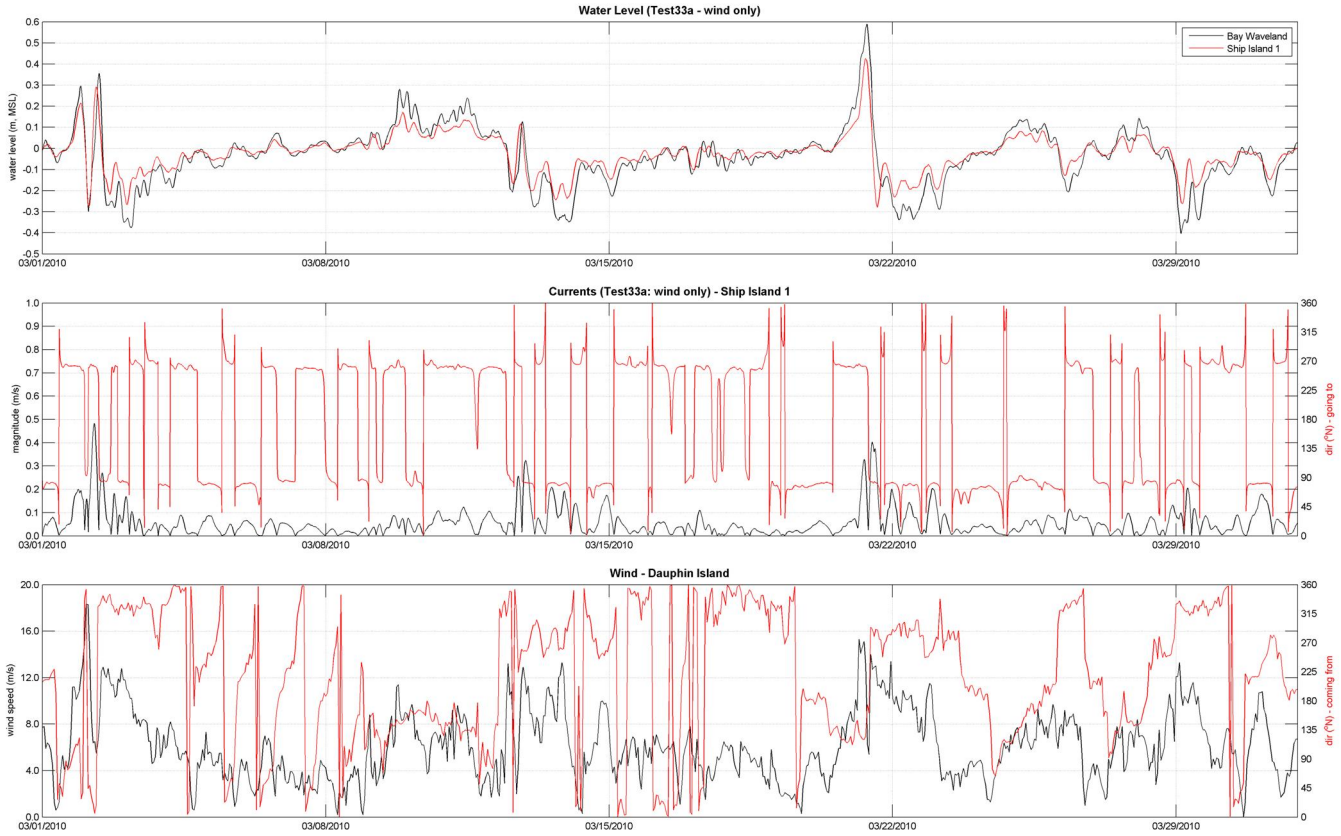

Figure D.7 Time-series of computed water levels (top) and currents (mid) and measured wind (bottom) for March 2010

Figure 4.10 shows the effect of wind on water levels and currents when wind speeds are generally in excess of about 8 to 10m/s. With low wind speeds, the water levels are around zero and the currents are undetermined.

Correlation between wind, water levels and currents

Correlation between wind and water level is presented in Figure B.8 as scatter plots. The water levels are computed at location Ship Island 1 during a 'normal' month (March 2010).

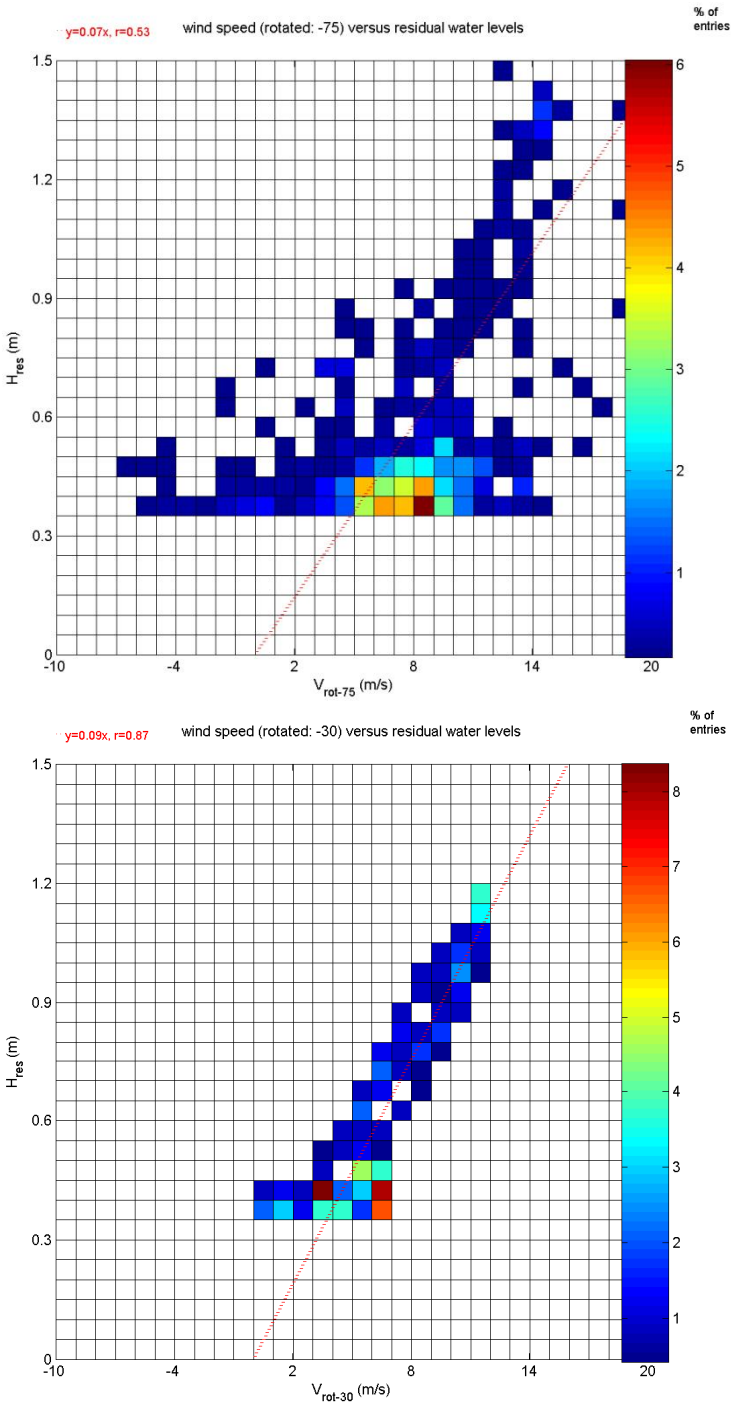

Figure D.8 Density scatter diagrams for Bay Waveland Yacht Club (top) and New Canal Station (bottom) showing correlation between residual water levels and wind speeds (NW component)

Similar comparison, but for a 'normal 1 month period (March 2010), is presented in Figure B.8.

The scatterplots in Figure B.9 show negative water levels (surge) during wind coming from 240°N to 30°N (WSW to NNE) and positive water levels (surge) during wind coming from 90°N to 180°N (E to S).

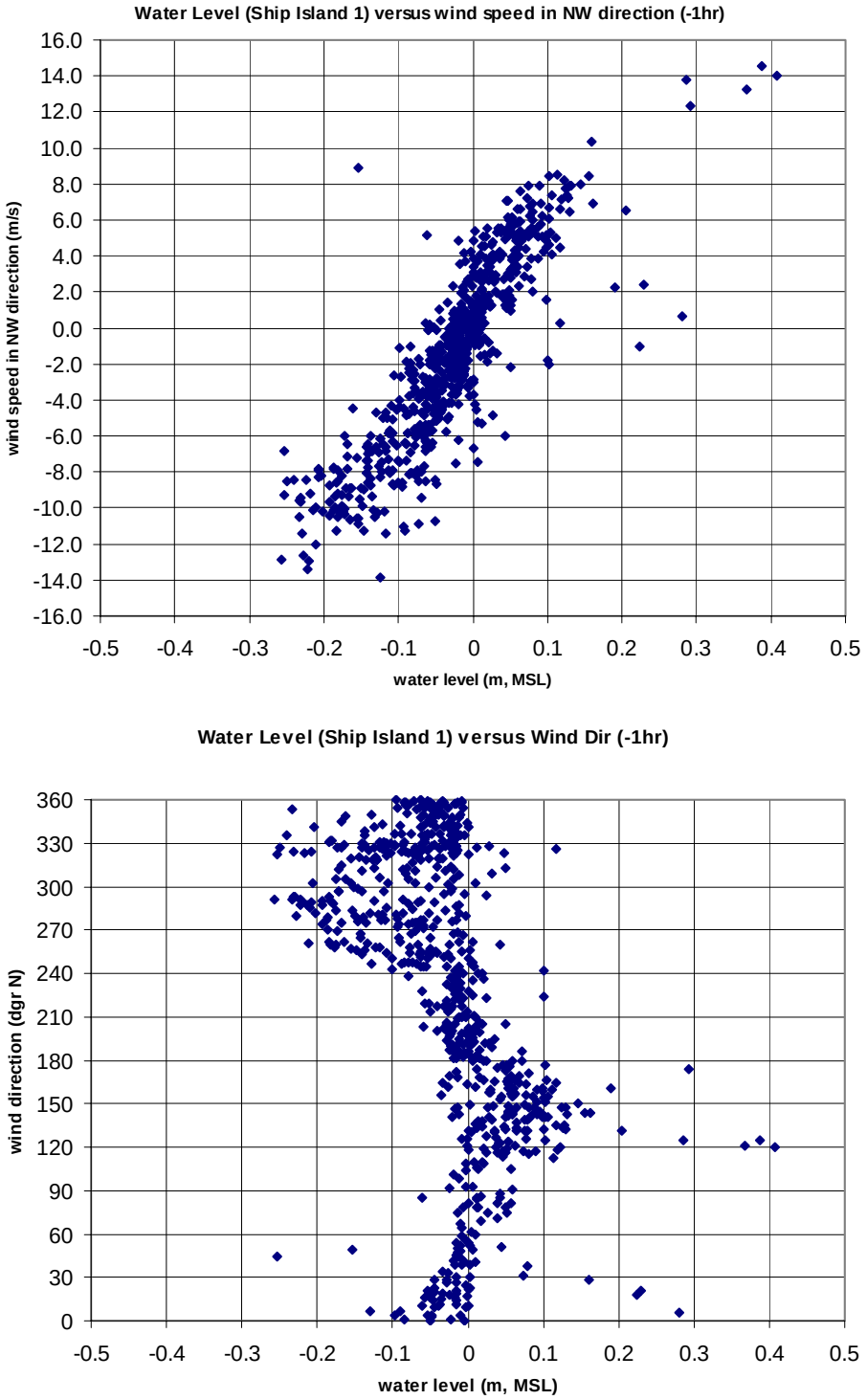

Figure D.9 Scatter plots of water level versus NW directed wind speed (top) and water level versus wind direction (bottom) for March 2010

Figure B.10 shows a scatter plot of current speed as computed at Ship Island 1 for the 'normal' month March 2010 versus wind speed measured at Dauphin Island. This figure shows that above (hourly) wind speeds of 8m/s significant wind-induced currents are generated. According to Figure 2 (joint-occurrence plot of wind), an hourly wind speed of 8m/s is exceeded about 16% of time.

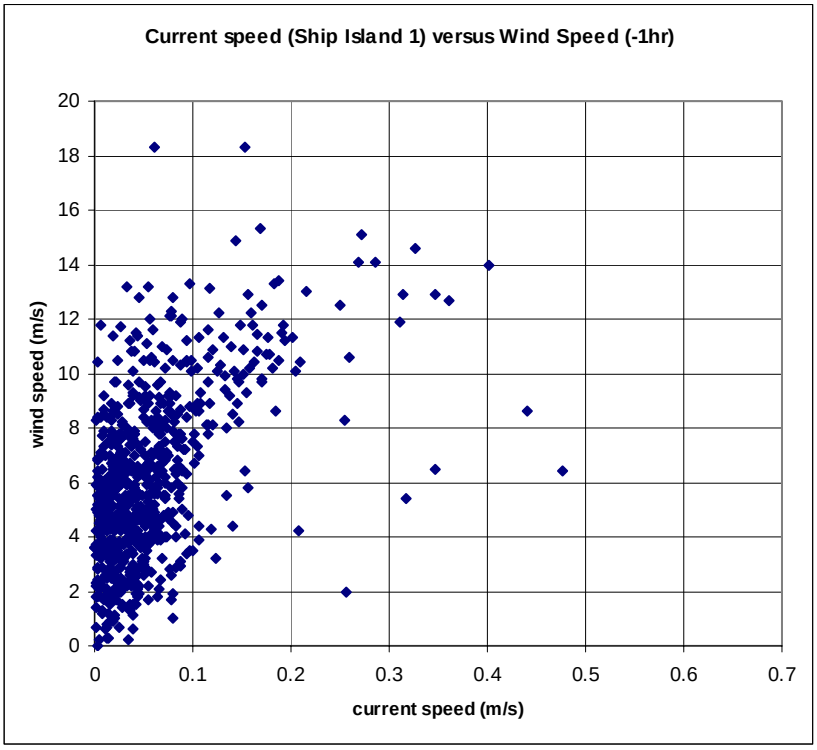

Figure D.10 Scatter plot of current speed as computed at Ship Island 1 for the 'normal' month March 2010 versus wind speed measured at Dauphin Island.

Conclusion of effect of wind

The above presented brief analysis of wind, water level and current data indicates the significance of wind-induced water levels (surges) and currents in the study area. During the process of data analysis, it was found that the magnitude of wind-induced currents in the study area can be in the same order as the magnitude of tidal currents, and can hence probably not be neglected.

Since inclusion of the wind effect in the model input schematisation is not straightforward, this effect will be addressed by means of sensitivity runs.

E Description of applied software

Delft3D

Xbeach

Unibest-CL+

E.1 Delft3D

The Delft-3D model is a state-of the art-model that has been tested for many sites and skill-assessed in different applications and environments and is generally accepted by the research community as evidenced in peer-reviewed literature. In the 3D mode, the model integrates tidal currents and wave interactions to better enable the prediction of sand movements near inlets, on beaches and around reefs and rock outcrops. More detailed hydrodynamic forcing factors, such as strong winds or air pressure differences can also be accounted for in the model. Delft3D is ideal to address the challenges of predicting the movement of sand from inlet bypassing and beach nourishments to improve project performance.

The morphological module of Delft3D is the worldwide frontrunner for application on coastal areas. Recent developments in Delft3D-3DMOR potentially relevant for the morphological issues along the Mississippi coast are:

- Multiple sediment fractions (sand and silt).
  Multiple sediment fractions can be implemented in the model in a very detailed manner, so that the vertical stratification of different sediment layers can be prescribed. In this way, fine and coarser sand fractions can be included in the model as well as silt fractions.
- Extensive dredging and dumping features
  The dredging and dumping module enables a variety of dredging and dumping functionality for specified areas in the computational domain. This feature updates the bed levels during the morphological computation given the prescribed dredge and dump characteristics. All kinds of dredging and dumping options can be taken into account, e.g. dredging at specified rates or to a certain level, flexible dump options, nourishments, etc. In case of nourishments, even a specific grain diameter, possibly finer or coarser than the local grain size, can be applied.
- Three-dimensional domain (3D)
  Delft3D can be run in depth-averaged mode or in a fully three-dimensional (3D) mode. In coastal waters, Delft3D is often applied in 3D mode to resolve the complex vertical flow structures. In 3D computations, the undertow during wave conditions can be included which is an important process in the cross-shore transport dynamics.
- Sediment tracking
  As mentioned above, the morphological model can handle multiple sediment fractions. It is of course also possible to define several sediment fractions with similar grain size. The availability of these sediment fractions can be prescribed for each location in the computational domain. Hence, this feature enables sediment tracking; i.e. the movement of sediments through the domain, and provides insight in the movement and fate of sediments.
- Profile model
  The profile model is actually just one grid cell wide and can represent a cross-shore transect. This model can handle vertical layers and in this way a 2DV model is obtained. This type of model has proven to be a very flexible tool for assessing the cross-shore variability of the coastal profile during different tidal and wave conditions, e.g. storm conditions.
- Re-suspension of sediments
  Within Delft3D the re-suspension of sediments from the bed can be computed. The sediment at the bed can be characterized by different fractions (from fine to coarse)

representing the gradation of sediment at the bed. Under sufficiently strong currents or wave action, the finer fractions will be picked up from the bed, whilst the coarser material may still be stable. The fine sediments may be transported away from their source location. The sediment gradation at the source then changes (becomes coarser), representing the process of armoring.

Selected References:

Benedet, L. and List, J.H., 2008. Evaluation of the physical process controlling beach changes adjacent to nearshore pits. Coastal Engineering, Vol. 55, p. 1224-1236

Geleynse, N., J.E.A. Storms, M.J.F. Stive, H.R.A. Jagers, and D.J.R. Walstra, 2009. Modeling of a mixed-load fluvio-deltaic system. Geophysical Research Letters, Vol. 37, L05402, doi:10.1029/2009GL042000, 2010

Grunnet, N.M., D.J.R. Walstra and B.G. Ruessink, 2004. Process-based modelling of a shoreface nourishment. Coastal Engineering, Volume 51, Issue 7, September 2004, Pages 581-607

Grunnet, N.M., B.G. Ruessink and D.J.R. Walstra , 2005. The influence of tides, wind and waves on the redistribution of nourished sediment at Terschelling, The Netherlands. Coastal Engineering, Volume 52, Issue 7, July 2005, Pages 617-631.

Hartog, W.M.; Benedet, L.; Walstra, D.J.R.; Van Koningsveld, M.; Stive, M.J.F. and Finkl, C.W., 2008. Mechanisms that influence the performance of beach nourishment: a case study in Delray Beach, Florida, U.S.A. Journal of Coastal Research, 24(5), 1304–1319. West Palm Beach (Florida), ISSN 0749-0208.

Idier, D., Hommes, S., Brière, C., Roos, P.C., Walstra, D.J.R., Knaapen, M.A.F. and Hulscher, S.J.M.H., 2006. Review of morphodynamic models to study the impact of offshore aggregate extraction. Accepted for publication in Journal of Coastal Research.

Lesser, G. R., J. A. Roelvink, J. A. T. M. van Kester and G. S. Stelling, 2004. Development and validation of a three-dimensional morphological model. Coastal Engineering 51.

Reniers, A. J. H. M., A. R. van Dongeren, J. A. Battjes, and E. B. Thornton, Linear modeling of infragravity waves during Delilah, J. Geophys. Res., 107(C10), 3137, doi:10.1029/2001JC001083, 2002.

Reniers, A. J. H. M., J. A. Roelvink, and E. B. Thornton (2004), Morphodynamic modeling of an embayed beach under wave group forcing, J. Geophys. Res., 109, C01030, doi:10.1029/2002JC001586.

Roelvink, J. A. and D. J. R. Walstra, 2005. Keeping it simple by using complex models. In Advances in Hydro-Science and Engineering, vol. VI. 222.

Ruggiero, P., Walstra, D.J.R., Gelfenbaum, G., van Ormondt, M., 2009. Seasonal-scale nearshore morphological evolution: Field observations and numerical modeling. Coastal Engineering Vol 56,Pages 1153–1172, doi:10.1016/j.coastaleng.2009.08.003

Storms, J.E.A., Stive, M.J.F., Roelvink, J.A.,and Walstra, D.J.R., 2007. Initial Morphologic and Stratigraphic Delta Evolution Related to Buoyant River Plumes. Coastal Sediments '07.

Sutherland, J., D.J.R. Walstra, T. J. Chesher, L. C. van Rijn and H. N. Southgate, 2004. Evaluation of coastal area modelling systems at an estuary mouth. Coastal Engineering, Volume 51, Issue 2, April 2004, Pages 119-142.

Tung, T.T., Walstra, D.J.R., van de Graaff, J., Stive, M.J.F., 2009. Morphological modeling of tidal inlet migration and closure. Journal of Coastal Research, SI 56, 1080-184. ISSN 0749-0258.

Tonnon, P.K.,van Rijn, L.C. and Walstra, D.J.R., 2006. The Modelling Of Sand Ridges On The Shoreface. Coastal Engineering, Volume 54, Issue 4, April 2007, Pages 279-296.

Van Duin, M.J.P., N.R. Wiersma, D.J.R. Walstra, L.C. van Rijn and M.J.F. Stive, 2004. Nourishing the shoreface: observations and hindcasting of the Egmond case, The Netherlands. Coastal Engineering, Volume 51, Issues 8-9, October 2004, Pages 813-837.

Van Rijn, L.C., Walstra, D.J.R., Grasmeijer, B., Sutherland, J., Pan, S., and Sierra, J.P., 2003. The predictability of cross-shore evolution of sandy beaches at the time-scale of storms and seasons using process-based profile models. Coastal Engineering Vol. 47, p. 295-327

Van Rijn, L.C., Walstra, D.J.R. and van Ormondt, M., 2007. Unified view of sediment transport by currents and waves. IV: Application of morphodynamic model. Journal of Hydraulic Engineering-ASCE 133 (7): 776-793 JUL 2007.

Walstra, D.J.R., J.A. Roelvink and J. Groeneweg, 2000. Calculation of Wave-Driven Currents in a 3D Mean Flow Model. Int. Conf. on Coastal Engineering, Sydney, Australia.

Walstra, D.J.R., L.C. Van Rijn, S.E. Hoogewoning, S.G.J. Aarninkhof, 1999. Modelling Of Sedimentation Of Dredged Trenches And Channels Under The Combined Action Of Tidal Currents And Waves. Coastal Sediments Conference.

Walstra, D.J.R., L.C. Van Rijn, M. Boers and J.A. Roelvink, 2003. Offshore sand pits: verification and application of a hydrodynamic and morphodynamic model. Intl. Coastal Sediments Conference. Clearwater, USA.

Walstra, D.J.R., L.C. Van Rijn and A. Klein, 2004. Validation of a new transport formula (TRANSPOR2004) in a three-dimensional morphological model. Int. Conf. on Coastal Engineering, Lisbon, Portugal.

E.2 XBeach

Storm sensitivity can be assessed by applying the advance Xbeach storm/hurricane impact model which can also be coupled to Delft3D. This model, originally developed for the USACE's MORPHOS project (http://www.frf.usace.army.mil/morphos/morphos.shtml) by Deltares, has specifically been designed to assess the natural coastal response during time-varying storm and hurricane conditions, including dune erosion, overwash and breaching. An example of such a validation is shown in Figure 1 in which the XBeach model prediction is compared with field data at Santa Rosa Island after Hurricane Ivan.

XBeach is a new nearshore numerical model to assess the natural coastal response during time-varyingstorm and hurricane conditions, including dune erosion, overwash and breaching. It is validated with a series of analytical, laboratory and field test cases. Innovations include a non-stationary wave driver with directional spreading to account for wave-group generated surf and swash motions and an avalanching mechanism providing a smooth and robust solution for slumping of sand during dune erosion. The model performs well in different situations including dune erosion, overwash and breaching with specific emphasis on swash dynamics, avalanching and 2DH effects; these situations are all modelled using a standard set of parameter settings. The results show the importance of infragravity waves in extending the reach of the resolved processes to the dune front. The simple approach to account for slumping of the dune face by avalanching makes the model easily applicable in two dimensions and applying the same settings good results are obtained both for dune erosion and breaching.

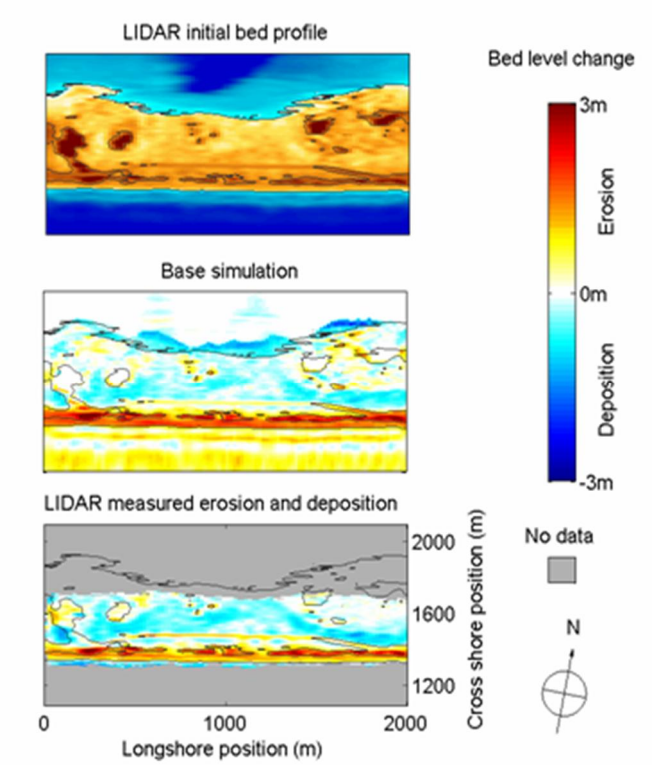

Figure 1 - Initial bed profile around the barrier island (first panel). Xbeach simulated erosion and deposition patterns after 36 h (middle panel). Measured regions of erosion and deposition (bottom panel). (Source: Deltares and USGS, McCall et al. (2010))

In McCall et al. (2010) the XBeach model is used to simulate overwash caused by Hurricane Ivan (2004) on Santa Rosa island. The model is forced using parametric wave and surge time

series based on field data and large-scale numerical model results. The model predicted beach face and dune erosion reasonably well as well as the development of washover fans. Furthermore, the model demonstrated considerable quantitative skill (upwards of 66% of variance explained, maximum bias −0.21 m) in hindcasting the poststorm shape and elevation of the subsurface barrier island when a sheet flow sediment transport limiter was applied. The prediction skill ranged between 0.66 and 0.77 in a series of sensitivity tests in which several hydraulic forcing parameters were varied. The sensitivity studies showed that the variations in the incident wave height and wave period affected the entire simulated island morphology while variations in the surge level gradient between the ocean and back barrier bay affected the amount of deposition on the back barrier and in the back barrier bay. The model sensitivity to the sheet flow sediment transport limiter, which served as a proxy for unknown factors controlling the resistance to erosion, was significantly greater than the sensitivity to the hydraulic forcing parameters.

References:

Baart, F., T. van der Kaaij, M. van Ormondt, A. van Dongeren, M. van Koningsveld and J.A. Roelvink (2009). Real-time forecasting of morphological storm impacts: a case study in the Netherlands. Journal of Coastal Research, SI 56 (Proceedings of the 10th International Coastal Symposium), Lisbon, Portugal.

Daly, C., J.A. Roelvink, A.R. van Dongeren, J.S.M van Thiel de Vries and R.T. McCall (2010). Evaluation of an advective-deterministic approach to short wave breaking. Submitted to Coastal Engineering.

McCall, R.T., et al., 2010. Two-dimensional time dependent hurricane overwash and erosion modeling at Santa Rosa Island. Coastal Engineering 57, 668 – 683. doi:10.1016/j.coastaleng.2010.02.006.

McCall, Robert, Nathaniel Plant, Jaap van Thiel de Vries, The effect of lonsghore topographic variation on overwash modelling, 2010. 32nd International Conference on Coastal Engineering, Shanghai, China.

Roelvink, J.A., et al., 2009. Modeling storm impacts on beaches, dunes and barrier islands. Coastal Engineering 56, 1133–1152. doi:10.1016/j.coastaleng.2009.08.006.

Van Dongeren, A.R., Bolle, M. Vousdoukas, T. Plomaritis, P.Eftimova, J. Williams, C.Armaroli, D. Idier, P. Van Geer, J. Van Thiel de Vries, P.Haerens, R.Taborda, J.Benavente, E. Trifonova, P. Ciavola, Y. Balouin and J.A. Roelvink, 2009. MICORE: Dune Erosion And Overwash Model Validation With Data From Nine European Field Sites, Proc. Coastal Dynamics.

Lindemer, C.A., N.G. Plant, J.A. Puleo, D.M. Thompson, T.V. Wamsley, 2010. Numerical Simulation of a Low-lying Barrier Island's Morphological Response to Hurricane Katrina. Accepted for publication in Coastal Engineering.

Van Thiel de Vries, Jaap, Robert McCall, Ap van Dongeren, Ad Reniers, The effect of the longshore dimension on dune erosion, 2010. 32nd International Conference on Coastal Engineering, Shanghai, China.

E.3 Unibest-CL+

The program UNIBEST-CL+ is a powerful tool to model longshore sediment transports and morphodynamics of coastlines. Shoreline migration is computed on the basis of computed longshore transports at specific locations along the coast. The model runs are very time-efficient, which allows for the evaluation of multiple scenarios as well as sensitivity analyses.

The model can be used for a wide range of coastal engineering projects. A typical application is the analysis of the large scale morphology of coastal systems to provide insight into the causes of coastal erosion or to predict the impact of planned coastal infrastructure (such as a port) on the coast. Shoreline evolution computations can be made over a period of decades, but also for considerations on a smaller time and spatial scale.

The shoreline is defined relative to a user-defined reference line which may be curved. This enables the modelling of complex coastal areas such as deltas, bays, circular shaped beaches and even complete islands. In these computations changes in the longshore transports with time due to re-orientation of the shoreline are taken into account. Longshore currents and sediment transports generated by obliquely incoming waves are computed. The effect of the tide can be included. The gradients in the (time-dependent) transports are used as input for the shoreline model. The model includes a wave propagation module to transform the offshore wave climate to the surf zone (assuming fairly uniform depth contours) and to compute the surfzone dynamics, according to the Battjes-Stive model (1984) for wave propagation and wave decay. Principal processes are accounted for, such as changes in wave energy as a result of bottom refraction, shoaling and dissipation induced by wave breaking and bottom friction. The distribution of the longshore current along the coastal profile is derived from the depth-averaged momentum equation alongshore.

Longshore transport and its distribution along the coastal profile can be evaluated according to several total-load sediment transport formulae for sand (such as Bijker, van Rijn) or gravel (Van der Meer & Pilarczyk). The transports respond to local wave- and current conditions in an instantaneous, quasi-steady way. The net longshore transport can be computed on the basis of (up to) hundreds of combinations of wave- and tidal conditions. Also the gross contributions in both directions can be derived. An essential aspect of coastline modelling is the strong relationship between the orientation of the coast and the longshore transport for each cross-shore ray. This relationship is presented in a so-called S-ϕ curve. This curve forms the basis for the shoreline modelling since it provides information on transport gradients caused by a curvature of the coastline, as well as on the time-dependent response of the longshore transport on changes of the coast-orientation with time.

The shoreline movement in the coastline model is computed on the basis of a continuity equation for sediment, computed longshore transports (from the S-ϕ curve) and an active profile height. Various initial and boundary conditions may be introduced so as to represent a variety of coastal situations. A non-uniform offshore or nearshore wave climate along the coast (e.g. due to structures) and resulting gradients in the longshore transport can be modelled.